AD_____

Award Number: DAMD17-03-1-0287

TITLE: Development of km23-Based Diagnostics and Therapeutics

PRINCIPAL INVESTIGATOR: Kathleen M. Mulder, Ph.D.

CONTRACTING ORGANIZATION: Pennsylvania State University
Hershey, PA 17033

REPORT DATE: May 2005

TYPE OF REPORT: Annual

PREPARED FOR: U.S. Army Medical Research and Materiel Command
Fort Detrick, Maryland 21702-5012

DISTRIBUTION STATEMENT: Approved for Public Release;
Distribution Unlimited

The views, opinions and/or findings contained in this report are those of the author(s) and should not be construed as an official Department of the Army position, policy or decision unless so designated by other documentation.

20060503171

REPORT DOCUMENTATION PAGE

Form Approved
OMB No. 074-0188

Public reporting burden for this collection of information is estimated to average 1 hour per response, including the time for reviewing instructions, searching existing data sources, gathering and maintaining the data needed, and completing and reviewing this collection of information. Send comments regarding this burden estimate or any other aspect of this collection of information, including suggestions for reducing this burden to Washington Headquarters Services, Directorate for Information Operations and Reports, 1215 Jefferson Davis Highway, Suite 1204, Arlington, VA 22202-4302, and to the Office of Management and Budget, Paperwork Reduction Project (0704-0188), Washington, DC 20503

1. AGENCY USE ONLY	2. REPORT DATE	3. REPORT TYPE AND DATES COVERED
	May 2005	Annual(15 Apr 2004 - 14 Apr 2005)

4. TITLE AND SUBTITLE
Development of km23-Based Diagnostics and Therapeutics

5. FUNDING NUMBERS
DAMD17-03-1-0287

6. AUTHOR(S)

Kathleen M. Mulder, Ph.D.

7. PERFORMING ORGANIZATION NAME(S) AND ADDRESS(ES)
Pennsylvania State University
Hershey, PA 17033

E-Mail: kmm15@psu.edu

8. PERFORMING ORGANIZATION REPORT NUMBER

9. SPONSORING / MONITORING AGENCY NAME(S) AND ADDRESS(ES)
U.S. Army Medical Research and Materiel Command
Fort Detrick, Maryland 21702-5012

10. SPONSORING / MONITORING AGENCY REPORT NUMBER

11. SUPPLEMENTARY NOTES

Original contains color plates: ALL DTIC reproductions will be in black and white

12a. DISTRIBUTION / AVAILABILITY STATEMENT
Approved for Public Release; Distribution Unlimited

12b. DISTRIBUTION CODE

13. ABSTRACT (Maximum 200 Words)

Similar to other solid tumors, ovarian cancers are resistant to the growth inhibitory effects of the natural epithelial growth inhibitor TGFβ, suggesting that alterations in TGFβ pathways contribute to ovarian cancer progress-sion. The TGFβ resistance is frequent, perhaps exceeding 75% of cases, especially for recurrent ovarian cancers. Despite the high frequency of TGFβ resistance that occurs in ovarian cancers, thus far, no clinically useful agents, which target the signaling pathways of any of the TGFβ superfamily members, have been developed for this disease. Accordingly, there is a great need to develop TGFβ-based agents and indicators for the diagnosis, therapy, and prognosis of ovarian cancer. Further, TGFβ and some of its signaling components can function as tumor suppressors. We have identified a novel TGFβ signaling component (km23) that is altered in 42% of ovarian cancer patient tumors. Our results suggest that the growth inhibitory effects of km23 may be lost in human ovarian cancers expressing altered forms of km23; km23 may normally function as a tumor suppressor. Our studies are likely to lead to significant new information regarding the development and progression of ovarian cancer, and to the development of novel diagnostics and therapeutics for this disease.

14. SUBJECT TERMS
TGFβ, km23, dynein, ovarian cancer, motor protein, signal transduction, tumor suppressor mutations, CNAPS

15. NUMBER OF PAGES
166

16. PRICE CODE

17. SECURITY CLASSIFICATION OF REPORT	18. SECURITY CLASSIFICATION OF THIS PAGE	19. SECURITY CLASSIFICATION OF ABSTRACT	20. LIMITATION OF ABSTRACT
Unclassified	Unclassified	Unclassified	Unlimited

Table of Contents

INTRODUCTION

We have identified a TGFβ receptor-interacting protein that appears to be a novel tumor suppressor for ovarian cancer. This protein, termed km23, is also a light chain of the motor protein dynein. As a dynein light chain (DLC), km23 would be expected to recruit intracellular cargoes (i.e., signaling complexes) to the rest of the dynein motor for transport along microtubules (MTs) toward the minus ends (generally toward the nucleus). We have identified mutations in km23 in 42% of ovarian cancer patients, which are not present in normal tissues. Our functional studies thus far demonstrate that these alterations block the binding of km23 to the dynein intermediate chain (DIC), and thereby diminish TGFβ-mediated transcriptional events. Moreover, expression of wild-type (wt) km23 in an ovarian cancer cell line with an altered form of km23 results in a reduction of growth in both monolayer culture and in soft agar. Forced expression of km23 in untransformed cells results in an induction of specific TGFβ responses. Further, blockade of km23 using siRNA approaches blocks the ability of TGFβ to inhibit cell growth or to induce fibronectin, two major TGFβ responses. Thus, km23 is a novel TGFβ signaling intermediate that appears to function as a tumor suppressor.

BODY

As described in the last Progress Report, we had largely completed Task 1 in the Statement of Work (SOM). However, we were still working on sub-task 1g at that time. We have now completed this sub-task as well. These studies are described by the abstract below (Liu et al, 2005a).

In addition, we have accomplished several sub-tasks under Task 2, including a-c, and f-i, some of which are described below in Ding et al (2005). Task 2c is also described in Jin et al., 2005. Tasks 2a-c and 2g-i are also described in the following abstracts: Mulder et al., 2005, Liu et al., 2005, Gao and Mulder, 2005, and Zhong et al., 2005. Tasks 2a, 2g-2i are described in Jin et al., 2005; Ding et al., 2005; and Ilangovan et al., 2005, all published papers, and thus, reportable outcomes. We have decided that we do not need to examine other cell lines at this time (sub-task h).

We have now completed Task 3 and we are preparing the paper describing this work now (see Liu et al., 2005a below).

Under Task 4, we have continued with sub-tasks a and b. Since PSCOM was unable to provide us useful samples in a timely manner (sub-task c), we have begun a collaboration with Dr. Gordon Mills at M. D. Anderson. He has agreed to provide sufficient samples to continue our work. We are also continuing with sub-tasks 4d, e, and g-i. Under sub-task 4f, we have found that the alterations are not present in DNA and that we cannot use paraffin-embedded samples. Thus, we will continue to use the RT-PCR methodologies we have developed. Future studies (outside the scope of this grant) will address the mechanisms underlying the development of the km23 alterations in RNA (ie, splicing or editing defects).

Under Task 5, we have completed sub-tasks a-c (see Liu et al., 2005b below). Since we were unable to obtain appropriately collected serum samples from PSCOM in a timely fashion, we are continuing these studies with CHTN, and will also receive samples from G. Mills, as discussed above. Using these samples, we are continuing with sub-tasks 5e-j at this time (see Liu et al, 2005b below). We anticipate being able to analyze a larger number of samples during the next project period.

Stable expression of wild-type km23 in human ovarian cancer cells expressing a mutant form of km23 causes growth suppression. (Described in Liu, X, Ding, W., Sun, B., and Mulder, K. M., In Preparation, 2005a).

We have previously shown that the human ovarian cancer cell line SK-OV-3 expresses an altered form of km23, missing exon 3, similar to one of the alterations we have identified in human ovarian cancer tissues. This cell line is highly aggressive and TGFβ-resistant. In order to determine whether expression of wt km23 in the SK-OV-3 cells would reduce the malignant behavior of the cells, we established SK-OV-3 pools and clones stably expressing wt km23 or the empty vector (EV) in a tet-off conditional expression system. In this system removal of doxycycline (dox) resulted in an induction of the stably expressed wt km23 within 4-5 days in both the km23 pool and in a representative clone that had been selected (#14). In contrast, stable expression of the EV construct in the same SK-OV-3-pBig2r system (EV pool) did not result in induction of km23 upon dox removal. Using this system, monolayer cell growth of the km23 and EV pools was assessed at various times after dox removal using a crystal violet assay. Induction of km23 resulted in a significant decline in viable cell number, while cell growth was unaffected by dox removal in the EV pool. Similarly, expression of km23 by removal of dox in both the km23 pool and clone #14 resulted in a 5- to 6-fold decrease in the number of colonies formed in soft agar, compared to the number of colonies formed by withdrawal of dox from the EV pool cells. Tumorigenicities were also reduced by induction of km23 *in vivo*. Our data suggest that expression of wt km23 inhibited both the anchorage-dependent and anchorage-independent growth of ovarian cancer cells that normally express an altered form of km23. The tumor suppressive effect of km23 was also apparent in a xenograft model *in vivo*.

km23: A dynein light chain frequently mutated in human ovarian cancer. (Described in Ding, W., Tang, Q., Espina, V., Liotta, L. A., Mauger, D., and Mulder, K. M., Cancer Res, 2005; 65(15):6526-33).

Using laser-capture microdissection (LCM) and nested reverse-transcription polymerase chain reaction (RT-PCR), we found that km23, which interacts with the TGFβ receptor complex, is altered at a high frequency in human ovarian cancer patients. A novel form of km23, missing exon 3 (Δexon3-km23), was found in two out of nineteen tumor tissues from patients with ovarian cancer. In addition to this alteration, a stop codon mutation (TAA→CAC) was detected in two patients. This alteration results in an elongated protein, encoding 107 amino-acid residues (Δ107km23), instead of the wild-type 96-amino acid form of km23. Furthermore, five missense mutations (T38I, S55G, T56S, I89V, and V90A) were detected in four patients, providing a total alteration rate of 42.1% (8 out of 19 cases) in ovarian cancer. No km23 alterations were detected in 15 normal tissues. Such a high alteration rate in ovarian cancer suggests that km23 may play an important role in either TGFβ resistance or tumor progression in this disease. In keeping with these findings, the functional studies described herein indicate that both the Δexon3-km23 and S55G/I89V-km23 mutants displayed a disruption in binding to the DIC *in vivo*, suggesting a defect in cargo recruitment to the dynein motor complex. In addition, the Δexon3-km23 resulted in an inhibition of TGFβ-dependent transcriptional activation of both the p3TP-lux and activin responsive element (ARE) reporters. Collectively, our results suggest that km23 alterations found in ovarian cancer patients result in altered dynein motor complex formation and/or aberrant transcriptional regulation by TGFβ.

Identfication of km23 alterations in tissues and CNAPs from ovarian cancer patients, relative to normal controls. (Liu, X., Thomas, K. M., and Mulder, K. M., In Preparation, 2005b)

We have already obtained a significant number of matched serum and tissue samples from CHTN. Additional samples are being obtained from G. Mills (MD Anderson). We have been and will continue to catalogue the matches, with their associated pathology reports. We do not anticipate any problems obtaining the specimens. The number of specimens required depends upon the results obtained, and upon the statistical analyses to be performed in association with

D. Mauger (PSU). We have shown that we can amplify wt km23 from normal serum using the methodologies we have developed. We have also considered various methods for quantitating the input RNA. For example, as part of the Core Facility at PSU, we have access to an Agilent 2100 Bioanalyzer, on which we can detect as low as 200 pg of RNA using a 6000 Pico LabChip kit (Xiao et al, 2005). This instrument can also evaluate the quality of the RNA simultaneously. Since we are currently having success with serum, we will only analyze plasma samples if difficulties arise. We expect to find km23 alterations in CNAPS at a relatively high frequency (approx 40%), based upon our previous results in the tumor tissues. However, if it turns out that the km23 alterations in serum are rare variant forms as cnaps, it may be necessary to try different enrichment methods to enhance the ratios of altered km23 to wt km23, as described for other genetic alterations (Gocke et al, 2000)

KEY RESEARCH ACCOMPLISHMENTS:

- Blockade of km23 expression using siRNA led to a reduction in the ability of TGFβ to inhibit DNA synthesis; km23 was necessary but not sufficient for mediating TGFβ growth inhibition.
- The km23 members comprise a distinct family within the larger superfamily of robl-like/LC7/bxd-like members; the km23 family appears to function as TGFβ signaling components.
- km23 is the human homologue of the Drosophila protein robl; defects in robl result in an increase in mitotic index and accumulation of cargoes inside cells.
- TGFβ induces the interaction of km23 with DIC within 2 min of TGFβ addition.
- The kinase activity of TGFβ receptor RII is required for km23 interaction with DIC.
- km23 interacts with Smad2 in both GST pull-down and IP/blot analyses.
- km23 is co-localized with Smad2 at early times after TGFβ addition to cells (before nuclear translocation of Smad2).
- Blockade of endogenous km23 using siRNA results in a decrease in TGFβ-dependent Smad2 phosphorylation, translocation, and regulation of transcription.
- Addition of wild-type km23 to ovarian cancer cells with an altered form of km23 causes growth suppression in monolayer culture and in semi-solid medium.

REPORTABLE OUTCOMES:

Publications:

1. Jin, Q., Ding, W., Staub, C.M., Gao, G., Tang, Q., and **Mulder, K.M.** Requirement of km23 for TGFβ-mediated growth inhibition and induction of fibronectin expression. *Cell. Signalling*, 2005; 17:1363-72..
2. Jin, Q, Ding, W., and **Mulder, K.M.** Requirement for km23 in a Smad2-dependent TGFβ signaling pathway. In Revision, *J. Biol. Chem.*, 2005.
3. **Mulder, K.M.** A new target for the development of anti-cancer diagnostics and therapeutics. In Preparation, *Amer. Clin. Lab.*, 2004.
4. Ding, W., Tang, Q., Espina, V., Liotta, L.A., Mauger, D.T., and **Mulder, K.M.** A TGFβ receptor-interacting protein frequently mutated in human ovarian cancer. *Cancer Res.*, 2005; 65(15):6526-33.

5. Liu, G., Chen, L., Neiman, J., and **Mulder, K.M.** Role of the c-AMP-responsive element in mediating TGFβ-induction of TGFβ3 gene transcription. In Revision, *J. Biol. Chem.*, 2005.
6. Ilangovan, U., Ding, W., Wilson, C.L., Groppe,J.C., Trbovich, J.T., Zuniga, J., Demeler, B., Tang, Q., Gao, G., **Mulder, K.M.**, and Hinck, A.P. Structure and dynamics of the homodimeric dynein light chain km23. *J. Molec. Biol.*, 2005; 352:338-54.
7. Liu, X., Ding, W., Sun, B., and **Mulder, K.M.** Suppression of tumor growth by stable expression of wild-type km23 in human ovarian cancer cells expressing a mutant form of km23. In Preparation, 2005.

Abstracts:

1. Mulder, K.M., Jin, Q., Liu, X., and Ding, W. Requirement for the TGFβ receptor interacting protein km23 in a Smad2-dependent TGFβ signaling pathway. AACR Annual Meeting, April, 2005.
2. Liu, G., Chen, L., Neiman, J., and **Mulder, K.M.** Role of the c-AMP Responsive Element in Mediating TGFβ induction of TGFβ3 Gene Transcription. AACR Annual Meeting, April, 2005.
3. Gao, G.F. and Mulder, K.M. A new light chain of the motor protein dynein (km23-2) is involved in transforming growth factor-β signaling. FASEB Summer Research Conference, Snowmass Village, CO., June 2005.
4. Zhong, Y., Ding, W., Tang, Q., and Mulder, K.M. km23 phosphorylation controls its function in transforming growth factor-β signaling. FASEB Summer Research Conference, Snowmass Village, CO., June 2005.

Invited Speaker:

University of South Carolina School of Medicine, Columbia, SC	2004
Medical University of South Carolina, Charleston, SC	2005
University of Arizona Cancer Center & College of Medicine, Tucson, AZ	2005
University of Hawaii School of Medicine, Manoa, HI	2005

CONCLUSIONS

1. We have developed a highly sensitive and specific assay to detect genetic alterations in km23 in cancer patient tissues by combining two micro-scale technologies -- LCM and nested RT-PCR.

2. Various mutations in km23 were detected in tumors from 8 out of 19 ovarian cancer patients, providing a total km23 alteration rate of 42%. These mutations were not present in tumor-free tissue groups.

3. The km23 alterations in cancer patients reduce or block DIC interaction and TGFβ-/Smad2-dependent transcriptional activation, suggesting that mutations in km23 may block the intracellular transport of TGFβ signaling components, thereby altering TGFβ responses.

4. Our results indicate that km23 alterations found in ovarian cancer patients result in altered dynein motor complex formation and aberrant transcriptional regulation by TGFβ.

5. Stable, inducible expression of wild-type km23 in human ovarian cancer cells with altered km23 results in blockade of both monolayer and soft agar growth.

6. km23 represents a novel target for the development of ovarian cancer diagnostics and therapeutics.

SO WHAT SECTION:

- Our results provide the first demonstration of a link between cytoplasmic dynein and a natural, growth inhibitory cytokine, namely TGFβ.
- km23 appears to specify the signaling intermediates that are transported along microtubules by the dynein motor after TGFβ receptor activation.
- km23 appears to be a motor receptor important for transporting TGFβ signaling components to their cellular sites of action, thereby maximizing the efficiency of signal propagation and maintaining signal specificity.
- km23 represents a novel target for the development of ovarian cancer diagnostics and therapeutics.
- km23 appears to function as a tumor suppressor, blocking cancer cell growth under normal conditions. In contrast, km23 alterations in human ovarian cancer abrogate the tumor suppressive function of km23.
- Several therapeutic approaches can be employed to repair or replace the loss of tumor suppressor protein functions (i.e., gene therapy approaches, blockade of binding proteins, etc); these are also applicable to km23.
- We anticipate that future studies will lead to the identification of novel agents that can restore the normal functions of km23, or replace the altered forms/functions of km23.
- We hope to develop a screening assay for ovarian cancer that will enable identification of patients with km23-dependent ovarian cancer, so that the km23-based therapeutics we plan to develop can be utilized in a patient-tailored manner.

REFERENCES

Ding, W., Tang, Q., Espina, V., Liotta, L.A., Mauger, D.T., and **Mulder, K.M.** A TGFβ receptor-interacting protein frequently mutated in human ovarian cancer. *Cancer Res.*, 65(15):6526-33, 2005.

Gocke CD, Benko FA, Kopreski MS, Evans DB. Enrichment methods for mutation detection. Annals N Y Acad Sci 906:31-38, 2000.

Liu, G., Chen, L., Neiman, J., and **Mulder, K.M.** Role of the c-AMP-responsive element in mediating TGFβ-induction of TGFβ3 gene transcription. In Revision, *J. Biol. Chem.*, 2005.

Xiao R, Bader TM, Simmen FA. Dietary exposure to soy or whey proteins alters colonic global gene expression profiles during rat colon tumorigenesis. Molecular Cancer 4(1):1, 2005.

APPENDICES

1. **Publication**: Jin, Q., Ding, W., Staub, C.M., Gao, G., Tang, Q., and **Mulder, K.M.** Requirement of km23 for TGFβ-mediated growth inhibition and induction of fibronectin expression. *Cell. Signalling*, 2005; 17:1363-72.
2. **Publication:** Ding, W., Tang, Q., Espina, V., Liotta, L.A., Mauger, D.T., and **Mulder, K.M.** A TGFβ receptor-interacting protein frequently mutated in human ovarian cancer. *Cancer Res.*, 2005; 65(15):6526-33.

3. **Manuscript In Revision:** Liu, G., Chen, L., Neiman, J., and **Mulder, K.M.** Role of the c-AMP-responsive element in mediating TGFβ-induction of TGFβ3 gene transcription. In Revision, *J. Biol. Chem.*, 2005.

4. **Manuscript In Revision**: Jin, Q., Ding, W., and **Mulder, K.M.** Requirement for km23 in a Smad2-dependent TGFβ signaling pathway. In Revision, *J. Biol. Chem.,* 2005.

5. **Publication:** Ilangovan, U., Ding, W., Wilson, C.L., Groppe, J.C., Trbovich, J.T., Zuniga, J., Demeler, B., Tang, Q., Gao, G., **Mulder, K.M.,** and Hinck, A.P. Structure and dynamics of the homodimeric dynein light chain km23. *J. Molec. Biol.*, 352:338-54, 2005.

6. **Abstract: Mulder, K.M.**, Jin, Q., Liu, X., and Ding, W. Requirement for the TGFβ receptor interacting protein km23 in a Smad2-dependent TGFβ signaling pathway. AACR Annual Meeting, April, 2005, # 4498.

7. **Abstract:** Liu, G., Chen, L., Neiman, J., and **Mulder, K.M.** Role of the c-AMP responsive element in mediating TGFβ induction of TGFβ3 gene transcription. AACR Annual Meeting, April, 2005, # 3726.

8. **Abstract:** Gao, G. F. and **Mulder, K. M.** A new light chain of the motor protein dynein (km23-2) is involved in transforming growth factor-β signaling. FASEB Summer Research Conference, Snowmass Village, CO., June 2005.

9. **Abstract:** Zhong, Y., Ding, W., Tang, Q., and **Mulder, K. M.** km23 phosphorylation controls its function in transforming growth factor-β signaling. FASEB Summer Research Conference, Snowmass Village, CO., June 2005.

10. **Curriculum Vitae:** Kathleen M. Mulder, Ph.D.

Available online at www.sciencedirect.com

SCIENCE DIRECT

Cellular Signalling 17 (2005) 1363–1372

CELLULAR SIGNALLING

www.elsevier.com/locate/cellsig

Requirement of km23 for TGFβ-mediated growth inhibition and induction of fibronectin expression

Qunyan Jin[a], Wei Ding[a], Cory M. Staub[a,1], Guofeng Gao[a,b], Qian Tang[a,2], Kathleen M. Mulder[a,b,*]

[a]*Department of Pharmacology, Pennsylvania State University College of Medicine, 500 University Dr., Hershey, PA 17033, United States*
[b]*Intercollege Graduate Program in Genetics, Pennsylvania State University College of Medicine, 500 University Dr., Hershey, PA 17033, United States*

Received 29 April 2004; received in revised form 4 February 2005; accepted 15 February 2005
Available online 31 March 2005

Abstract

We previously identified km23 as a novel TGFβ receptor-interacting protein. Here we show that km23 is ubiquitously expressed in human tissues and that cell-type specific differences in endogenous km23 protein expression exist. In addition, we demonstrate that the phosphorylation of km23 is TGFβ-dependent, in that EGF was unable to phosphorylate km23. Further, the kinase activity of both TGFβ receptors appears to play a role in the TGFβ-mediated phosphorylation of km23, although TGFβ RII kinase activity is absolutely required for km23 phosphorylation. Blockade of km23 using small interfering RNAs significantly decreased key TGFβ responses, including induction of fibronectin expression and inhibition of cell growth. Thus, our results demonstrate that km23 is required for TGFβ induction of fibronectin expression and is necessary, but not sufficient, for TGFβ-mediated growth inhibition.
© 2005 Elsevier Inc. All rights reserved.

Keywords: TGFβ; Signal transduction; siRNA; Growth; Fibronectin; km23; EGF; Dynein

1. Introduction

Transforming growth factor β (TGFβ) is the prototype for a family of highly conserved ubiquitous peptides that show a remarkable diversity in the biological actions they mediate. These biological responses include effects on cell growth, cell death, cell differentiation, and the extracellular matrix (ECM) [1–3]. TGFβ is growth inhibitory for normal cells of endothelial, hematopoietic, neuronal, and epithelial origin [1,4,5]. However, cancers are often refractory to this growth inhibitory effect, due to genetic loss of TGFβ signaling components or, more commonly, perturbation of TGFβ signaling pathways [1,4].

TGFβ initiates its signals by producing an active tetrameric receptor complex consisting of TGFβ RI (TβRI) and TGFβRII (TβRII) serine/threonine kinase receptors. After TGFβ binds to TβRII, it transphosphorylates, and thereby activates TβRI. The active receptor complex then propagates signals to downstream cellular components and regulatory proteins [2,3,6]. Two primary signaling cascades downstream of the TGFβ receptors have been elucidated: the Smads and the Ras/mitogen-activated protein kinase (MAPK) pathways [1,2,7]. In addition, several TGFβ receptor-interacting factors [1] and Smad-interacting factors [8] have been reported. However, additional TGFβ signaling components and pathways are likely required to mediate the diverse biological responses of this polypeptide factor.

Abbreviations: TGFβ, Transforming growth factor β; ECM, Extracellular matrix; TβRI, TGFβ RI receptor; TβRII, TGFβ RII receptor; JNK, Jun N-terminal kinases; siRNA, Small interfering RNA; NC siRNA, Negative control siRNA; MDCK, Madin Darby canine kidney; Ab, Antibody; DIC, Dynein intermediate chain; DIC Ab, Dynein intermediate chain antibody; EGF, Epidermal growth factor; hkm23, Human km23; FACS; Fluorescence-activated cell sorting.

* Corresponding author. Tel.: +1 717 531 6789; fax: +1 717 531 5013.
E-mail address: kmm15@psu.edu (K.M. Mulder).
[1] Current address: Fox Chase Cancer Center, Philadephia, PA, 19111-2497, United States.
[2] Current address: Lexicon Genetics Inc., 8800 Technology Forest Place, The Woodlands, TX 77381-1160, United States.

0898-6568/$ - see front matter © 2005 Elsevier Inc. All rights reserved.
doi:10.1016/j.cellsig.2005.02.004

Fibronectin, a major component of the ECM, plays important roles in cell adhesion, migration, growth, and differentiation [9,10]. TGFβ is one of the most potent stimulators of the ECM, and it has been shown to play a significant role in the accumulation of specific ECM components such as fibronectin and collagen [1,11,12]. Despite the suggestion that Smads play a critical role in TGFβ-mediated responses, the signaling mechanisms leading to TGFβ-mediated accumulation of ECM proteins are unclear. For example, Hocevar et al. [13] have shown that TGFβ can induce fibronectin synthesis through a Jun N-terminal kinase (JNK)-dependent pathway, but that Smad4 was not involved. In addition, Gooch et al. [14] reported that calcineurin was involved in TGFβ-mediated regulation of ECM accumulation. It is likely that other novel TGFβ signaling intermediates are required for mediating the diverse effects of TGFβ on such a large repertoire of biological responses, which include the effects on ECM.

We have previously identified a novel TGFβ receptor-interacting protein that is also a light chain of the motor protein dynein [15]. This TGFβ signaling intermediate, termed km23, interacts with the receptor complex through TβRII and is phosphorylated after activation of the TGFβ receptor complex. Here we show that km23 is a ubiquitously expressed cytoplasmic protein. Further, TGFβ mediated a rapid increase in km23 phosphorylation, and the kinase activity of both receptors appeared to play a role in this phosphorylation event. Blockade of km23 using small interfering RNAs (siRNAs) decreased the ability of TGFβ to both inhibit cell growth and induce fibronectin expression in Madin Darby canine kidney (MDCK) epithelial cells. Our findings indicate that km23 is a mediator of the growth inhibitory effects of TGFβ and is also required for the induction of fibronectin expression by TGFβ.

2. Materials and methods

2.1. Reagents

The anti-Flag M2 (F3165) antibody (Ab) and mouse IgG were from Sigma-Aldrich (St. Louis, MO). The anti-dynein intermediate chain (DIC) monoclonal Ab (MAB1618) and anti-Lamin A/C Ab (MAB3211) were from Chemicon (Temecula, CA). The rabbit IgG was from Santa Cruz Biotechnology, Inc. (Santa Cruz, CA). The anti-fibronectin Ab (610078) was from BD Biosciences Transduction Laboratories (Palo Alto, CA). Protein A or G agarose were purchased from Invitrogen (Carlsbad, CA). ^{32}P-orthophosphate (NEX-053) was from PerkinElmer Life Sciences (Boston, MA). TGFβ$_1$ was purchased from R & D Systems (Minneapolis, MN). Epidermal growth factor (EGF) was purchased from Upstate Cell Signaling Solutions (Lake Placid, NY). Lipofectamine 2000 (11668-019) was from Invitrogen (Carlsbad, CA). Propidium iodide (537059) was from Calbiochem (San Diego, CA). Ribonuclease A (R4875) and Sodium citrate (C7254) were from Sigma Aldrich (St. Louis, MO). FuGENE 6 Transfection Reagent (11814443001) was from Roche Diagnostics (Indianapolis, IN).

2.2. Antibody production

The rabbit km23 anti-serum was prepared against the following sequence: GIPIKSTMDNPTTTQYA (corresponding to amino acids 27–43) of human km23 (hkm23) (Strategic BioSolutions, Newark, DE, or Covance Reseach Products, Denver, PA). Each company also provided pre-immune serum.

2.3. Cell culture

Mv1Lu (CCL-64), 293 (CRL-1573), and COS-1 (CRL-1650) cells were purchased from American Type Culture Collection (Manassas, VA) and were grown in DMEM supplemented with 10% FBS. MDCK cells (CCL-34) and HepG2 cells (HB-8065) were also obtained from ATCC and were grown in MEM-α supplemented with 10% FBS. 293T cells were obtained from T-W. Wong (Bristol-Myers Squibb, Princeton, NJ) and were maintained as for 293 cells. OVCA 433 cells were obtained from R.C. Bast Jr. (M.D. Anderson Cancer Center, Houston, TX) and were maintained in MEM supplemented with 10% FBS. FET cells were maintained as described previously [16]. Cultures were routinely screened for mycoplasma using Hoechst 33258 staining.

2.4. Transient transfections, IP/blot, Westerns, and In vivo phosphorylation assays

Transient transfections, IP/blot, Westerns, and In vivo phosphorylation assays were performed essentially as described previously [13,15,17–19].

2.5. siRNAs

The km23 siRNAs used for the [^{3}H]thymidine incorporation assays were purchased from Dharmacon Research (Lafayette). The double-stranded km23 siRNA corresponded to nucleotides 77–97 of the hkm23 coding region (5′-AAGGCATTCCCATCAAGAGCA-3′). The siRNAs were transfected using Oligofectamine (12252-011; Invitrogen). For the FACS and fibronectin experiments (Figs. 5 and 6), siRNA plasmids were constructed as follows. The sense strand of the hairpin km23 siRNA-1 corresponded to nucleotides 230–250 of the km23 coding region (5′-AAATTATGGTTGCACCAGATA-3′). The sense strand of hairpin km23 siRNA-2 corresponded to nucleotides 130–150 of the km23 coding region (5′-AACCTCATGCACAACTT-CATC-3′). km23 siRNA-1 and km23 siRNA-2 plasmids were transfected using Lipofectamine 2000 reagent for the fibronectin experiments. The sense strand of the hairpin km23 siRNA-3 corresponded to nucleotides 251–271 of the

km23 coding region (5′-AAGACTATTTCCTGATTGTGA-3′). This km23 siRNA-3 plasmid was transfected using FuGENE 6 Transfection Reagent for the FACS experiments. In addition, we have made a negative control siRNA (NC siRNA) plasmid, the sequence of which does not match any genes by alignment with the NCBI database using BLAST. All of these constructs contain a human RNA polymerase III U6 promoter and can form a hairpin structure in vivo that is quite similar to chemically synthesized double-stranded siRNA. The pSIREN empty vector was purchased from BD Clontech (Cat# 631529).

2.6. Cellular fractionation

The NE-PER Nuclear and Cytoplasmic Extraction Reagent kit (78833; Pierce, Rockford, IL) was used to fractionate Mv1Lu cells according to the manufacturer's protocol.

2.7. Growth assays

The TGFβ growth inhibitory responsiveness of the cells was assessed by [^{3}H]thymidine incorporation assays, performed as described [20].

2.8. Fluorescence-activated cell sorting (FACS) analysis

Cell-cycle distribution was determined by FACS analysis of propidium iodide-labeled cells. Twenty-four hours after transfection of siRNA plasmids, Mv1Lu cells treated for 24 h in the absence or presence of TGFβ (5 ng/ml) were stained for 15 min before FACS analysis of 50,000 cells per sample [21]. Samples were acquired on a Becton Dickinson FACScan using the CellQuest software package (BD Bioscience, Palo Alto, CA), and data were analyzed using ModFitLT (Verity Software House, Topsham, ME).

2.9. Statistical analyses

A Student's *t*-test was used to determine the level of statistical significance of the decrease in [^{3}H]thymidine incorporation by TGFβ between km23 siRNA-transfected and control-transfected MDCK cells.

3. Results

We have demonstrated previously that km23 is a novel TGFβ receptor-interacting protein that is also a light chain

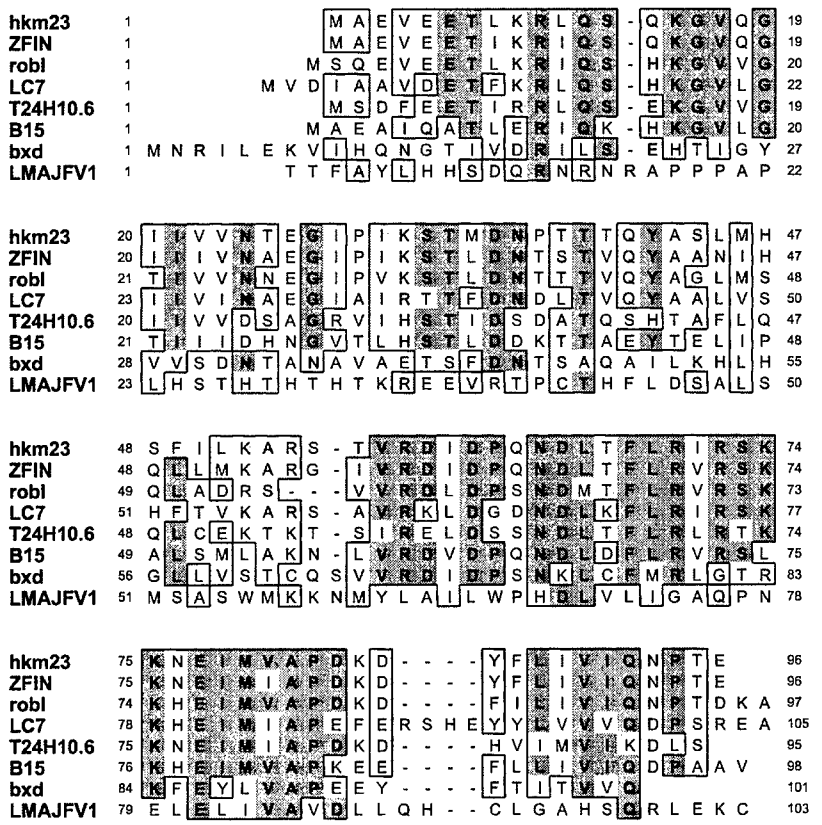

Fig. 1. Alignment of amino acid sequences comparing km23 family members. The coding region for the following km23 family members are aligned to illustrate the relative identities: hkm23 (accession # AY026513), ZFIN (accession # AAH46084; 74% homology to hkm23), robl (accession # AF141920; 67% homology to hkm23), LC7 (accession # AF140239; 59% homology to hkm23), T24H10.6 (accession # Z54216; 56% homology to hkm23), B15 (accession # AJ243446; 56% homology to hkm23), bxd (accession # M27999; 40% homology to hkm23), and LMAJFV1 (accession # AQ850960; 33% homology to hkm23).

of the motor protein dynein [15]. As indicated in Fig. 1, hkm23 is very similar to the *Danio Rerio* (Zebrafish) ZFIN (80% identity or 93% similarity), *Drosophila* robl (68% identity or 82% similarity), and *Chlamydomonas* LC7 (55% identity or 81% similarity) sequences. In addition, a counterpart of km23 in *Caenorhabditis elegans* (T24 H10.6) displays 56% homology to hkm23, and the predicted protein would be 76% similar. In contrast, hkm23 displays 71% similarity to *Spermatozopsis* B15 [22], 54% similarity to *Drosophila* bithoraxoid (bxd), and only 33% homology (predicted protein would be 32% similar) to *Leishmania* LMAJFV1 [23]. The single-celled flagellar parasite *Leishmania* is an animal-like, protozoan form of Protista, the Kingdom that also includes plant-like forms of green algae, such as *Chlamydomonas* and *Spermatozopsis*. Thus, km23 displays a considerable degree of conservation across different Kingdoms and Phyla.

In order to determine the tissue distribution of hkm23, we performed Northern blot analysis using a human tissue blot obtained from BD Biosciences Clontech. The km23 was ubiquitously expressed, with a calculated hkm23 mRNA size of approximately 0.7 kb (data not shown). Similarly, it was of interest to determine whether the km23 protein was expressed in different cell types. In order to proceed with these studies, we developed a polyclonal anti-serum against amino acids 27–43 of hkm23 and performed initial Western blot analyses in MDCK epithelial cells to determine whether the km23 anti-serum was specific. As indicated in Fig. 2A, the rabbit km23 anti-serum specifically recognized a single band of 11 kDa by Western blot analysis (lane 1). No band was visible when pre-immune serum was used (lane 2). Thus, the km23 serum was specific.

In order to further demonstrate the specificity of the rabbit km23 anti-serum and to determine whether it could also detect transfected km23, we performed Western blot analysis after subcellular fractionation of the cells. As indicated in Fig. 2B, the anti-Flag Ab could only detect expressed km23-Flag in the cytoplasmic fraction (lane 3, top panel). In contrast, the rabbit km23 anti-serum could detect both endogenous and expressed km23 in the cytoplasmic fraction (lanes 1–3, middle panel). This cytoplasmic localization of km23 is consistent with the fact that km23 does not contain a nuclear localization sequence based upon nuclear localization sequence motifs previously published [24]. As expected, endogenous Lamins A and C were not detectable in the cytoplasmic fraction (lanes 1–3, bottom

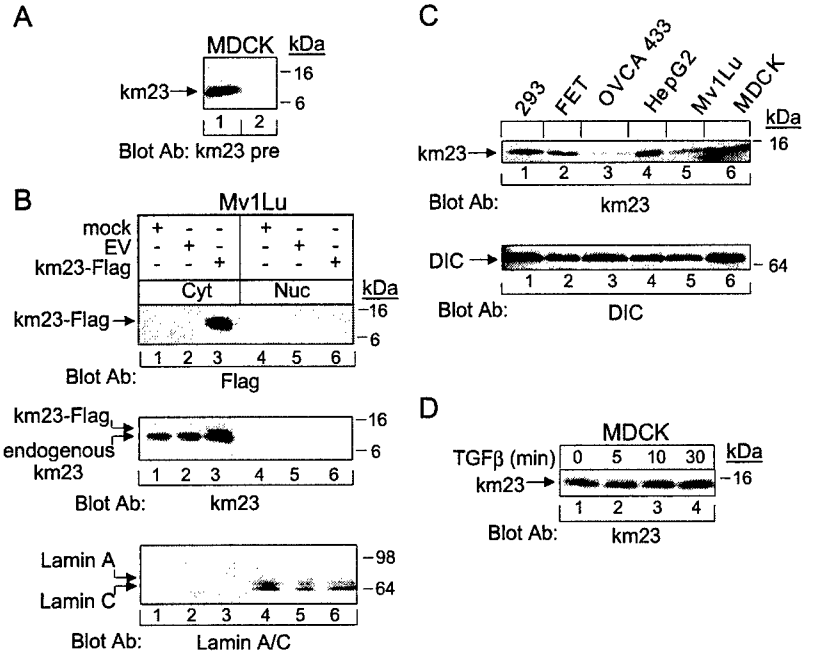

Fig. 2. Development and specificity assessment of a rabbit polyclonal antiserum for detection of km23 protein expression. A: MDCK cell lysates were analyzed by SDS-PAGE (15%) and transferred to a PVDF membrane. The membrane was then incubated with rabbit km23 anti-serum (lane 1), pre-immune rabbit serum as a control (lane 2), respectively, followed by incubation with an anti-rabbit IgG secondary antibody (1:7500) to demonstrate the specificity of the km23 Ab. B: Mv1Lu cells were either mock transfected or transiently transfected with EV or km23-Flag. Twenty-four hours later, cells were then fractionated as described in "Materials and Methods." Top panel, both cytoplasmic and nuclear fractions were subjected to SDS-PAGE (15%), transferred to a PVDF membrane, and blotted with anti-flag Ab. Middle panel, membrane was then reprobed with rabbit km23 anti-serum. Bottom panel, the membrane was then reprobed with anti-lamin A/C Ab as a nuclear marker. C: Top panel, protein lysates (75 μg) were prepared from 293, FET, OVCA 433, HepG2, Mv1Lu, and MDCK cells, and analyzed as in Fig. 3A. Equal loading was confirmed by blotting with a DIC Ab. D: MDCK cell lysates were incubated in serum-free MEM-α medium for 1 h in the absence (lane 1) or presence of (lanes 2–4) TGFβ (10 ng/ml). Lysates were analyzed by SDS-PAGE (15%) and transferred to a PVDF membrane. The membrane was then incubated with rabbit km23 polyclonal anti-serum, followed by incubation with an anti-rabbit IgG secondary antibody (1:7500). The results shown are representative of two similar experiments.

panel). Further, both endogenous and expressed km23 were absent in the nuclear fraction (lanes 4–6, top panel), whereas Lamins A and C were easily detectable in this compartment (lanes 4–6, bottom panel) [25]. The results indicate that km23 is a cytoplasmic protein and that the rabbit anti-serum can specifically recognize both endogenous and expressed km23.

Since we had demonstrated the specificity of our Ab, we could now assess km23 protein expression levels across multiple species. Thus, we examined the relative expression levels of endogenous km23 in several mammalian cell types. As shown in Fig. 2C, our Ab can detect km23 at high levels in HepG2 human hepatoma cells (lane 4, top panel) and in MDCK cells (lane 6, top panel), whereas lower levels were detectable in Mv1Lu mink lung epithelial cells (lane 5, top panel). We also found that km23 was barely detectable in the TGFβ-resistant, human ovarian cancer cell line OVCA 433 (lane 3, top panel), compared with all of the other cell lines. The km23 levels were intermediate in 293 human embryonic kidney cells (lane 1, top panel) and in partially TGFβ–responsive FET human colon cancer cells (lane 2, top panel). Equal loading was confirmed by blotting with a dynein intermediate chain antibody (DIC Ab) (bottom panel), since we have previously determined that DIC levels are relatively constant among such cell lines. Thus, our Ab could detect endogenous km23 across multiple species, and in malignant cells as well.

Since TGFβ often modulates gene expression, it was of interest to determine whether km23 levels were regulated by TGFβ at various times after TGFβ addition to cells. Thus, we performed Western blot analysis using the rabbit km23 anti-serum. As shown in Fig. 2D, equal amounts of km23 were detectable from 5 to 30 min after TGFβ treatment (lanes 1–4). Equal loading was confirmed by blotting with a DIC Ab (data not shown). Thus, TGFβ did not induce the expression of endogenous km23.

The serine/threonine kinase activity of the TGFβ receptors mediates phosphorylation of downstream molecules to affect TGFβ responses. We have previously shown that km23 was phosphorylated by the TGFβ receptor complex in human embryonic kidney 293T cells [15]. Since TGFβ increased the phosphorylation levels of km23, it was of interest to determine whether another growth factor ligand could produce a similar effect. EGF is known to phosphorylate many downstream targets after activation of its receptor [26]. For example, Shc, Src, STATs, PLC-γ and PPARγ [27–30] have all been shown to be phosphorylated within 30 min of EGF treatment. In order to determine whether km23 could be phosphorylated by EGF, we performed in vivo phosphorylation assays after transient expression of km23-Flag, RI-HA, and RII-HA in the absence and presence of TGFβ or EGF. However, as indicated in Fig. 3A (right side), EGF did not stimulate km23 phosphorylation during a treatment period of 0–30 min (lanes 7–9). EGF has been shown to phosphorylate

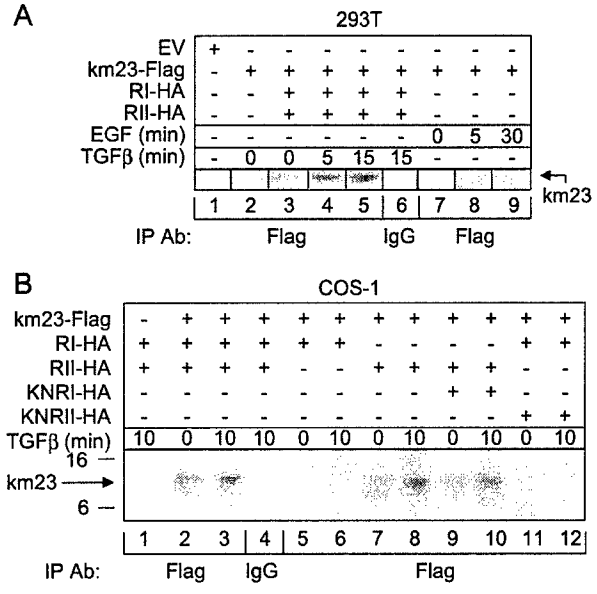

Fig. 3. The kinase activity of both TβRI and TβRII plays a role in the TGFβ–dependent phosphorylation of km23. A: Human embryonic kidney 293T cells were transiently transfected with either EV, km23-Flag, and/or RI-HA and RII-HA as indicated. Twenty-four hours after transfection, cells were labeled for 3 h with [$^{32}P_i$] in the absence or presence of TGFβ (5 ng/ml) (lanes 1–6) or EGF (100 ng/ml) (lanes 7–9) for the indicated times. Thereafter, cells were lysed and immunoprecipitated with anti-Flag. In vivo phosphorylation of km23-Flag was visualized by SDS-PAGE (15%) and autoradiography. B: COS-1 cells were transiently transfected with either EV, km23-Flag, and/or wild-type or mutant TβRI and TβRII as indicated and were analyzed as for A. The results shown are representative of three similar experiments.

other substrates during this time period in this cell line [31]. As expected, km23 was phosphorylated upon co-expression of both types of TGFβ receptors (lane 3). A ligand-dependent increase in km23 phosphorylation was observed at 5 and 15 min after TGFβ treatment (lanes 4 and 5). As shown previously, km23 was not auto-phosphorylated (lane 2), nor was there phosphorylation in the EV (lane 1), or the IgG (lane 6) control lanes. Collectively, our results suggest that km23 phosphorylation may be mediated specifically by TGFβ.

We have also previously shown that the kinase activity of TβRII was required for the phosphorylation of km23 [15]. However, it was unclear whether the kinase activity of TβRI was also required for this phosphorylation event. In order to address the role of the kinase activity of TβRI in the TGFβ-mediated phosphorylation of km23, the in vivo phosphorylation assays in Fig. 3B were performed using either a wild-type or kinase-deficient form of TGFβ RI receptor (KNRI) alone or in combination with TβRII. Co-expression of TβRII with KNRI (lanes 9 and 10) resulted in a reduction in km23 phosphorylation, relative to that observed after expression of both receptors (lanes 2 and 3), or after expression of TβRII alone (lanes 7 and 8). As expected, co-expression of TβRI and TβRII without km23 resulted in no detectable phosphorylation

(lane 1). The IgG control (lane 4) was also negative. Thus, phosphorylation of km23 by TGFβ can occur in the absence of TβRI, but the kinase activity of TβRI does enhance km23 phosphorylation by TβRII to some extent. The mechanism underling the role of TβRI in km23 phosphorylation is the subject of future investigations.

We have previously shown that TβRII kinase activity was required for km23 phosphorylation and interaction with the rest of the dynein motor, and that forced expression of km23 resulted in activation of known TGFβ signaling components and responses [15]. Thus, we suggested that TGFβ signaling components might be the cargo transported by km23. Accordingly, km23 may function as a TGFβ signaling intermediate by assisting with the transport of TGFβ signaling complexes to the appropriate cell locations to mediate TGFβ responses. In order to more definitively establish whether km23 was required for mediating specific TGFβ responses, we utilized siRNA approaches. We examined the effect of blocking km23 expression on two major TGFβ responses, namely growth inhibition and induction of extracellular matrix protein expression.

Since a prominent biological effect of TGFβ in epithelial cells is growth inhibition [1,4,5], we initially examined the effect of siRNA blockade of km23 on TGFβ inhibition of [^{3}H]thymidine incorporation. In order to establish that the km23 siRNA could block endogenous km23 expression, we

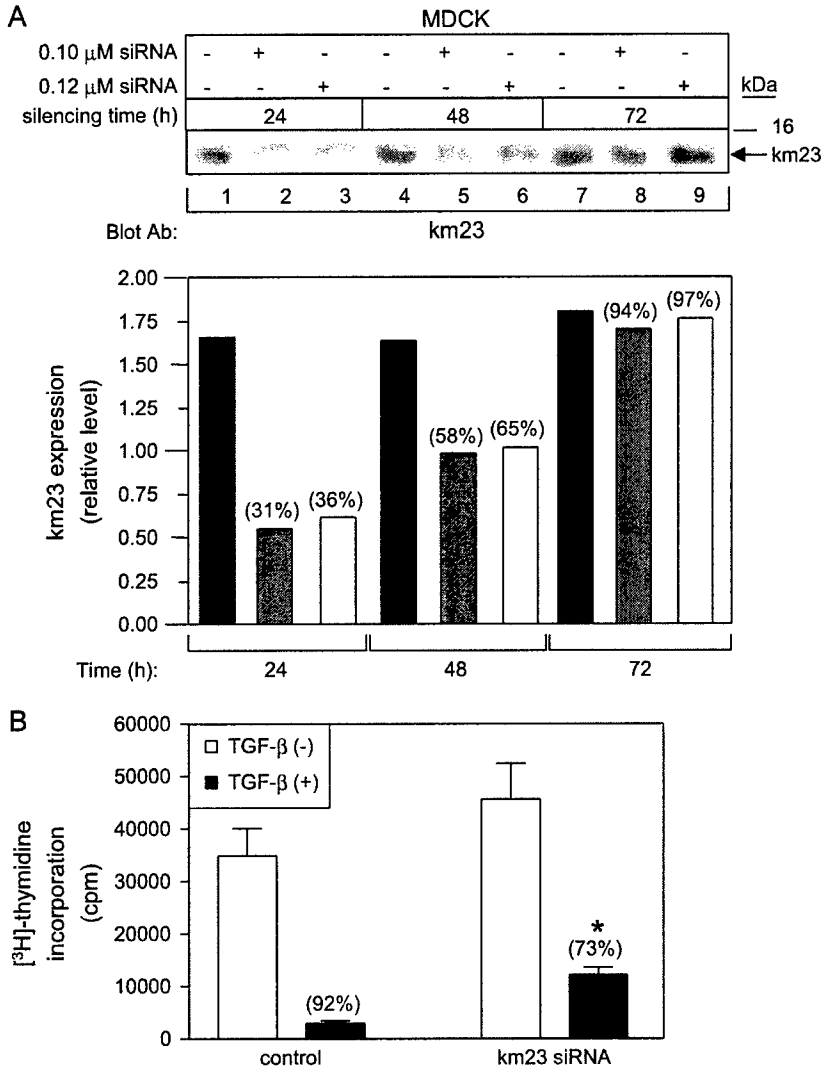

Fig. 4. The siRNA blockade of km23 expression results in a partial loss of the ability of TGFβ to inhibit DNA synthesis. A: Top panel, MDCK cells were transfected with 0.10 μM or 0.12 μM double-stranded siRNA as described in "Materials and Methods." After incubation for 24–72 h, expression levels of endogenous km23 were analyzed via Western blot analysis using rabbit km23 anti-serum (1:500) as described for Fig. 2. Bottom panel, plot of densitometric results from top panel. The values in parentheses indicate a percent of control relative to the corresponding control values. B: MDCK cells were transfected with 0.1 μM siRNA as described in A. Twenty-four hours after transfection, [^{3}H]thymidine incorporation analyses were performed as described in "Materials and Methods." The asterisk indicates a statistically significant difference (Student's t-test, $p < 0.01$) in the inhibition of DNA synthesis by TGFβ between km23 siRNA-transfected and control-transfected MDCK cells.

transfected MDCK cells with the siRNA using Oligofectamine as described in the "Materials and Methods." Western blot analysis was then performed as shown in Fig. 4A. Transfection with either 0.10 μM or 0.12 μM siRNA resulted in a marked decrease (compared to control cells) in km23 levels at both 24 h (lanes 1–3) and 48 h (lanes 4–6) after addition of the siRNA. The decrease in endogenous km23 was maximal at 24 h after transfection of siRNA (lanes 2 and 3, top panel), with a reduction of km23 expression by approximately 65%. The silencing effect was apparent for at least an additional 24 h, and was similar when a slightly higher siRNA concentration was used (0.12 μM; lanes 2, 3, 5, and 6, top panel). After 72 h, there was no difference in endogenous km23 levels between the control and siRNA-transfected cells (lanes 7–9, top panel). The bottom panel of Fig. 4A depicts the results of desitometric scans of the top panel, with the percent of control values provided above the relevant bars.

Since 0.1 μM siRNA resulted in maximal silencing at 24 h after addition to MDCK cultures, we examined TGFβ effects on [^{3}H]thymidine incorpration in MDCK cells in the presence and absence of 0.1 μM siRNA at this time point. The results in Fig. 4B indicate that blockade of endogenous km23 caused a reduction in the ability of TGFβ to inhibit DNA synthesis. While TGFβ inhibited the control cells by 92%, cells transfected with km23 siRNA displayed only a 73% inhibition by TGFβ. This difference was statistically significant ($p<0.01$). Thus, km23 is partially required for the repression of DNA synthesis by TGFβ.

To specifically identify km23 as a mediator of TGFβ-induced growth inhibition, we examined the effect of siRNA blockade of km23 on the cell cycle distribution induced by TGFβ using FACS analysis. Since Mv1Lu cells are extremely sensitive to growth inhibition by TGFβ, and the reduction of cells in the S phase after TGFβ treatment is well documented in these cells [32], we chose Mv1Lu cells for these experiments. In order to demonstrate the ability of km23 siRNA-3 to block km23 expression, we either mock-transfected the cells, or transiently transfected them with either km23-Flag and NC siRNA, or km23-Flag and km23 siRNA-3. Western blotting analysis was then performed as shown in Fig. 5A. No band was detected in the mock-transfected cells as expected (lane 1, top panel). The km23 siRNA-3 totally blocked km23-Flag expression (lane 3, top panel), compared with NC siRNA (lane 2, top panel). Equal protein loading was confirmed by blotting with a DIC Ab (bottom panel).

Since we have shown that km23 siRNA-3 could specifically knockdown km23 in Mv1Lu cells, we transiently transfected Mv1Lu cells with either NC siRNA and km23-Flag or km23 siRNA-3 and km23-Flag, and then performed FACS analysis as described in the "Materials and Methods." The cell cycle distribution in the absence and presence of TGFβ is shown in Fig. 5B. In cells co-transfected with NC siRNA and km23-Flag (top panel),

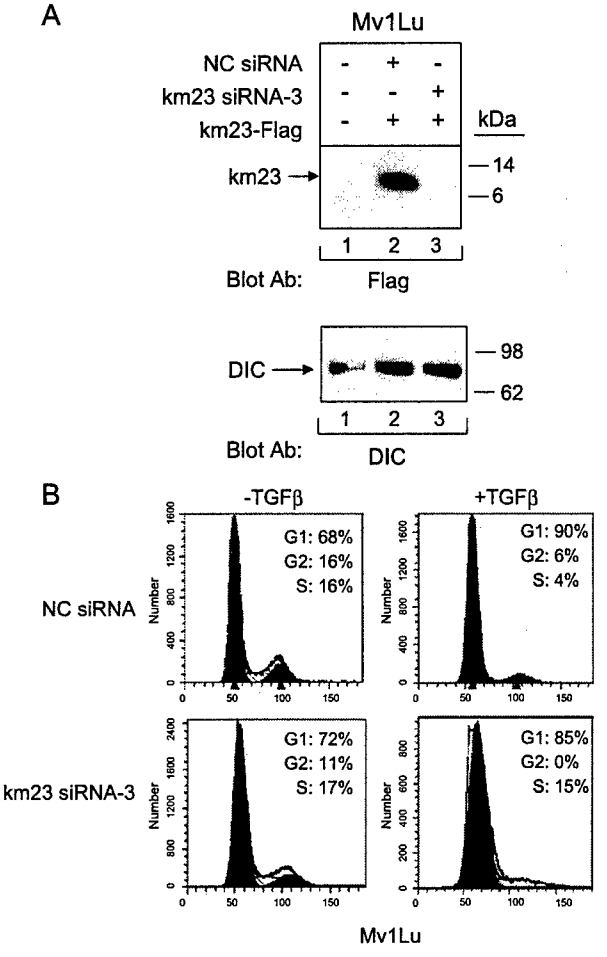

Fig. 5. The siRNA blockade of km23 expression results in a partial loss of the ability of TGFβ to inhibit cell cycle progression. A: Mv1Lu cells were either mock-transfected (lane 1), or transiently transfected km23-Flag and NC siRNA (lane 2), or km23-Flag and km23 siRNA-3 (lane 3). Top panel, blockade of km23-Flag was analyzed via Western blotting with an anti-Flag M2 Ab (1:1000). Bottom panel, equal loading was confirmed by blotting with an anti-DIC Ab. B: km23 siRNA-3 or NC siRNA was co-transfected with km23-Flag into Mv1Lu cells. Twenty-four hours after transfection of plasmids, Mv1Lu cells were incubated in serum-free medium for 60 min before addition of TGFβ (5 ng/ml) for additional 24 h. FACS analysis was then performed as described in the "Materials and Methods." The results shown are representative of two similar experiments.

exposure to TGFβ resulted in an increase in the percentage of cells in the G1 phase of the cell cycle (90%) and a decrease in the percentage of cells in S phase (4%), compared to the same cells in the absence of TGFβ (G1: 68%; S: 16%). This result is consistent with a previous report by another group [32]. However, in cells co-transfected with km23 siRNA-3 and km23-Flag (bottom panel), TGFβ displayed little effect on the percentage of cells in the G1 (85%) or S (15%) phases of the cell cycle, compared with cells left untreated (G1: 72%; S: 17%). Together, these results suggest that blockade of km23 expression results in a reduction in the ability of TGFβ to inhibit cell growth.

TGFβ has been shown to potently induce fibronectin expression at both the mRNA and protein levels [33,34]. In addition, Hocevar et al. [13] have shown that the JNK pathway is required for the induction of fibronectin by TGFβ. We have previously shown that over-expression of km23 could induce JNK activation and result in phosphorylation of the downstream target c-Jun [15], suggesting that km23 regulates the JNK pathway and may contribute to fibronectin induction in some manner. Thus, it was of interest to determine whether blockade of km23 would also decrease TGFβ induction of fibronectin expression. Therefore, we transiently transfected MDCK cells with km23 siRNA-1 or km23 siRNA-2 as described in the "Materials and Methods" and performed Western blot analysis to examine fibronectin induction by TGFβ. As shown in Fig. 6A, both km23 siRNA-1 and km23 siRNA-2 resulted in a marked decrease in endogenous km23 levels (lanes 2 and 3, top panel) compared to control (lane 1, top panel). Equal protein loading was confirmed by blotting with a DIC Ab (bottom panel). Fig. 6B indicates that, as expected, TGFβ induced fibronectin expression in the controls (lanes 1 and 2, top panel). In contrast, both km23 siRNAs resulted in a decrease in the ability of TGFβ to induce fibronectin expression, both in the absence and presence of TGFβ (lanes 3–6, top panel). Blockade of endogenous km23 was confirmed by blotting with km23 anti-serum (bottom panel). Thus, km23 siRNA can block fibronectin induction by both autocrine and exogenous TGFβ. These results suggest that km23 is required for TGFβ induction of fibronectin expression.

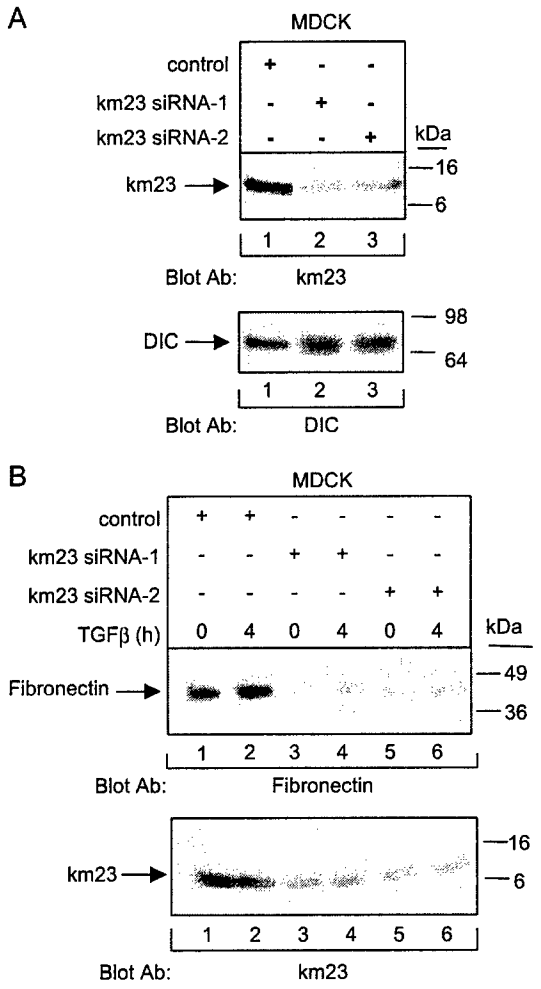

Fig. 6. The siRNA blockade of km23 expression reduces TGFβ induction of fibronectin expression. A: MDCK cells were transiently transfected with the siRNA plasmids indicated: control (lane 1), km23 siRNA-1 (lane 2), km23 siRNA-2 (lane 3). Top panel, blockade of endogenous km23 was analyzed via Western blotting with rabbit km23 anti-serum (1 : 500). Bottom panel, equal loading was confirmed by blotting with an anti-DIC Ab. B: MDCK cells were transiently transfected with siRNA plasmids as indicated: control (lanes 1–2), km23 siRNA-1 (lanes 3–4), km23 siRNA-2 (lanes 5–6). Twenty-four hours after transfection, MDCK cells were incubated in serum-free medium for 60 min before addition of TGFβ (5 ng/ml) for the indicated times. Top panel, fibronectin expression was detected by Western blot analysis using a mouse monoclonal anti-fibronectin Ab. Bottom panel, blockade of km23 was confirmed by blotting with rabbit km23 anti-serum. The results shown are representative of two similar experiments.

4. Discussion

We have isolated km23 via its ability to interact with the intracellular portions of the TGFβ receptors, and have shown that this protein is also a light chain of the motor protein dynein [15]. Further, we have demonstrated that this TGFβ receptor-interacting protein is associated with the TGFβ receptor complex through TβRII, and that its expression can mediate some of the biological responses of TGFβ. In the current report, we show that although the kinase activity of TβRII is absolutely required for km23 phosphorylation, the kinase activity of TβRI is also involved. Further, km23 phosphorylation appeared to be induced specifically by TGFβ, since EGF was unable to alter the phosphorylation status of km23. More importantly, we demonstrate for the first time, using siRNA approaches, that km23 is required for TGFβ induction of fibronectin expression and that it is necessary, but not sufficient, for growth inhibition by TGFβ. Thus, our results support an important role for km23 in TGFβ signaling.

The partial requirement of km23 for TGFβ-mediated inhibition of DNA synthesis and cell cycle progression is not an unexpected finding, as other pathway components are known to be involved in mediating this complex biological response. For example, TGFβ activation of Ras is also partially required for TGFβ-mediated growth inhibition, and for some of the cell cycle effects that mediate this response [35–37]. TGFβ activation of extracellular signal-regulated kinases (Erks) and of stress-activated protein kinases/Jun N-terminal kinases (SAPK/JNKs) was also found to be required for negative growth control by TGFβ [7,18,38]. Further, over-expression of the p65 subunit of the NF-κB/Rel family in Hs578

T cells abrogated the ability of TGFβ to inhibit cell growth [39], suggesting that TGFβ regulation of NF-κB/Rel activity is also associated with TGFβ-mediated growth inhibition. Thus, several TGFβ-regulated components appear to be required for mediating the growth inhibitory response to TGFβ. The km23 may represent a novel member of this group of signaling components.

As mentioned above, we have demonstrated herein that silencing of km23 resulted in a blockade of the ability of TGFβ to mediate another major TGFβ response, namely induction of fibronectin expression. The induction of fibronectin by TGFβ was previously shown to be mediated by an activation of JNK and was Smad4-independent [13]. In addition, we have previously shown that stable expression of km23 resulted in a super-activation of JNK, as well as an increase in the phosphorylation of the downstream JNK target c-Jun, suggesting that km23 was involved in the activation of JNK by TGFβ [15]. Thus, our novel findings here are in keeping with our previous results, and the results of others, and suggest that km23 may function as a signaling intermediate for the TGFβ induction of fibronectin expression, possibly via the JNK pathway.

In summary, we have provided the following evidence to indicate that km23 is an important TGFβ signal transducer. First, we have shown that TGFβ, but not EGF, can induce phosphorylation of km23 in a ligand-dependent fashion. Second, our data indicate that the kinase activity of both TGFβ receptors plays a role in phosphorylation, although the TβRII kinase activity is obligatory. Third, siRNA blockade of km23 expression resulted in a partial loss of the ability of TGFβ to inhibit cell cycle progression, as indicated by the partial reversal of TGFβ-mediated repression of DNA synthesis and the decrease in the fraction of cells in the S phase after TGFβ treatment. Fourth, siRNA blockade of km23 expression blocked the ability of TGFβ to induce the extracellular matrix protein fibronectin. Our results also reveal that km23 is a highly conserved, ubiquitously-expressed, cytoplasmic protein, which can be detected in several species and cell types, in keeping with the ubiquitous and multifunctional nature of TGFβ. Future studies will unravel the precise signaling pathways and mechanisms involved in the km23-mediated TGFβ responses examined herein.

Acknowledgments

We specially thank Nate Sheaffer (the Cell Science/Flow Cytometry Core Facility of the Section of Research Resources, Penn State College of Medicine) for FACS technical support. We thank J. Massague (Memorial Sloan–Kettering Cancer Center, New York, NY) for KNRI-HA, KNRII-HA and pCMV5-HA-TbRII; J. Wrana (Samuel Lunenfeld Research Institute, Toronto, Canada) for pCMV5-HA-TbRI; H. Moses (Vanderbilt) for the T204D-HA. We also thank R.C. Bast Jr. (M.D. Anderson Cancer Center, Houston, TX) for the OVCA 433 cells and T-W. Wong (Bristol–Myers Squibb, Princeton, NJ) for the 293T cells. This work was supported by National Institutes of Health Grants CA90765, CA92889, and CA100239, and Dept of Defense IDEA AWAD # DAMD17-03-1-0287 (to K.M.M).

References

[1] J. Yue, K.M. Mulder, Pharmacol. Ther. 91 (2001) 1.
[2] R. Derynck, Y.E. Zhang, Nature 425 (2003) 577.
[3] Y.G. Shi, J. Massague, Cell 113 (2003) 685.
[4] R.J. Akhurst, R. Derynck, Trends Cell Biol. 11 (2001) S44.
[5] A.B. Roberts, L.M. Wakefield, Proc. Natl. Acad. Sci. U. S. A. 100 (2003) 8621.
[6] A. Mehra, J.L. Wrana, Biochem. Cell. Biol. 80 (2002) 605.
[7] K.M. Mulder, Cytokine Growth Factor Rev. 11 (2000) 23.
[8] P. ten Dijke, M.J. Goumans, F. Itoh, S. Itoh, J. Cell. Physiol. 191 (2002) 1.
[9] E.H.J. Danen, K.M. Yamada, J. Cell. Physiol. 189 (2001) 1.
[10] R. Pankov, K.M. Yamada, J. Cell Sci. 115 (2002) 3861.
[11] J. Massague, S.W. Blain, R.S. Lo, Cell 103 (2000) 295.
[12] A.B. Roberts, A. Russo, A. Felici, K.C. Flanders, Ann. N. Y. Acad. Sci. 995 (2003) 1.
[13] B.A. Hocevar, T.L. Brown, P.H. Howe, EMBO J. 18 (1999) 1345.
[14] J.L. Gooch, Y. Gorin, B.X. Zhang, H.E. Abboud, J. Biol. Chem. 279 (2004) 15561.
[15] Q. Tang, C.M. Staub, G. Gao, Q. Jin, Z. Wang, W. Ding, R.E. Aurigemma, K.M. Mulder, Mol. Biol. Cell 13 (2002) 4484.
[16] P.A. Zipfel, B.L. Ziober, S.L. Morris, K.M. Mulder, Cell Growth Differ. 4 (1993) 637.
[17] J. Yue, R.S. Frey, K.M. Mulder, Oncogene 18 (1999) 2033.
[18] J. Yue, M.T. Hartsough, R.S. Frey, T. Frielle, K.M. Mulder, J. Cell. Physiol. 178 (1999) 387.
[19] J. Yue, K.M. Mulder, J. Biol. Chem. 275 (2000) 30765.
[20] M.T. Hartsough, K.M. Mulder, J. Biol. Chem. 270 (1995) 7117.
[21] I. Hoffmann, G. Draetta, E. Karsenti, EMBO J. 13 (1994) 4302.
[22] V. Dole, C.R. Jakubzik, B. Brunjes, G. Kreimer, Biochim. Biophys. Acta 1490 (2000) 125.
[23] N.S. Akopyants, S.W. Clifton, J. Martin, D. Pape, T. Wylie, L. Li, J.C. Kissinger, D.S. Roos, S.M. Beverley, Mol. Biochem. Parasitol. 113 (2001) 337.
[24] I.W. Mattaj, L. Englmeier, Annu. Rev. Biochem. 67 (1998) 265.
[25] S.D. Georgatos, J. Meier, G. Simos, Curr. Opin. Cell Biol. 6 (1994) 347.
[26] R.N. Jorissen, F. Walker, N. Pouliot, T.P.J. Garrett, C.W. Ward, A.W. Burgess, Exp. Cell Res. 284 (2003) 31.
[27] K. Sakaguchi, Y. Okabayashi, Y. Kido, S. Kimura, Y. Matsumura, K. Inushima, M. Kasuga, Mol. Endocrinol. 12 (1998) 536.
[28] W. Mao, R. Irby, D. Coppola, L. Fu, M. Wloch, J. Turner, H. Yu, R. Garcia, R. Jove, T.J. Yeatman, Oncogene 15 (1997) 3083.
[29] M. David, L. Wong, R. Flavell, S.A. Thompson, A. Wells, A.C. Larner, G.R. Johnson, J. Biol. Chem. 271 (1996) 9185.
[30] M.I. Wahl, S. Nishibe, J.W. Kim, H. Kim, S.G. Rhee, G. Carpenter, J. Biol. Chem. 265 (1990) 3944.
[31] H.S. Camp, S.R. Tafuri, J. Biol. Chem. 272 (1997) 10811.
[32] M. Laiho, J.A. DeCaprio, J.W. Ludlow, D.M. Livingston, J. Massague, Cell 62 (1990) 175.

[33] R.A. Ignotz, J. Massague, J. Biol. Chem. 261 (1986) 4337.
[34] J.L. Wrana, C.M. Overall, J. Sodek, Eur. J. Biochem. 197 (1991) 519.
[35] K.M. Mulder, S.L. Morris, J. Biol. Chem. 267 (1992) 5029.
[36] M.T. Hartsough, R.S. Frey, P.A. Zipfel, A. Buard, S.J. Cook, F. McCormick, K.M. Mulder, J. Biol. Chem. 271 (1996) 22368.
[37] J. Yue, A. Buard, K.M. Mulder, Oncogene 17 (1998) 47.
[38] R.S. Frey, K.M. Mulder, Cancer Res. 57 (1997) 628.
[39] M.A. Sovak, M. Arsura, G. Zanieski, K.T. Kavanagh, G.E. Sonenshein, Cell Growth Differ. 10 (1999) 537.

A Transforming Growth Factor-β Receptor–Interacting Protein Frequently Mutated in Human Ovarian Cancer

Wei Ding,[1] Qian Tang,[1] Virginia Espina,[3] Lance A. Liotta,[3] David T. Mauger,[2] and Kathleen M. Mulder[1]

Departments of [1]Pharmacology and [2]Health Evaluation Sciences, Pennsylvania State University College of Medicine, Hershey, Pennsylvania and [3]National Cancer Institute Clinical Proteomics Program, Laboratory of Pathology, Center for Cancer Research, National Cancer Institute, Bethesda, Maryland

Abstract

Ovarian carcinomas, particularly recurrent forms, are frequently resistant to transforming growth factor-β (TGF-β)–mediated growth inhibition. However, mutations in the TGF-β receptor I and receptor II (*TβR-I* and *TβR-II*) genes have only been reported in a minority of ovarian carcinomas, suggesting that alterations in TGF-β–signaling components may play an important role in the loss of TGF-β responsiveness. Using laser-capture microdissection and nested reverse-transcription-PCR, we found that km23, which interacts with the TGF-β receptor complex, is altered at a high frequency in human ovarian cancer patients. A novel form of *km23*, missing exon 3 (*Δexon3-km23*), was found in 2 of 19 tumor tissues from patients with ovarian cancer. In addition to this alteration, a stop codon mutation (TAA → CAC) was detected in two patients. This alteration results in an elongated protein, encoding 107-amino-acid residues (Δ107km23), instead of the wild-type 96-amino-acid form of km23. Furthermore, five missense mutations (T38I, S55G, T56S, I89V, and V90A) were detected in four patients, providing a total alteration rate of 42.1% (8 of 19 cases) in ovarian cancer. No *km23* alterations were detected in 15 normal tissues. Such a high alteration rate in ovarian cancer suggests that km23 may play an important role in either TGF-β resistance or tumor progression in this disease. In keeping with these findings, the functional studies described herein indicate that both the Δexon3-km23 and S55G/I89V-km23 mutants displayed a disruption in binding to the dynein intermediate chain *in vivo*, suggesting a defect in cargo recruitment to the dynein motor complex. In addition, the Δexon3-km23 resulted in an inhibition of TGF-β–dependent transcriptional activation of both the p3TP-lux and activin responsive element reporters. Collectively, our results suggest that km23 alterations found in ovarian cancer patients result in altered dynein motor complex formation and/or aberrant transcriptional regulation by TGF-β. (Cancer Res 2005; 65(15): 6526-33)

Introduction

Epithelial ovarian cancer is often diagnosed at an advanced stage and is the leading cause of death from gynecologic neoplasia, accounting for >14,300 deaths per year (1). Despite advances in surgical approaches and chemotherapeutic agents, the overall survival rates for women with this cancer have not improved significantly because the majority of women are diagnosed with ovarian cancer at an advanced stage, when it has already metastasized to remote organs (1, 2).

Overall, the molecular changes that underlie the initiation and development of this tumor are poorly understood. It has been reported that >75% of ovarian carcinomas are resistant to transforming growth factor-β (TGF-β), particularly recurrent ones (3, 4). The loss of TGF-β responsiveness may play an important role in the pathogenesis and/or progression of ovarian cancer. It has been shown that *TGF-β*$_1$, the TGF-β receptors (*TβR-II* and *TβR-I*), and the TGF-β-signaling component *Smad2* are altered in ovarian cancer (5–8). Alterations in *TβR-II* have been identified in 25% of ovarian carcinomas (5), whereas mutations in *TβR-I* were reported in 33% of such cancers (6). Loss of function mutations of TGF-β1, TβR-I, and TβR-II can lead to disruption of TGF-β-signaling pathways and subsequent loss of cell cycle control (5–7). However, these alterations only account for a minority of TGF-β-resistant ovarian carcinomas, suggesting that other alterations in TGF-β-signaling components may be involved in the pathogenesis of this type of cancer.

Recently, we have identified a novel TGF-β-signaling component, termed km23, which is also a light chain of the motor protein dynein (9). Our previous studies have shown that is a TβRII-interacting protein that can be phosphorylated on serine residues after TGF-β binding (9). Forced expression of km23 induced specific TGF-β responses, including c-jun NH_2-terminal kinase (JNK) activation, c-Jun phosphorylation, and cell growth inhibition (9). Furthermore, TGF-β induced the recruitment of km23 to the dynein intermediate chain (DIC). A kinase-deficient form of TGF-β RII prevented both km23 phosphorylation and interaction with DIC (9). From these studies, we have proposed a model for km23 function, whereby the binding of km23 to the DIC after TGF-β receptor activation is important for specifying the nature of the cargo (i.e., TGF-β-signaling components) that will be transported along the microtubules (9, 10). In keeping with this model, any disruption of the binding of km23 to the DIC should disrupt cargo binding and subsequent TGF-β signaling. In this way, km23 may not only be an important component in TGF-β signaling, but any alterations in km23 sequence may contribute to dysregulated TGF-β signaling.

Here, we report the analysis of sequence alterations in human *km23* in epithelial ovarian cancer tissues using laser-capture microdissection (LCM) and nested reverse-transcription-PCR (RT-PCR) approaches. We found a high incidence (42.1%) of *km23* mutations in human ovarian carcinomas, whereas normal tissues did not contain such alterations ($P < 0.005$). This is the first

Note: Q. Tang is currently at the Lexicon Genetics, Inc., 8800 Technology Forest Place, The Woodlands, TX 77381. V. Espina and L. A. Liotta are currently at George Mason University, Department of Molecular and Microbiology, Center for Applied Proteomics and Molecular Medicine, Manassas, VA.

Requests for reprints: Kathleen M. Mulder, Department of Pharmacology-MC H078, Pennsylvania State College of Medicine, 500 University Drive, Hershey, PA 17033. Phone: 717-531-6789; Fax: 717-531-5013; E-mail: kmm15@psu.edu.

©2005 American Association for Cancer Research.

report of alterations in a cytoplasmic dynein light chain (DLC) in epithelial ovarian cancer. Furthermore, we found that both the Δexon3-km23 and S55G/I89V-km23 mutants resulted in a disrupted interaction with the DIC. The Δexon3-km23 mutant form of km23 also inhibited TGF-β-dependent activation of both p3TP-lux and ARE-lux transcription. In addition, two phosphorylation site mutants, S32A-km23 and S73A-km23, disrupted the interaction with DIC. Overall, our results show that altered forms of this novel TGF-β-signaling component found in ovarian cancer patients can result in altered dynein motor interactions and/or altered regulation of TGF-β-dependent gene transcription.

Materials and Methods

Cell cultures. 293T cells and Mink lung epithelial cells CCL-64 (Mv1Lu) were purchased from American Type Culture Collection (Rockville, MD). 293T and Mv1Lu cells were cultured in DMEM with glutamine. All medium was supplemented with 10% heat-inactivated fetal bovine serum. Cells were maintained in 5% CO_2 at 37°C. Cultures were routinely screened for *Mycoplasma* using Hoechst staining.

Ovarian tissues. Nineteen ovarian carcinoma tissues and 12 normal ovarian tissues were provided by Cooperative Human Tissue Network (Eastern division, Philadelphia, PA and Midwestern division, Columbus, OH). Tissues were obtained within 1 hour of surgery, snap frozen, sent on dry ice, and stored at −80°C before use. The Institutional Review Board approval for this study was received from the Penn State College of Medicine (Hershey, PA).

H&E staining. Sections of frozen tissues (10 μm) were mounted on slides (SL Microtest, Jena, Germany). H&E staining was done as described by Goldsworthy et al. (11). All reagents for H&E staining were prepared with diethyl-pyrocarbonate–treated distilled water.

Laser-capture microdissection. LCM was done using a μCut Laser Microdissection system (SL Microtest) according to the manufacturer's instructions. After microdissection of each specimen, the thermoplastic film-coated cap containing the captured tissue was placed in a 0.5-mL microtube.

RNA isolation. Total RNA was isolated from normal ovarian tissues using TRIzol reagent according to the manufacturer's protocol (Invitrogen, Life technologies, Carlsbad, CA). Total RNA was isolated from tissues subjected to LCM using a Total RNA Microprep Kit (Stratagene, La Jolla, CA) according to the manufacturer's recommendations.

Nested reverse-transcription-PCR and DNA sequencing. cDNA synthesis was done using Sensicript Reverse Transcriptase (Qiagen, Valencia, CA), according to the manufacturer's protocol. Nested PCR was done using two pairs of primers spanning the whole open reading frame of *km23*. The forward primer for the first round of PCR was 5′-GTTTTGACAGAAACCTTTGCG-3′ and the reverse primer was 5′-TTGGTGCACACAGGGGTTC-3′. The conditions used for the first round of PCR were 30 cycles at 94°C for 50 seconds, at 54°C for 50 seconds, and at 72°C for 1 minute. The second round of PCR was done using the first round of PCR products as a reaction template (forward primer, 5′-ACTCGCTAAGTGTTCGCTACG-3′; reverse primer, 5′-TGCCATGTGCTAGTCCACTGA-3′), with the following conditions: 33 cycles at 94°C for 50 seconds, at 62°C for 50 seconds, and at 72°C for 1 minute. All PCR assays were done using recombinant Pfu polymerase with 3′ to 5′ exonuclease activity (Stratagene). The PCR products were electrophoresed on 2% agarose gels, visualized with ethidium bromide staining, and purified using a QIAquick Gel Extraction Kit (Qiagen). DNA sequencing was done in both directions using the primers for the second round of PCR.

DNA constructs. Flag-tagged wt-km23, Δexon3-km23, and S55G/I89V-km23 constructs were generated by inserting the corresponding PCR products into pFlag-CMV5a vector (Sigma-Aldrich, St. Louis, MO) after digestion with *Bgl*II and *Sal*I restriction enzymes. The Flag-tagged S32A-km23, S55A-km23, and S73A-km23 constructs were produced using the QuikChange Site-Directed Mutagenesis Kit (Stratagene) following the manufacturer's protocols.

Immunoprecipitation/immunoblotting. 293T cells were transiently transfected with the indicated Flag-tagged forms of km23. Twenty-four hours after transfection, cells were harvested using radioimmunoprecipitation assay buffer (1× PBS, 1% NP40, 0.5% sodium deoxycholate, and 0.1% SDS) supplemented with protease inhibitor cocktail (Roche Applied Science, Indianapolis, IN). Immunoprecipitation/blot assays were done as described previously (9, 12). The anti-DIC antibody for immunoprecipitation analyses was purchased from Chemicon (Temecula, CA), and the anti-Flag antibody for immunoblot analysis was purchased from Sigma-Aldrich.

Luciferase reporter assays. TGF-β-dependent p3TP-lux and ARE-lux reporter assays were done in Mv1Lu cells. Mv1Lu cells were cotransfected either with p3TP-lux (13) or ARE-Lux (along with forkhead activin signal transducer-1, FAST-1; ref. 14), and the indicated amounts of either wild-type (wt) km23 or Δexon3-km23. The reporter assays were done as described previously (15). All assays were done in triplicate.

Statistics. The statistical difference in alteration rate between the ovarian carcinoma tissues and the tumor-free ovarian tissue groups was calculated using Fisher's exact test.

Phosphorylation site prediction. Phosphorylation site prediction for km23 was done using PROSITE[4] and NetPhos 2.0 Server (16).[5]

Results

A truncated form of *km23*, missing exon 3 (*Δexon3-km23*), was detected in 2 of 19 ovarian carcinoma tissues. Because alterations in TGF-β-signaling components and pathways have been reported in several types of human cancers (17, 18), including epithelial ovarian cancer (5–8), it was of interest to investigate whether km23, a novel TGF-β receptor-interacting protein, was altered in ovarian cancer patients. To examine whether sequence alterations in *km23* existed in ovarian cancer patients, we developed a novel approach to detect *km23* mutations using two microscale technologies. First, LCM was done on ovarian cancer tissues from patients to separate epithelial tumor cells from adjacent tumor-free normal cells. Nested RT-PCR and DNA sequencing were then done to analyze *km23* sequence alterations in the RNA isolated from the tissues subjected to LCM. Using these two microscale technologies, we amplified a PCR fragment of 424 bp in 19 ovarian cancer tissues from patients, using forward and reverse primers located in the 5′-untranslated region (UTR) and 3′-UTR regions, respectively. This 424-bp fragment spans the entire coding region of human *km23*. As shown in Fig. 1*A*, a smaller band of 256 bp, in addition to the 424-bp product, was detectable by agarose gel electrophoresis in 2 of 19 tumor tissues (cases 3 and 8). DNA sequencing indicated that this short fragment is a truncated form of *km23* (*Δexon3-km23*). It is missing exon 3 and contains only 123 nucleotides, as opposed to the 291 nucleotides in the coding region of wt-km23. In case 8, we also analyzed the *km23* sequence in tumor-free stromal cells and found no alterations in km23.

To illustrate the important sites that would be lost in the *Δexon3-km23* mutant, a schematic of the human *km23* sequence is depicted in Fig. 1*B*. km23 consists of four exons encoding 96 amino acids. Among these exons, exon 3 is the largest and encodes a region from amino acids 27 to 82 (shown by underline). From the sequencing results for *Δexon3-km23* mutant, the predicted size for Δexon3-km23 is 40 amino acids. Because the 56 amino acids in exon 3 are missing, this large truncation of the km23 protein is likely to cause significant alterations in km23 function.

[4] http://us.expasy.org/prosite
[5] http://www.cbs.dtu.dk/services/NetPhos/

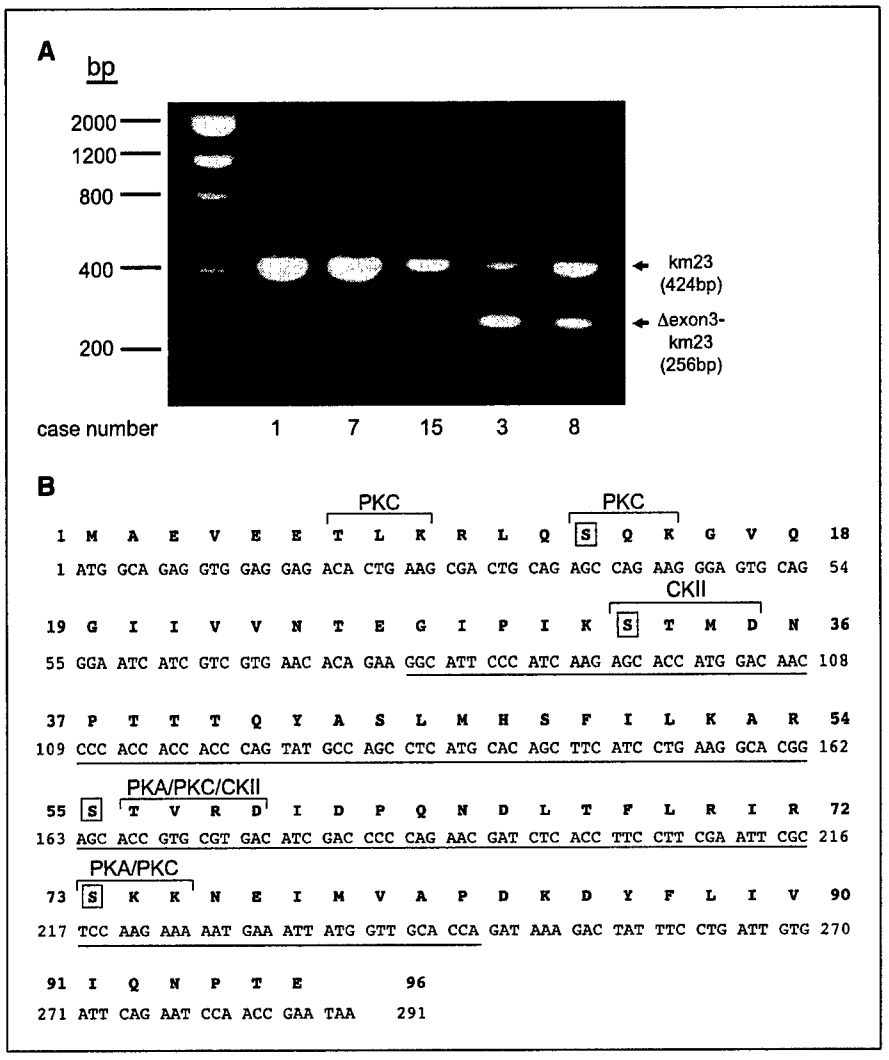

Figure 1. *A*, detection of a truncated form of *km23* (*Δexon3-km23*) in 2 of 19 ovarian carcinoma tissues. Agarose electrophoresis (2%) of nested RT-PCR products. In addition to a 424-bp fragment, which corresponds to the *wt-km23*, a truncated form of *km23* (*Δexon3-km23*, 256 bp) was detected in two patients (cases 3 and 8). This short fragment was not present in the other tumor samples (cases 1, 7, and 15). *B*, schematic of human *km23* sequence depicting exon 3 and potential phosphorylation sites. *wt-km23* consists of four exons. Among them, exon 3 is the largest and encodes a region of 56 amino acids (*underlined*). The predicted size for the Δexon3-km23 mutant is 40 amino acids. Potential phosphorylation sites for PKA, PKC, and/or CKII were predicted using NetPhos 2.0 Server and PROSITE (16). Four serine residues that are conserved among the mammalian km23 forms are boxed. Among them, three are located in exon 3.

To determine whether exon 3 of km23 contains any important functional domains, we also did phosphorylation site prediction analysis using NetPhos 2.0 Server (16) and PROSITE. As shown in Fig. 1*B*, there are several potential phosphorylation sites for protein kinase A (PKA), protein kinase C (PKC), and/or casein kinase II (CKII) in km23. For these sites, the prediction scores for serine and threonine were all over 0.91, indicating that the probability of these sites being true phosphorylation sites is quite high (16). In addition, there are four serine residues that may potentially be phosphorylated and are conserved among the mammalian km23 forms (shown by boxes). Among these, three are located in exon 3. Thus, the Δexon3-km23 mutant may have defective phosphorylation reactions as well.

Six missense mutations in *km23* were detected in 31.6% of epithelial ovarian carcinoma tissues. In addition to the above-mentioned findings, we obtained six missense mutations in *km23* in six patients (Table 1). In case 1, the 163rd nucleotide of the coding region was changed from an adenine to a guanine (A → G). As shown in Fig. 2*A*, this alteration corresponds to an amino acid change from a serine to a glycine (S55G). Also in this patient, the 265th nucleotide of the coding region was altered from an adenine to a guanine (A → G), corresponding to an amino acid change in residue 89 of km23 from an isoleucine to a valine (I89V; Fig. 2*A*). Furthermore, in two other cases (cases 4 and 14), the stop codon of *km23* was altered from TAA to CAC, as shown in Fig. 2*B*. This alteration results in a larger protein, encoding 107-amino-acid residues, instead of the wt 96-amino-acid form of km23. In addition to these alterations, the three other missense mutations detected in three other patients (cases 7, 15, and 18) were T38I, T56S, and V90A (Table 1). Because these alterations were detected in RNA, the possibility exists that not all these alterations are genomic mutations.

Table 1 also compares the clinical characteristics of eight patients with *km23* alterations, summarizing the age of onset, histology, and stage and grade of the tumor. In these cases, only one patient was diagnosed at stage I (case 7), and two other patients were diagnosed at stage II (cases 3 and 15). Five other patients were diagnosed at a later stage (stage IIIA-IV). In addition, most of the tumors from these eight patients were moderately or poorly differentiated (Table 1). This sample population is representative of the general population, in that most ovarian cancer patients are diagnosed at a later stage of tumor progression.

No similar alterations in *km23* were detectable in normal tissues. It was of interest to determine whether the *km23* alterations found in the malignant tissues were also present in

Table 1. Clinical characteristics of eight ovarian carcinomas with *km23* alterations from 19 patients

Case no.	Age (y)	Histology*	Stage/grade†	Mutations
1	58	Serous	IIIA/2	S55G, I89V
3	51	Serous	IIB/2	exon 3 missing
4	48	Serous	IIIA/2	elongated km23 107aa
7	49	Serous	IC/2	T56S
8	72	Serous	IIIC/2-3	exon 3 missing
14	57	Endometrioid	IV/3	elongated km23 107aa
15	47	Endometrioid	IIA/2	T38I
18	57	Metastatic ovarian cancer	IV/–	V90A

*Serous, serous cystadenocarcinoma; endometrioid, endometrioid adenocarcinoma.
†Stage and grade classified according to the criteria standardized by the International Federation of Gynecology and Obstetrics. –, not available.

normal ovarian tissues. Thus, we analyzed 12 normal ovarian samples, as well as three tumor-free stroma samples (procured from cases 8, 9, and 11 by LCM), using the nested PCR strategy. In all 15 normal samples, the *km23* sequence was not altered. Our findings show a statistically significant difference in the *km23* alteration rate between cancer and noncancer groups (42.1% versus 0%; $P < 0.005$, Fisher's exact test, Table 2). Thus, the *km23* alterations we have observed are specific to the malignant cells.

Δexon3-km23 disrupted the interaction with dynein intermediate chain. Because the major function of DLCs such as km23 is to bind to the DIC (9, 19, 20), it was of interest to determine whether km23 mutants could still interact with DIC. Immunoprecipitation/blot analyses were done in 293T cells transfected with Flag-tagged versions of either wt-km23 or Δexon3-km23. As shown in Fig. 3, compared with the wt-km23 (*lane 3*), the interaction of Δexon3-km23 (*lane 4*) with the DIC was disrupted. No interactions were detectable in lysates from cells expressing only the empty vector or when using normal mouse IgG as the immunoprecipitation antibody (*lanes 1* and *2*). The expression and inputs of the Flag-tagged proteins used for the immunoprecipitation reaction were verified by Western blotting as shown in Fig. 3 (*bottom*). Thus, the Δexon3-km23 mutant we identified in the ovarian cancer patients prevent the association of km23 with the rest of the dynein motor complex.

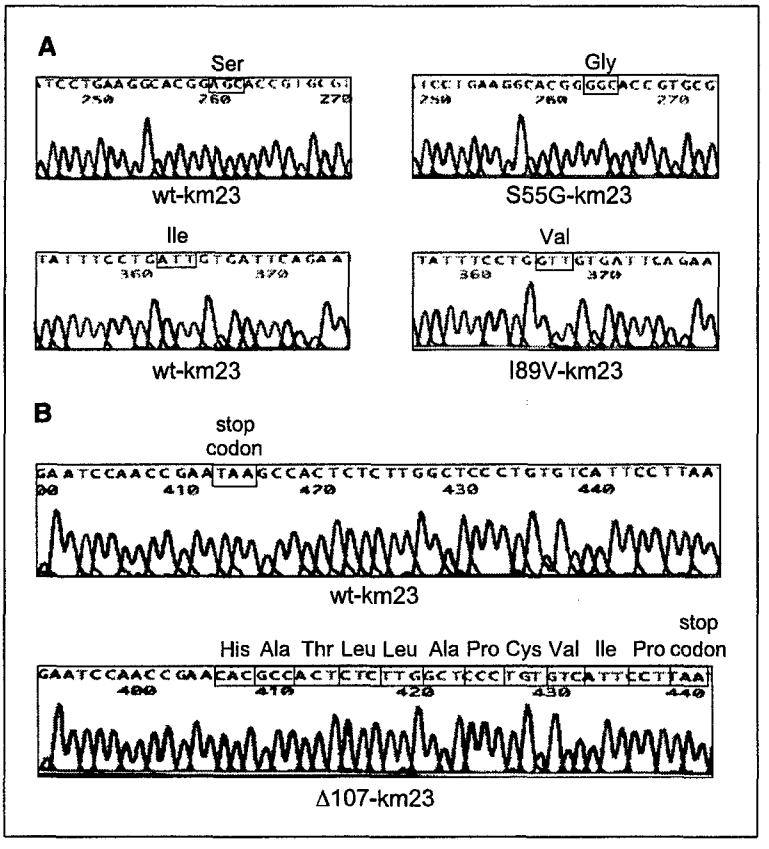

Figure 2. Nested RT-PCR and DNA sequencing results for the mutations found in ovarian cancer patients. *A*, S55G/I89V alterations found in one patient. The DNA sequence from one normal tissue showing *wt-km23* (*left top* and *bottom*). In one patient with ovarian cancer (case 1), the 163rd nucleotide of the coding region of *km23* was altered from A to G, and the corresponding amino acid was substituted from a serine to a glycine (S55G; *top right*). In the same patient, another mutation from A → G occurred at 265th nucleotide, resulting in an isoleucin → valine substitution (I89V; *bottom right*). *B*, a stop codon mutation was detected in two patients. In two patients (cases 4 and 14), the stop codon of *km23* was altered from TAA (*top*) to CAC (*bottom*). This alteration results in a larger protein, with an additional 11 amino acids at the COOH terminus, encoding a protein of 107-amino-acid residues (*bottom*), instead of the 96-amino-acid residues wt-km23 (*top*).

Table 2. Comparison of *km23* alteration rate between ovarian carcinoma and normal ovarian tissues

	Normal ovarian tissues	Ovarian carcinoma tissues
Alteration	0	8
No Alteration	15	11
Total	15	19
Alteration rate (%)	0	42.1*

*Statistical calculation using Fisher's exact test demonstrated a significant difference in the km23 alteration rate between ovarian carcinoma and normal ovarian tissues ($P < 0.005$).

Δexon3-km23 inhibited transforming growth factor-β–dependent transcriptional activation of p3TP-lux and ARE-lux reporters. As mentioned above, we have identified km23 as a novel TGF-β receptor–interacting protein (9) and have shown that Δexon3-km23 can disrupt binding to the DIC. Based upon our model for km23 function (9, 10), it was conceivable that alterations in km23 could disrupt TGF-β signaling. To assess whether TGF-β signaling was still intact in the presence of the truncated form of km23 (Δexon3-km23), we did TGF-β-dependent reporter assays in Mv1Lu cells. First, we tested the effect of either wt-km23 or Δexon3-km23 on TGF-β-inducible transcriptional activity of the p3TP-lux reporter, a TGF-β-regulated reporter frequently used to evaluate TGF-β signaling (13, 21, 22). This reporter construct contains three consecutive 12-*O*-tetradecanoylphorbol-13-acetate response elements and a TGF-β-inducible 100-bp fragment of the plasminogen activator inhibitor-1 promoter (13). Mv1Lu cells were cotransfected with p3TP-lux and the indicated amounts of either wt-km23 or Δexon3-km23. As shown in Fig. 4*A*, TGF-β induced a 13-fold increase in p3TP-lux activity after expression of EV, as previously reported (23). Similarly, after expression of wt-km23, TGF-β induced a 17- to 18-fold activation of the p3TP-lux reporter. In contrast, the ability of TGF-β to activate the p3TP-lux reporter was reduced to only 5- to 7-fold after expression of Δexon3-km23. Thus, the Δexon3-km23 mutant results in a repression of ligand-dependent p3TP-lux activation.

To determine whether Δexon3-km23 displayed similar effects on other TGF-β-dependent promoters, we also examined induction of the activin-responsive element (ARE) promoter reporter from the *Xenopus Mix.2* gene (14). This reporter has been shown to be activated by TGF-β or activin in a Smad2-dependent manner (24). Mv1Lu cells were transfected with the indicated amounts of either wt-km23 or Δexon3-km23, along with the ARE-lux reporter and FAST-1. As shown in Fig. 4*B*, compared with wt-km23, Δexon3-km23 resulted in an elevation of the basal level of ARE-lux activity, suggesting aberrant regulation of this promoter in the absence of TGF-β. Furthermore, the ability of

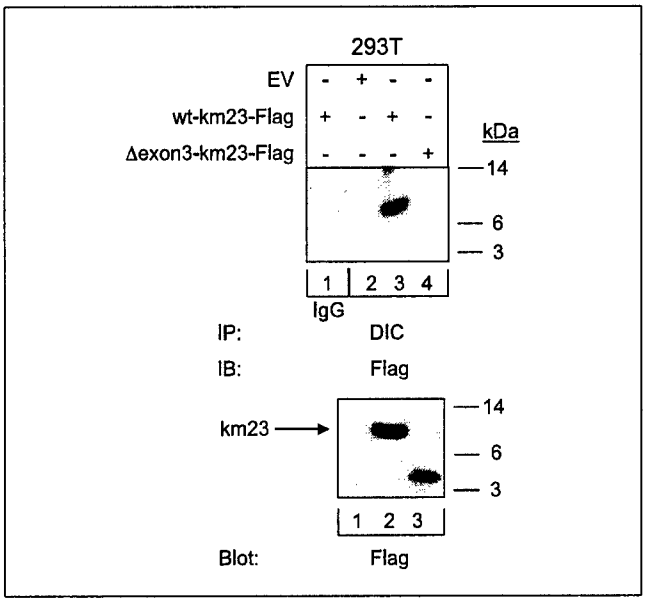

Figure 3. Δexon3-km23 disrupts binding to the DIC. Total lysates were prepared from 293T cells that had been transfected with the indicated forms of km23 and immunoprecipitation (*IP*)/immunoblotting assays were done. Flag-tagged wt-km23 (*lane 3*) and Δexon3-km23 (*lane 4*) were immunoprecipitated using an anti-DIC antibody. The interacting proteins were analyzed by SDS-PAGE and immunoblotting using an anti-Flag antibody (*top*). Normal mouse IgG and lysates from empty vector-transfected cells were used as negative controls (*lanes 1* and *2, top*). Equal expression and inputs of Flag-tagged proteins were verified by Western blotting (*bottom*). Representative of two experiments.

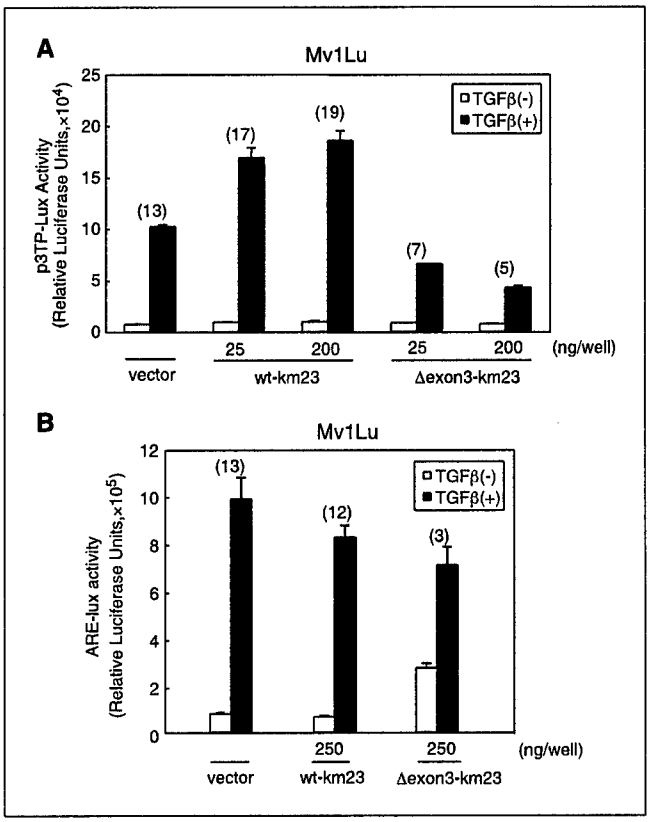

Figure 4. Δexon3-km23 inhibits TGF-β-dependent transcriptional activation in p3TP-lux and ARE-lux reporter assays. Mv1Lu cells were transfected with the indicated amounts of either wt-km23 or Δexon3-km23 along with the p3TP-lux reporter (*A*) or the ARE-lux reporter and FAST-1 (*B*). Twenty-four hours after transfection, the medium was replaced with serum-free medium for 1 hour, and the cells were incubated in the absence (*open columns*) or presence (*black columns*) of TGF-β_1 (5 ng/mL) for an additional 18 hours. The fold induction of luciferase activity by TGF-β is indicated (*parentheses on top of relevant columns*). *Bars*, SE. Representative of at least two experiments, each done in triplicate.

TGF-β to induce ARE reporter activity was significantly repressed, from 13-fold for wt-km23 to 3-fold for Δexon3-km23. Thus, our results show a loss of ligand-dependent regulation of the ARE promoter as well.

S55G/I89V-km23 but not S55A-km23 disrupts the interaction with dynein intermediate chain. The results from Figs. 3 and 4 indicated that Δexon3-km23 not only disrupted the interaction with DIC but also inhibited TGF-β-dependent transcriptional activation of the p3TP-lux and ARE-lux promoters. Thus, disruption of the km23-DIC interaction blocks TGF-β-mediated transcriptional events. To examine whether another mutant identified in human ovarian cancer could also block the DIC interaction, we did immunoprecipitation/blot analyses in 293T cells. As shown in Fig. 5*A*, compared with wt-km23 (*lane 3*), the S55G/I89V-km23 mutant (*lane 4*) completely blocked the interaction with DIC. As expected, no bands were observed in the negative control lanes (*lanes 1* and *2*).

Because we have previously shown that km23 phosphorylation is critical for km23's DIC-binding function (9, 10), it is conceivable that the S55G/I89V-km23 mutant might not have interacted with DIC due to the S55G mutation. However, this mutant also contains an I89V alteration. Accordingly, to determine whether the blockade of DIC binding was due to the S55G mutation alone, we did immunoprecipitation/blot assays using an S55A-km23 construct lacking the I89V alteration. In this construct, the serine residue at position 55 was converted to an alanine by site-directed mutagenesis. As shown in Fig. 5*A*, the S55A-km23 mutant could still bind to DIC (*lane 5*). Collectively, these data indicate that S55 is not a critical site for km23-DIC interaction, but that I89 is crucial for the DIC-binding function of km23.

Ser^{32} and Ser^{73} are both required for km23 binding to the dynein intermediate chain. As mentioned earlier, there are four conserved serine residues in km23 that could potentially be phosphorylated by TGF-β. Of these four serine residues, three are located in exon 3 (S32, S55, and S73). Our data above have shown that S55 is not required for the km23-DIC interaction, suggesting that this site may not be a critical phosphorylation site. However, we have previously shown that the kinase activity of TβRII was required for the km23-DIC interaction (9, 10), indicating that km23 phosphorylation is a critical event for km23 function. To address whether two other serine residues, S32 and S73, were pivotal for the binding to the DIC, we did immunoprecipitation/blot assays using Flag-tagged S32A-km23 and S73A-km23 constructs, in which the corresponding serine residues were converted to alanine by site-directed mutagenesis. As shown in Fig. 5*B*, wt-km23 (*lane 3*) was immunoprecipitated by the anti-DIC antibody, whereas neither S32A-km23 nor S73A-km23 interacted with DIC (*lanes 4* and *5*). No interactions were detectable when cells were transfected with only the EV or using normal mouse IgG as the immunoprecipitation antibody (Fig. 5*B*, *top, lanes 1*, and *2*). The expression of the Flag-tagged proteins used for the immunoprecipitation reaction was verified by Western blotting as shown in Fig. 5B (*bottom*). These results indicate that S32 and S73, both of which are missing in the Δexon3-km23 mutant, are critical phosphorylation sites for the recruitment of km23 to the DIC.

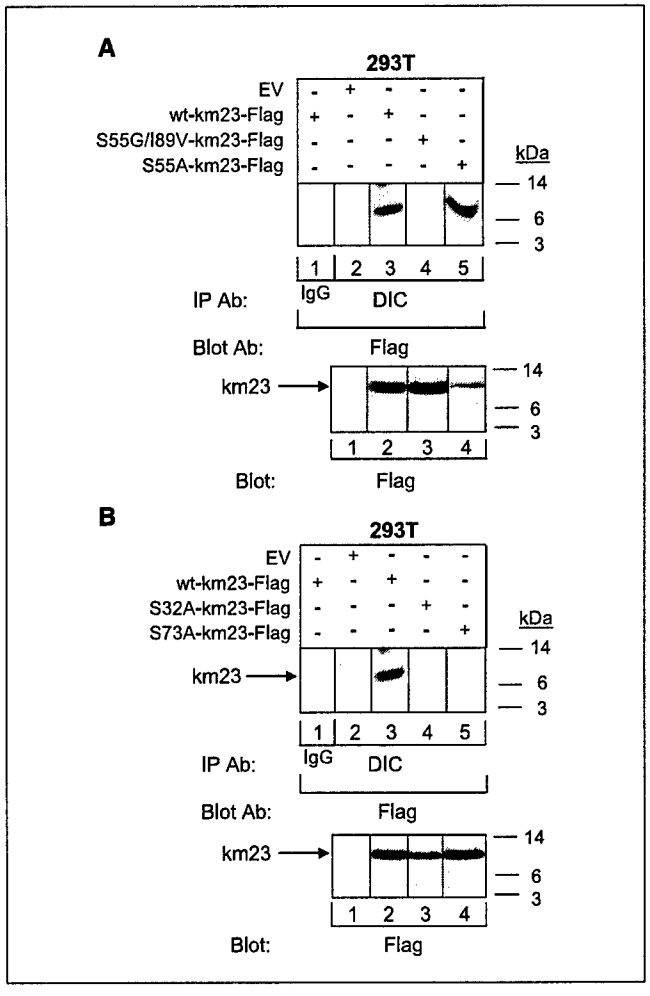

Figure 5. The double-mutant S55G/I89V-km23 but not the single mutant S55A-km23 disrupts the interaction with DIC, and Ser^{32} and Ser^{73} of km23 are required for DIC binding. *A*, S55G/I89V-km23 blocks the interaction with DIC, whereas S55A-km23 is without effect. Immunoprecipitation (*IP*)/blot assays were done using total lysates prepared from 293T cells that had been transfected with the indicated forms of km23. Flag-tagged wt-km23, S55G/I89V-km23, and S55A-km23 (*top, lanes 3, 4*, and *5*, respectively) were immunoprecipitated using an anti-DIC antibody. The interacting proteins were analyzed by SDS-PAGE and immunoblotting using an anti-Flag antibody (*top*). Normal mouse IgG and lysates from EV-transfected cells were used as negative controls (*top, lanes 1* and *2*). The expression and inputs of Flag-tagged proteins were verified by Western blotting (*bottom*). *B*, both S32A-km23 and S73A-km23 disrupt the interaction with DIC. Immunoprecipitation/blot assays were done as in (*A*) using cell lysates prepared from 293T cells transfected with wt-km23, S32A-km23, and S73A-km23 (*top, lanes 3, 4*, and *5*, respectively). The expression and inputs of Flag-tagged proteins were verified by Western blotting (*bottom*). Representative of two experiments.

Discussion

In the present study, we report that km23, a TGF-β receptor-interacting protein and a dynein motor protein light chain, was altered with high frequency (42.1%) in tissues from ovarian cancer patients. In 2 of 19 patients, a truncated form of *km23* missing exon3 (*Δexon3-km23*) was detected. In addition to this alteration, six other missense mutations have been detected in an additional six patients. None of these alterations were detectable in normal ovarian tissue samples. Furthermore, functional studies showed that the km23 mutant Δexon3-km23 not only disrupted the interaction with DIC but also inhibited transcriptional activation of the TGF-β-dependent reporters p3TP-lux and ARE-lux. In addition, our results indicate that alterations in km23 disrupt TGF-β-signaling events, thereby

implicating km23 in the TGF-β resistance associated with ovarian cancer development and/or progression. This report is the first demonstration of a link between cytoplasmic dynein and ovarian cancer.

Our results of the predicted potential phosphorylation sites for PKA, PKC, and/or CKII in km23 (Fig. 1*B*) suggest that these kinases might be involved in modifications of km23 required for subsequent signaling events. Furthermore, the Δexon3-km23 alteration, which is missing multiple phosphorylation sites that may potentially be modulated by TGF-β or other kinases, not only resulted in an abrogation of the DIC-km23 interaction, but TGF-β-dependent gene transcription was also inhibited. In addition, the S32A and S73A phosphorylation mutants both resulted in a blockade of km23 binding to DIC. Thus, the loss of key phosphorylation sites in km23 may be another mechanism underlying the TGF-β resistance associated with ovarian tumors.

Interestingly, a deletion mutant found in the *roadblock* (*robl*) gene, a homologue of *km23* in *Drosophila*, is similar to the *Δexon3-km23* mutant we identified in ovarian cancer patients. This *Drosophila robl* mutant lacks portions of intron 2 and exon 3 (25). The phenotype of this mutant exhibits a variety of defects in intracellular transport, including those of axonal transport, accumulation of cargo in intra-axonal areas, severe axonal degeneration, and an increase in mitotic index (25). Accordingly, we propose that Δexon3-km23 may resemble this *Drosophila* mutant and result in altered intracellular trafficking and accumulation of cargoes in an aberrant manner or in aberrant compartments. Such an outcome for the km23 mutants is consistent with our results herein, which show that Δexon3-km23 caused defects in both DIC binding and TGF-β-dependent transcriptional events.

In *Drosophila*, the km23/robl mutant homozygotes cannot be fully rescued by the genomic or cDNA rescue constructs, showing that this mutation can act in a dominant fashion to inhibit the action of wt-km23/robl (25). In addition, here we have shown that both *wt-km23* and *Δexon3-km23* were present together in two ovarian cancer patients (Fig. 1*A*). Thus, we suggest that the Δexon3-km23 may behave like the km23/robl mutant in *Drosophila* to inhibit the normal function of wt-km23 in a dominant fashion. Future studies will address this possibility in more detail.

To date, three classes of cytoplasmic DLCs have been identified in mammals, including Tctex-1/rp3, DLC8, and km23/roadblock (9, 19, 20, 25–27), which have been shown to directly bind to the DIC at distinct regions (28). Together with the dynein intermediate chains and light-intermediate chains, they form the base of the dynein complex and are important for cargo binding and cargo transport along microtubules (19, 20, 26, 27). It has been shown that a 72-amino-acid domain of DIC, spanning amino acids 243 to 314, is required for its binding to km23/roadblock (28). However, the site on km23 that is necessary for binding to DIC has still not been identified. Δexon3-km23 disrupted the interaction with DIC, suggesting that the third exon of km23 may contain the binding domain required for the DIC-km23 interaction. Alternatively, this large truncation of the km23 protein may completely disrupt the folding of km23, secondarily impairing km23-DIC interactions.

Our previous work showed that TGF-β receptor activation was required for recruitment of km23 to the dynein motor complex (9). Thus, upon receptor activation, TGF-β-signaling components might be transported along microtubules through the interaction of km23 with the DIC. If this were the case, the disruption of the DIC-km23 interaction by the km23 alterations we report here would be expected to alter TGF-β-signaling events. The abrogation of the TGF-β transcriptional events we have observed is consistent with this function for km23.

Δexon3-km23 inhibited the transcriptional activity of the p3TP-lux reporter in Mv1Lu cells, suggesting that this alteration disrupts TGF-β signaling through several transcriptional factors. The p3TP-lux reporter, an artificial construct, contains three activator protein-1 (AP-1) sites that are regulated by Ras and both the extracellular signal-regulated kinase (Erk) and JNK/mitogen-activated protein kinase pathways (17, 18, 29–31). It has also been reported, for a wide variety of cell types, that TGF-β can activate the Ras/Erk pathways, as well as p38 and JNK (17, 18, 30–35). Furthermore, our previous data indicated that forced expression of km23 induced specific TGF-β responses, including JNK activation and c-Jun phosphorylation. These results suggest that km23 may also be involved in a JNK pathway (9). Therefore, collectively, our results suggest that the Δexon3-km23 mutant might disrupt a JNK/AP-1-dependent pathway activated by TGF-β.

Δexon3-km23 also inhibited the transcriptional activity of the Smad-dependent ARE promoter. This reporter is a natural promoter from the *Xenopus Mix.2* gene (14, 24, 36–39). The activin-responsive factor (ARF), which is composed of Smad2, Smad4, and either FAST-1 or FAST-2, is required for binding to the ARE and activation of the *Mix.2* promoter (14, 24, 36–39). Because we show that Δexon3-km23 inhibited TGF-β stimulation of the ARE-lux reporter, Δexon3-km23 might disrupt transcription factors that are required for binding to the ARE. Future studies will address which ARF component(s) might be motor cargo for recruitment by km23.

In summary, we show that *km23* is altered at high frequency in epithelial ovarian cancer. In addition, all of the alterations we have identified were specific to the tumor tissues. More importantly, all of the km23 alterations tested to date disrupted the DIC-binding function of km23. Furthermore, the Δexon3-km23 mutant displayed a significant inhibition of the transactivation of TGF-β-dependent reporters. Of note, the S55G/I89V-km23 mutant found in the ovarian cancer patients abrogated binding of km23 to the DIC, whereas the single phosphorylation site mutant S55A-km23 did not. In contrast, two other phosphorylation site mutants completely blocked the interaction with DIC. Collectively, our results indicate that km23 is an important mediator of TGF-β-signaling events, due to its ability to bind to the DIC, and regulate TGF-β-dependent transcriptional events. Thus, alterations in km23 would be expected to play a role in ovarian cancer formation or progression, through a mechanism involving a loss of TGF-β signaling. As such, our results suggest that km23 may represent a critical target for the development of ovarian cancer diagnostics, prognostics, and/or therapeutics.

Acknowledgments

Received 12/8/2004; revised 4/15/2005; accepted 5/22/2005.

Grant support: NIH grants CA-51452, CA-100239, CA-90765, and CA-92889 and Department of Defense award DAMD 17-03-1-0287 (K.M. Mulder). This research was also supported in part by a General Clinical Research Center grant from NIH (M01RR10732) awarded to the Pennsylvania State University College of Medicine.

The costs of publication of this article were defrayed in part by the payment of page charges. This article must therefore be hereby marked *advertisement* in accordance with 18 U.S.C. Section 1734 solely to indicate this fact.

We thank the Cooperative Human Tissue Network for providing the ovarian tissues, W. Stewart (Department of Histology, Penn State College of Medicine) for assistance with tissue sectioning, S. Gestl (Jake Gittlen Cancer Research Institute, Penn State College of Medicine) and D. Shearer (Department of Obstetrics/Gynecology, Penn State College of Medicine) for assistance with the LCM, J. Massague (Memorial Sloan-Kettering Cancer Center, New York, NY) for providing us with p3TP-lux construct, and M. Whitman (Harvard Medical School, Boston, MA) for providing us with the ARE-lux and FAST-1 constructs.

References

1. Jemal A, Murray T, Samuels A, Ghafoor A, Ward E, Thun MJ. Cancer statistics, 2003. CA Cancer J Clin 2003; 53:5–26.
2. Ozols RF, Bookman MA, Connolly DC, et al. Focus on epithelial ovarian cancer. Cancer Cell 2004;5:19–24.
3. Hu W, Wu W, Nash MA, Freedman RS, Kavanagh JJ, Verschraegen CF. Anomalies of the TGF-β postreceptor signaling pathway in ovarian cancer cell lines. Anticancer Res 2000;20:729–33.
4. Yamada SD, Baldwin RL, Karlan BY. Ovarian carcinoma cell cultures are resistant to TGF-β1-mediated growth inhibition despite expression of functional receptors. Gynecol Oncol 1999;75:72–7.
5. Lynch MA, Nakashima R, Song H, et al. Mutational analysis of the transforming growth factor β receptor type II gene in human ovarian carcinoma. Cancer Res 1998;58:4227–32.
6. Chen T, Triplett J, Dehner B, et al. Transforming growth factor-β receptor type I gene is frequently mutated in ovarian carcinomas. Cancer Res 2001;61: 4679–82.
7. Cardillo MR, Yap E, Castagna G. Molecular genetic analysis of TGF-β1 in ovarian neoplasia. J Exp Clin Cancer Res 1997;16:49–56.
8. Wang D, Kanuma T, Mizunuma H, et al. Analysis of specific gene mutations in the transforming growth factor-β signal transduction pathway in human ovarian cancer. Cancer Res 2000;60:4507–12.
9. Tang Q, Staub CM, Gao G, et al. A novel TGFβ receptor-interacting protein that is also a light chain of the motor protein dynein. Mol Biol Cell 2002;13:4484–96.
10. Ding W, Mulder KM. km23: a novel TGFβ signaling target altered in ovarian cancer. In: Kumar R, editor. Molecular targeting and signal transduction. Boston/ New York/Dordrecht/London: Kluwer Academic Publishers; 2004. p. 315–27 (Cancer Treat Res, vol. 119).
11. Goldsworthy SM, Stockton PS, Trempus CS, Foley JF, Maronpot RR. Effects of fixation on RNA extraction and amplification from laser capture microdissected tissue. Mol Carcinog 1999;25:86–91.
12. Jin Q, Ding W, Staub CM, Gao G, Tang Q, Mulder KM. Requirement of km23 for TGFβ-mediated growth inhibition and induction of fibronectin expression. Cell Signal. In press 2005.
13. Wrana JL, Attisano L, Carcamo J, et al. TGFβ signals through a heteromeric protein kinase receptor complex. Cell 1992;71:1003–14.
14. Chen X, Rubock MJ, Whitman M. A transcriptional partner for MAD proteins in TGF-β signalling. Nature 1996;383:691–6.
15. Yue J, Mulder KM. Requirement of Ras/MAPK pathway activation by transforming growth factor β for transforming growth factor β1 production in a Smad-dependent pathway. J Biol Chem 2000;275: 30765–73.
16. Blom N, Gammeltoft S, Brunak S. Sequence and structure-based prediction of eukaryotic protein phosphorylation sites. J Mol Biol 1999;294:1351–62.
17. Yue J, Mulder KM. Transforming growth factor-β signaling transduction in epithelial cells. Pharmacol Ther 2001;91:1–34.
18. Massague J, Blain SW, Lo RS. TGFβ signaling in growth control, cancer, and heritable disorders. Cell 2000;103:295–309.
19. King SM. The dynein microtubule motor. Biochim Biophys Acta 2000;1496:60–75.
20. Vallee RB, Williams JC, Varma D, Barnhart LE. Dynein: an ancient motor protein involved in multiple modes of transport. J Neurobiol 2004;58:189–200.
21. Lee HJ, Lee JK, Miyake S, Kim SJ. A novel E1A-like inhibitor of differentiation (EID) family member, EID-2, suppresses transforming growth factor (TGF)-β signaling by blocking TGF-β-induced formation of Smad3-Smad4 complexes. J Biol Chem 2004;279:2666–72.
22. Abecassis L, Rogier E, Vazquez A, Atfi A, Bourgeade MF. Evidence for a role of MSK1 in transforming growth factor-β-mediated responses through p38α and Smad signaling pathways. J Biol Chem 2004;279: 30474–9.
23. Souchelnytskyi S, Tamaki K, Engstrom U, Wernstedt C, ten Dijke P, Heldin CH. Phosphorylation of Ser^{465} and Ser^{467} in the C terminus of Smad2 mediates interaction with Smad4 and is required for transforming growth factor-β signaling. J Biol Chem 1997;272:28107–15.
24. Felici A, Wurthner JU, Parks WT, et al. TLP, a novel modulator of TGF-β signaling, has opposite effects on Smad2- and Smad3-dependent signaling. EMBO J 2003; 22:4465–77.
25. Bowman AB, Patel-King RS, Benashski SE, McCaffery JM, Goldstein LS, King SM. *Drosophila* roadblock and *Chlamydomonas* LC7: a conserved family of dynein-associated proteins involved in axonal transport, flagellar motility, and mitosis. J Cell Biol 1999;146: 165–80.
26. Gunawardena S, Goldstein LS. Cargo-carrying motor vehicles on the neuronal highway: transport pathways and neurodegenerative disease. J Neurobiol 2004;58: 258–71.
27. Vale RD. The molecular motor toolbox for intracellular transport. Cell 2003;112:467–80.
28. Susalka SJ, Nikulina K, Salata MW, et al. The roadblock light chain binds a novel region of the cytoplasmic dynein intermediate chain. J Biol Chem 2002;277:32939–46.
29. Eferl R, Wagner EF. AP-1: a double-edged sword in tumorigenesis. Nat Rev Cancer 2003;3:859–68.
30. Mulder KM. Role of Ras and Mapks in TGFβ signaling. Cytokine Growth Factor Rev 2000;11:23–35.
31. Derynck R, Zhang YE. Smad-dependent and Smad-independent pathways in TGF-β family signalling. Nature 2003;425:577–84.
32. Mulder KM, Morris SL. Activation of $p21^{ras}$ by transforming growth factor β in epithelial cells. J Biol Chem 1992;267:5029–31.
33. Hartsough MT, Mulder KM. Transforming growth factor β activation of p44mapk in proliferating cultures of epithelial cells. J Biol Chem 1995;270:7117–24.
34. Hartsough MT, Frey RS, Zipfel PA, et al. Altered transforming growth factor β signaling in epithelial cells when ras activation is blocked. J Biol Chem 1996;271: 22368–75.
35. Frey RS, Mulder KM. Involvement of extracellular signal-regulated kinase 2 and stress-activated protein kinase/Jun N-terminal kinase activation by transforming growth factor β in the negative growth control of breast cancer cells. Cancer Res 1997;57:628–33.
36. Chen X, Weisberg E, Fridmacher V, Watanabe M, Naco G, Whitman M. Smad4 and FAST-1 in the assembly of activin-responsive factor. Nature 1997;389:85–9.
37. Yeo CY, Chen X, Whitman M. The role of FAST-1 and Smads in transcriptional regulation by activin during early *Xenopus* embryogenesis. J Biol Chem 1999;274: 26584–90.
38. Watanabe M, Whitman M. FAST-1 is a key maternal effector of mesoderm inducers in the early *Xenopus* embryo. Development 1999;126:5621–34.
39. Liu B, Dou CL, Prabhu L, Lai E. FAST-2 is a mammalian winged-helix protein which mediates transforming growth factor β signals. Mol Cell Biol 1999;19:424–30.

Role of the c-AMP Responsive Element in Mediating TGFβ-induction of TGFβ3 Gene Transcription*

Guangming Liu, Lipai Chen, Jill Neiman, and Kathleen M. Mulder‡

Department of Pharmacology, Penn State College of Medicine,

500 University Drive, Hershey, PA 17033

Running Title: CRE Mediates TGFβ3 Expression

*This work was supported by NIH grants CA90765, CA92889, CA100239, and DAMD17-03-1-0287 to KMM

‡To whom correspondence should be addressed: Dept. of Pharmacology, Penn State College of Medicine, 500 University Dr., Hershey, PA 17033. Tel.: 717-531-6789; Fax: 717-531-5013; E-mail: kmm15@psu.edu.

[1]The abbreviations used are: TGFβ, Transforming growth factor β; CRE: c-AMP-responsive element; CREB1: CRE binding protein 1; AP-1, activator protein-1; siRNA, small interfering RNA; IEC4-1, untransformed intestinal epithelial cell clone 4-1; EMSAs, electrophoretic mobility shift assays.

ABSTRACT

In tumor cells that have lost responsiveness to the growth inhibitory effects of transforming growth factor β (TGFβ), increased TGFβ production by the tumor cells contributes to cancer progression primarily through paracrine mechanisms. Identification of critical points that can be targeted to block TGFβ production in cancer cells is therefore important. In order to determine how regulation of TGFβ3 expression differs from that of the other TGFβ isoforms, here we have examined the TGFβ3 promoter region that is critical for TGFβ3 gene transcription. Using TGFβ3 promoter reporter assays, we have found that TGFβ-stimulated transactivation of the TGFβ3 promoter in a time-dependent manner. EMSA supershift assays indicated that CRE binding protein 1 (CREB1) and Smad3, but not Smad4, were the major components present in this TGFβ-inducible complex bound at the TGFβ3 promoter. This TGFβ3 promoter region contains an AP-2 site, a Smad binding element (SBE), and a c-AMP responsive element (CRE). Mutation of these sites demonstrated that the CRE site was the most critical for complex formation. Further, TGFβ induction of TGFβ3 transactivation was suppressed by both the JNK-selective inhibitor SP600125 and the p38-selective inhibitor SB203580, but not by the MEK/ERK inhibitor PD98059 or the PKA inhibitor H89. Moreover, both siRNA-CREB1 and siRNA-

Smad3 significantly inhibited TGFβ stimulation of this complex formation. Our results indicate that activation of the TGFβ3 promoter CRE site by TGFβ required TGFβRII, JNK, p38, and Smad3, but was independent of PKA and ERK.

INTRODUCTION

TGFβ is the prototype of a large super-family of multifunctional cytokines that are differentially expressed and function in a wide range of target cells (1). TGFβ suppresses the proliferation of normal cells. However, in malignant cells, TGFβ production often enhances tumor progress, especially once the cells have lost the negative growth control signals imparted by TGFβ. Therefore, identification of critical points that can be targeted to block TGFβ production in cancer cells is important (2, 3). A better understanding of the mechanisms underlying TGFβ auto-regulated secretion will assist in identifying these critical branch points.

The TGFβ family has three homologous forms: TGFβ1, TGFβ2, and TGFβ3. Although the three TGFβs share 60% to 80% identity, they are encoded by distinct genes and their expression is controlled by different regulatory sequences and promoters (4-6). They also show different physiological and pathological activities in certain cell types and systems.

TGFβ3 is expressed in structures undergoing morphogenesis during early stages of development, while TGFβ2 is expressed in mature and differentiating epithelium at later stages of development (7, 8). TGFβ3 plays a critical role during palate development, since mutations of the TGFβ3 gene give rise to cleft palate in both humans and mice (9). In

lactotropes, TGFβ3 stimulates cell proliferation indirectly by acting on folliculostellate cells, whereas TGFβ1 inhibits cell proliferation by acting directly on lactotropes (10, 11). TGFβ3 is ubiquitously abundant in the rat brain (12), and is the major TGFβ isoform released in the brain (13). TGFβ3 is also the primary TGFβ isoform present in human umbilical cord, where it is developmentally regulated (14).

At the level of receptor activation, the different TGFβ isoforms also display unique characteristics. TGFβ3, as well as TGFβ1, directly combine with the type II TGFβ receptor (RII). This complex activates the type I TGFβ receptor (RI) and signaling proceeds. In contrast, TGFβ2 needs the type III TGFβ receptor (RIII, betaglycan) in order to combine with RII (15). Recent studies on the crystal structure of TGFβ3, and on its dynamics-modulated biological activity, revealed important structural and internal dynamic differences between TGFβ3 and the other TGFβ isoforms (16, 17). For example, in TGFβ3 the central α-helix *H3* and the C-terminal part of its pre-helix loop are extremely flexible in solution, which makes TGFβ3 significantly different from the other TGFβ isoforms (16).

The expression of all TGFβ isoforms is under the control of an auto-feedback loop (18). In TGFβ-null heterozygous mice, circulating and tissue

TGFβ protein levels are dramatically decreased to only 10-30% that of wild type TGFβ, indicating that cellular produced TGFβ plays a significant role in its own regulation (18). TGFβ auto-regulation is an important mechanism for amplifying TGFβ expression and production. Due to the critical roles that TGFβ plays in regulating physiological and pathophysiological functions such as proliferation, cell cycle, apoptosis, angiogenesis, metastasis, and invasiveness in cells and tissues, any changes in the signaling pathways mediating TGFβ3 auto-regulation may lead to severe abnormalities of a broad nature. It is, therefore, important to understand the mechanisms underlying TGFβ auto-regulation, as well as the signal transduction pathways mediating TGFβ-induced TGFβ3 expression.

The auto-regulation of TGFβ appears to be mediated through specific sites in the promoter regions of the distinct isoforms (19). While these sites have been examined for the TGFβ1 promoter (19), little is known about the relevant regions in the TGFβ3 promoter. The promoter area of the TGFβ3 gene has little structural or functional similarity to the TGFβ1 promoter. Similarly, the transcriptional regulation of this gene has significantly diverged from that of the other TGFβs (6). It has been reported that a region proximal to the TATA box in the 5'-flanking region of the TGFβ3 gene might be important in regulating TGFβ3 expression (6). However, no

conclusive studies have defined the critical sites required for TGFβ induction of TGFβ3 expression.

Here we have determined that the TGFβ-inducible region of the TGFβ3 promoter contains three transcription factor binding consensus sites: a cAMP-responsive element (CRE) at –45 to –39 (GACGTCA), a Smad binding element (SBE) at –49 to –46 (CAGA), and an activator protein 2 (AP-2) site at –57 to –50 (CCCCAGGC). We have investigated the transcriptional regulation of each of these TGFβ3 gene promoter regions in response to TGFβ exposure. We have also defined the signal transduction pathways mediating TGFβ induction of the TGFβ3 promoter regions. Our studies provide new insights into TGFβ3 auto-feedback regulatory mechanisms. Blockade of TGFβ3 production by targeting these critical points would be expected to suppress tumor growth.

MATERIALS AND METHODS

Cell culture — The untransformed rat intestinal epithelial cell line 4-1 (IEC4-1, TGFβ-sensitive) was isolated as described previously (20, 21). Cells were routinely maintained in SMIGS medium, consisting of McCoy's 5A (Life Technology, Inc.), supplemented with amino acid pyruvate, antibiotics (streptomycin, penicillin), insulin (4μg/ml), glucose (4.5mg/ml), and 5% fetal bovine serum. IEC4-1 cells, stably transfected with dominant-negative RII (DN RII), and empty vector (EV), were prepared as previously described (22). The transfectants were maintained in SMIGS medium under the suppression of 5 μg/ml blasticidin. CCL64-L20 and CCL64-Smad3C mink lung epithelial cells were routinely maintained in Dulbecco's modified Eagle's medium plus 10% fetal bovine serum as previously described (19).

Electrophoretic mobility shift assays (EMSAs) — EMSAs were performed as described (23). Nuclear protein extracts were prepared from either IEC4-1 or CCL64 cells by a method described previously (23). Briefly, the cells were cultured in 10-cm dishes and treated with TGFβ3 (10 ng/ml) for 1 h. The cells were then disrupted in 500 μl of lysis buffer A [25 mM HEPES (pH 7.8), 50 mM KCl, 0.5% NP-40, 100 μM DTT, 10 μg/ml leupeptin, 25 μg/ml aprotinin, and 1 mM PMSF]. After a 1-min centrifugation (16,000 x *g*, 4°C), the pellet containing the nuclei was washed

once with 500 µl of buffer B (buffer A without NP-40), resuspended in 120 µl of extraction buffer (buffer B but with 500 mM KCl and 10% glycerol), and incubated with shaking at 4°C for 30 min. The nuclear extracts were stored at -70°C until analysis. The DNA binding reaction (for EMSA) was carried out at room temperature for 30 min in a mixture containing 4 µg of nuclear protein, 1 µg of poly (dI-dC), and 15,000 cpm of ^{32}P-labeled double-stranded oligonucleotide. The samples were fractionated through a 5% polyacrylamide gel. Gels were dried and analyzed using the Storm 840 Phospho-Image System (Molecular Dynamics).

The oligonucleotides used for probe labeling were: Tβ3-P61/35, –61 CCCA CCCCAGGC CAGA GACGTCA TGGG –35; mutated AP-2 in Tβ3-P61/35, –61 CCCA CCCtcaGC CAGA GACGTCA TGGG –35; mutated SBE in Tβ3-P61/35, –61 CCCA CCCCAGGC CgtA GACGTCA TGGG –35; mutated CRE in Tβ3-P61/35, –61 CCCA CCCCAGGC CAGA GACactA TGGG –35; TGFβ2/E-Box promoter –59 to –35 motif, –59GAAGGCAGACACGTGGTTCAGAGAG –35; SBE consensus binding motif, GTCTAGAC. The SBE consensus sequence was purchased from Santa Cruz Biotechnology, Inc. (Santa Cruz, CA). All other oligonucleotides were synthesized by Integrated DNA Technologies (Coralville, IA). Electrophoretic mobility supershift assays were performed

by preincubating 4 μg of nuclear protein with 4 μg of the relevant specific antibody against CREB (Santa Cruz Biotechnology, Inc., Santa Cruz, CA), Smad3 (Zymed Laboratories Inc., San Francisco, CA), or Smad4 (Santa Cruz), or control normal rabbit IgG (Santa Cruz) at 4°C for 2 h, and then processing samples as described above. The gels were dried and exposed to X-ray film.

siRNA transfections — siRNA-CREB-1 was purchased from Santa Cruz. siRNA-Smad3 was purchased from Cellogenetics, Inc. (Baltimore, MD). The siRNA products were annealed duplexes of RNA. Transfection of siRNA into the cells was carried out according to the manufacturer's instruction. A non-targeting siRNA was used as a control for non-sequence-specific effects of the siRNA transfection (Dharmacon, Inc., Dallas, TX)

Construction of TGFβ3 promoter luciferase reporter plasmid — The Tβ3-P221/110-Luc encodes a TGFβ3 promoter region from –221 to +110. The nucleotide sequence was PCR- amplified. The primers used were: sense, 5'-actcgaACGCGTtgtggcaggagtgattccaaga-3' (the capital letters indicate an *Mlu*I restrict enzyme digestion site), antisense: 5'-gcacgcAGATCTcttggacttgactctctgcttcc-3' (the capital letters indicate a *Bgl*II restrict enzyme digestion site). The PCR products and the basic pGL3 Luciferase Reporter Vector (Promega, Madison, WI) were digested using

*Mlu*I and *Bgl*II, and the products were gel-purified and inserted into the vector using Quick ligase (New England Biolabs, Beverly, MA). The sequence of the resulting Tβ3-P221/110-Luc luciferase reporter plasmid was confirmed by sequence analysis.

Luciferase reporter assays — IEC4-1 and CCL64 cells were seeded in 24-well plates and grown to 70-80% confluence. Cells were transfected with 0.4 μg Tβ3-P221/110-Luc, siRNA plasmids at the indicated concentrations, and 0.1 μg renilla luciferase control reporter (pRL-SV40) per well, using Lipofectamine™ 2000 (Invitrogen, Carlsbad, CA), as described in the user manual. TGFβ3 (10 ng/ml) was added 24h after transfections, and luciferase activity was measured at 24 h after TGFβ3 treatment. Transfection efficiency was determined by co-transfecting with renilla luciferase.

Western immunoblotting — IEC4-1 cells were transfected with the siRNA plasmids indicated and the cells were lysed and prepared at 36h after transfection. Western immunoblotting for CREB-1, Smad3, and phosphorylated-CREB-1 proteins was carried out using specific antibodies, according to the supplier's recommendations. Anti-CREB-1 antibody (#9192) and anti-phospho-CREB-1 antibody (#9191) were from Cell

Signaling Technology (Beverly, MA). Anti-Smad3 antibody (#51-1500) was from Zymed Laboratories, Inc. (South San Francisco, CA)

Statistical analysis — Data were analyzed and significant differences determined using the Student's *t* test. The results are expressed as the mean ± SE.

RESULTS

The CRE consensus site in Tβ3-P61/35 is critical for TGFβ3 responsiveness — It has been reported that a sequence from –490 to +100 in the 5' flanking region of the TGFβ3 gene might be important in regulating TGFβ3 expression (6). This region contains two ubiquitously expressed transcription factor SP-1 DNA binding sites (–420 to –415 and –363 to –358), an AP-2 site (–57 to –50), and a CRE site (–45 to –39). The CRE site has been shown to be involved in TGFβ3 transcription, although its TGFβ-inducible expression was not examined (6). Besides the AP-2 and CRE sites, we also identified an SBE site (–49 to –46), between the AP-2 and CRE sites, sites which can also be induced by TGFβ (24). We presumed that the SBE and/or CRE sites, but not the SP-1 sites, in the TGFβ3 promoter region might be important for TGFβ induction of TGFβ3 gene expression, since SP-1 has relatively little effects in the activation of the promoter (6). In order to address this issue, we constructed a Tβ3-P221/110-Luc luciferase reporter plasmid using the DNA sequence from the TGFβ3 5'-flanking region (–221 to +110) of the promoter. This sequence contains the AP-2, SBE, and CRE sites. We treated IEC4-1 cells with TGFβ to stimulate the auto-induction loop, and measured Tβ3-P221/110-Luc reporter activity. The IEC4-1 cells used in these studies represent a good

model for TGFβ regulation in untransformed epithelial cells, due to their high level of TGFβ sensitivity and to their well-characterized TGFβ pathways (21, 22, 25, 26). Here we show that TGFβ affected a time-dependent increase in Tβ3-P221/110-Luc activity. The TGFβ stimulation of Tβ3-P221/110-Luc activity reached a peak at 24h after TGFβ3 treatment (Fig.1A). These results indicate that Tβ3-P221/110 is important in TGFβ auto-induction of TGFβ3 gene transcription.

In order to determine whether these three DNA binding sites [AP-2 (–57 to –50), SBE (–49 to –46), and CRE (–45 to –39)] within the –221 to +110 region of the TGFβ3 promoter were involved in TGFβ induction of TGFβ3 gene transcription, we also examined the DNA binding activity of a sequence containing these three sites (Tβ3-P61/35) in response to TGFβ3. As shown in Fig. 1B, TGFβ significantly increased complex formation at the Tβ3-P61/35 in a time-dependent manner, with peak levels occurring at 1h after TGFβ treatment. Thus, our results indicate that a TGFβ-inducible complex formed at Tβ3-P61/35 in response to TGFβ treatment.

During the TGFβ signaling process, TGFβ binds to RII, which then recruits RI into the active complex (27). To investigate whether the TGFβ receptors were required for auto-regulation of TGFβ3 expression, we

performed EMSAs with Tβ3-P61/35 after expression of a dominant-negative TGFβ receptor II (DN RII) (22). As shown in Fig. 2A, the Tβ3-P61/35 DNA binding activity stimulated by either TGFβ1 or TGFβ3 was significantly suppressed in the DN RII-expressing IEC4-1 cells (Fig. 2A, lane 6 and 7 vs. lane 2 and 3). In contrast, DN RII had no effect in the PMA-induced cells (Fig. 2A, lane 8 vs. lane 4). These results indicate that RII is required for TGFβ3 auto-loop regulation.

In order to determine which DNA binding sites are required for TGFβ3 production, we performed site-directed mutagenesis to mutate the relevant sites, and then repeated the EMSAs using labeled versions of these as probes. As shown in Fig. 2B, mutation of the CRE site completely abolished DNA binding activity at Tβ3-P61/35 (lane 10 to 12), whereas mutation of the AP-2 (lane 4 to 6) or SBE (lane 7 to 9) sites had no effect. The TGFβ-inducible complex formed at the wild-type Tβ3-P61/35 is shown for comparison (lane 2, 3). These results indicate that DNA binding activity at the CRE site is critical for mediating the TGFβ3 auto-induction loop. A 10-fold excess of unlabeled cold probe was used throughout the EMSA experiments as controls. As shown in figure 2 B (lanes 1, 4, 8, and 10), the 10-fold excess of unlabeled probe completely competed for DNA binding of

the radioisotope-labeled probe, indicating that the bands observed represented specific binding to Tβ3-P61/35.

CREB-1 and Smad3, but not Smad4, are bound at the Tβ3-P61/35 — It is known that CREB-1 can recognize and bind to CRE consensus sites in various gene promoters. Since we have demonstrated that the CRE site in Tβ3-P61/35 is critical for TGFβ auto-induction of TGFβ3, we examined whether the CREB-1 protein was a component in the transcription factor complex bound at this Tβ3-P61/35. As shown in Fig. 3A by EMSAs, TGFβ-inducible complex formation (lanes 1, 2) was reduced when the CREB-1 antibody was present (lane 4), but not when rabbit IgG was present (lane 3). A suppershift was also observed using the CREB-1 antibody (lane 4). Thus, CREB-1 was in the transcription factor complex bound to the Tβ3-P61/35 region.

We further explored whether Smad3 and Smad4 might be present in the complex at Tβ3-P61/35, since Smads are known to play important roles in TGFβ3 signaling and since an SBE site is present in Tβ3-P61/35. As shown in Fig. 3A, lane 5, the anti-Smad3 antibody reduced the TGFβ-inducible DNA binding, indicating that Smad3 was present in the transcription factor complex bound to Tβ3-P61/35. Since activated Smad2 or Smad3 can form a dimer with Smad4 prior to stimulation of transcriptional activation of target

genes through SBE sites, it was of interest to determine whether Smad4 was also in this complex bound to Tβ3-P61/35. As shown in Fig. 3A, lane 6, the anti-Smad4 antibody had no effect on DNA binding of Tβ3-P61/35, suggesting that Smad4 may not be involved in the transcription factor complex bound to Tβ3-P61/35.

In order to verify the specificity of the anti-Smad3 and anti-Smad4 antibodies used, a full palindromic SBE sequence was used in the supershift EMSAs. As shown in Fig. 3B, both Smad3 and Smad4 were present in the transcription factor complex bound to the consensus SBE site (lane 5, 6). Fig. 3B (lane 1) shows that a 10-fold excess of unlabeled cold probe completely competed for TGFβ induction of the DNA binding of the radioisotope-labeled probe, indicating that the band observed was specific for the consensus palindromic SBE site. Lane 2 indicates that in the absence of TGFβ, there was no binding to the consensus palindromic SBE site in IEC4-1 cells. Lane 3 shows TGFβ induction of DNA binding at the consensus palindromic SBE site. Lane 4 indicates that addition of rabbit IgG to the EMSAs had no effect on TGFβ induction of DNA binding at the consensus palindromic SBE site. Thus, the anti-Smad3 and anti-Smad4 antibodies we used (Fig. 3A) were capable of competing effectively for DNA binding at the consensus SBE in the EMSA supershift assays.

As a control for TGFβ specificity, we used a different stimulus in the EMSAs. As shown in Fig. 3C, while stimulation by PMA also induced complex formation at Tβ3-P61/35 (lane 1 to 3), CREB-1, but not Smad3, was present in the transcription factor complex bound at this TGFβ3 promoter region (Fig. 3C, lane 4 vs. lane 5 and 6). The phorbol ester PMA is a known inducer of CRE DNA binding, but it cannot activate Smads (28). Thus, the Smad3 binding in Fig. 3A appears to be specific for TGFβ.

Smad3 is required for TGFβ induction of TGFβ3 promoter DNA Binding Activity — We have demonstrated above that Smad3 is present in the transcription factor complex bound to Tβ3-P61/35 after induction by TGFβ. Since there is an SBE site upstream of the CRE site in Tβ3-P61/35, which was not required for TGFβ-inducible DNA binding to Tβ3-P61/35 (Fig. 2B), we employed CCL64-Smad3C cells, and their parental CCL64-L20 cells, to further examine whether Smad3 plays any role in the TGFβ-inducible complex formation at Tβ3-P61/35. CCL64-Smad3C cells stably express a dominant-negative form of Smad3 (29). In this cell line, TGFβ is unable to induce phosphorylation of Smad3, and overexpression of the dominant-negative mutant of Smad3 blocks the inhibitory effect of TGFβ on cell growth (29). Thus, normal Smad3 function in this cell line is lost. According to the results of the EMSAs in Fig. 4A, TGFβ induction of

complex formation at Tβ3-P61/35 was blocked in the CCL64-Smad3C cells, compared to control L20 cells (Fig. 4A, lane 5 vs. lane 2). In contrast, the PMA-induced complex formation at Tβ3-P61/35 was not diminished, when compared to control L20 cells (Fig. 4A, lane 6 vs. lane 3).

We also examined Tβ3-P221/110-Luc luciferase activity after transfection of CCL64 cells with Tβ3-P221/110-Luc. As shown in Fig. 4B, TGFβ induced a 5.9-fold increase of Tβ3-P221/110-Luc luciferase activity in the L20 cells, but only a 1.6-fold increase in the Smad3C cells. Collectively, our results demonstrate that Smad3 not only binds to Tβ3-P61/35, but it is also functionally required for TGFβ3 auto-regulation.

Jun N-terminal kinase (JNK) and p38, but not cAMP-dependent protein kinase A (PKA) or the extracellular signal-regulated protein kinases (ERKs), are required for TGFβ3 auto-regulation — We have previously demonstrated that TGFβ induction of DNA binding to Tβ3-P61/35 occurs through the TGFβ receptors (Fig. 2A). Accordingly, it was of interest to explore whether downstream signaling events were also involved in TGFβ induction of TGFβ3 transcription. Further, it is known that mitogen-activated protein kinases (MAPKs) and PKA are upstream kinases of CREB-1 (30-32). Upon activation, these kinases translocate to the nucleus where they phosphorylate CREB-1 and initiate its DNA binding to the

consensus CRE site. In order to determine whether JNK, ERK, p38, or PKA were required for TGFβ3 auto-regulation, we employed the following specific inhibitors: SP600125 as a selective JNK inhibitor, SB203580 as a selective p38 inhibitor, PD98059 as a selective MEK inhibitor, and H89 as a selective inhibitor of PKA. Our results indicate that SP600125 and SB203580 effectively suppressed TGFβ induction of Tβ3-P61/35 DNA binding activity (Fig. 5A) and transactivation (Fig.5B) in a dose-dependent manner. However, PD98059 had no effect on either DNA binding to Tβ3-P61/35 or Tβ3-P221/110-Luc activity (Fig. 5A and 5B) at concentrations previously demonstrated to be effective in blocking TGFβ activation of ERKs in IEC4-1 cells (33). All three inhibitors had little effects on basal Tβ3-P61/35 DNA binding activity (data not shown).

Unexpectedly, H89 (10μM) had no effect on either DNA binding to Tβ3-P61/35, or Tβ3-P221/110-Luc luciferase activity, either in the absence or presence of TGFβ (Fig. 5C and 5D). H89 has previously been shown to be effective in selectively blocking PKA in several cell types over the concentration range of 5-20μM (34-38). Thus, a concentration of 10μM H89 would be expected to completely block PKA activity in our system. Therefore, our results suggest that the signaling pathways mediating TGFβ3 auto-regulation are independent of PKA.

siRNA-CREB-1 and siRNA-Smad3 both suppress TGFβ induction of Tβ3-P61/35 DNA binding and Tβ3-P221/110-Luc luciferase activity — Since we have shown that CREB-1 and Smad3 were both present in the complex at Tβ3-P61/35, it was of interest to confirm our results using siRNA-CREB-1 and siRNA-Smad3 transfectants in the EMSA and luciferase repoter experiments. Commercially available double-stranded siRNA was purchased and transfected into IEC4-1 cells to block target gene protein expression. As shown in Fig. 6A, both CREB-1 and Smad3 were detectable using either an anti-CREB-1 (lane 1, panel 1) or an anti-Smad3 (lane 1 panel 3) antibody. Lane 2 of panels 1 and 3 indicates that the scrambled control siRNAs had no effect on expression levels of either CREB-1 (lane 2, panel 1) or Smad3 (lane 2, panel 3). Fig. 6A (lane 3, panel 1) also indicates that the expression levels of CREB-1 in IEC4-1 cells transfected with siRNA-CREB-1 were significantly suppressed compared to untransfected IEC4-1 cells (lane 1) or to IEC4-1 cells transfected with the scrambled control siRNA (lane 2). In contrast, as expected, siRNA-Smad3 did not suppress CREB-1 levels (lane 4, panel 1). Fig. 6A (lane 3) also demonstrates that siRNA-Smad3 completely blocked Smad3 expression (lane 4), while siRNA-CREB-1 (lane 3) was ineffective. β-actin was used as

a loading control (panel 2 and 4). Thus, siRNA-CREB-1 and siRNA-Smad3 could effectively block the expression of their respective target proteins.

CREB-1 is activated by phosphorylation at ser133, which is critical for its biological function. Although we have demonstrated that siRNA-CREB-1 effectively suppressed CREB-1 protein expression (Fig. 6A), it was of interest to investigate, further, whether siRNA-CREB-1 suppressed TGFβ induction of CREB-1 phosphorylation specifically at ser133. Accordingly, we incubated IEC4-1 cells and their respective transfectants with or without TGFβ and performed Western immunoblotting using an antibody specific for the activated form of phospho-CREB-1 (Fig. 6B, upper panel). Since this antibody also detects the phosphorylated form of the CREB-related protein ATF-1, two bands should be visible, with the lower band of these representing phospho-ATF-1 (39). As shown in Fig. 6B, siRNA-CREB-1 significantly blocked both basal and TGFβ-induced phosphorylation of CREB-1 at ser133. Densitometric scanning of the phospho-CREB-1 bands from Western analysis demonstrated that TGFβ could induce a 3-fold increase in phosphorylation of CREB-1 in IEC4-1 cells or IEC4-1 cells transfected with the siRNA-control (Fig. 6B, lower panel). However, TGFβ only induced a 1.4-fold increase of phosphorylation in CREB-1 in IEC4-1 cells transfected with siRNA-CREB-1, indicating that siRNA-CREB-1

suppressed TGFβ induction of phosphorylation of the protein. Interestingly, siRNA-Smad3 also suppressed TGFβ induction of CREB-1 phosphorylation with only 1.6-fold increase, being observed. Thus, Smad3 might also be involved in the pathway mediating TGFβ induction of CREB-1 phosphorylation.

Since we have demonstrated that both CREB-1 and Smad3 are involved in the transcription factor complex formed at the CRE site in Tβ3-P61/35 in response to TGFβ treatment, we performed EMSAs using siRNA-CREB-1 and siRNA-Smad3 to examine whether CREB-1 and Smad3 were required for DNA binding at Tβ3-P61/35. As shown in Fig. 6C, TGFβ induced an increase in DNA binding at Tβ3-P61/35 in both control IEC4-1 cells (lane 5 vs. lane 1) and IEC4-1 cells transfected with the siRNA scrambled control (lane 6 vs. lane 2). siRNA-CREB-1 or siRNA-Smad3 significantly blocked TGFβ induction of Tβ3-P61/35 DNA binding activity (lane 7 vs. 3 and lane 8 vs. 4), indicating that both CREB-1 and Smad3 were required for the DNA binding at Tβ3-P61/35. siRNA-CREB-1 also repressed basal levels of Tβ3-P61/35 DNA binding activity (lane 3 vs. 2), which is consistent with the results shown in Fig. 6B, indicating that siRNA-CREB-1 also inhibited basal levels of phospho-CREB-1. Thus, both CREB-1 and Smad3 were required for TGFβ induction of Tβ3-P61/35 DNA binding activity.

Since we have demonstrated that both CREB-1 and Smad3 were required for DNA binding at Tβ3-P61/35 in response to TGFβ treatment, we performed Tβ3-P221/110-Luc luciferase activity assays to examine whether CREB-1 and Smad3 were functionally required for initiating promoter transactivation. As shown in Figure 6D, TGFβ induced a 4.7-fold increase of Tβ3-P221/110-Luc activity in control IEC4-1 cells (Control). TGFβ also induced a 5.6-fold increase of Tβ3-P221/110-Luc activity in IEC4-1 cells transfected with siRNA scrambled control reagent (siRNA-Ctrl). In contrast, TGFβ induction of Tβ3-P221/110-Luc activity was suppressed in siRNA-CREB-1 transfected IEC4-1 cells to 2.3-fold (siRNA-CREB-1) and in siRNA-Smad3 transfected IEC4-1 cells to 2.4-fold (siRNA-Smad3). These results established that both CREB-1 and Smad3 were not only present in the transcription factor complex bound at Tβ3-P61/35, but were also functionally required for initiation of promoter transactivation in response to TGFβ treatment.

Schematic model for TGFβ3 auto-regulation — Based upon the results in the preceeding figures, we have defined the signal transduction pathways that mediate TGFβ3 auto-regulation, specifically focusing on TGFβ3 induction of TGFβ3 expression, as depicted in the schematic diagram in Fig. 7. According to this model, TGFβ activates Smad3 through the TGFβ

receptors. TGFβ can also activate JNKs and p38 (40, 41). JNKs and p38 phosphorylate CREB-1 (42, 43), and phospho-CREB-1 forms a transcription factor complex at the CRE site (–45 to –39) in the TGFβ3 promoter region Tβ3-P61/35. Phospho-Smad3 is also present in this complex. Based upon the results in Figs. 1A, 4B, 5C, and 6D, the activation of this complex by TGFβ results in an increase in TGFβ3 transcriptional activity.

DISCUSSION

In the present study, we demonstrate that TGFβ3 can induce Tβ3-P221/110-Luc luciferase activity and DNA binding at Tβ3-P61/35 in a time-dependent manner in IEC4-1 cells. The Tβ3-P61/35 region contains an AP-2 site, a Smad binding element (SBE), and a c-AMP responsive element (CRE). Mutation of the CRE site in Tβ3-P61/35, but not the AP-2 or the SBE sites, totally abolished complex formation. EMSA supershift assays indicated that CREB1 and Smad3, but not Smad4, were the major components of this complex. siRNA-CREB1 and siRNA-Smad3 significantly inhibited complex formation at Tβ3-P61/35, and Tβ3-P221/110-Luc activity in IEC4-1 cells. In addition, dominant-negative TGFβRII effectively blocked the DNA binding activity induced by either TGFβ1 or TGFβ3, indicating that RII is required for this TGFβ3 auto-loop regulation. TGFβ induction of complex formation at Tβ3-P61/35 and Tβ3-P221/110-Luc activity were both suppressed by both the JNK-selective inhibitor SP600125 and the p38-selective inhibitor SB203580, but not by the MEK/ERK inhibitor PD98059 or the PKA inhibitor H89. Thus, JNK and p38, but not PKA, were involved in mediating this TGFβ3 production loop. Collectively, our results indicate that the CRE site is critical for mediating TGFβ3 gene expression, with CREB1 and Smad3 being the major

components bound at this site in response to TGFβ in untransformed epithelial cells. Further, activation of the TGFβ3 promoter CRE site by TGFβ required TGFβRII, JNK, p38, and Smad3, but was independent of PKA.

In this report, we have shown that TGFβ stimulated complex formation at the TGFβ3 promoter region Tβ3-P61/35. After TGFβ treatment, instead of Smad3 binding to the SBE site in this region, it appears to bind to the CRE site in Tβ3-P61/35, where CREB-1 also bound. Moreover, Smad4 was not present in this binding complex. Smad3 knockdown significantly blocked TGFβ induction of Tβ3-P61/35 DNA binding and Tβ3-P221/110-Luc activity. Thus, not only is Smad3 present in the complex bound at Tβ3-P61/35, it is also functionally required for TGFβ-inducible TGFβ3 expression. There are reports that Smad3, but not Smad4, associates with both a binding protein of CREB-1 (CBP) and the structurally related p300 protein in response to TGFβ exposure (44). In keeping with these previous findings, and our results herein, it is conceivable that Smad3 may actually form a complex with CREB-1 in response to TGFβ exposure, although this has not been previously reported. Further studies will address this possibility.

It should be pointed out that while Smads are critical to TGFβ signaling, TGFβ also stimulates other intracellular signaling pathways, such as JNKs, ERKs and p38 (19, 45, 46). Further, such MAPKs have been shown to be required for the signaling of TGFβ effects on growth, apoptosis, and gene expression (45, 46). MAPKS have also been identified as kinases upstream of CREB (47). In our current report, selective inhibitors of JNKs and p38 effectively blocked DNA binding to the TGFβ3 promoter region Tβ3-P61/35, indicating that JNKs and p38 were required for TGFβ activation of complex formation at this site. Notably, the selective MEK1 inhibitor failed to suppress the DNA binding to Tβ3-P61/35, although there are reports that ERKs are involved in CREB activation, particularly in specific neuronal cell cultures (48, 49). Our data demonstrate that JNK and p38, but not ERK, are involved in TGFβ induction of TGFβ3 gene transcription.

Taken together, our data provide evidence that TGFβ stimulates TGFβ3 gene transcription through an auto-regulatory mechanism involving the TGFβ receptors, JNKs, p38, Smad3, and CREB-1. The CRE site in the Tβ3-P61/35 promoter region is critical for TGFβ3 promoter DNA binding and transactivation, whereas the AP-2 and SBE sites do not appear to play critical roles. The transcription factor complex bound to Tβ3-P61/35

contains CREB-1 and Smad3. Both are functional in mediating DNA binding and subsequent luciferase reporter activity.

Identifying factors that modulate TGFβ3 auto-regulation improves our understanding of the mechanisms underlying TGFβ3 production. Our results may enable the design of novel strategies to regulate TGFβ3 secretion in pathological conditions by manipulating factors that are involved in this pathway. For example, blockade of TGFβ3 production in late-stage solid cancers using siRNA approaches may prevent the invasiveness and metastatic nature of such cancers.

Acknowledgments — We thank H. F. Lodish (MIT, Cambridge, MA) for the CCL64-Smad3C cells.

REFERENCES

1. Massague, J. (1998) *Annu. Rev. Biochem.* **67**, 753-791
2. Parada, D., Arciniegas, E., Moreira, O., and Trujillo, E. (2004) *Arch Esp Urol.* **57**, 93-99
3. Lammerts, E., Roswall, P., Sundberg, C., Gotwals, P. J., Koteliansky, V. E., Reed, R. K., Heldin, N. E., and Rubin, K. (2002) *Int J Cancer* **102**, 453-462
4. Kim, S. J., Glick, A., Sporn, M. B., and Roberts, A. B. (1989) *J. Biol. Chem.* **264**, 402-408
5. Samatar, A. A., Wang, L., Mirza, A., Koseoglu, S., Liu, S., and Kumar, C. C. (2002) *J. Biol. Chem.* **277**, 28118-28126
6. Lafyatis, R., Lechleider, R., Kim, S. J., Jakowlew, S., Roberts, A. B., and Sporn, M. B. (1990) *J. Biol. Chem.* **265**, 19128-19136
7. Pelton, R. W., Saxena, B., Jones, M., Moses, H. L, and Gold, L. I. (1991) *J. Cell Biol.* **115**, 1091-1105
8. Roberts, A. B., and Sporn, M. B. (1992) *Mol. Repro. Dev.* **32**, 91-98
9. Tudela, C., Formoso, M. A., Martinez, T., Perez, R., Aparicio, M., Maestro, C., Del Rio, A., Martinez, E., Ferguson, M., and Martinez-Alvarez, C. (2002) *Int. J. Dev. Biol.* **46**, 333-336
10. Hentges. S., Boyadjieva. N., and Sarkar. D. K. (2000) *Endocrinology*

141, 859–867

11. Chaturvedi, K., and Sarkar, D. K. (2004) *Endocrinology* **145**, 706-715
12. Unsicker, K., Flanders, K. C., Cissel, D. S., Lafyatis, R., and Sporn, M. B. (1991) *Neuroscience* **44**, 613-625
13. Yamazaki, H., Arai, M., Matsumura, S., Inoue, K., and Fushiki, T. (2002) *Am. J. Physiol. Endocrinol. Metab.* **283**, E536-544
14. Copland, I. B., Adamson, S. L., Post, M., Lye, S. J., and Caniggia, I. (2002) *Placenta* **23**, 311-321
15. Lopez-Casillas, F., Wrana, J. L., and Massague, J. (1993) *Cell* **73**, 1435-1444
16. Bocharov, E. V., Korzhnev, D. M., Blommers, M. J., Arvinte, T., Orekhov, V. Y., Billeter, M., and Arseniev, A. S. (2002) *J. Biol. Chem.* **277**, 46273-46279
17. Hart, P. J., Deep, S., Taylor, A. B., Shu, Z., Hinck, C. S., and Hinck, A. P. (2002) *Nat. Struct. Biol.* **9**, 203-208
18. Tang, B., Bottinger, E. P., Jakowlew, S. B., Bagnall, K. M., Mariano, J., Anver, M. R., Letterio, J. J., and Wakefield, L. M. (1998) *Nat. Med.* **4**, 802-807
19. Yue, J., and Mulder, K. M. (2000) *J. Biol. Chem.* **275**, 30765-30773

20. Mulder, K. M., Segarini, P. R., Morris, S. L., Ziman, J. M., and Choi, H. G. (1993) *J. Cell. Physiol.* **154**, 162-174

21. Mulder, K. M., and Morris, S. L. (1992) *J. Biol. Chem.* **267**, 5029-5031

22. Yue, J., Sun, B., Liu, G., and Mulder, K. M. (2004) *J. Cell Physiol.* **199**, 284-292

23. Liu, G., Chen, N., Kaji, A., Bode, A. M., Ryan, C. A., and Dong, Z. (2001) *Proc. Natl. Acad. Sci. U.S.A.* **98**, 7510-7515

24. Shi, Y., Wang, Y. F., Jayaraman, L., Yang, H., Massague, J., and Pavletich, N. P. (1998) *Cell* **94**, 585-594

25. Hartsough, M. E., and Mulder, K. M. (1995) *J. Biol. Chem.* **270**, 7117-7124

26. Yue, J., Buard, A., and Mulder, K. M. (1998) *Oncogene* **17**, 47-55

27. Wrana, J. L., Attisano, L., Wieser, R., Ventura, F., and Massagué, J. (1994) *Nature* **370**, 341-347

28. Biggs, J. R., Kraft, A. S. (1999) *J. Biol. Chem.* **274**, 36987-36994

29. Liu, X., Sun, Y., Constantinescu, S. N., Karam, E., Weinberg, R. A., and Lodish, H. F. (1997) *Proc. Natl. Acad. Sci. U.S.A.* **94**, 10669-10674

30. Shaywitz, A. J., and Greenberg, M. E. (1999) *Annu. Rev. Biochem.* **68**,

821-861

31. Nishihara, H., Hwang, M., Kizaka-Kondoh, S., Eckmann, L., and Insel, P.A. (2004) *J. Biol. Chem.* **279**, 26176-26183

32. Gustin, J. A., Pincheira, R., Mayo, L. D., Ozes, O. N., Kessler, K. M., Baerwald, M. R., Korgaonkar, C. K., Donner, D. B. (2004) *Am. J. Physiol. Cell Physiol.* **286**, C547-555

33. Yue, J., Frey, R. S., and Mulder, K. M. (1999) *Oncogene* **18**, 2033-2037

34. Oki, N., Takahashi, S.-I., Hidaka, H., and Conti, M. (2000) *J. Biol. Chem.* **275**, 10831 – 10837

35. Davies, S. P., Reddy, H., Caivano, M., and Cohen, P. (2000) *Biochem J.* **351**, 95-105

36. Chijiwa, T., Mishima, A., Hagiwara, M., Sano, M., Hayashi, K., Inoue, T., Naito, K., Toshioka, T., and Hidaka, H. (1990) *J. Biol. Chem.* **265**, 5267 – 5272

37. Yang, F., Kawedia, J. D., and Menon, A. G. (2003) *J. Biol. Chem.* **278**, 32173 – 32180

38. Ranganathan, G., Phan, D., Pokrovskaya, I. D., McEwen, J. E., Li, C., and Kern, P. A. (2002) *J. Biol. Chem.* **277**, 43281 – 43287

39. Tan, Y., Rouse, J., Zhang, A., Cariati, S., Cohen, P., and Comb, M. J.

(1996) *EMBO J.* **15**, 4629-4642

40. Tuli, R., Tuli, S., Nandi, S., Huang, X., Manner, P. A., Hozack, W.J, Danielson, K. G., Hall, D. J., and Tuan, R. S. (2003) *J Biol Chem.* **278**, 41227-41236

41. Watanabe, H., de Caestecker, M. P., and Yamada, Y. (2001) *J. Biol. Chem.* **276**, 14466–14473

42. Dong, C., Davis, R. J., and Flavell, R. A. (2002) *Annu. Rev. Immunol.* **20**, 55–72

43. Bhat, N. R., Feinstein, D. L., Shen, Q., and Bhat, A. N. (2002) *J. Biol. Chem.* **277**, 29584–29592

44. Feng, X.-H., Zhang, Y., Wu, R. Y., Derynck, R. (1998) *Genes Dev.* **12**, 2153-2163

45. Mulder, K. M. (2000) *Cytokine Growth Factor Rev.* **11**, 23-35

46. Yue, J., and Mulder, K. M. (2000) *Methods Mol. Biol.* **142**, 125-131

47. Mora-Garcia, P., Cheng, J., Crans-Vargas, H. N., Countouriotis, A., Shankar, D., Sakamoto, K. M. (2003) *Stem. Cells* **21**, 123-130

48. Masutani, H., Bai, J., Kim, Y. C., and Yodoi, J. (2004) *Mol. Neurobiol.* **29**, 229-242

49. Weeber, E. J., and Sweatt, J. D. (2002) *Neuron* **33**, 845-848

FIGURE LEGENDS

FIG 1. **TGFβ increases Tβ3-P221/110-Luc activity and induces DNA binding at Tβ3-P61/35.** *A*, IEC4-1 cells were seeded in 24-well plates and grown to 70-80% confluence. Cells were transfected with 0.4 μg Tβ3-P221/110-Luc and 0.1 μg renilla luciferase control reporter (pRL-SV40) per well using Lipofectamine™ 2000 (Invitrogen, Carlsbad, CA), as described in the user manual. 24h after the transfection, the cells of the TGFβ3 group were exposed to TGFβ3 (10 ng/ml), whereas the control group was not treated. The cells were harvested at the time points indicated and luciferase assays were performed as described in the "Materials and Methods." Data are plotted as mean ± SE of triplicate samples for each of three independent experiments. Numbers on top of each bar indicate the fold-increase compared to control. *B*, IEC4-1 cells were incubated in the absence or presence of TGFβ3 (10 ng/ml). Nuclear protein was harvested at the time points indicated and EMSAs were performed as described in the "Materials and Methods." The arrow indicates the relevant DNA binding complex. Three independent experiments were carried out and representative figures are shown.

FIG 2. **DN RII and the CRE site in Tβ3-P61/35 are required for TGFβ3 induction of DNA complex formation at Tβ3-P61/35.**

A, IEC4-1 DN RII cells were incubated in the absence or presence of TGFβ1 or TGFβ3 (10 ng/ml), or PMA (100 ng/ml) for 1h. Nuclear extracts were subjected to EMSAs using Tβ3-P61/35 as the probe as described in the "Materials and Methods." Three independent experiments were carried out and representative figures are shown. *B*, IEC4-1 cells were incubated in the absence or presence of TGFβ3 (10 ng/ml) and EMSAs were performed as described in the "Materials and Methods." The probes used for wild type (WT), mutated AP-2 (mAP-2), mutated SBE (mSBE), and mutated CRE (mCRE) of Tβ3-P61/35 were described in the "Materials and Methods." A 10-fold excess of unlabeled Tβ3-P61/35 (cold probe) competed TGFβ-inducible Tβ3-P61/35 DNA binding respectively (lanes 1, 4, 7 and 10). TGFβ3-inducible DNA binding to the TGFβ3 promoter was abolished when mCRE was used as the probe (lane 10, 11, and 12), but not when mAP-2 (lane 4, 5, and 6) or mSBE (lanes 7, 8, and 9) were used as probes. Three independent experiments were carried out and representative figures are shown.

FIG 3. **CREB-1 and Smad3 are the primary components present in the transcription factor complex binding at Tβ3-P61/35.**
Nuclear protein was extracted from IEC4-1 cells and EMSA super shift assays using the antibodies indicated were performed as described in the

"Materials and Methods." *A*, Cells were incubated in the absence or presence of TGFβ3 (10 ng/ml). The probe used was Tβ3-P61/35 as described in the "Materials and Methods." The arrow indicates the super-shifted band. *B*, Cells were incubated in the absence or presence of TGFβ3 (10 ng/ml). The probe used was the full palindromic SBE sequence as described in the "Materials and Methods." *C*, Cells were incubated in the absence or presence of PMA (100 ng/ml). The probe used was Tβ3-P61/35 as described in the "Materials and Methods." The arrow indicates the super-shifted band.

FIG. 4. **Smad3 is required for TGFβ induction of Tβ3-P61/35 DNA binding and Tβ3-P221/110-Luc luciferase reporter activity.** *A*, CCL64 L20 or CCL64 Smad3C cells were incubated in the absence or presence of TGFβ3 (10 ng/ml) or PMA (100 ng/ml) for 1h. Nuclear protein was harvested and EMSAs were performed as described in the "Materials and Methods." Three independent experiments were carried out and representative figures are shown. *B*, CCL64 L20 or CCL64 Smad3C cells were transfected with Tβ3-P221/110-Luc. 24h after the transfection, the cells in the TGFβ3 group were exposed to TGFβ3 (10 ng/ml), whereas the control group was not treated. The cells were harvested after an additional 24 h and luciferase assays were performed as described in the "Materials and

Methods." Data are plotted as mean ± SE of triplicate samples for each of three independent experiments. Numbers on top of each bar indicate the fold-increase compared to control.

FIG. 5. **JNKs and p38, but not PKA or ERKs, are required for TGFβ induction of Tβ3-P61/35 DNA binding and Tβ3-P221/110-Luc luciferase reporter activity.** *A*, IEC4-1 cells were pretreated with either SB203580, PD98059, or SP600125 (Calbiochem, San Diego, CA) at the concentrations indicated for 30 min. Cells were then incubated in the absence or presence of TGFβ3 (10 ng/ml) for 1 h. Nuclear protein was harvested and EMSAs were performed as described in the "Materials and Methods." Three independent experiments were performed and a representative figure is shown. *B*, IEC4-1 cells were transfected with Tβ3-P221/110-Luc. 24h after the transfection, the cells were pretreated with either SB203580, PD98059, or SP600125 at the concentrations indicated for 30 min and then incubated in the absence or presence of TGFβ3 (10 ng/ml) for an additional 24h. The cells were harvested and luciferase assays were performed as described in the "Materials and Methods." Data plotted are the mean ± SE of triplicate samples from one of three independent experiments. Asterisks (*) indicate a statistically significant difference ($p<0.01$) compared with TGFβ3-treated cells in the absence of any inhibitors. *C*, IEC4-1 cells

were pretreated with H89 at the concentrations indicated for 30 min and were then incubated in the absence or presence of TGFβ3 (10 ng/ml) for 1h. Nuclear protein was harvested and EMSAs were performed as described in the "Materials and Methods." Three independent experiments were performed and a representative figure is shown. *D*, IEC4-1 cells were transfected with Tβ3-P221/110-Luc. 24 h after the transfection, the cells were pretreated with H89 at the concentrations indicated for 30 min and were then incubated in the absence or presence of TGFβ3 (10 ng/ml) for an additional 24h. The cells were harvested and luciferase assays were performed as described in the "Materials and Methods." Data plotted are the mean ± SE of triplicate samples from one of three independent experiments.

FIG. 6. **siRNA-CREB-1 and siRNA-Smad3 both suppress TGFβ induction of Tβ3-P61/35 DNA binding and Tβ3-P221/110-Luc luciferase reporter activity.** *A*, IEC4-1 cells transfected with the indicated siRNA plasmids were harvested. Cell lysates were subjected to Western immunoblotting using CREB-1 and Smad3 antibodies as described in the "Materials and Methods." As a loading control, β-actin protein was also detected in the same membrane using an anti-β-actin antibody. The siRNA-Ctrl used was an siRNA-scrambled sequence from Ambion. *B*, upper panel: siRNA transfected IEC4-1 cells as described in *A* were incubated in the

absence or presence of TGFβ3 (10 ng/ml) for 30 min. The cells were then harvested, lysates were prepared, and Western immunoblotting was performed with phospho-CREB-1 and phospho-Smad3 antibodies, as described in the "Materials and Methods." As a loading control, the β-actin protein was also detected in the same membrane using an anti-β-actin antibody. The siRNA-Ctrl used was an siRNA-scrambled sequence from Ambion. Lower panel: Quantitative analysis of the bands in upper panel. The numbers atop the column indicate fold increases compared to control. *C*, siRNA transfected IEC4-1 cells as described in *A* were incubated in the absence or presence of TGFβ3 (10 ng/ml) for 1h. The nuclear protein was harvested and EMSAs were performed as described in the "Materials and Methods." The arrow indicates the relevant DNA complex. Three independent experiments were performed and a representative figure is shown. *D*, IEC4-1 cells were co-transfected with Tβ3-P221/110-Luc and the indicated siRNA plasmids. 24h after the transfection, the cells were incubated in the absence or presence of TGFβ3 (10 ng/ml). The cells were harvested after an additional 24h, and luciferase assays were performed as described in the "Materials and Methods." Data plotted are the mean ± SE of triplicate samples for one of three independent experiments. Asterisks (*)

indicate a statistically significant difference ($p< 0.01$) relative to siRNA-Ctrl.

Fig. 7. **Schematic model for TGFβ3 auto-regulation.** TGFβ3 induces activation of Smad3, JNKs, and p38 through the TGFβ receptors. JNKs and p38 phosphorylate CREB-1 (61, 62), and phospho-CREB-1 forms a transcription factor complex at the Tβ3-P61/35 region of the TGFβ3 promoter, where phospho-Smad3 also binds. The DNA binding of the complex to the TGFβ3 promoter initiates TGFβ3 gene transcription and subsequent TGFβ3 production. The produced TGFβ3 can bind to the TGFβ receptors and stimulate the process again, thus forming an auto-regulatory loop.

Liu & Mulder Fig. 1A

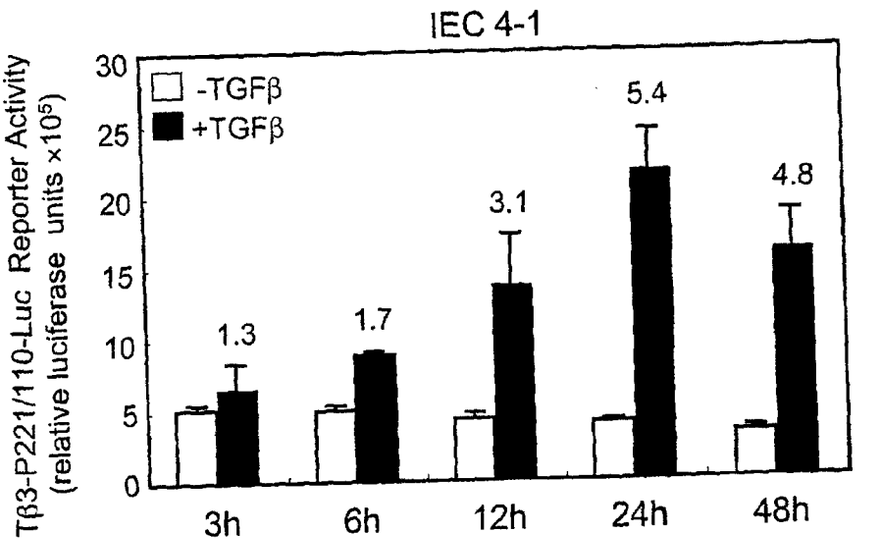

Liu & Mulder Fig. 1B

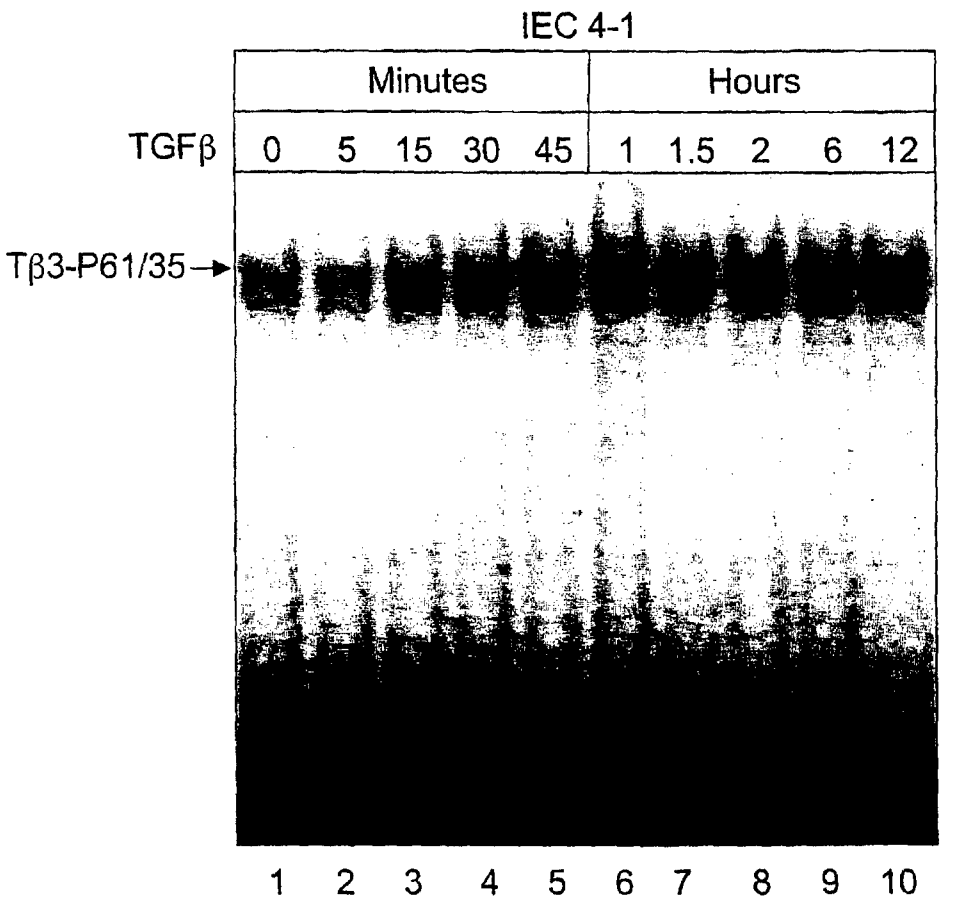

Liu & Mulder Fig. 2A

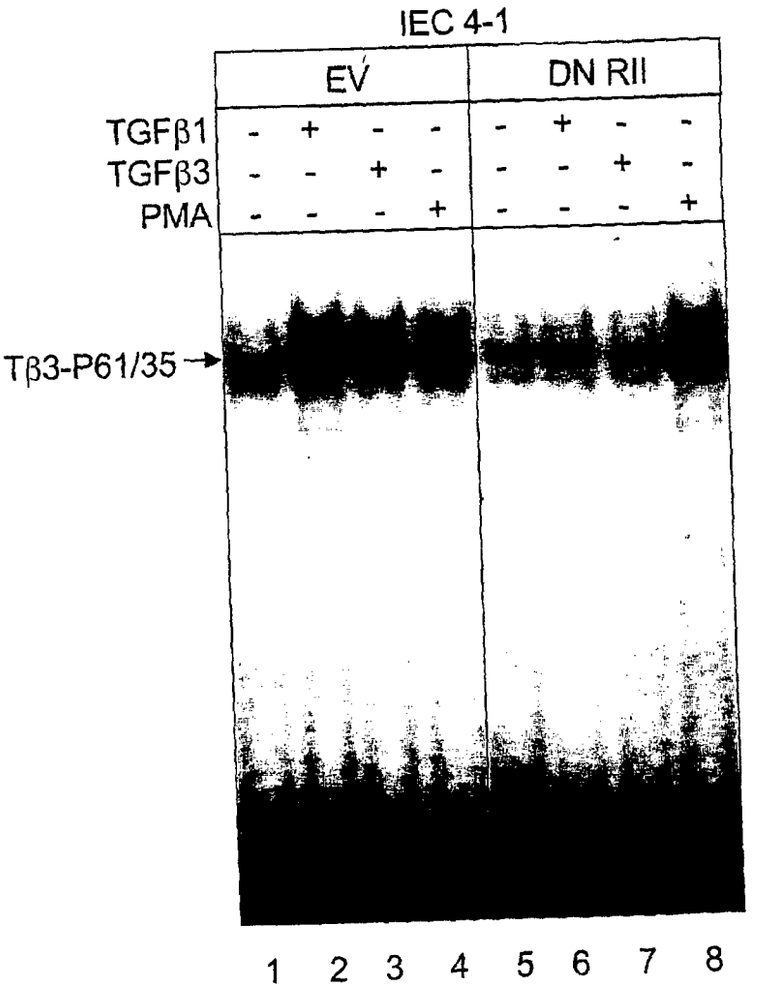

Liu & Mulder Fig. 2B

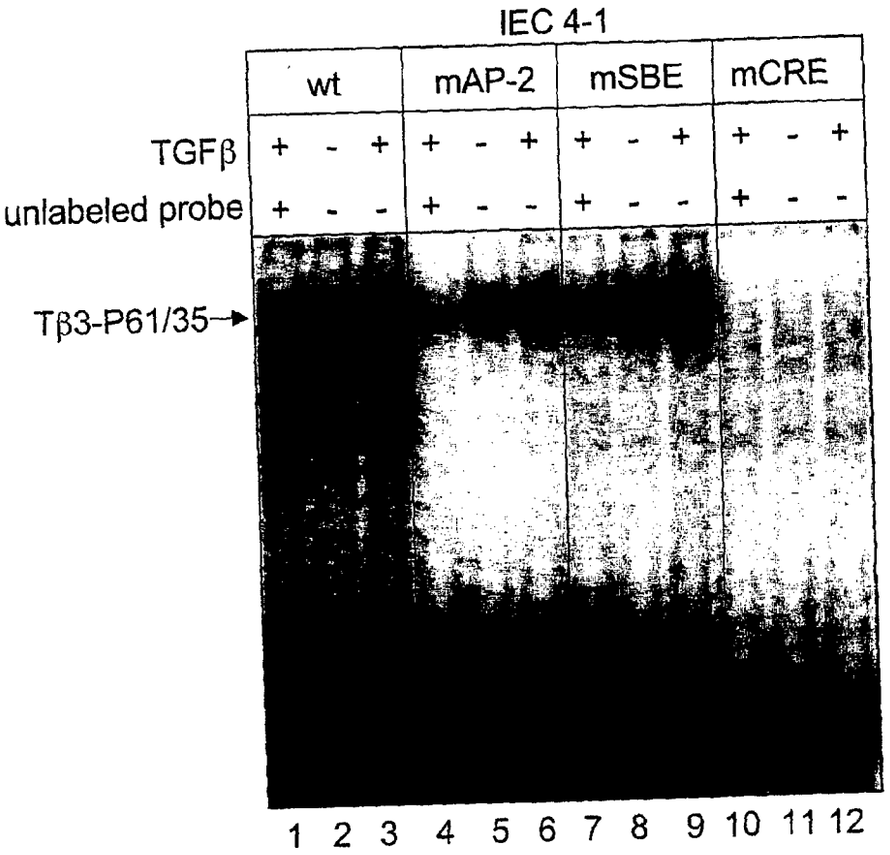

Liu & Mulder Fig. 3A

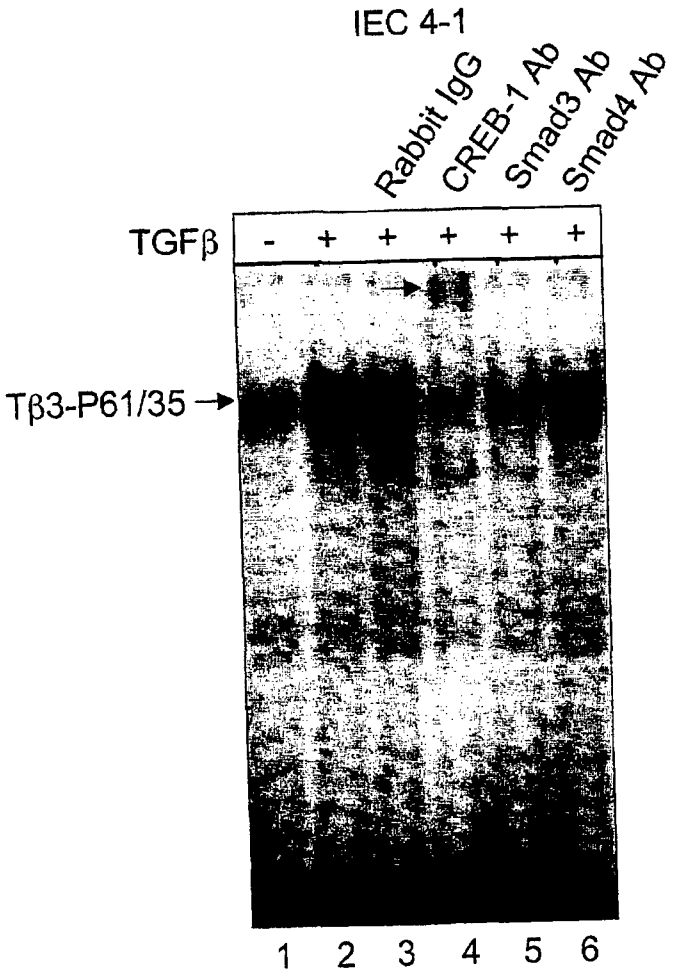

Liu & Mulder Fig. 3B

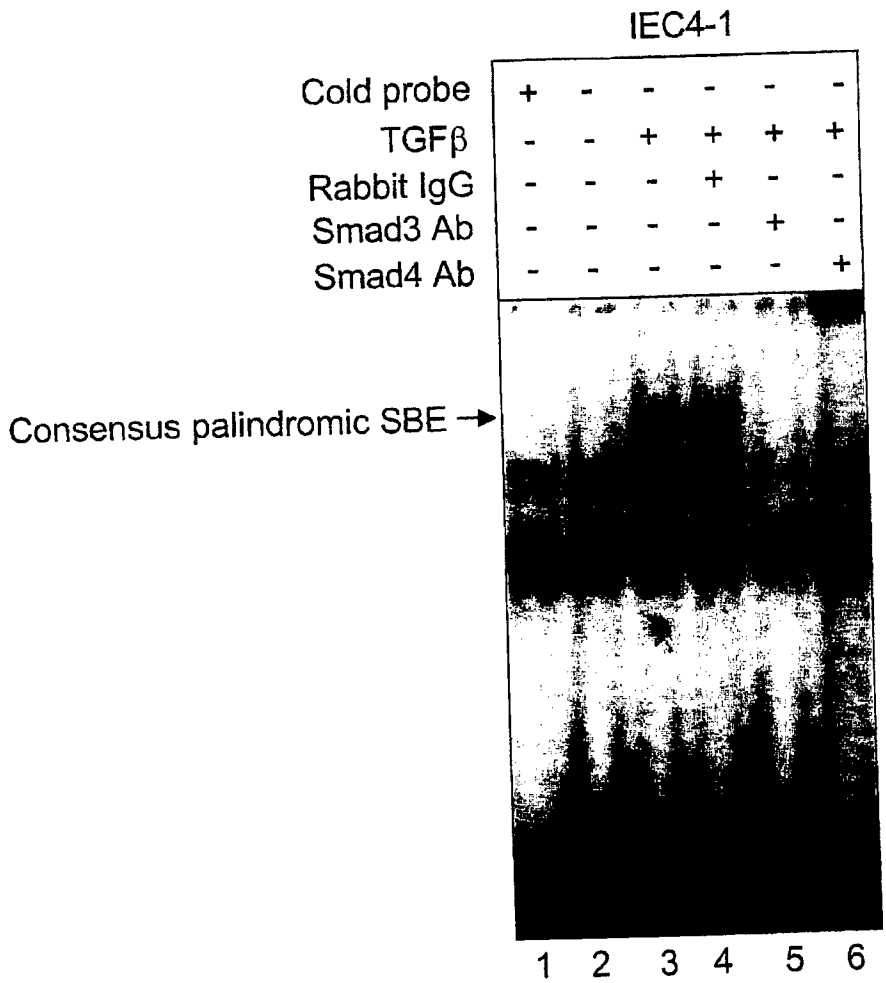

Liu & Mulder Fig. 3C

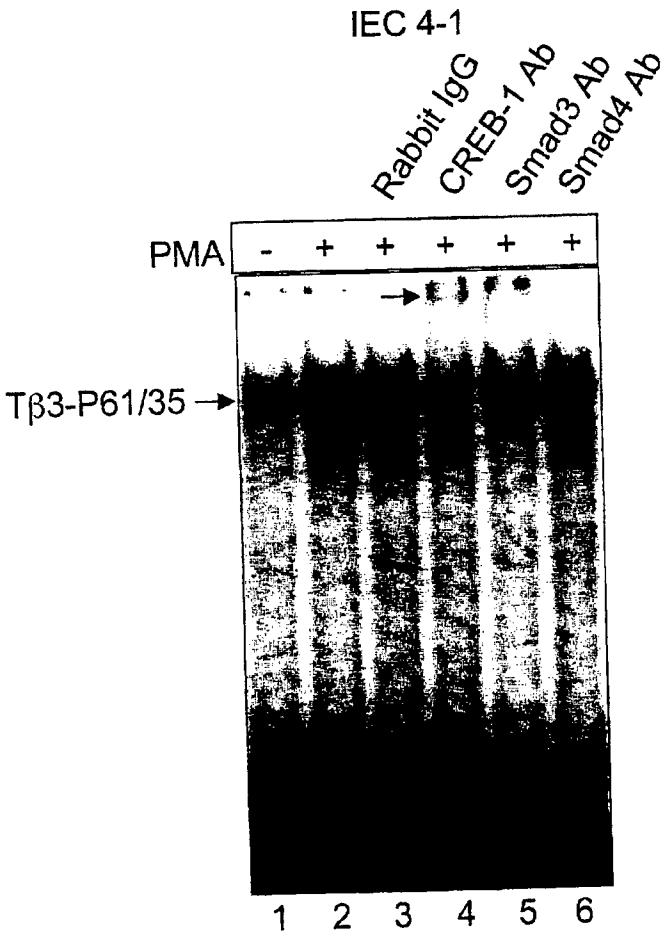

Liu & Mulder Fig. 4A

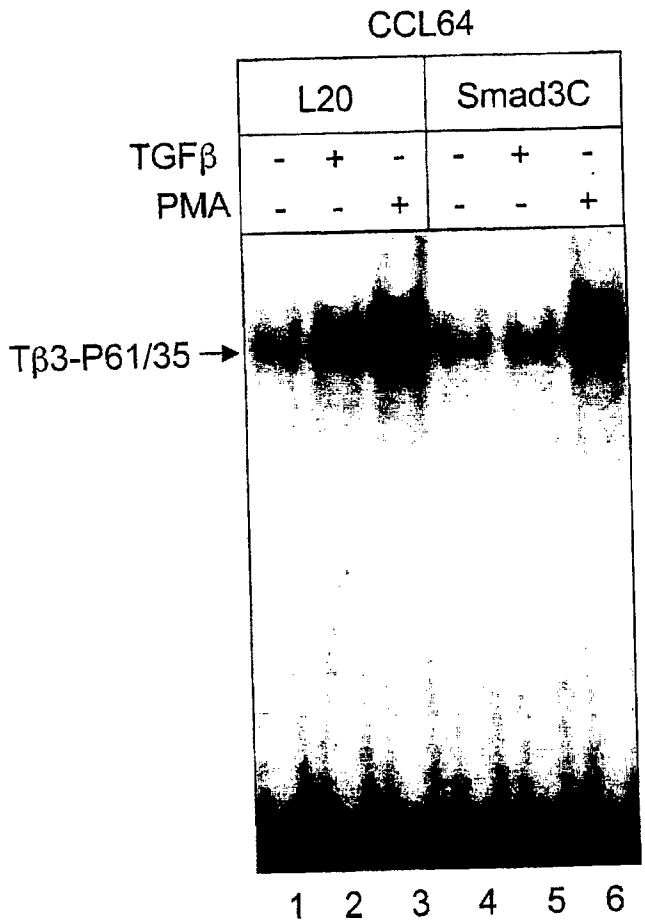

Liu & Mulder Fig. 4B

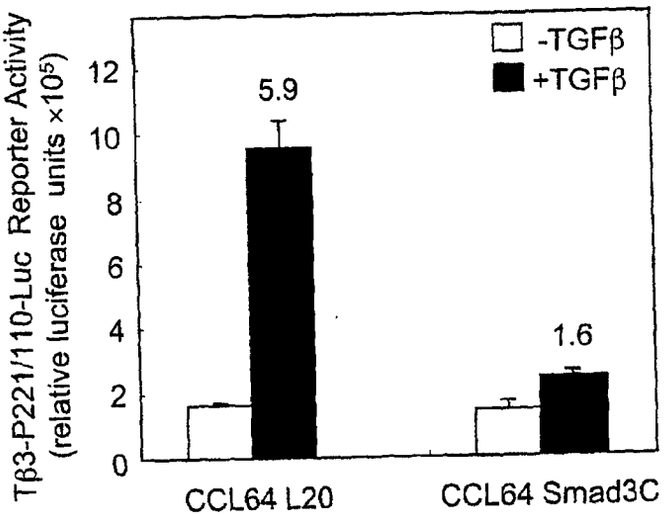

Liu & Mulder Fig. 5A

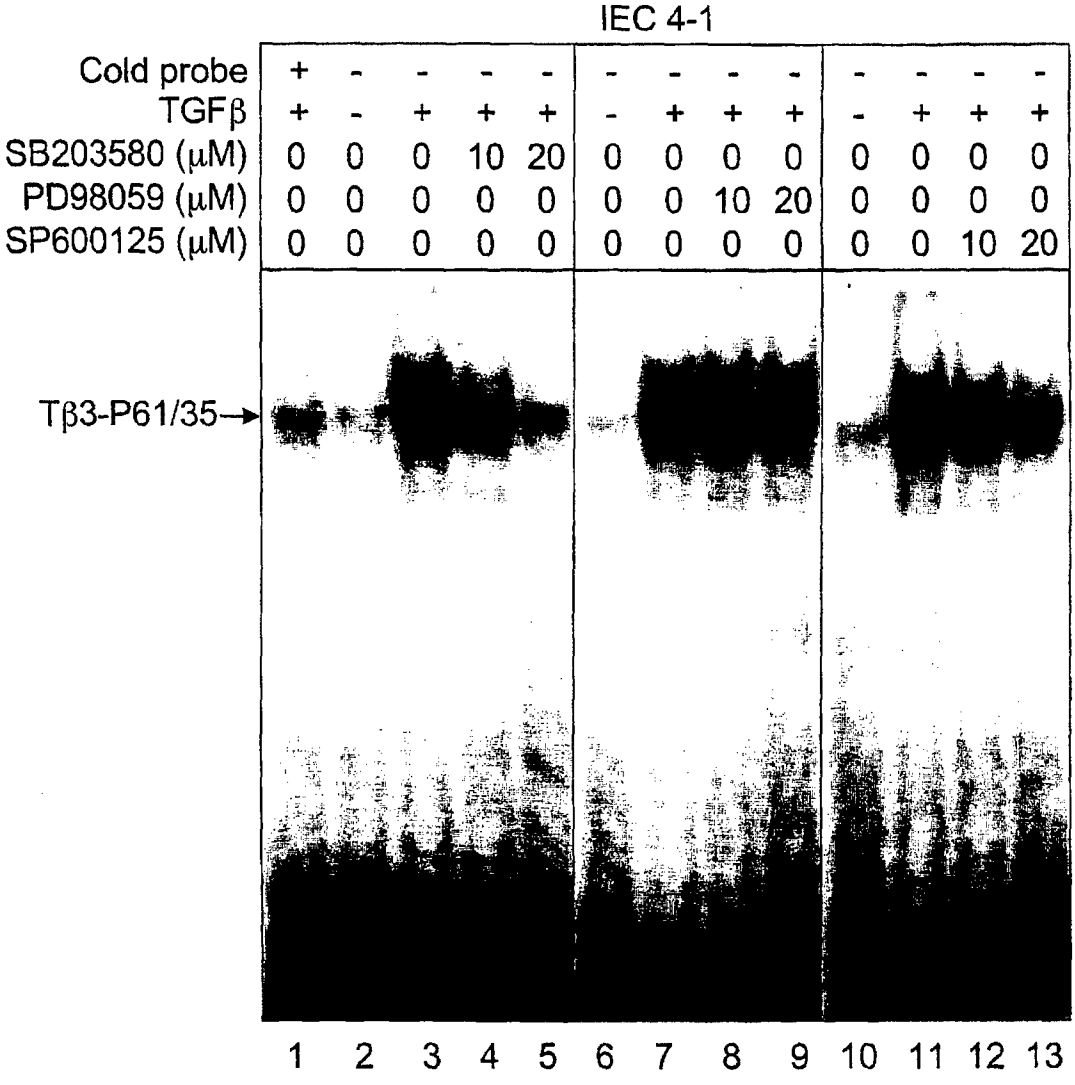

Liu & Mulder Fig. 5B

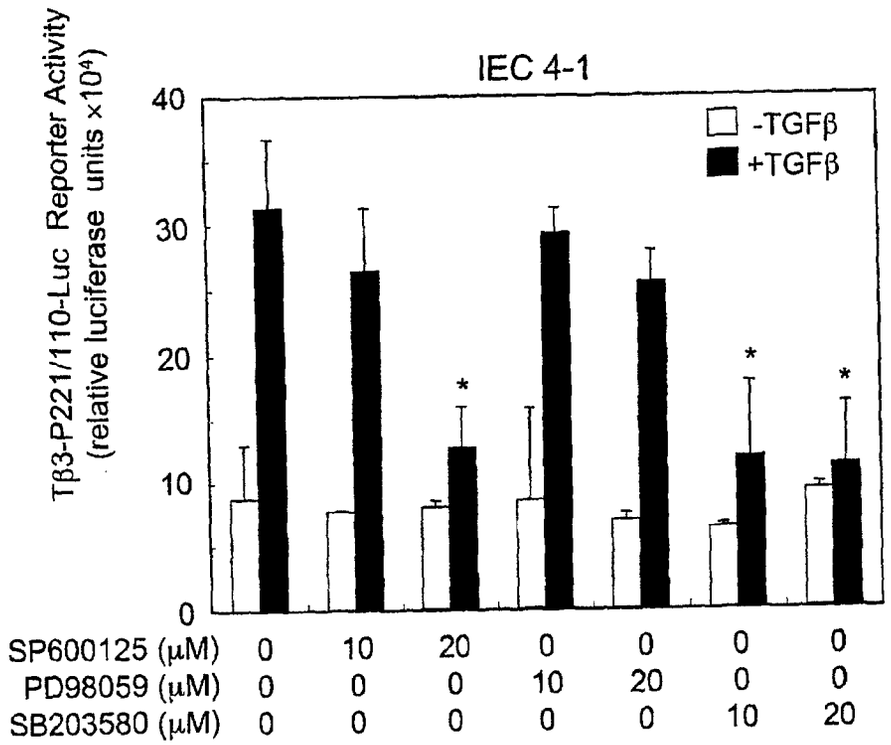

Liu & Mulder Fig. 5C

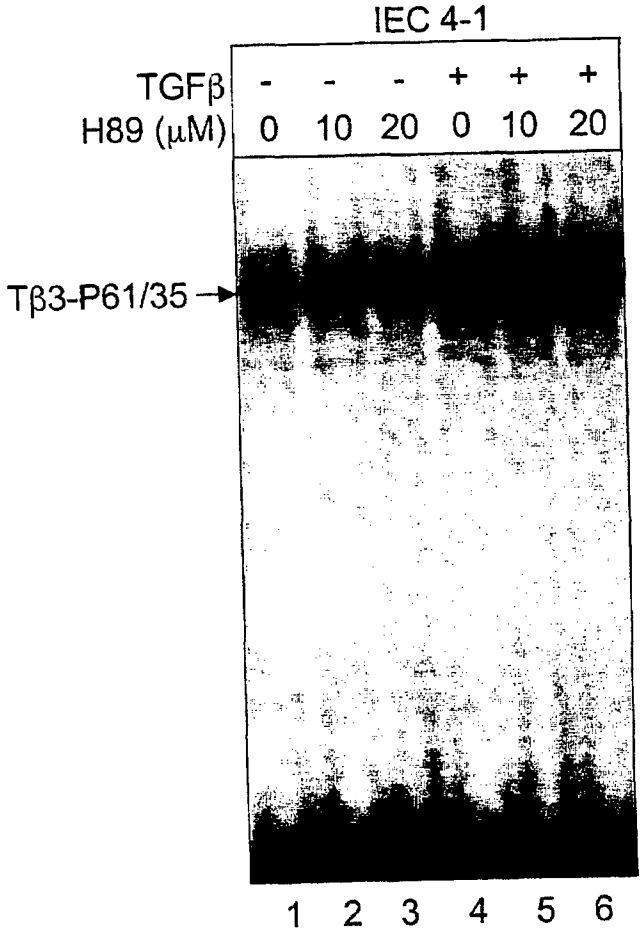

Liu & Mulder Fig. 5D

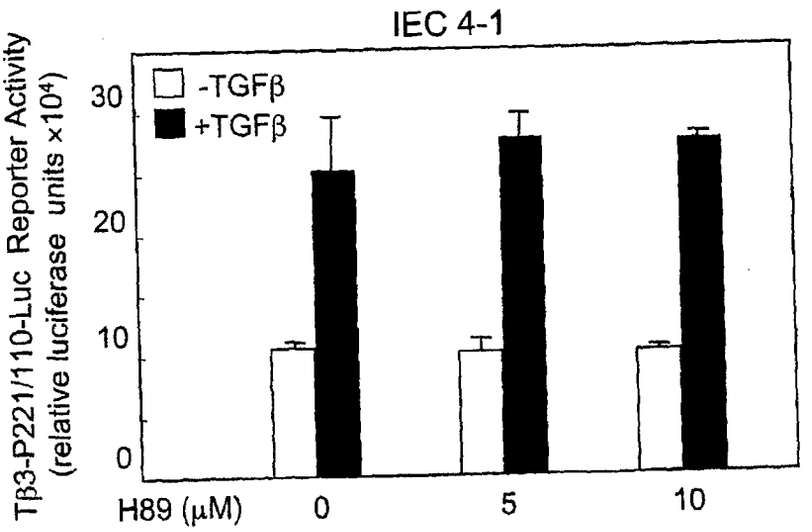

Liu & Mulder Fig. 6A

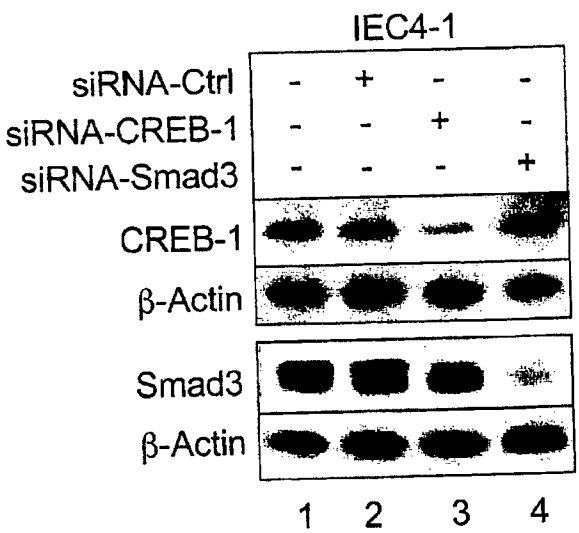

Liu & Mulder Fig. 6B

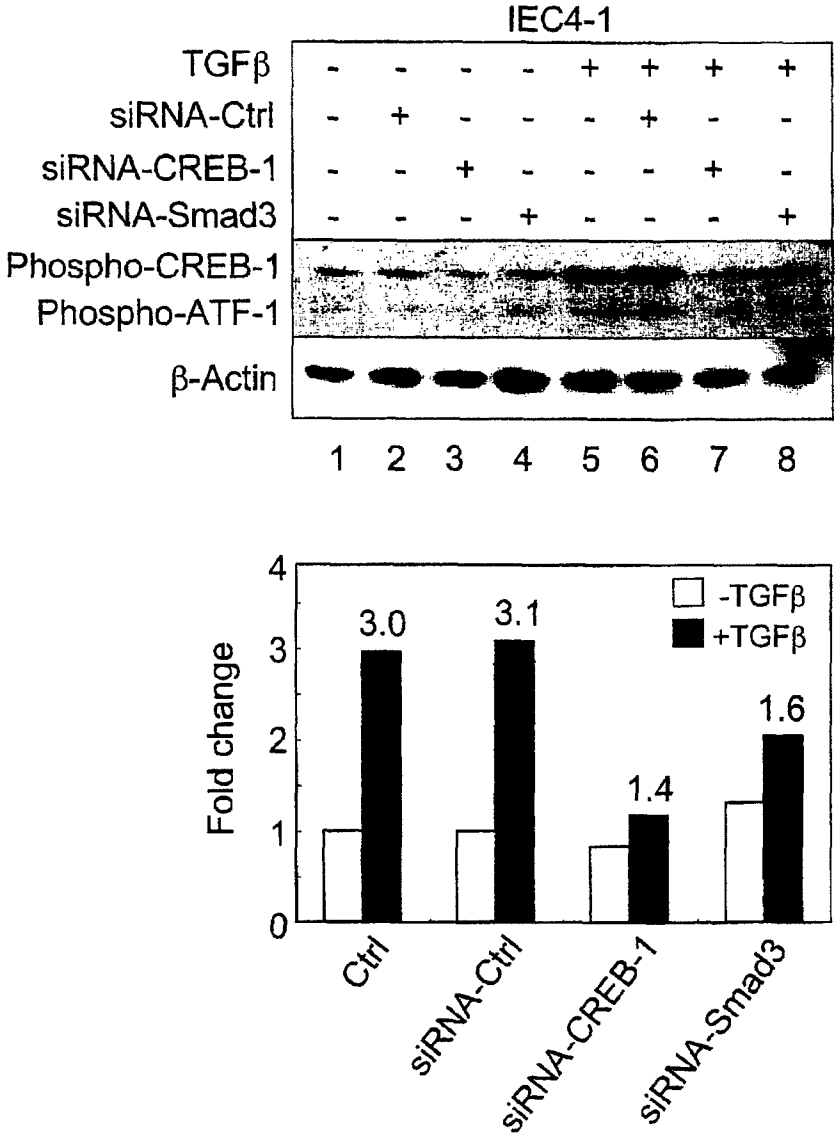

Liu & Mulder Fig. 6C

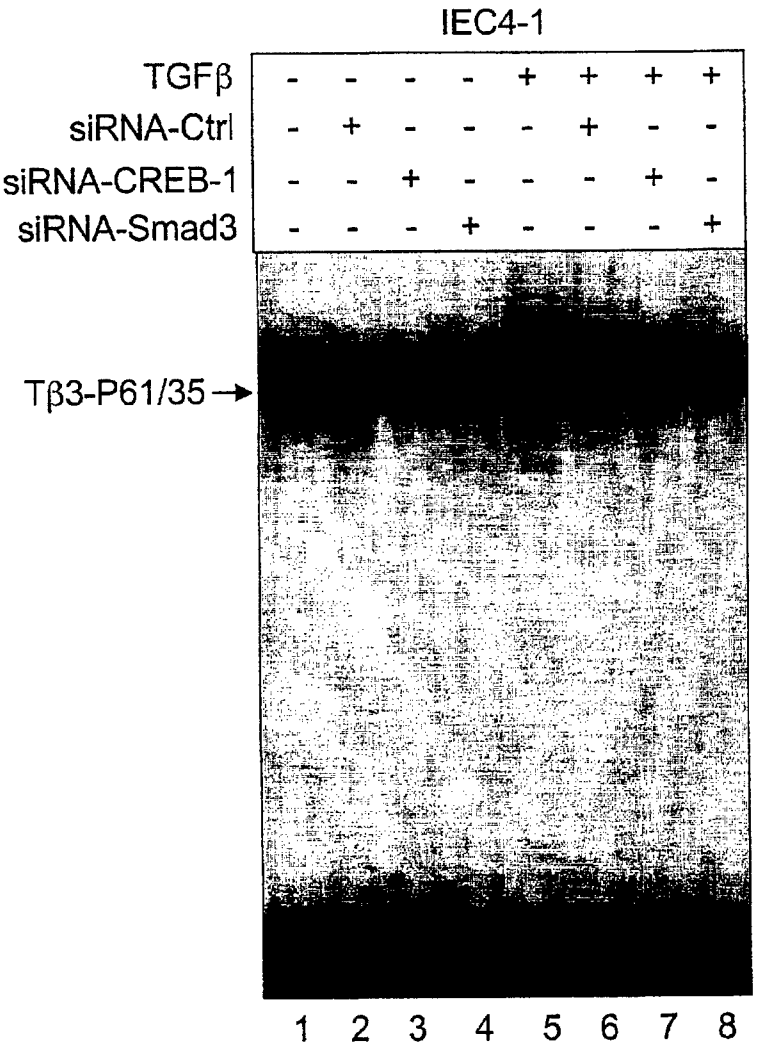

Liu & Mulder Fig. 6D

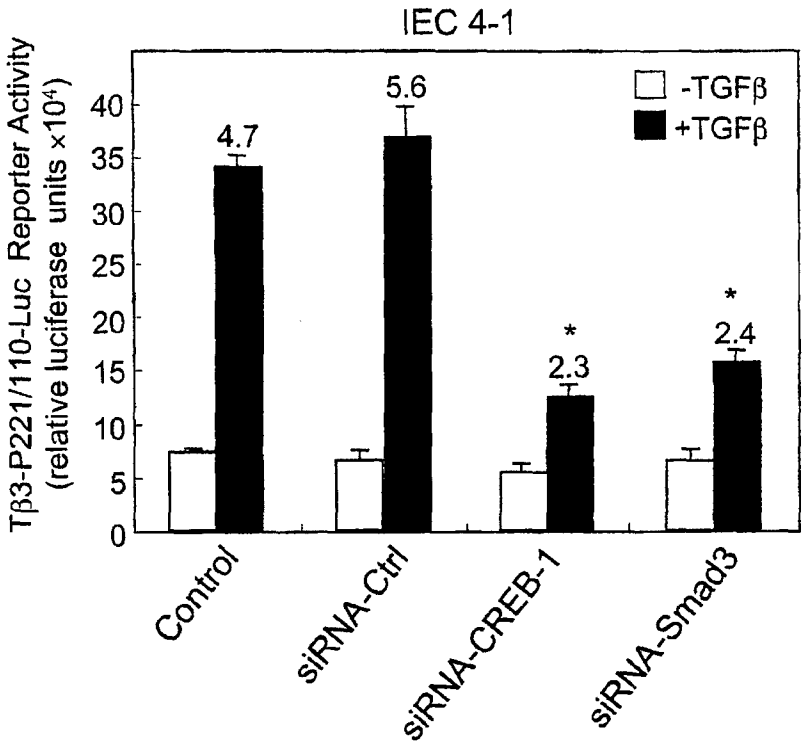

Liu & Mulder Fig. 7

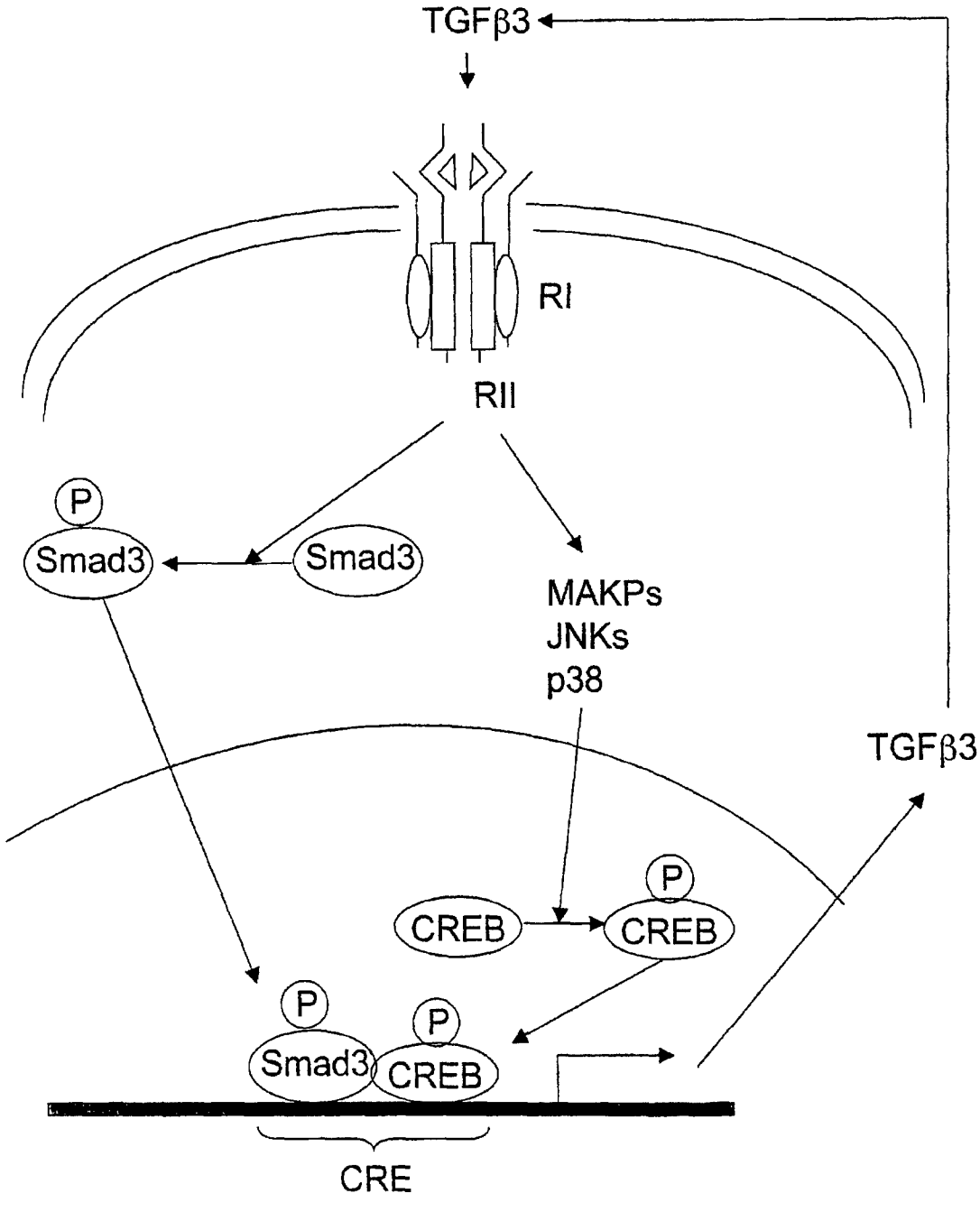

J. Biol. Chem., In Revision, 2005

Requirement for km23 in a Smad2-dependent TGFβ signaling pathway

Qunyan Jin*, Wei Ding*, and Kathleen M. Mulder*[¶]

*Department of Pharmacology, Pennsylvania State University

College of Medicine, 500 University Dr., Hershey, PA 17033

[¶]To whom correspondence should be addressed:

Department of Pharmacology---MC H078

Penn State College of Medicine

500 University Drive, Hershey, PA 17033

Telephone: 717-531-6789; FAX: 717-531-5013

E-mail: kmm15@psu.edu

Running title: km23 in Smad2 signaling

Key words: TGFβ, siRNA, Smad2, km23, dynein

ABSTRACT

We have identified km23 as a novel transforming growth factor β (TGFβ) receptor-interacting protein that is also a light chain of the motor protein dynein. Here we show that km23 is co-localized with the TGFβ signaling component Smad2 at early time periods after TGFβ treatment of Madin Darby canine kidney (MDCK) epithelial cells, prior to translocation of Smad2 to the nucleus. Further, km23 interacted with Smad2, but not Smad3, in both immunoprecipitation (IP) /blot and glutathione-S-transferase (GST) pull-down assays. More significantly, km23 interacted with Smad2 once it had been phosphorylated by constitutively active TGFβ RI in vivo. Further, blockade of km23 using small interfering RNA (siRNA) significantly reduced the levels of phosphorylated Smad2, nuclear expression of Smad2, and TGFβ-dependent Smad2 transcriptional activation. Our findings demonstrate that km23 is required in a Smad2-dependent TGFβ signaling pathway.

INTRODUCTION

TGFβ is the prototype of a large family of structurally related growth and differentiation factors that show remarkable diversity in the biological actions they mediate (Yue and Mulder, 2001; Derynck and Zhang, 2003; Shi and Massague 2003). These biological responses include effects on cell growth, cell death, cell differentiation, and the extracellular matrix. The effects are often cell type and context dependent (Yue and Mulder, 2001; Derynck and Zhang, 2003; Shi and Massague 2003).

TGFβ initiates its signals by producing an active tetrameric receptor complex consisting of RI and RII serine/threonine kinase receptors. After TGFβ binds to RII, it transphosphorylates, and thereby activates RI. The activated form of RI can phosphorylate Smad2 and Smad3, and these receptor-activated Smads (RSmads) then form a complex with Smad4. The TGFβ-activated, heteromeric Smad complexes are translocated to the nucleus, where they induce or repress transcription of defined genes, either directly by binding to congnate DNA consensus sites, or indirectly by interaction with other transcription factors, such as forkhead activin signal transducer (FAST)-1, FAST-2, c-jun, and c-fos (Derynck and Zhang, 2003; Roberts et al, 2003; Shi and Massague, 2003).

In addition to the RSmads, several other TGFβ receptor-interacting proteins have been identified. Some of these appear to play a role in TGFβ receptor internalization and vesicular trafficking, events involving Smad recruitment to the receptors (Derynck and Zhang, 2003). For example, SARA

and Dab2 bind both the TGFβ receptors and the RSmads, to promote RSmad phosphorylation and TGFβ signaling (Hocevar, 2001; Di Guglielmo et al., 2003). In addition, cytoskeletal proteins play a role in the localization and signaling of Smads (Denryck and Zhang, 2003). For example, unphosphorylated Smads2/3/4 bind microtubules (MTs), and TGFβ treatment induces their dissociation from these cytoskeletal components (Dong et al., 2000). Filamin, an actin crosslinking factor and scaffolding protein, also associates with Smads and positively regulates transduction of Smad signals (Sasaki et al., 2001). Collectively, these findings indicate that the interactions among TGFβ receptors, Smads, adaptor/scaffolding proteins, and cytoskeletal elements represent important regulatory mechanisms in TGFβ signaling.

km23 was identified as a novel TGFβ receptor-interacting protein that is also a light chain of the motor protein dynein (Tang et al., 2002). We have previously shown that TGFβ RII is absolutely required for km23 phosphorylation and interaction of km23 with the dynein intermediate chain (DIC). Collectively, our previous results suggested that TGFβ pathway components (such as Smads) might use km23 as an adaptor or motor receptor for their recruitment and transport along MTs (Tang et al., 2002; Wei and Mulder, 2004).

We demonstrate here that km23 is co-localized with the TGFβ signaling component Smad2 at early time periods after TGFβ treatment, prior to translocation of Smad2 to the nucleus. km23 interacted with Smad2, once this RSmad had been phosphorylated by constitutively active TGFβ RI in vivo. We also demonstrate a direct interaction between km23 and Smad2 in vitro. Further,

blockade of km23 reduced the levels of phosphorylated Smad2, nuclear expression of Smad2, and TGFβ-dependent Smad2 transcriptional activation. Thus, km23 appears to be a signaling intermediate in a Smad2-dependent TGFβ pathway.

MATERIALS AND METHODS

Reagents--The anti-Flag M2 (F3165) antibody (Ab) and mouse IgG were from Sigma-Aldrich (St. Louis, MO). The anti-DIC monoclonal Ab (MAB1618) was from Chemicon (Temecula, CA). The rabbit IgG was from Santa Cruz Biotechnology, Inc. (Santa Cruz, CA). TGFβ_1 was purchased from R & D Systems (Minneapolis, MN). The phospho-Smad2 Ab (3101) was from Cell Signaling Technology (Beverly, MA). The rabbit Smad2 Ab (51-1300) was from Zymed (South San Francisco, CA). The mouse anti-Smad2/3 (610843) was from BD Biosciences Transduction Laboratories (Palo Alto, CA). The Fugene 6 transfection reagent was from Roche Applied Science (Indianapolis, IN).

Antibody production-- The rabbit polyclonal km23 anti-serum used for the immunofluorescence studies was prepared against the following sequence: MAEVEETLKRLQS (corresponding to amino acids 1-13 of human km23) (Strategic BioSolutions, Newark, DE). The rabbit km23 anti-serum used for Western blotting analysis was prepared against the following sequence: GIPIKSTMDNPTTTQYA (corresponding to amino acids 27-43) of human km23 (Strategic BioSolutions, Newark, DE). The company also provided pre-immune serum.

Cell culture-- Mv1Lu (CCL-64) cells and 293T cells were purchased from American Type Culture Collection (Manassas, VA) and were grown in DMEM supplemented with 10% FBS. MDCK cells (CCL-34) was also obtained from

ATCC and were grown in MEM-α supplemented with 10% FBS. Cultures were routinely screened for mycoplasma using Hoechst 33258 staining.

Transient transfections, IP/blot, Westerns-- were performed essentially as described previously (Hocevar et al., 1999; Yue et al., 1999a; b; Yue and Mulder, 2000; Tang et al., 2002).

GST Pull –Downs-- were performed essentially as described previously (Tang et al; 2002).

siRNAs --a km23 siRNA pSIREN construct to target the human km23 (251st~271st nucleotide, 5'-AAGACTATTTCCTGATTGTGA-3') was prepared. This km23 siRNA also can knock down rat and mouse km23, since this targeting sequence is identical among human, rat, and mouse. In addition, we have made a negative control siRNA (NC siRNA) plasmid, the sequence of which does not match any genes by alignment with the NCBI database using BLAST. All of these constructs contain a human RNA polymerase III U6 promoter and can form a hairpin structure in vivo that is quite similar to chemically synthesized double-stranded siRNA. The pSIREN empty vector was purchased from BD Clontech (Cat# 631529).

Immunofluorescence -- For km23 and Smad2 co-localization experiments, MDCK cells were fixed with 4% paraformaldehyde in phosphate-buffered saline for 20 min at room temperature, and permeabilized with 0.5% Triton X-100 in phosphate-buffered saline for 5 min. Subsequently, these cells were incubated with km23 rabbit anti-serum (1:200) and 5 μg/ml anti-Smad2/3 monoclonal Ab for 1 h, respectively. The bound primary antibodies were visualized with 2 μg/ml

Alexa 594 goat anti-rabbit IgG or Alexa 488 goat anti-mouse IgG, respectively. Immunofluorescence images were captured using a Nikon Diaphot microscope with a Retiga 1300 CCD camera (BioVision Technologies, Inc., Exton, PA) running IPLab v3.6.3 software (Scanalytics, Inc., Fairfax, VA). For immunofluorescence analysis to study the effects of siRNA's on nuclear translocation of Smad2 by TGFβ, the cells were analyzed as for the co-localization studies, except that the cells were incubated only with 5μg/ml anti-Smad2/3 monoclonal Ab, and then the bound Ab was visualized with 2 μg/ml Alexa 594 goat anti-mouse IgG. One hundred green fluroscence protein (GFP) positive cells were counted for cultures with both km23 siRNA-transfected and NC siRNA-trasnsfected cells. DAPI staining designates individual cells. Triplicate fields are shown for each condition.

Luciferase reporter assay– Mv1Lu cells were plated at 1×10^4 cells/cm^2 in 12-well plates. Twenty-four hours after plating, the cells were transfected with the indicated amounts of either km23 siRNA or NC siRNA, together with activin-responsive element (ARE)-Lux and FAST-1 (Chen et al; 1996) or Smad-binding element (SBE)-Luc (Zawel et al; 1998). Renilla was used to normalize transfection efficiencies, and pcDNA3.1 was used to normalize the amount of total DNA transfected. Twenty-four hours after transfection, the medium was replaced with DMEM serum-free medium. One hour after incubation, Mv1Lu cells were cultured in the absence or presence of TGFβ (5ng/ml) for another 18 h. The luciferase activity was measured using Promega's Dual-luciferase

Reporter Assay System (Cat# E1960) following the manufacturer's instructions.

All assays were performed in triplicate. Data are expressed as mean±SEM.

RESULTS

Our previous data suggested that km23 might function as a "motor receptor" to recruit TGFβ signaling complexes to the dynein motor complex for intracellular transport along MTs toward the nucleus (Tang et al; 2002). Since Smad2/3 is a critical intracellular mediator of TGFβ responses (Attisano and Wrana, 1998, Massague 1998), co-localized with RII in specific endosomal compartments after receptor endocytosis (Hayes et al., 2002), it was conceivable that Smad2/3 might function as one of the cargo that km23 could recruit for intracellular transport. If this were the case, we would expect that km23 could interact with Smad2/3. Thus, we performed GST pull-down assays after transfection of either empty vector, Smad2-Flag, or Smad3-Flag into 293T cells. Cell lysates were incubated with sepharose-bound, bacterial-expressed GST alone or GST-km23. An anti-Flag Ab was used as the blotting Ab to detect Smad2-Flag in the GST-km23 complex. As shown in Fig. 1A, Smad2 was visible in the GST-km23 immunoprecipitates (lane 4), but not in the immunoprecipitates from GST only (lane 3). Empty vector control lanes were also negative (lanes 1, 2). Since both Smad2 and Smad3 are regulated by TGFβ, we also examined whether Smad3 could bind km23 in vitro. However, in contrast to Smad2, Smad3 was not observed in the GST-km23 immunoprecipites (lane 6). The interaction between the Smad binding domain (SBD) of SARA and Smad2-Flag (Tsukazaki et al; 1998) is shown as a positive control for comparison (lane 8).

Our results indicate that km23 interacts with Smad2, but not Smad3, in vitro. Differential binding of Smad2 and Smad3 to signaling components has been reported previously. For example, PKB/Akt has been shown to modulate TGFβ signaling through a direct interaction with Smad3, but not Smad2 (Remy et al; 2004). In addition, Smad2 and Smad3 have been shown to be activated by different pool of receptors (Felici et al; 2003). Thus, it is not unexpected that a different dynein light chain would be involved Smad binding to the motor machinery.

Since Smad2 interacted with km23 in vitro, we proceeded to examine whether the two proteins could interact in vivo. For these studies, we performed IP/blot analyses after transfection of km23-Flag and Smad3-Flag or Smad2-Flag, in the absence or presence of constitutively activated TGFβ RI (T204D-HA). As shown in Fig. 1B, in the presence of T204D-HA, immunoprecipitation of the Smad2 protein with anti-Smad2, resulted in co-IP of km23-Flag and Smad2 (lane 4). This km23-Smad2 interaction did not occur in the absence of activated TGFβ RI (T204D-HA) (lane 3). Further, Smad3 did not interact with km23 under similar conditions (lanes 6-7), indicating specificity for Smad2 as in Fig. 1A. As expected, no band was visible for the IgG control (lanes 2, 5). The data suggest that Smad2 phosphorylation by constitutively active TGFβ RI is required for Smad2 interaction with km23.

Since we have shown that km23 interacted with Smad2 in two different assays, we would expect that Smad2 might be co-localized with km23 in a vesicular compartment intracellularly. Thus, we performed immunofluorescence

studies in TGFβ-responsive MDCK cells, using km23-specific rabbit anti-serum prepared against amino acids 1-13. As indicated in Fig. 2A, in the absence of TGFβ treatment, endogenous km23 was present in perinuclear puncta, whereas Smad2 displayed a somewhat different pattern of punctate staining. TGFβ treatment resulted in a greater co-localization of Smad2 with km23 at both 2 min (Fig. 2B) and 5 min (Fig. 2C) after TGFβ addition to MDCK cells. In contrast, once Smad2 had translocated to the nucleus by 15 min after TGFβ treatment (Fig. 2D), km23 was still localized in the cytoplasm and was no longer co-localized with Smad2. For all studies, the preimmune serum and relevant IgG controls were negative, confirming the spcecificity of the km23 Ab. Thus, our results clearly indicate that km23 and Smad2 are co-localized intracellularly at 2 and 5 min after TGFβ treatment, prior to the entry of Smad2 into the nucleus.

If km23 could function as a motor receptor to transport Smad2 intracellularly along MTs by means of the dynein motor, it might expected that blockade of endogenous km23 would block Smad2-dependent events such as phosphorylation, nuclear expression, and transcriptional regulation. In order to explore this possibility, we developed km23 siRNA to knock down km23 expression. As shown in Fig. 3A, we transiently transfected Mv1Lu cells with km23 siRNA or NC siRNA and GFP-km23, and evaluated the level of km23 siRNA and NC siRNA blockade of GFP-km23 expression as described in Materials and Methods. There are approximately 20% GFP-positive cells in the NC siRNA-transfected cultures (top panels, right). In contrast, there are only a few positive cells in the km23 siRNA-transfected cells (bottom panels, right),

suggesting a significant level of knockdown of km23 expression. A similar result was observed at 48 h post-transfection (data not shown).

To determine whether km23 siRNA could specifically knock down endogenous km23, we transiently transfected 293T cells with either km23 siRNA or NC siRNA. As shown in Fig.3B, km23 siRNA resulted in a marked decrease (compared to NC siRNA) in km23 levels at both 24 h (lanes 1-2) and 48 h (lanes 3-4) after addition of the siRNAs. Collectively, the results in Fig. 3 indicate that the km23 siRNA could specifically block expression of the km23 protein.

Since km23 siRNA resulted in maximal silencing at 24h after addition to Mv1Lu cells, we performed Western blot analysis to examine whether blockade of km23 would block TGFβ induction of Smad2 phosphorylation during this time period. As shown in Fig. 4, TGFβ treatment of NC siRNA-transfected cells resulted in phosphorylation of Smad2 as early as 5 min after TGFβ treatment (left, top panel). Levels of phosphorylated Smad2 continued to increase to values 9-fold above basal levels by 15 min after TGFβ (left, bottom panel). In contrast, in the km23 siRNA-transfected cells TGFβ induction of Smad2 phosphorylation was reduced to values 2-4 fold above baseline levels at similar time points (right, top and bottom panels). Equal Smad2 expression was confirmed by Western blotting (middle panel). The results in Fig. 4 indicate that km23 is partially required for the TGFβ-mediated increase in phospho-Smad2 levels that occurs at early times after TGFβ treatment (5-15 min).

We also performed immunofluorescence studies to determine whether blockade of km23 could block nuclear expression of Smad2 by TGFβ in

individual cells. Mv1Lu cells were transiently transfected with either NC siRNA or km23 siRNA and GFP. As shown in Fig. 5A, in the absence of TGFβ, the NC siRNA-transfected cells and the km23 siRNA-transfected cells displayed the same pattern of punctate staining. However, while the NC siRNA-transfected, GFP-positive cells still displayed nuclear expression of Smad2 in response to TGFβ (Fig. 5B), the km23 siRNA-transfected, GFP-positive cells displayed barely detectable levels of nuclear Smad2 expression (Fig. 5C). As expected, the non-transfected cells in Figs. 5B and C responded to TGFβ with significant Smad2 translocation.

In order to quantify siRNA effects on TGFβ-mediated nuclear expression of Smad2, we counted one hundred GFP positive cells in cultures of either km23 siRNA-transfected or NC siRNA-trasnsfected cells treated with TGFβ (5ng/ml). Of these 100 GFP-positive cells, the cells showing nuclear expression of Smad2 were counted as described in Materials and Methods. As shown in Table1, in NC siRNA-transfected cells, 93% of the GFP-positive cells displayed Smad2 nuclear expression in response to TGFβ. As expected, 100% of the GFP-negative cells responded to TGFβ with Smad2 translocation, whether NC or km23 siRNA had been transfected. In contrast, in the km23 siRNA-transfected cells, 89% of the GFP-positive cells displayed barely detectable levels of nuclear Smad2 expression. Thus, only 11% of the km23 siRNA, GFP-positive cells still displayed nuclear expression of Smad2. Our results demonstrate that km23 is required for the nuclear expression of Smad2 induced by TGFβ.

The transcriptional activity of Smad2 is dependent upon its prior phosphorylation and translocation (Macias-Silva et al; 1996). Since blockade of km23 could reduce both the levels of phosphorylated Smad2 and the nuclear expression of Smad2, it was of interest to determine whether blockade of km23 could also influence the transcriptional activity of the Smad2 protein. To assess this, we transiently transfected Mv1Lu cells with either km23 siRNA or NC siRNA and ARE-Lux/FAST-1 for analysis of ARE luciferase reporter activity. This reporter has previously been shown to be activated by TGFβ or activin in a Smad2-dependent manner (Chen et al; 1996). As shown in Fig. 6A, a strong (up to 28-fold) activation the ARE-Lux reporter by TGFβ was achieved in both mock-transfected and NC siRNA-transfected cells. However, the cells transfected with km23 siRNA displayed a significant decrease in TGFβ-stimulated ARE-Lux induction to levels of only 10-fold. The results in Fig. 6A indicate that km23 is required for TGFβ induction of Smad2-dependent transcriptional activity.

Since an interaction between km23 and Smad3 was not observed in either GST pull-down or IP/blot assays, we would not expect the km23 siRNA to influence the transcriptional activity of the Smad3 protein. In order to examine whether this was case, we transiently transfected Mv1Lu cells with either km23 siRNA or NC siRNA and the SBE-Luc reporter in the absence or in the presence of TGFβ treatment. The SBE-Luc reporter has been used previously to demonstrate whether a Smad3/4–specific response can been induced by TGFβ (Zawel et al; 1998). Our results demonstrate that blockade of km23 had no effect

on Smad3-dependent TGFβ signaling (Fig. 6B), further confirming that km23 is specifically required for Smad2-dependent TGFβ signaling.

DISCUSSION

We have previously reported that km23 is both a TGFβ receptor-interacting protein and a light chain of the motor protein dynein. Kinase-active TGFβ receptors are required for km23 phosphorylation and recruitment of km23 to the dynein motor complex, suggesting that subsequent to receptor activation, TGFβ signaling components may be transported along MTs through the interaction of km23 with DIC (Tang et al; 2002). Here, we show that km23 interacts with the TGFβ signaling intermediate Smad2 both in vitro and in vivo. Furthermore, km23 partially co-localizes with Smad2 in a TGFβ-dependent manner. More importantly, using siRNA approaches, we demonstrate for the first time, that km23 is required for TGFβ stimulation of Smad2 phosphorylation, nuclear expression of Smad2, and Smad2-dependent ARE transcriptional activation.

Previous work has indicated that Smad2/3 activation by TGFβ is dependent upon receptor internalization (Penheiter et al., 2002). Further, activated TGFβ receptors are known to be internalized into EEA1/SARA-enriched endosomes where Smad2 is recruited by SARA (Hayes et al., 2002; Di Guglielmo et al., 2003). Smad2/3 can then be phosphorylated by the TGFβ receptors to promote TGFβ signaling, prior to receptor degradation. From our results, it appears that km23 is being phosphorylated by the activated TGFβ receptors and is recruited to the dynein motor complex in approximately the same time frame as RSmad activation (Tang et al; 2002). Thus, km23 may

function at a point after Smad2 has become localized to a specific endosomal compartment to affect the next step in the intracellular transport process. In this way, km23 may provide a key link in the signaling of Smad2-specific TGFβ responses.

Although Smad2 and Smad3 are highly homologous and share some overlapping activities, they have distinct functions and are regulated differentially (Liu, 2003; Roberts and Wakefield 2003). For example, Smad2 and Smad3 have opposite activities on the goosecoid (gsc) promoter, in that Smad2 activates it, while Smad3 represses it (Labbe et al; 1998). Moreover, a recent study about a receptor-associated protein has led to a model whereby Smad2 and Smad3 are activated by different pools of TGFβ receptors (Felici et al; 2003). Thus, there appears to be some specificity for RSmad segregation into vesicular compartments. Our studies support such a model, since we have shown that activated Smad2 can bind km23, whereas activated Smad3 cannot. We also show that blockade of km23 reduces TGFβ- and Smad2-dependent ARE-Lux transcriptional activity. However, km23 knockdown is without effect on TGFβ- and Smad3-dependent SBE-Luc activity. Thus, it appears that km23's critical function in mediating the phosphorylation, nuclear expression, and transcriptional activation of Smad2 is specific to this RSmad. Perhaps a km23-like protein regulates Smad3 in a similar fashion. Whether this is the case requires further investigation.

It is noteworthy that when comparing Figs. 5B and 5C, there was no corresponding increase in cytoplasmic Smad2, when nuclear Smad2 expression

was blocked by the km23 siRNA. This finding is consistent with the degradation of Smad2 occurring when km23 function is blocked. Ubiquitin-proteaseome-mediated degradation is known to control the levels of Smads post-translationally (Derynck and Zhang, 2003; Izzi et al; 2004). Since our data demonstrate that blockade of km23 decreased Smad2 expression levels in the cytoplasm, as well as in the nucleus, it is possible that blockade of km23 stimulates a Smad2 ubiquitin–mediated degradation pathway. For example, a degradation pathway involving Smuf2, which could directly target Smad2 for degradation, could play a role (Lin et al; 2000). However, we cannot rule out a mechanism for Smad2 degradation that may involve specific km23 functions. Future studies will explore this issue more completely.

Blockade of km23 reduced the levels of Smad2 phosphorylation, nuclear expression of Smad2, and Smad2-dependent transcriptional activity, suggesting a critical role for km23 in mediating Smad2-dependent responses. However, Smad2 phosphorylation and activation can also be regulated by TGFβ-dependent activation of the Erk, JNK, and p38 pathways (Derynck and Zhang, 2003; Fu et al; 2003). For example, activation of MEKK1, which functions upstream of JNK, has been shown to enhance Smad2 phosphorylation, association with Smad4, nuclear accumulation, and transcriptional activity (Brown et al; 1999). Since we have previously shown that forced expression of km23 enhances JNK activation, it may be that km23 serves as a bridge to link the Smad2 and JNK signaling pathways. Thus, Smad2 may not be the only

TGFβ signaling component regulated by km23. Identification of other TGFβ signaling components that are regulated by km23 will require additional studies.

ACKNOWLEDGMENTS

We thank Dr. Joan Massague (Memorial Sloan-Kettering Cancer Center, New York, NY) for the T204D-HA; Dr. Scott E. Kern (John Hopkins Oncology Center, Baltimore, MD) for SBE-Luc. We also thank Dr. Malcolm Whitman (Harvard Medical School, Boston, MA) for the ARE-Lux and FAST-1 constructs. The work was supported by National Institutes of Health Grants CA90765, CA92889, and CA100239, and Dept of Defense # DAMD17-03-01-0287 (to K.M.M).

FOOTNOTES

The abbreviations used are: Ab, antibody; ARE, activin-responsive element; DIC, dynein intermediate chain; FAST, forkhead activin signal transducer; IP, immunoprecipitation; GFP, green fluroscence protein; GST, glutathione-S-transferase; MTs, microtubules; NC, negative control; RSmads, receptor-activated Smads; siRNA, small interfering RNA; TGFβ, Transforming growth factor β

REFERENCES

Attisano, L., and Wrana, J. L. (1998). Mads and Smads in TGFβ signaling. *Curr. Opin. in Cell Biol.* **10**, 188-194.

Brown, J. D., DiChiara, M. R., Anderson, K. R., Gimbrone, M. A. Jr, and Topper, J. N. (1999). MEKK-1, a component of the stress (stress-activated protein kinase/c-Jun N-terminal kinase) pathway, can selectively activate Smad2-mediated transcriptional activation in endothelial cells. *J. Biol. Chem.* **274**, 8797-8805.

Chen, X, Rubock, M. J., and Whitman, M. (1996). A transcriptional partner for MAD proteins in TGF-β signalling. *Nature* **384**, 648.

Derynck, R., and Zhang, Y. E. (2003). Smad-dependent and Smad-independent pathways in TGFβ- family signaling. *Nature* **425**, 577-584.

Di Guglielmo, G. M., Le Roy, C., Goodfellow, A. F., and Wrana, J. L. (2003). Distinct endocytic pathways regulate TGF-β receptor signalling and turnover. *Nat. Cell Biol.* **5**, 382-384.

Ding, W., and Mulder, K. M. (2004). km23: a novel TGFβ signaling target altered in ovarian cancer. In: Molecular Targeting and Signal Transduction (ed. R. Kumar), pp.315-327. Norwell, MA: Kluwer Academic Publishers.

Dong, C., Li, Z., Alvarez, Jr., R., Feng, X. H., and Goldschmidtch-Clermont, P. J. (2000). Microtubule binding to Smads may regulate TGF-β activity. *Mol. Cell* **5**, 27-34.

Felici, A., Wurthner, J. U., Parks, W. T., Glam, L. R., Reiss, M., Karpova, T. S., McNally, J. G., and Roberts, A. B. (2003). TLP, a novel modulator of TGF-β signaling, has opposite effects on Smad2- and Smad3-dependent signaling. *EMBO J.* **22**, 4465-4477.

Fu, Y., O'Connor, L. M., Shepherd, T. G., and Nachtigal, M. W. (2003). The p38 MAPK inhibitor, PD169316, inhibits transforming growth factor -β induced Smad signaling in human ovarian cancer cells. *Biochem. Biophys. Res. Commun.* **310**, 391-397.

Hocevar, B. A., Brown, T. L., and Howe, P. H. (1999). TGF-β induces fibronectin synthesis through a c-Jun N-terminal kinase-dependent, Smad4-independent pathway. *EMBO J.* **18**, 1345-1356.

Hocevar, B. A., Smine, A., Xu, X. X., and Howe, P. H. (2001). The adaptor molecule Disabled-2 links the transforming growth factor-β receptors to the Smad pathway. *EMBO J.* **18**, 2789-2801.

Izzi, L., and Attisano, L. (2004). Regulation of the TGF-β signalling pathway by ubiquitin-mediated degradation. *Oncogene.* **23**, 2071-2078.

Labbe, E., Silvestri, C., Hoodless, P. A., Wrana, J. L., and Attisano, L. (1998). Smad2 and Smad3 positively and negatively regulate TGFβ -dependent transcription through the forkhead DNA-binding protein FAST2. *Mol. Cell* **2**, 109-120.

Lin, X., Liang, M., and Feng, X. H. (2000). Smurf2 is a ubiquitin E3 ligase mediating proteasome-dependent degradation of Smad2 in transforming growth factor-β signaling. *J. Biol. Chem.* **275**, 36818-36822.

Liu, F. (2003). Receptor-regulated Smads in TGF-β signaling. *Front Biosci.* **8**, 1280-1303.

Macias-Silva, M., Abdollah, S., Hoodless, P. A., Pirone, R., and Attisano, L., Wrana, J. L. (1996). MADR2 is a substrate of the TGFβ receptor and its phosphorylation is required for nuclear accumulation and signaling. *Cell* **87**, 1215-1224.

Massague, J. (1998). TGF-β signal transduction. *Annu. Rev. Biochem.* **67**, 753-791.

Penheiter, S. G., Mitchell, H., Garamszegi, N., Edens, M., Dore, J. J. Jr., and Leof, E. B. (2002). Internalization-dependent and -independent requirements for transforming growth factor-β receptor signaling via the Smad pathway. *Mol. Cell Biol.* **22**, 4750-4759.

Remy, I., Montmarquette, A. and Michnick, S. W. (2004). PKB/Akt modulates TGF-β signalling through a direct interaction with Smad3. *Nature Cell Biology* **6**, 358 - 365.

Roberts, A. B., and Wakefield, L. M. (2003). The two faces of transforming growth factor-β in carcinogenesis. *Proc. Natl. Acad. Sci. U S A* **100**, 8621-8623.

Sasaki, A., Masuda, Y., Ohta, Y., Ikeda, K., and Watanabe, K. (2001). Filamin associates with Smads and regulates transforming growth factor-β signaling. *J. Biol. Chem.* **276**, 17871-17877.

Shi, Y. G., and Massague, J. (2003). Mechanism of TGF-β signaling from cell membrane to the nucleus. *Cell* **113**, 685-700.

Tang, Q., Staub, C. M., Gao, G., Jin, Q., Wang, Z., Ding, W., Aurigemma, R. E., and Mulder, K. M. (2002). A novel transforming growth factor-β receptor interacting protein that is also a light chain of the motor protein dynein. *Mol. Biol. Cell* **13**, 4484-4496.

Tsukazaki, T., Chiang, T. A., Davison, A. F., Attisano, L. and Wrana J. L. (1998). SARA, a FYVE domain protein that recruits Smad2 to the TGFβ receptor. *Cell* **95**, 779-791.

Yue, J., Frey, R. S., and Mulder, K. M. (1999a). Cross-talk between the Smad1 and Ras/MEK signaling pathways for TGFβ. *Oncogene* **18**, 2033-2037.

Yue, J., Hartsough, M. T., Frey, R. S., Frielle, T., and Mulder, K. M. (1999b). Cloning and expression of a rat Smad1: regulation by TGFβ and modulation by the Ras/MEK pathway. *J. Cell Physiol.* **178**, 387-96.

Yue, J., and Mulder, K.M. (2001). Transforming growth factor-β signal transduction in epithelial cells. *Pharmacol. Ther.* **91**, 1-34.

Zawel, L., Dai J. L., Buckhaults, P., Zhou, S., Kinzler, K. W., Vogelstein, B., and Kern, S. E. (1998). Human Smad3 and Smad4 are sequence-specific transcription activators. *Mol. Cell* **1**, 611-617.

FIGURE LEGENDS

Fig. 1. km23 interacts with Smad2, not Smad3 in GST pull-down and IP/blot assays. **A:** Top panel, 293T cells were transfected with either empty vector, Smad2-Flag, or Smad3-Flag and lysates were incubated with sepharose bound, bacterially-expressed GST alone or GST-km23. GST-bound proteins were analyzed by SDS-PAGE and were immunoblotted with an anti-Flag Ab. Smad2 interacts with GST-km23 (lane 4), but Smad3 does not interact with GST-km23 (lane 6). Empty vector control lanes (lanes 1, 2) and GST control lane were negative (lanes 1, 3, 5, 7). Bottom panel, equal amounts of GST or GST-km23 was visualized by Coomassie staining. **B:** 293T cells were transfected with km23-flag and Smad3-Flag or Smad2-Flag, and/or T204D-HA as indicated. Twenty-four hours after transfection, 293T cells were lysed, and IP/blot analyses were performed using Smad2 or Smad3 as the IP Ab and a Flag Ab as the blotting Ab.

Fig. 2. km23 colocalizes with Smad2 in a TGFβ-dependent manner. **A:** MDCK cells were cultured in the absence of TGFβ, and then were fixed and permeabilized. Endogenous km23 was detected using rabbit km23 anti-serum, followed by Alexa 594 goat anti-rabbit IgG (left, top row). Smad2 was detected using a mouse monoclonal Smad2/3 Ab and Alexa 488 goat anti-mouse IgG (left, middle row). The merge photos show potential co-localization of km23 and Smad2 as yellow punctate staining (left, bottom row) and an enlarged inset (right, bottom row). No signal was detected in the controls (right, top and middle rows).

B: MDCK cells were incubated in serum-free medium for 1h before addition of TGFβ (5 ng/ml) for 2 min, and then analyzed as in A. **C:** MDCK cells were incubated in serum-free medium for 1h before addition of TGFβ (5 ng/ml) for 5 min, and then analyzed as in A. **D:** MDCK cells were incubated in serum-free medium for 1h before addition of TGFβ (5 ng/ml) for 15 min, and then analyzed as in A. The results shown are representative of three similar experiments.

Fig. 3. Demonstration of the specificity of km23 siRNA for blocking endogenous km23. **A:** Mv1Lu cells were transiently transfected with either NC siRNA and GFP-km23 (top panels) or km23 siRNA and GFP-km23 (bottom panels). Twenty-four hours after transfection, cells were fixed and analyzed by immunofluorescence as described in " Material and Methods." DAPI staining (left) is shown to visualize individual cells. The results shown are representative of two similar experiments. **B:** 293T cells were transiently transfected with either km23 siRNA or NC siRNA. Top panel, after incubation for 24-48 h, expression levels of endogenous km23 were analyzed via Western blot analysis using rabbit km23 anti-serum (1:500). Bottom panel, equal loading was confirmed by Western blotting analysis with a DIC Ab. The results shown are representative of three similar experiments.

Fig. 4. siRNA blockade of endogenous km23 reduced the TGFβ–dependent increase in phosphorylated Smad2. Mv1Lu cells were transiently transfected with either km23 siRNA or NC siRNA. Twenty-four hours after transfection, cells

were incubated in serum-free medium for 1h before addition of TGFβ (5 ng/ml) for the indicated times. Top panel, cells were lysed and then analyzed by Western blot analysis with anti-phospho-Smad2. Middle panel, total Smad2 levels were confirmed by Western blotting. Bottom panel, plot of densitometric scan of results in top panel. The results shown are representative of two similar experiments.

Fig. 5. siRNA blockade of endogenous km23 reduced the nuclear expression of Smad2 induced by TGFβ. **A:** Mv1Lu cells were transiently co-transfected with either GFP and NC siRNA, or GFP and km23 siRNA. Twenty-four hours after transfection, cells were fixed and endogenous Smad2 was detected using a mouse monoclonal Smad2/3 Ab and Alexa 594 goat anti-mouse IgG (red). DAPI staining permits visualization of individual cells (blue). GFP is used as a marker to designate cells transfected with siRNA (green). Triplicate fields are shown for each condition. **B:** Mv1Lu cells were transiently co-transfected with GFP and NC siRNA. Twenty-four hours after transfection, cells were incubated in serum-free medium before addition of TGFβ (5 ng/ml) for 15 min, and then analyzed as in A. **C:** Mv1Lu cells were transiently co-transfected with GFP and km23 siRNA. Twenty-four hours after transfection, cells were incubated in serum-free medium before addition of TGFβ (5 ng/ml) for 15 min, and then analyzed as in A. The results shown are representative of two similar experiments.

Fig. 6. siRNA blockade of endogenous km23 inhibits Smad2/4-dependent

transcription in TGF-β/activin reporter assays, but has no effect Smad3/4-dependent transcriptional activation. **A:** Mv1Lu cells were transfected with increasing amounts of either km23 siRNA or NC siRNA (0.125 μg and 0.500 μg) along with 0.2 μg ARE-lux and 0.2 μg FAST-1. To normalize transfection efficiencies, 0.2 μg renilla was co-transfected as an internal control. Twenty-four hours after transfection, the medium was replaced with serum-free medium for 1 h, followed by incubation of cells in the absence (open bar) and presence (black bar) of TGFβ (5ng/ml) for an additional 18 h. Luciferase activity was measured using the Dual Luciferase Reporter Assay System. All reporter assays were performed in triplicate. The results shown are representative of two similar experiments. **B:** Mv1Lu cells were transfected with increasing amounts of either km23 siRNA or NC siRNA (0.125 μg and 0.500 μg) along with 0.2 μg SBE-Luc, and then analyzed as in A. The results shown are representative of two similar experiments.

Table1: Quantitation of siRNA effects on TGFβ-mediated nuclear expression of Smad2

	GFP+NC siRNA	GFP+km23 siRNA
Transfection efficiency[1]	19.4%±0.4	20%±2
Cells with nuclear expression of Smad2[2]/GFP positive cells	93%±2	11%±2
Cells with nuclear expression of Smad2 /GFP negative cells	100%±0	99.7%±0.3

1. GFP-positive cells divided by total DAPI-positive cells in the relevant fields.
2. Nulcear staining of Smad2 after addition of TGFβ (5ng/ml) for 15min.

Fig. 1A

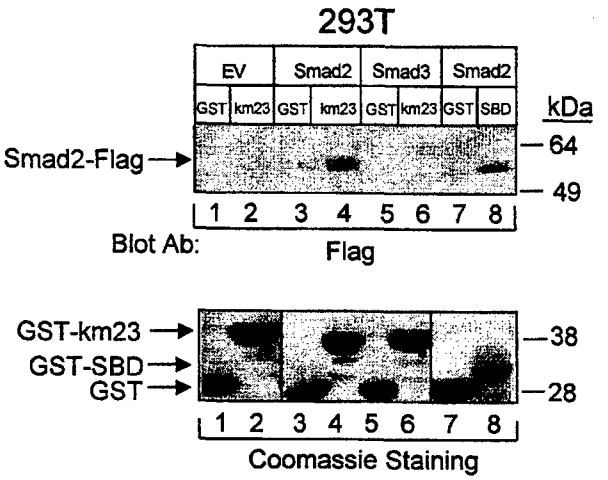
293T
EV
Smad2
Smad3
Smad2
GST
km23
GST
km23
GST
km23
GST
SBD
kDa
Smad2-Flag
64
49
1 2 3 4 5 6 7 8
Blot Ab:
Flag
GST-km23
GST-SBD
GST
38
28
1 2 3 4 5 6 7 8
Coomassie Staining

Fig. 1B

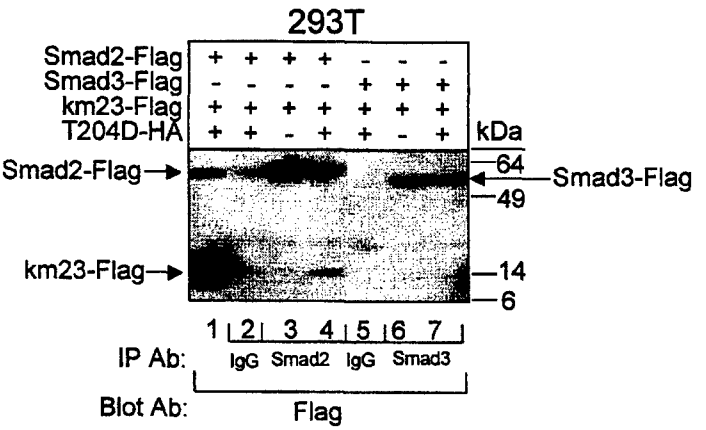
293T
Smad2-Flag + + + + - - -
Smad3-Flag - - - - + + +
km23-Flag + + + + + + +
T204D-HA + + - + + - +
kDa
Smad2-Flag
64
Smad3-Flag
49
km23-Flag
14
6
1 2 3 4 5 6 7
IP Ab:
IgG Smad2 IgG Smad3
Blot Ab:
Flag

Fig. 2A

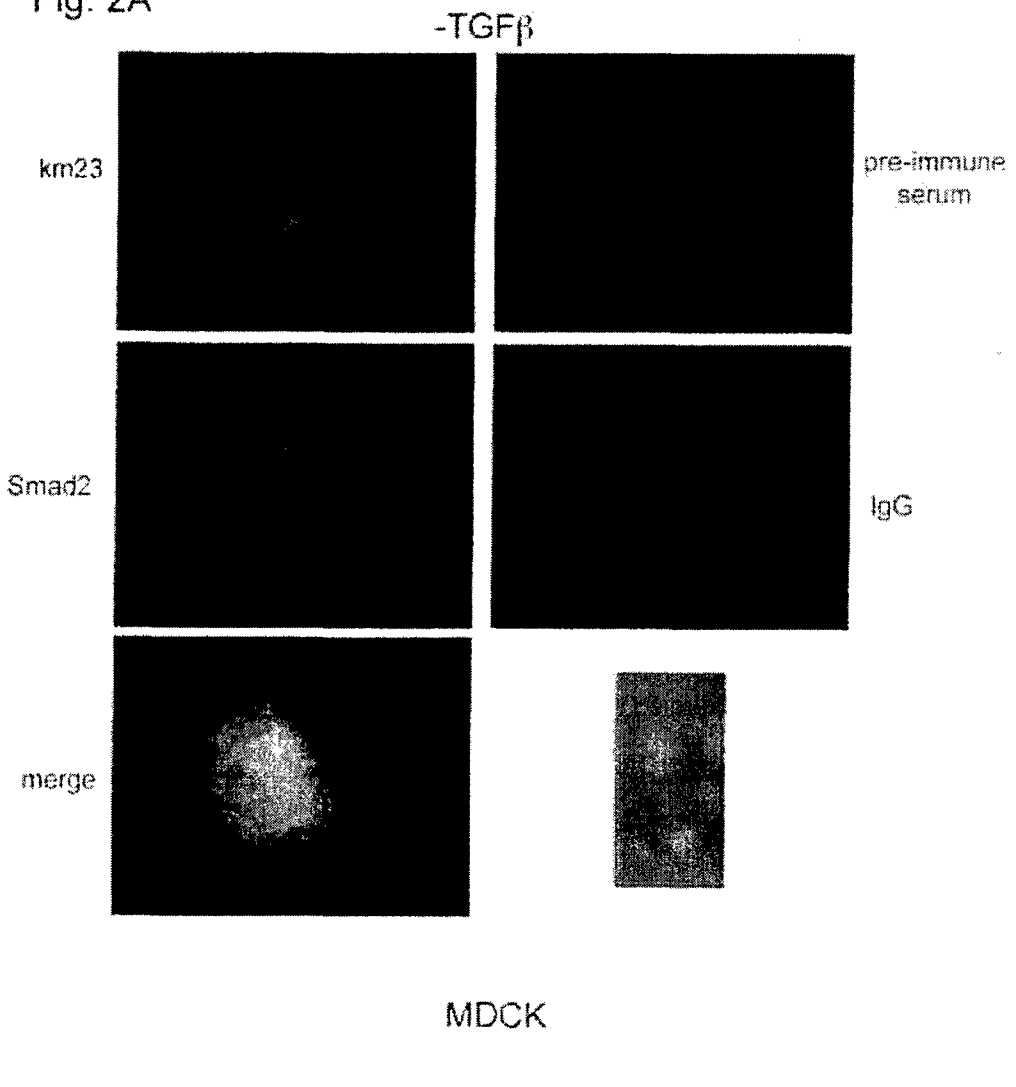

Fig. 2B

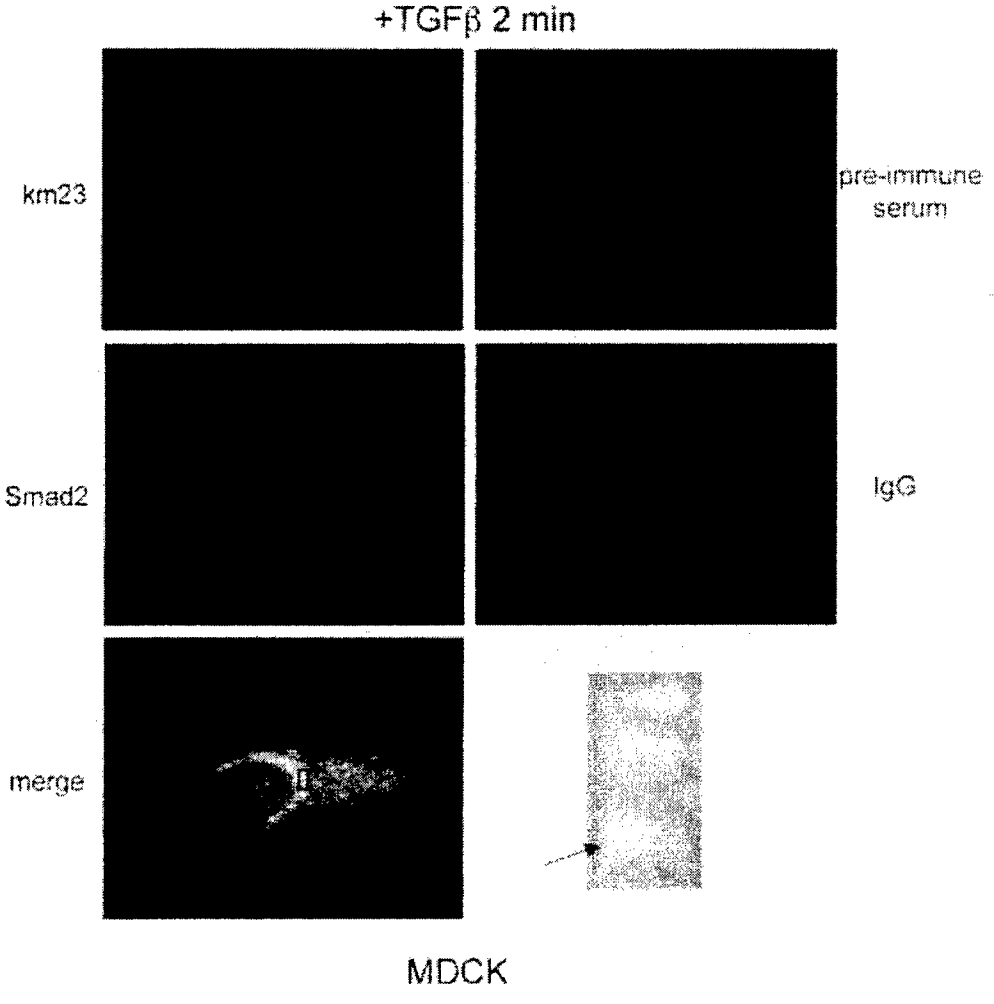

Fig. 2C

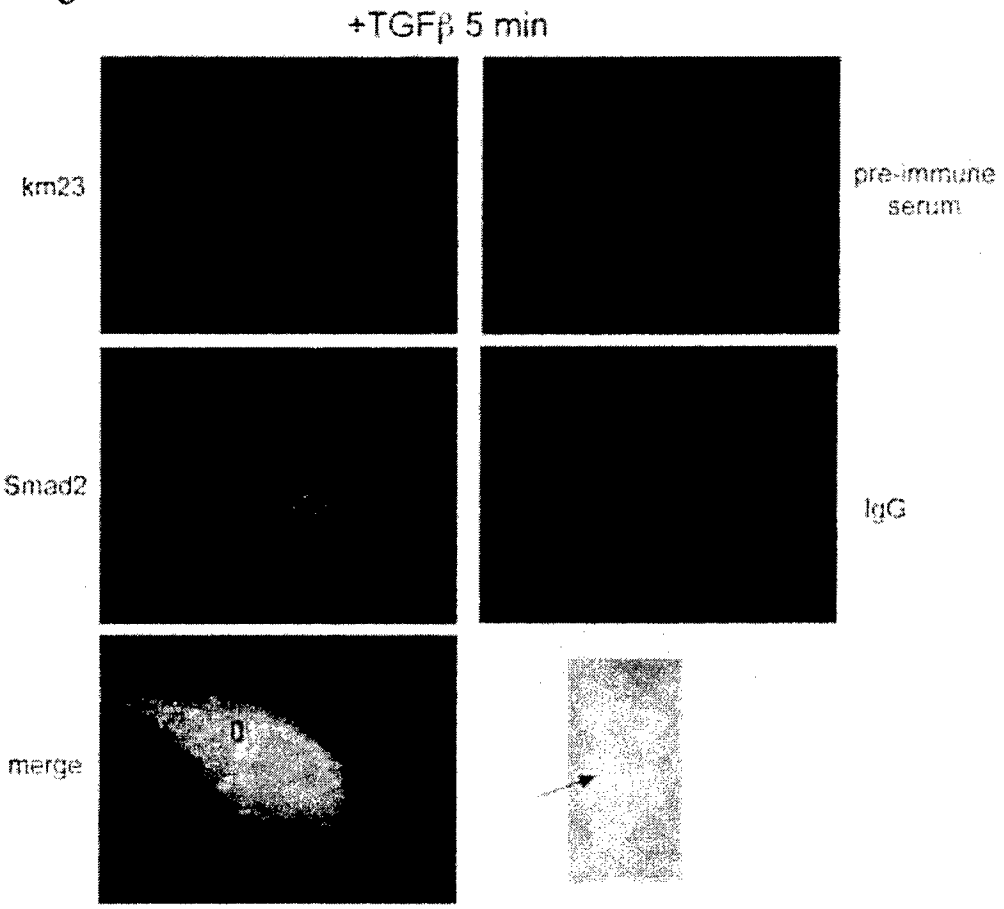

Fig. 2D

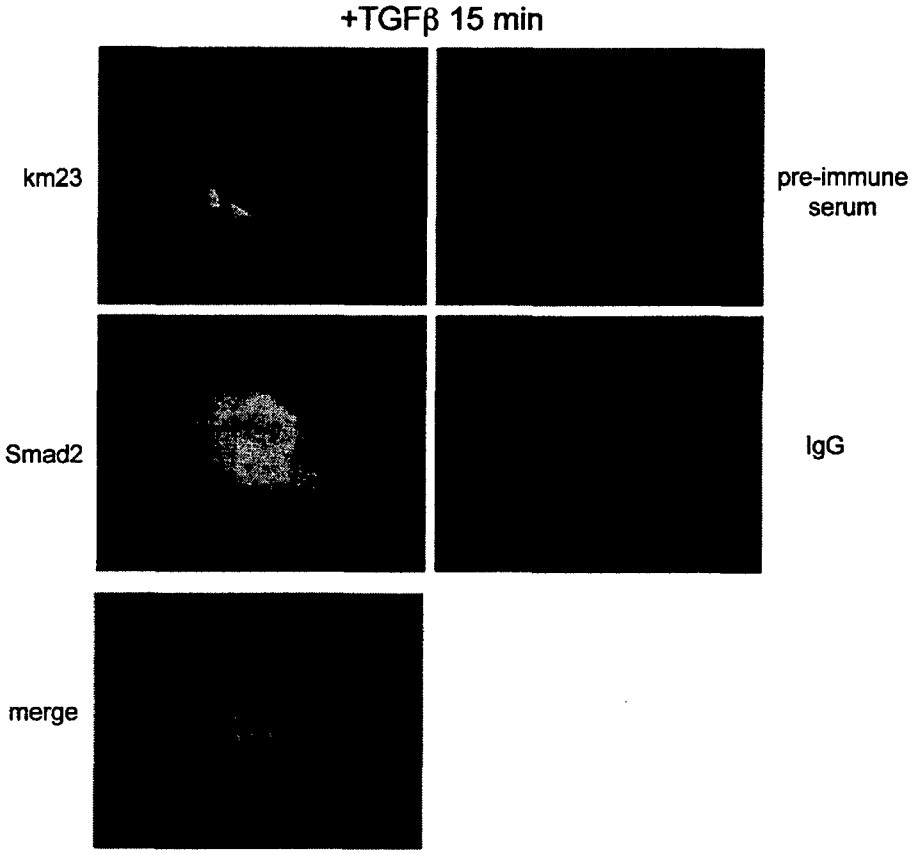

Fig.3A

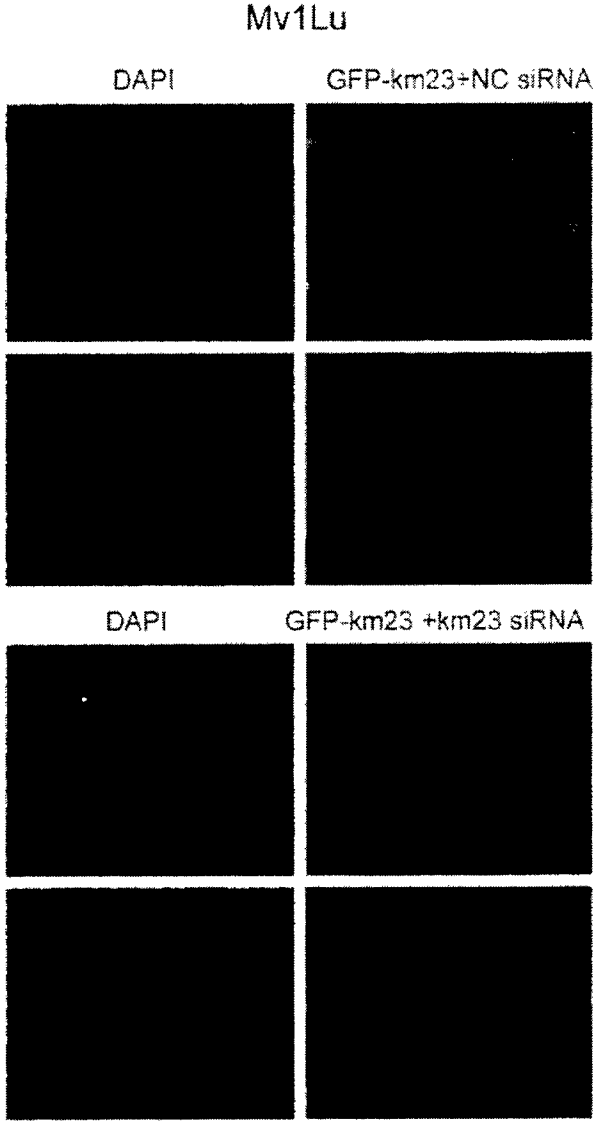

Fig.3B

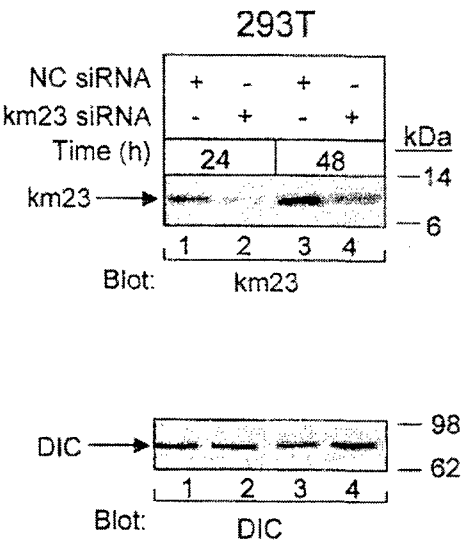
293T
NC siRNA
km23 siRNA
Time (h)
24
48
kDa
km23
14
6
1 2 3 4
Blot:
km23
DIC
98
62
1 2 3 4
Blot:
DIC

Fig.4

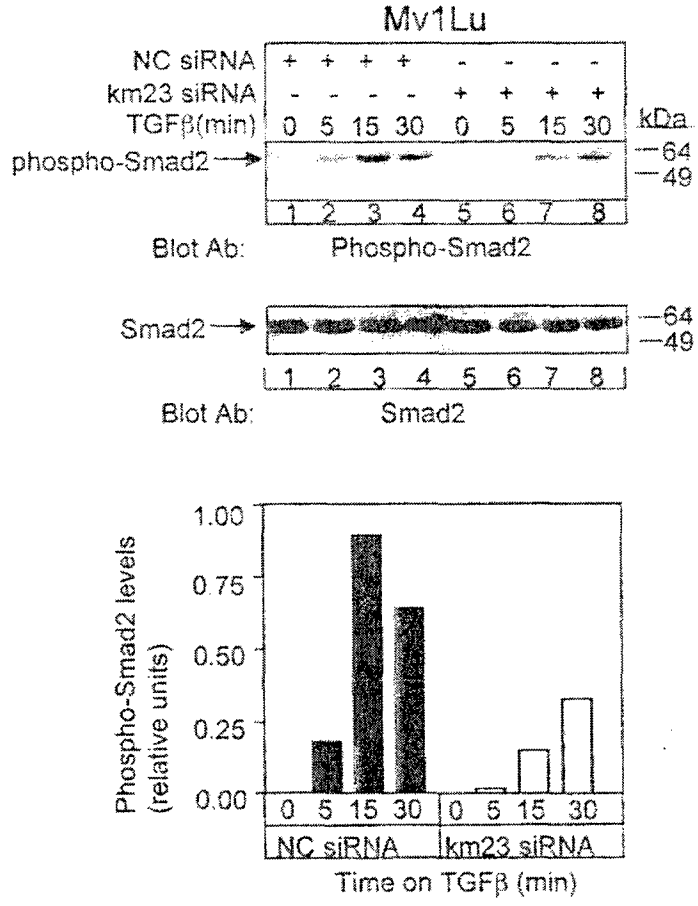
Mv1Lu
NC siRNA + + + + - - - -
km23 siRNA - - - - + + + +
TGFβ(min) 0 5 15 30 0 5 15 30
kDa
phospho-Smad2
64
49
1 2 3 4 5 6 7 8
Blot Ab: Phospho-Smad2
Smad2
64
49
1 2 3 4 5 6 7 8
Blot Ab: Smad2
Phospho-Smad2 levels (relative units)
1.00
0.75
0.50
0.25
0.00
0 5 15 30 0 5 15 30
NC siRNA
km23 siRNA
Time on TGFβ (min)

Fig.5A

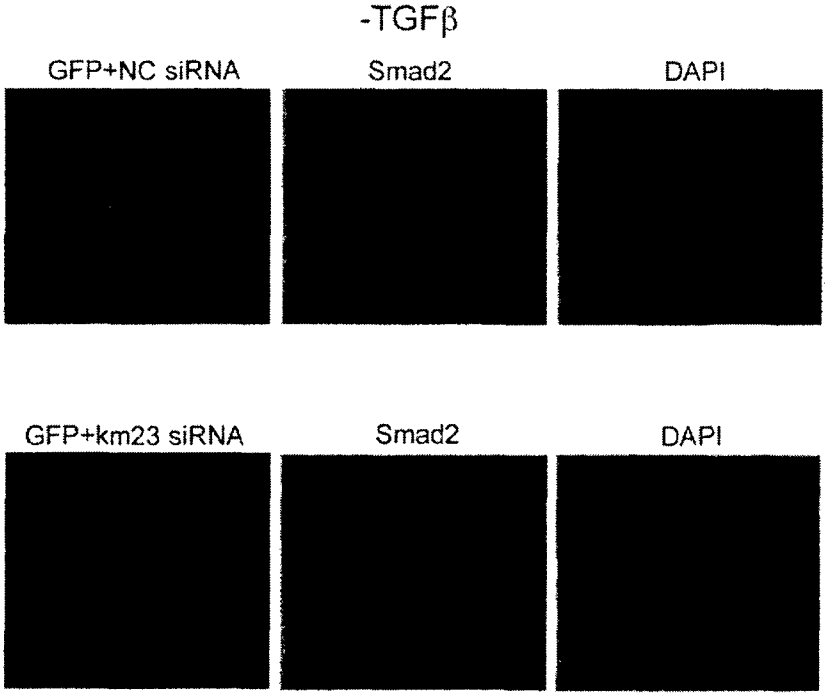

Fig.5B

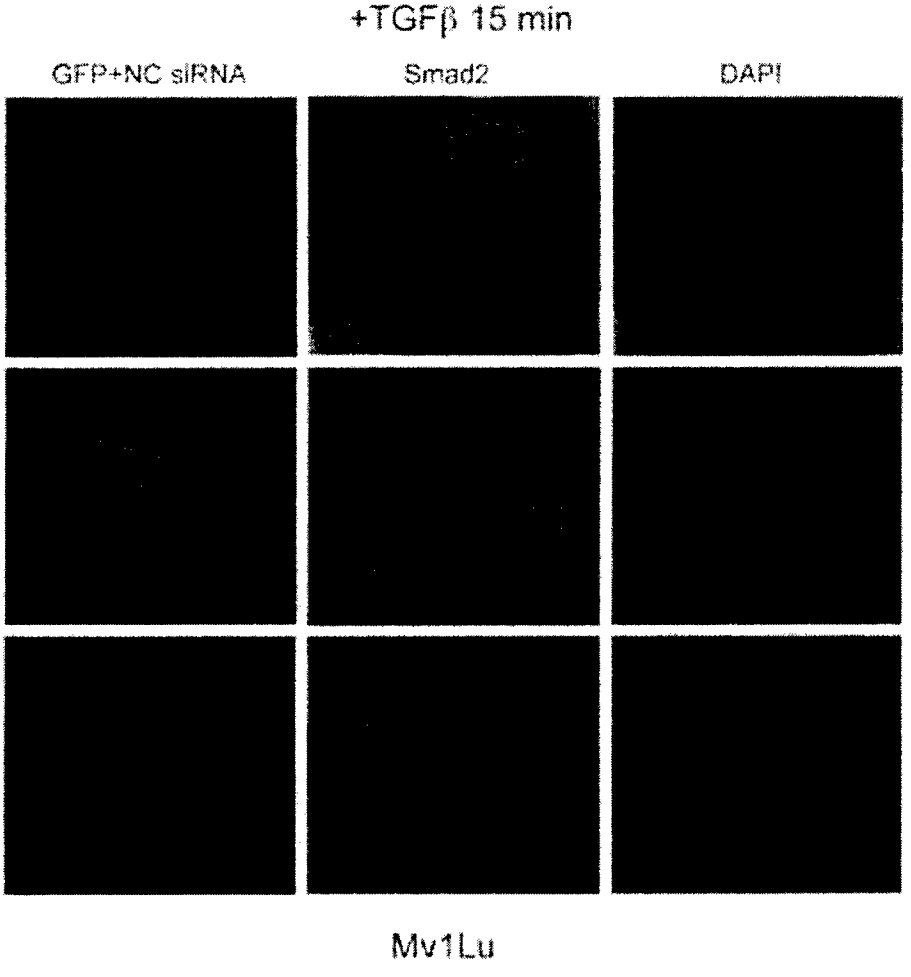

Fig.5C

+TGFβ 15 min

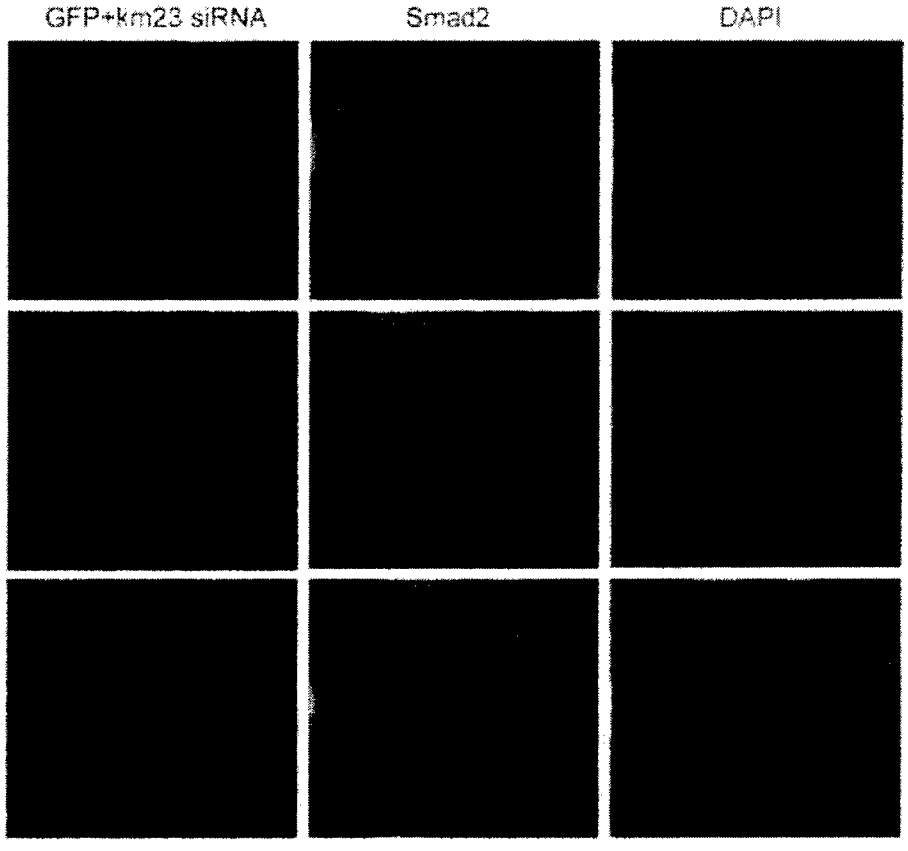

Mv1Lu

Fig.6A

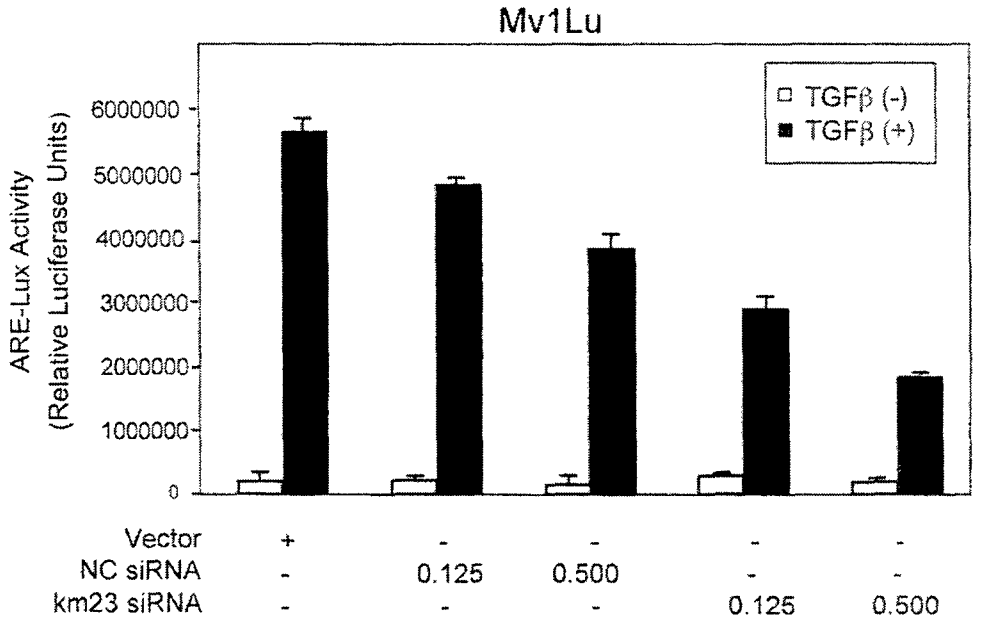
Mv1Lu
TGFβ (-)
TGFβ (+)
ARE-Lux Activity
(Relative Luciferase Units)
6000000
5000000
4000000
3000000
2000000
1000000
0
Vector + - - - -
NC siRNA - 0.125 0.500 - -
km23 siRNA - - - 0.125 0.500

Fig. 6B

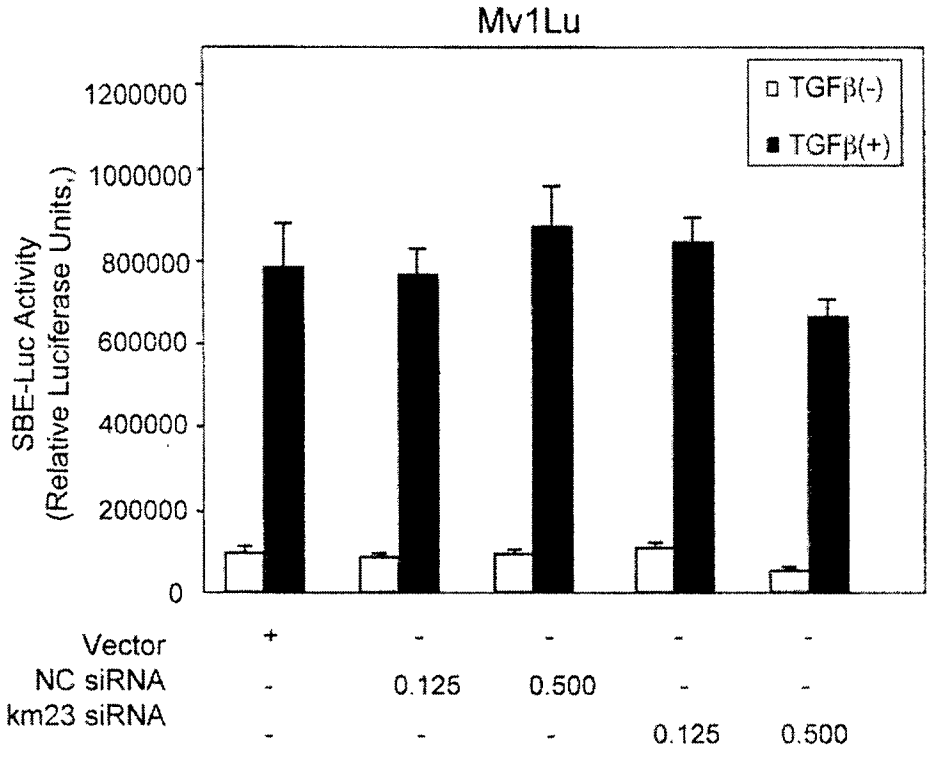
Mv1Lu
TGFβ(-)
TGFβ(+)
SBE-Luc Activity
(Relative Luciferase Units,)
1200000
1000000
800000
600000
400000
200000
0
Vector + - - - -
NC siRNA - 0.125 0.500 - -
km23 siRNA - - - 0.125 0.500

doi:10.1016/j.jmb.2005.07.002 J. Mol. Biol. (2005) 352, 338–354

JMB

Available online at www.sciencedirect.com

SCIENCE DIRECT®

ELSEVIER

Structure and Dynamics of the Homodimeric Dynein Light Chain km23

Udayar Ilangovan[1]†, Wei Ding[2]†, Yan Zhong[2], Christina L. Wilson[2] Jay C. Groppe[1], James T. Trbovich[1], Jorge Zúñiga[1], Borries Demeler[1] Qian Tang[2], Guofeng Gao[2], Kathleen M. Mulder[2]* and Andrew P. Hinck[1]*

[1]*Department of Biochemistry University of Texas Health Science Center at San Antonio San Antonio, TX 78229, USA*

[2]*Department of Pharmacology Penn State College of Medicine Hershey, PA 17033, USA*

**Corresponding authors*

km23 (96 residues, 11 kDa) is the mammalian ortholog of *Drosophila* roadblock, the founding member of LC7/robl/km23 class of dynein light chains. km23 has been shown to be serine-phosphorylated following TGFβ receptor activation and to bind the dynein intermediate chain in response to such phosphorylation. Here, we report the three-dimensional solution structure of km23, which is shown to be that of a homodimer, similar to that observed for the heterodimeric complex formed between p14 and MP1, two distantly related members of the MglB/robl superfamily, but distinct from the LC8 and Tctex-1 classes of dynein light chains, which also adopt homodimeric structures. The conserved surface residues of km23, including three serine residues, are located predominantly on a single face of the molecule. Adjacent to this face is a large cleft formed by the incomplete overlap of loops from opposite monomers. As shown by NMR relaxation data collected at two fields, several cleft residues are flexible on the ns–ps and ms–μs timescales. Based on these observations, we propose that the patch of conserved residues on the central face of the molecule corresponds to the site at which km23 binds the dynein intermediate chain and that the flexible cleft formed between the overlap of loops from the two monomers corresponds to the site at which km23 binds other partners, such as the TGFβ type II receptor or Smad2.

© 2005 Elsevier Ltd. All rights reserved.

Keywords: NMR; flexibility; dynein light chains; km23; TGFβ

Introduction

Cytoplasmic dynein is a motor complex that transports membrane vesicles and diverse motor cargoes along microtubules (MTs) in a retrograde manner.[1–4] It plays a pivotal role in mitotic spindle assembly and orientation, positioning of the Golgi apparatus, and transport of intracellular organelles, including endosomes and lysosomes.[5,6] The dynein motor complex consists of two heavy chains (~530 kDa), two intermediate chains (~74 kDa), light-intermediate chains (~50–60 kDa), and several light chains (8–22 kDa).[1–4] Dynein heavy chains contain the MT binding sites and the ATP hydrolysis sites that are essential for force production and the movement of the motor complex along MTs.[7,8] The intermediate chains, light-intermediate chains, and light chains form the base of the dynein complex and are important for cargo binding.[1–4]

Three classes of cytoplasmic dynein light chains (DLCs) have been identified in mammals, including LC8, Tctex-1/rp3, and LC7/robl/km23.[1–4,9,10] In addition to binding the dynein intermediate chain (DIC) at distinct regions,[11] light chains have also been shown to directly interact with a number of proteins to exert diverse functions. LC8, for example, binds to neuronal nitric oxide synthase (nNOS),[12,13] the proapoptotic Bcl-2 family members Bim and Bmf,[14,15] the *Drosophila* mRNA localization protein Swallow,[16] and the rabies virus P protein.[17] LC8 has also been reported to be a physiologically

† U.I. & W.D. contributed equally to this work.

Abbreviations used: DLC, Dynein light chain; DIC, dynein intermediate chain; EV, empty vector; IP, immunoprecipitation; HSQC, heteronuclear single quantum coherence; NOE, nuclear Overhauser effect; NOESY, NOE spectroscopy; CSI, chemical shift index; RDC, residual dipolar coupling.

E-mail addresses of the corresponding authors: kmm15@psu.edu; hinck@uthscsa.edu

0022-2836/$ - see front matter © 2005 Elsevier Ltd. All rights reserved.

interacting substrate of p21-activated kinase 1 (Pak1).[18] Pak1 interacts with the complex of LC8 and Bim, and phosphorylates both proteins.[18] Tctex-1 has been shown to interact with Doc2,[19] $p59^{fyn}$ Src family tyrosine protein kinase,[20] and the C-terminal tail of rhodopsin.[21]

LC8 has been studied using both NMR[22,23] and X-ray crystallography[24] and has been shown to adopt a homodimeric structure stabilized by an extensive array of contacts between edge β-strands. Tctex-1 has also been studied structurally and has been shown to adopt a homodimeric structure similar to that of LC8.[25,26] The mechanism of nNOS and Bim peptide binding by LC8 has been investigated by NMR.[22,27] These studies have shown that despite their disparate sequences, each binds in a similar manner in a flexible groove at the homodimer interface.

LC7 was initially identified as a component of the *Chlamydomonas* outer dynein arm,[9] whereas robl was identified in *Drosophila* in a mutant screen for sluggish motility.[9] km23 (96 residues, 11 kDa) and km23-2, a km23 homolog with 77% sequence identity, are the mammalian orthologs of *Chlamydomonas* LC7 and *Drosophila* robl.[10] km23 was discovered in a novel screen for TGFβ receptor-interacting proteins, and has been shown to function both as a DLC and a TGFβ signaling intermediate.[10,28]

The hormone-like polypeptide growth factor TGFβ is known to be an important negative regulator of cell growth and a potent inducer of extracellular matrix synthesis.[29,30] TGFβ initiates its response by binding and bringing together two pairs of structurally similar, single-pass transmembrane receptors, classified as types I (TβRI) and II (TβRII). The ligand-mediated assembly of these two receptor types triggers an intracellular phosphorylation cascade initiated by the serine-threonine kinase domain of the type II receptor, which *trans*-phosphorylates the adjacent type I kinase. The type I kinase in turn phosphorylates the nuclear-translocating Smad proteins, which together with various transcriptional coactivators and corepressors, regulate transcription of target genes.[29,30]

km23 has also been shown to undergo rapid phosphorylation on serine after TGFβ receptor activation, in keeping with the kinase specificity of TβRI and TβRII.[10] TGFβ has been further shown to induce, in a manner dependent upon the kinase activity of TβRII, recruitment of km23 to the DIC.[10] Overexpression of km23 has been shown to induce specific TGFβ responses, including Jun N-terminal kinase (JNK) activation, c-Jun phosphorylation, and cell growth inhibition,[10] while blockade of km23 expression using small interfering RNA (siRNA) results in a decrease in cellular responses to TGFβ, including induction of fibronectin expression and inhibition of cell cycle progression.[28] Thus, km23 appears to play an important role in TGFβ signaling, which may explain the high frequency (42%) with which km23 is altered in cancerous, but not normal ovarian tissue.[28,31]

LC7/robl/km23 DLCs belong to an ancient superfamily of proteins, known as the MglB/robl superfamily, with representative members in all three kingdoms of life.[9,10,32] Members of the MglB family have been implicated in NTPase regulation in bacteria and archae and in regulating the mitogen-activated protein kinase (MAPK) and other signaling pathways in eukaryotes. Recently, the crystal structure of a heterodimer formed between two members of the MglB family, p14 and the MAPK scaffolding protein, MP1, was reported.[33,34] This revealed that the two chains adopt the same overall fold and that they interact through edge β-strands and through helix–helix contacts using hydrophobic residues conserved throughout the superfamily. The overall fold of the dimer is distinct relative to that of the LC8 and Tctex-1 dimers, which has led to the notion that proteins of the MglB/robl superfamily each adopt similar dimeric structures and that their ability to interact with one another to form dimers contributes to the diversity of their functions.[33]

The results presented here show that km23 also adopts the structure of a homodimer similar to that of the p14/MP1 heterodimer.[33,34] The conserved surface residues of km23, including three serine residues, are located predominantly on a single face of the molecule. There is adjacent to this face a large cleft formed by the incomplete overlap of loops from the two monomers. This region of km23 was demonstrated through analysis of NMR relaxation data at two fields to be flexible on the ms–μs and ns-ps timescales. Based on these observations, we propose that the patch of conserved residues on the central face of the molecule corresponds to the site at which km23 binds DIC and that the flexible cleft formed between the overlap of the two monomers corresponds to the site that accommodates both TβRII and Smads.

Results

km23 forms homo-oligomers and hetero-oligomers *in vivo*

Our initial studies to identify regions of km23 important for DIC binding were carried out by generating ten-residue deletions throughout the length of the protein. These deletions each abrogated DIC binding, indicating that the overall fold of the protein, or possibly its dimerization, might be required for its function. The initial goal, therefore, was to characterize km23 with respect to formation of higher-order structure.

Our *in vivo* characterization of higher-order structure was carried out by performing immunoprecipitation/immunoblotting (IP/blot) analyses in 293T cells transfected with V5-tagged km23 (km23-V5) together with either Flag-tagged km23 (km23-Flag) or empty vector (EV). The results, shown in Figure 1(a), revealed that km23-V5 and km23-Flag were in the same immunocomplex when

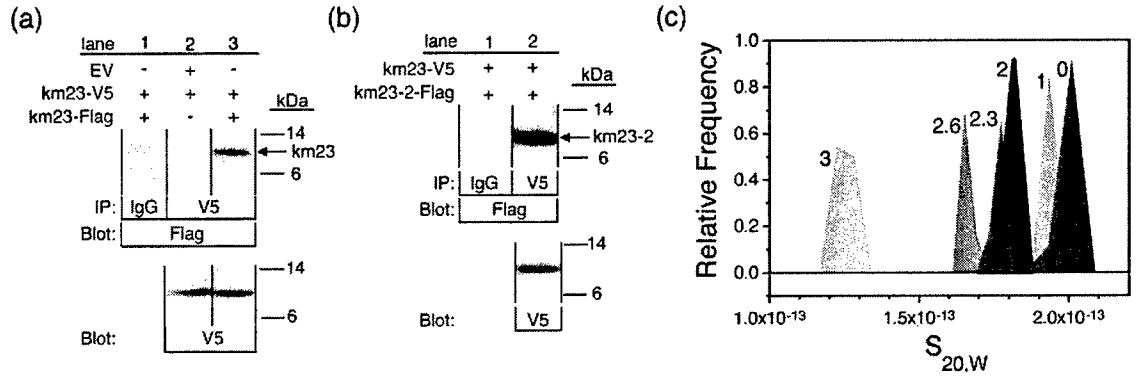

Figure 1. km23 isoforms form homo-oligomers and hetero-oligomers *in vivo* and *in vitro*. (a) km23 forms homo-oligomers as shown through IP-blot analysis of total lysates from 293T cells that had been transfected with V5 and Flag-tagged km23 constructs (top panel, lane 3). Specificity of the immunocomplex is demonstrated by the empty vector (EV) and antibody controls shown in lanes 1 and 2, respectively (top panel). Controls for the expression of km23-V5 were verified by Western blotting whole cell lysates using an anti-V5 antibody (bottom panel, lanes 2 and 3). (b) km23 forms hetero-oligomers with km23-2 as shown through IP-blot analysis of total lysates from 293T cells that had been transfected with V5-tagged km23 and Flag-tagged km23-2 (top panel, lane 2). Specificity of the immunocomplex is demonstrated by the antibody control shown in lane 1 (top panel). Controls for the expression of km23-V5 were verified by Western blotting whole cell lysates using an anti-V5 antibody (bottom panel, lane 2). (c) Sedimentation coefficient distributions for 0.3 mM km23 in 25 mM sodium acetate at pH 6.0 and 20 °C as a function of urea concentration (molar concentrations of urea are designated on the left side of each distribution). Sedimentation coefficient distributions were obtained with the $C(s)$ method[35] as implemented in UltraScan.[51] Increasing urea concentration causes a shift in the sedimentation coefficient consistent with the transition from homodimer to monomer.

both km23-V5 and km23-Flag were co-transfected (top panel, lane 3). In contrast, there was no detectable immunocomplex when cells were co-transfected with km23-V5 and EV (top panel, lane 2), a result attributable to the absence of km23-Flag as immunoblot analysis revealed that km23-V5 was expressed (bottom panel, lane 2). There was also no immunocomplex apparent when normal mouse immunoglobulin G (IgG) was used as the IP antibody (top panel, lane 1), thereby demonstrating the specificity of the IP antibody. The same type of analysis was carried out to determine whether km23 might form oligomeric complexes with km23-2, the other mammalian km23 isoform that shares 77% sequence identity with km23. This was accomplished by co-transfecting 293T cells with km23-V5 and km23-2-Flag and by carrying out IP/blot analyses as before. These results, shown in Figure 1(b), revealed that km23-V5 and km23-2-Flag indeed formed detectable immunocomplexes when the anti-Flag antibody (top panel, lane 2) but not the normal mouse antibody (top panel, lane 1) was used for the IP. These results, taken together, indicate that km23 forms homo-oligomers or hetero-oligomers with km23-2 *in vivo*.

km23 forms homodimers *in vitro*

The objective of the studies described here was to use sedimentation velocity analytical ultracentrifugation to determine whether the oligomeric complexes of km23 demonstrated through the cell-based experiments corresponded to that of a dimer, similar to that of the MglB family p14:MP1 dimer, or whether km23 formed higher-order oligomeric structures. To accomplish this, a structurally homogenous form of km23 was isolated by expressing the protein, together with an artificial 20 residue N-terminal segment encoding a hexahistidine tag, in *Escherichia coli*. The protein was then purified to homogeneity using immobilized metal affinity chromatography.

The sedimentation experiments were carried out by preparing recombinant km23 (116 residues, 13.1 kDa) at a concentration of 0.3 mM in 25 mM sodium acetate at pH 6.0 containing 0.0, 1.0, 2.0, 2.3, 2.6, and 3.0 M urea. The velocity profiles were then obtained by recording the absorbance at 280 nm as the samples were centrifuged at 20 °C. The resulting data were analyzed by both the $C(s)$ method[35] and by finite element analysis with a single ideal species.[36] The results of the $C(s)$ analysis, shown in Figure 1(c), revealed single narrow peaks with mean average sedimentation coefficients that decreased from 2.1×10^{-13} to 1.9×10^{-13} s over the range from 0 M to 2 M urea and from 1.9×10^{-13} to 1.1×10^{-13} s over the range from 2 M to 3 M urea. The sedimentation coefficients ($s_{20,W}$) and frictional ratios (f/f_o) obtained from the $C(s)$ method are listed in Table 1. These correlate closely with the corresponding values obtained using finite elements analysis (which are also listed in Table 1).

The $s_{20,W}$ and f/f_o values obtained from the 0–2 and 3 M urea samples translate into molecular masses of 20–23 kDa and 10.5–11.1 kDa, respectively (Table 1). This suggests that km23 forms a stable homodimer in solution and that only under the strongly denaturing conditions of 2.3 M urea and higher does it begin to dissociate to yield appreciable amounts of monomer. The fact that the km23 homodimer dissociates at urea concentrations

Table 1. Sedimentation velocity analysis of km23 as a function of the urea concentration

	C(*s*) Analysis[a]			Finite element analysis[a]		
[Urea] (M)	$\overline{s_{20,w}}$ ($\times 10^{-13}$ s^{-1})	Frictional ratio (f/f_o)	$\overline{MW}$ (kDa)	$\overline{s_{20,w}}$ ($\times 10^{-13}$ s^{-1})	Frictional ratio (f/f_o)	$\overline{MW}$ (kDa)
0.0	2.03	1.33	21.0	1.98	1.44	22.6
1.0	1.98	1.57	25.9	1.81	1.48	22.5
2.0	1.77	1.46	19.7	1.80	1.41	21.6
2.3	1.74	1.47	19.2	1.74	1.42	18.3
2.6	1.63	1.49	17.9	1.63	1.43	16.7
3.0	1.24	1.43	11.1	1.23	1.38	10.5

[a] Sedimentation coefficients, weight average molecular weights, and frictional ratios are as determined with the C(*s*) analyses[35] and the finite element analysis[36] as implemented in the UltraScan software.[51]

comparable to that at which many small globular proteins unfold indicates that the homodimer is stabilized by an extensive array of contacts similar in nature to those that stabilize globular proteins. These conclusions have been borne out by the structural analysis of km23 by NMR as discussed below.

NMR assignments

To define the tertiary and quaternary structure of km23, NMR spectroscopy was used. Towards this end, an ^{15}N isotopically labeled sample was prepared using the *E. coli* expression and purification procedure described above. This sample was then analyzed by recording a ^{1}H–^{15}N shift correlation heteronuclear single quantum coherence (HSQC) spectrum under non-denaturing conditions (25 mM sodium acetate, pH 6.0) at 20 °C where km23 was shown through analytical ultracentrifugation to be homodimeric. The HSQC revealed a well-dispersed pattern characteristic of a structurally ordered protein, although the total number of identifiable signals corresponding to backbone amides was fewer than that anticipated based upon the primary sequence (95 observed, 109 expected). This indicated that either the dimer is relatively weak and that the signals of monomeric and dimeric forms undergo fast exchange, or that the dimerization is relatively tight and that the signals of monomeric and dimeric forms undergo slow exchange (but that only signals of the dimeric form are present). To distinguish these possibilities, ^{1}H–^{15}N HSQC spectra were recorded in the buffer described above as the sample was diluted from 1.0 mM to 20 μM. There were no detectable changes in peak positions over this 50-fold concentration range, suggesting that km23 forms a tight dimer with the signals from the monomeric and dimeric forms falling in the slow exchange regime.

The sequence-specific backbone and side-chain resonance assignments of km23 were obtained by collecting three-dimensional triple resonance NMR data sets using 0.4–0.8 mM ^{13}C,^{15}N km23 samples. The solution conditions used for the assignments were those described above (25 mM sodium acetate, pH 6) although a higher temperature was used (42 °C) to optimize sensitivity. The HSQC pattern was not changed at 42 °C relative to that at 20 °C, indicating that the higher temperature had little or no effect upon formation of the dimer.

The triple-resonance data sets enabled assignment of the backbone and side-chain resonances of all but one residue (N36) in the region corresponding to km23 (designated residues 1–96) (Figure 2). The triple-resonance data in contrast enabled the assignment of only five of the 20 residues in the N-terminal segment derived from the vector (designated residues −20 to −1). Three of the five backbone amides assigned in this region (G(−8), V(−6), and G(−3)) were further shown to be of low intensity (Figure 2). These observations suggest that the inability to assign resonances in the N-terminal region is a consequence of rapid amide exchange, which is not surprising in the light of the expected random coil nature of this region. The underlying reason for our inability to assign N36 is not clear, although one possibility is exchange broadening.

Secondary structure

The secondary structure of km23 was determined from the pattern of short-range and medium-range nuclear Overhauser effect (NOE) connectivities observed in the 3-D ^{15}N and ^{13}C-edited NOESY spectra and the consensus chemical shift index (CSI).[37] Together, these data revealed the presence of five β-strands, β1 (17–24), β2 (29–32), β3 (66–73), β4 (76–82), and β5 (86–92) and two α-helices, α1 (2–10) and α2 (36–60). The β-strand regions are supported by weak or medium $d_{N\text{-}N}(i,i+1)$ and strong $d_{\alpha\text{-}N}(i,i+1)$ NOE connectivities and a positive consensus CSI. The α-helical regions are supported by strong $d_{N\text{-}N}(i,i+1)$, weak $d_{\alpha\text{-}N}(i,i+1)$, and medium-to-weak $d_{\alpha\text{-}N}$ $(i,i+3)$ NOE connectivities and a negative consensus CSI. The pairing of the five β-strands in an antiparallel fashion is supported by numerous H^{α}–H^{α}, H^{N}–H^{α}, and H^{N}–H^{N} long-range NOEs.

Tertiary structure

There were a significant number of NOEs involving protons on residues 38, 42, 45, and 49 on the N-terminal end of α-helix 2 with protons on residues 53, 56, and 60 on the C-terminal end of

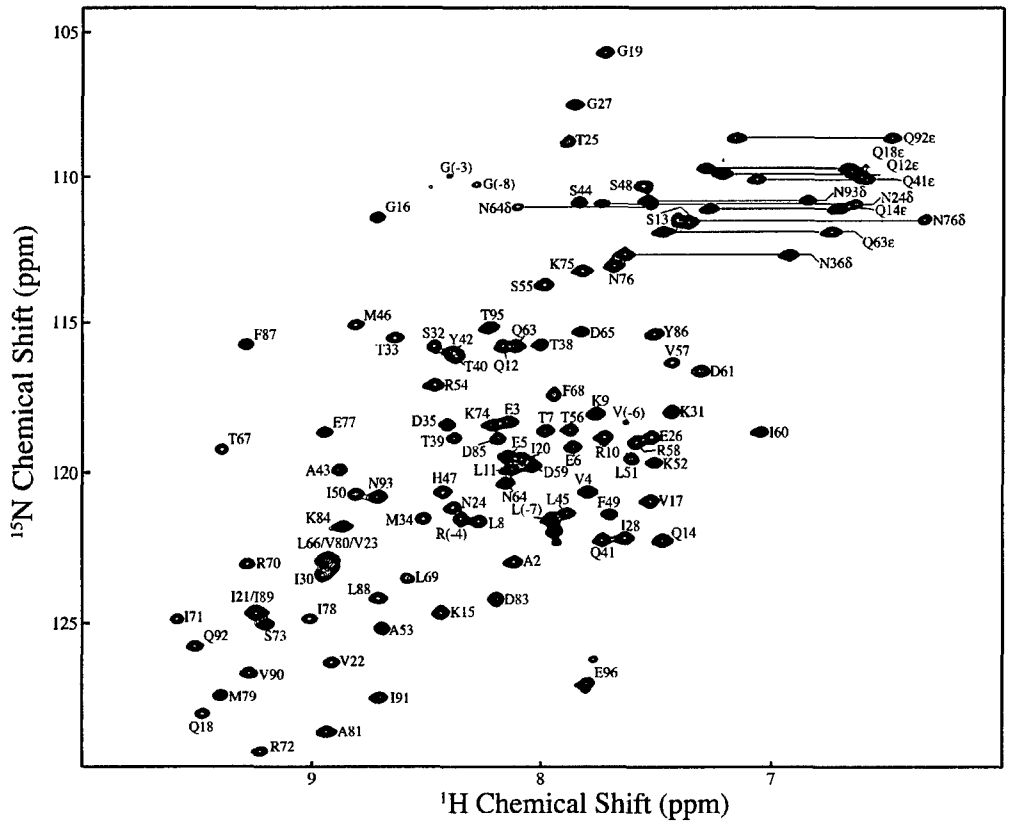

Figure 2. Two-dimensional ^{1}H–^{15}N HSQC spectrum of 0.5 mM ^{15}N km23 in 25 mM sodium acetate, 0.02% sodium azide (pH 6.0) recorded at 42 °C at a magnetic field strength of 14.1 *T* (600 MHz ^{1}H). Peaks are labeled according to their resonance assignments (numbers shown in parentheses correspond to those in the 20 residue N-terminal tail and are numbered −20 to −1; residues numbered 1 to 96 correspond to the 96 residues of human km23).

α-helix 2. These NOEs, when included in the structure calculations, required a bend in the helix near residues 51 and 52. This seemed unlikely since the $^{3}J_{HNH\alpha}$ couplings in α-helix 2 were found to range between 2.5 to 4.5 Hz, consistent with canonical helical phi values, −40° to −65°, but not with the phi values of residues 51 and 52, which fell between −80° and −90° and which had predicted $^{3}J_{HNH\alpha}$ couplings of 6.5 to 7.8 Hz. In addition, there were a number of NOEs observed between protons on residues 67, 68, and 69 on the N-terminal end of β-strand 3 with protons on residues 71, 72, and 73 of the C-terminal end of the strand. These NOEs similarly required a bend, this time at residue 70. This again seemed unlikely since the $^{3}J_{HNH\alpha}$ couplings in this region were found to range between 6.8 to 7.2 Hz, consistent with phi values characteristic of β-strand, −88° to −90°, but not with the phi value of residue 70, which was −150° and which had a predicted $^{3}J_{HNH\alpha}$ coupling of 9.2 Hz. These observations, together with the analytical ultracentrifugation results, suggest that the intra-helix and intra-strand NOEs thus observed correspond to intermolecular NOE contacts in the context of a km23 homodimer. To ascertain this, a km23 sample was prepared by mixing equivalent amounts of unlabeled and ^{13}C,^{15}N labeled km23 in denaturant (6 M urea) and by dialyzing the sample back into non-denaturing NMR buffer. Then, 3-D ^{12}C-filtered,^{15}N-edited and 3-D ^{12}C-filtered,^{13}C-edited NOESY experiments were recorded. These data sets revealed a total of 40 intermolecular contacts. The majority of these were, as anticipated, between residues on the N-terminal half of α-helix 2 or β-strand 3 of one subunit with residues on the C-terminal half of α-helix 2 or β-strand 3 of the other subunit, respectively. The observation of such NOEs unambiguously showed that km23 forms a stable homodimer in solution. These NOEs also show that the homodimer interface is formed by arranging α-helix 2 and β-strand 3 from each monomer in an antiparallel manner as in the p14/MP1 heterodimer.[33,34]

The three-dimensional structure of the km23 homodimer was then calculated using the distance geometry-simulated annealing protocol in torsion angle space as implemented in X-PLOR-NIH.[38] The structure was initially calculated using 1121 NOE and 140 chemical shift derived dihedral angle (TALOS[39]) restraints alone (Table 2). The overall fold thus obtained was consistent with expectations regarding the antiparallel arrangement of α2 and β3

noted above. To validate the structure, $^1D_{NH-HN}$, $^1D_{C\alpha H\alpha}$, $^1D_{C\alpha C'}$, $^1D_{NC'}$ and $^2D_{HNC'}$ residual dipolar couplings (RDCs) were measured using km23 samples in a solution containing 10 mg ml^{-1} Pf1 phage.[40] The 333 RDCs thus measured were then compared to those calculated from the NMR structure using the program PALES.[41] This revealed a correlation coefficient (r^2) of 0.71 between the experimental and calculated RDCs, which is typical of NMR structures refined without the use of RDCs.[42] The structures were then further improved by including the 333 RDCs, as well as 66 $^3J_{HNH\alpha}$ couplings, as restraints in the calculation (Table 2).

The stereoview of the ensemble of calculated structures consistent with the experimental NOE, chemical shift derived dihedral, $^3J_{HNH\alpha}$ coupling, and RDC restraints is shown in Figure 3(a). The ensemble of structures shows excellent precision (0.53 Å for backbone atoms in regular elements of secondary structure) and low overall energies (Table 2). The analysis of stereochemical quality by the program PROCHECK[43] revealed that on average 98% of the residues lie in the most favored or additionally allowed regions of the Ramachandran plot (Table 2). Those that fall in the disallowed region correspond to S13, K15, D35 and K84. These unfavorable geometries are likely due to the fact that each of these residues fall within loops (Figures 3(b) and 5) and are poorly restrained. A ribbon diagram depicting the energy-minimized average structure is shown in Figure 3(b). The overall fold of the monomer consists of two α-helices (α1-α2) and a five stranded antiparallel β-sheet (β1–β5) connected by six loops (L1–L6). The helices are arranged perpendicular to one another with the shorter of the two (α1) packed against one face of the β-sheet and the longer one (α2) packed against the other. To orient α2, which is seven turns in length, the flanking strands, β2 and β3, position themselves as the outermost strands, while the remaining strands, β1, β4 and β5, position themselves as inner strands. The ten-stranded antiparallel β-sheet of the homodimer, which is formed by the simultaneous arrangement of α2 and β3 in an antiparallel manner, is rectangular in shape with α2 placed along the diagonal. The side of the β-sheet upon which the α2 packs is relatively smooth and convex in shape. In contrast, the side of the β-sheet upon which α1 packs has a major depression formed by the space between the two N-terminal

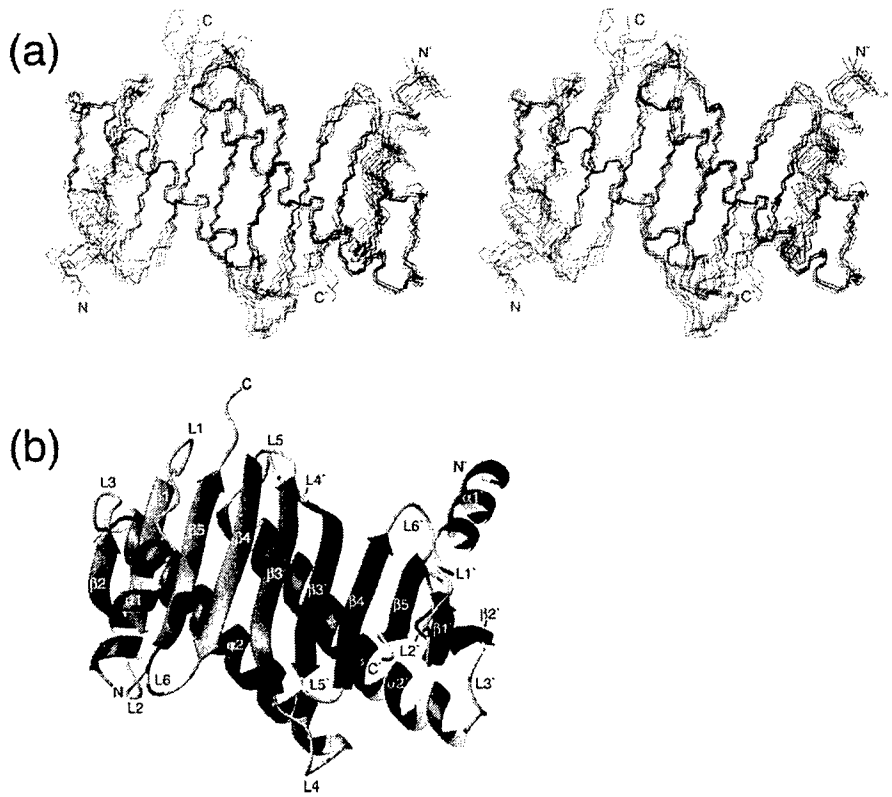

Figure 3. Solution structure of homodimeric km23. (a) A stereoview of the ensemble of eight lowest-energy structures superimposed on the basis of the deduced secondary structure, α1 (2–10), β1 (17–24), β2 (29–32), α2 (36–60), β3 (66–73), β4 (76–82), β5 (86–92). Monomers are colored red and blue. (b) Ribbon diagram of the km23 homodimer in which the regular elements of secondary structure are identified. Monomers are distinguished based upon the shading of the β-strands and α-helices (monomer 1, dark blue β-strands and red/yellow α-helices; monomer 2, light blue β-strands and magenta/yellow α-helices).

Table 2. Structural statistics for km23

Restraints		Experimental
Total restraints		1660
NOE distance restraints		
Intraresidue ($\|i-j\|=0$)		273
Sequential ($\|i-j\|=1$)		384
Short range ($2\leq\|i-j\|\leq5$)		214
Long range ($\|i-j\|>5$)		210
Intersubunit		40
Dihedral restraints		
ϕ		70
ψ		70
RDC restraints		
$^1D_{NH}$		63
$^1D_{C\alpha H\alpha}$		54
$^1D_{C\alpha C'}$		82
$^1D_{NC'}$		67
$^{2}D_{HNC'}$		67
Coupling restraints		
$^3J_{HNH\alpha}$		66
Deviation among ensemble		
Bonds (Å)		0.0033±0.0003
Angles (degrees)		0.85±0.03
Impropers (degrees)		0.87±0.095
Dihedral restraints (degrees)		2.4±0.8
RDC (Hz)		
$^1D_{NH}$		1.0±0.1
$^1D_{CH}$		2.1±0.1
$^1D_{C\alpha CO}$		3.9±0.2
$^1D_{NC'}$		2.6±0.1
$^{2}D_{NHC'}$		3.8±0.2
$^3J_{HN\alpha}$ restraints (Hz)		0.7±0.1
Ramachandran plot[a]		
Most favored (%)		79.1
Additionally allowed (%)		18.6
Generously allowed (%)		0.0
Disallowed (%)		2.3
Overall precision		
Secondary structure	Backbone[b]	0.53
	Heavy[b]	0.98
Ordered residues[c]	Backbone[b]	0.74
	Heavy[b]	1.25

Structural statistics are calculated for the ensemble of eight lowest energy structures.

[a] Calculated using the program PROCHECK.[43]

[b] Backbone atoms include N^H, C^α, and C^O; heavy includes all non-hydrogen atoms.

[c] Ordered corresponds to residues 21–112.

α-helices. This surface of the molecule, as discussed below, includes a number of solvent-exposed residues conserved among sequences from different species.

km23 dynamics

The internal flexibility of km23 has been investigated by measuring ^{15}N T_1, ^{15}N T_2, and ^{15}N-{^1H} NOE relaxation parameters at two magnetic field strengths (14.1 and 16.4 *T*). The raw relaxation data were analyzed to first determine the extent of diffusional anisotropy, which is important, as anisotropies as small as 1.2 have been shown to interfere with interpretation of relaxation data using the model-free formalism.[44]

To assess the extent of diffusional anisotropy for km23, the experimental T_1/T_2 data were fit to a diffusional model with axial symmetry.[45] The χ^2 value, which provides an indication of the agreement between the experimentally measured and modeled T_1/T_2 data, was found to be 6.7 and 4.4 for the data collected at 14.1 and 16.4 *T*, respectively (Table 3). These χ^2 values were lower than the corresponding ones obtained for the fit to an isotropic model (12.6 and 10.6 for the data collected at 14.1 and 16.4 *T*, respectively), indicating that km23 indeed tumbles anisotropically. To demonstrate that the improvement was specifically due to diffusional anisotropy, the experimental T_1/T_2 data were again fitted to an anisotropic model but with randomized N–H bond vector orientations. The χ^2 values obtained in this case ($\chi^2=11.8$ and 10.0 for the data collected at 14.1 and 16.4 *T*, respectively) (Table 3) were reduced relative to the values obtained with the isotropic model, but not nearly to the same extent as for the fit to the axially asymmetric model with non-randomized N–H bond vector orientations. The significance of the fit was further shown by the correspondence of the fitted parameters to those estimated from the calculated inertia tensor. Thus, the orientation of the principal axis of the experimentally fitted diffusion tensor, defined by the polar angles ϕ and ψ (Table 3A), agreed closely with ϕ and ψ values that define the principal axis of the calculated inertia tensor (Table 3B). The experimental estimates for the extent of anisotropy, $D_\parallel/D_\perp$ (Table 3A), also agreed with estimates based on the calculated inertial anisotropy (Table 3B). These observations are consistent with both that of the fitted tensor and the homodimeric structure of km23, as inertial calculations carried out on monomeric km23 predict a much lower degree of anisotropy ($D_\parallel/D_\perp=1.05$) and a principal axis that runs parallel to that of the β-strands, rather than perpendicular, as in the case of homodimeric km23.

The experimental T_1/T_2 data collected at the two different magnetic field strengths were also modeled assuming full diffusional asymmetry.[46] The χ^2 values in this case were slightly lower than those obtained by fitting to an axially symmetric model (5.8 and 3.7 for the data collected at 14.1 and 16.4 *T*, respectively). These fits, however, were not considered statistically significant, as the fitted parameters for the diffusion constants along the minor axes did not differ in a statistically significant way. This is consistent with the small degree of inertial anisotropy along the minor axes ($I_{yy}=1.80\pm0.07$ and $I_{zz}=2.01\pm0.06$) (Table 3B) and shows that the km23 homodimer is best described by an axially symmetric, not a fully asymmetric, diffusion tensor.

Model-free analyses were performed with the axially symmetric tensor described above using the program ModelFree4.[47] The model-free fits were carried out by simultaneously fitting the experimental relaxation data collected at the two magnetic field strengths using the procedure described by Mandel.[47] This yielded statistically significant fits for all residues, except L45, A81, T95 and E96. The S^2, τ_e, and R_{ex} values derived in this

Table 3. Modeling of the km23 diffusion tensor

A. *Experimental axially symmetric diffusion tensor*

Field	NH vectors	θ (degrees)	ϕ (degrees)	$D_{\|}/D_{\perp}$	τavg (ns)[a]	χ^{2} [b]
16.4 T	Experimental[c]	90.3±1.9	8.4±2.0	1.58±0.04	9.82±0.07	4.4±0.5
16.4 T	Random[d]	91.4±34.7	113.3±63.7	1.14±0.14	10.06±0.12	10.0±0.4
14.1 T	Experimental	90.3±3.9	11.3±2.7	1.68±0.06	9.53±0.03	6.7±04
14.1 T	Random	130.1±30.0	70.8±45.2	1.21±0.06	9.86±0.10	11.8±0.4

B. *Modeled axially symmetric diffusion tensor*[e]

I_{xx}	I_{yy}	I_{zz}	θ (degrees)	ϕ (degrees)	$D_{\|}/D_{\perp}$
1.00±0.00	1.80±0.07	2.01±0.06	89.3±0.1	−0.6±1.1	1.45±0.03

[a] The average correlation time defined according to the convention described by Woessner.[78]
[b] Normalized value of chi squared defined according to Tjandra.[45]
[c] NH bond vector orientations were calculated from the ten lowest energy km23 homodimer structures.
[d] NH bond vector orientations were calculated from the ten lowest energy km23 homodimer structures, but then randomized with respect to residue number.
[e] Euler angles (θ, ϕ) are based upon the calculated inertia tensor from the ten lowest energy km23 structures. Diffusional anisotropy, $D_{\|}/D_{\perp}$, is derived from the calculated inertia tensor from the ten lowest energy km23 homodimer structures using the relation $D_{\|}/D_{\perp} = [0.75(2(I_{\perp}/I_{\|})-1)]^{1/2}$.

manner are plotted in Figure 4. As shown, most residues exhibit S^2 values greater than 0.85, indicating that the backbone is relatively rigid on the ns to ps time-scale, although there are a few exceptions as shown by moderately decreased S^2 values and higher τ_e values for residues located near the N terminus (A2, E3 and V4) and in two loops (S13 and G16 in L1 and D85 in L6) (Figure 4). There are also residues that undergo motions on the ms to μs time-scales as satisfactory model-free fits of

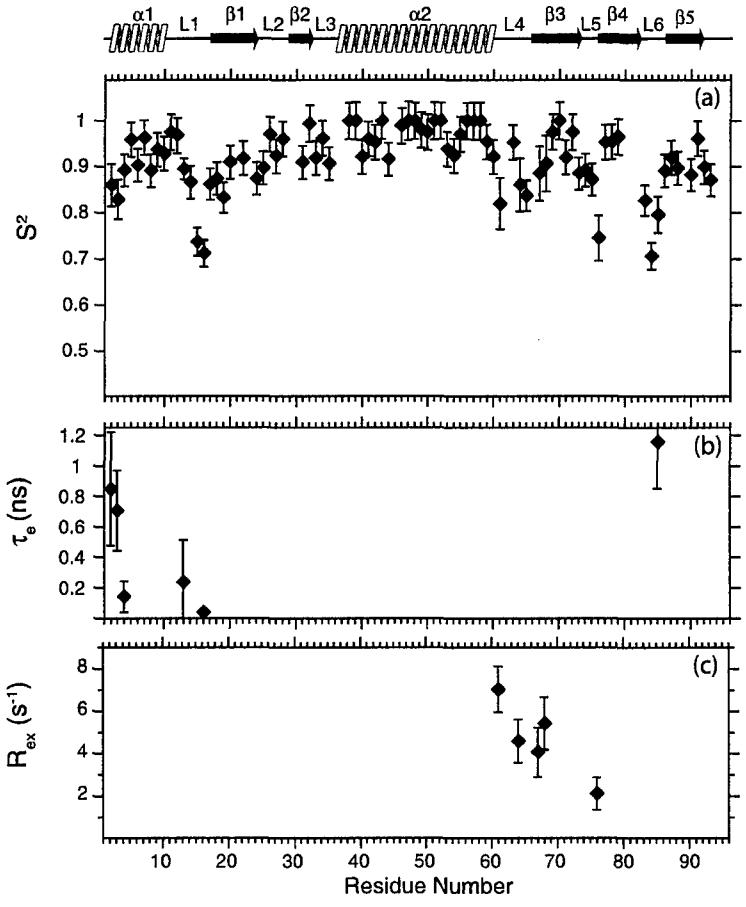

Figure 4. Model-free parameters for km23 backbone amides derived by simultaneous fitting of ^{15}N T_1, ^{15}N T_2, and ^{15}N-{^1H} NOE data recorded at magnetic field strengths of 14.1 and 16.4 *T*. The modeling was carried out using an axially symmetric diffusion tensor with $D_{\|}/D_{\perp}=1.63$, $\tau_{avg}=9.68$ ns, and N–H bond vector information derived from the average of the lowest energy km23 structures. Lipari-Szabo S^2, τ_e, and R_{ex} parameters are shown in (a), (b), and (c), respectively. Data points not shown for specific residues in (b) and (c) indicate that this parameter was not included in the motional model for that residue.

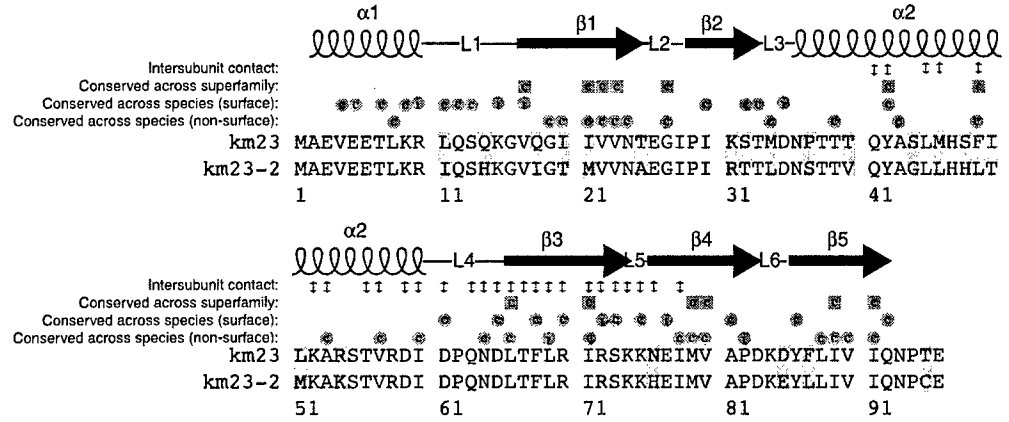

Figure 5. Conservation of km23 isoforms. Residues conserved across the MglB/robl superfamily are designated by purple squares with the letter c. Residues that are either invariant or conserved relative to that of km23 from different species are indicated by orange or light green circles with the letters i and c, respectively (surface and non-surface residues are distinguished based on their side-chain solvent accessible surface areas; those with greater than 40% exposure are considered surface; those with less than 40% exposure are considered non-surface). Residues that differ between human km23 and human km23-2 are shaded yellow. Residues that lie at the km23 homodimer interface are indicated by double-ended red arrows. Sequences used in the determination of the conservation across the MglB/robl superfamily were the 54 reported by Koonin and Aravind.[32] Sequences used in the determination of conservation of km23 across species were obtained from NCBI and included *H. sapiens, R. norvegicus, M. musculus, C. familiaris, G. gallus, D. rerio, C. reinhardtii, D. melanogaster, C. elegans, C. briggsae, S. similes, G. lamblia, A. gambiae, C. intestinalis, and T. nigrovirdis*. Sequence conservation was assessed using the program AMAS[49] with a conservation threshold of 7.

the relaxation data required non-zero R_{ex} terms for five residues. These are clustered in loop L4 (D61, N64, T67 and F68) as shown (Figure 4).

Discussion

Homodimeric nature of km23 provides a structural paradigm for the MglB/robl superfamily

The analytical ultracentrifugation and NMR experiments described here have shown that km23 is homodimeric in solution and that the dimerization is mediated by the simultaneous pairing of the edge β-strand (β3) of a five-stranded antiparallel β-sheet and by a seven turn α-helix (α2) that lies diagonally across the surface of the sheet. The interfacial contact is extensive, with each of the monomers burying 1255 Å^2 of solvent accessible surface at the interface. The residues that participate in the interface are 60% hydrophobic and 40% charged or polar (Figure 5, red double-ended arrows). The hydrophobic residues generally exhibit a low degree of solvent accessibility (8.6% on average) and are located mostly along α-helix 2 or β-strand 3. Those along α-helix 2 pack against the underlying β-sheet, whereas those along β-strand 3 pack against residues from β-strand 3 of the other monomer. The charged and polar residues generally exhibit a higher degree of solvent accessibility (29.2% on average) and are found both within the secondary structures that form the interface (α2 and β3), as well as in the connecting loops that approach one another at the interface (loop 4 from one monomer and loop 5 from the other monomer; see Figure 3(b)). The charged or polar residues found within α2 (Q41, K52, and D59) or β3 (R70 and R72) invariably exhibit a high degree of solvent accessibility and therefore are not likely important in terms of either stabilizing the dimer or in determining the specificity of the monomer-monomer pairing. The charged or polar residues in the connecting loops (D61, Q63, N64, and D65 in loop 4 and R70 and R72 in loop 5) exhibit a lower degree of solvent accessibility and engage one another through ion pairs (loop 4 D61–loop 5′ K75 and loop 4 D65–loop 5′ K74) and several side-chain–side-chain and side-chain–backbone hydrogen bonds. Thus, in contrast to the polar and charged residues noted above, those in loops 4 and 5 are likely important both in stabilizing the dimer and contributing to the specificity of the monomer-monomer pairing.

The km23 homodimer as noted is similar in architecture to the heterodimer formed between the MglB family proteins, p14 and MP1.[33,34] The structural similarity between the two dimers, as indicated by the RMSD in backbone atom positions of residues within the β1–β2–α2–β3–β4–β5 structural core, is 1.4 Å (Figure 6(a)). The largest structural difference between the two dimers involves the N-terminal α-helix (α1), which in km23 is positioned such that it initiates above the N-terminal end of β-strand 5 and proceeds in a direction parallel to that of the underlying strands, whereas in p14 it initiates above the N-terminal end of β-strand 2 and proceeds diagonally across the strands (Figure 6(b)). This change enables the

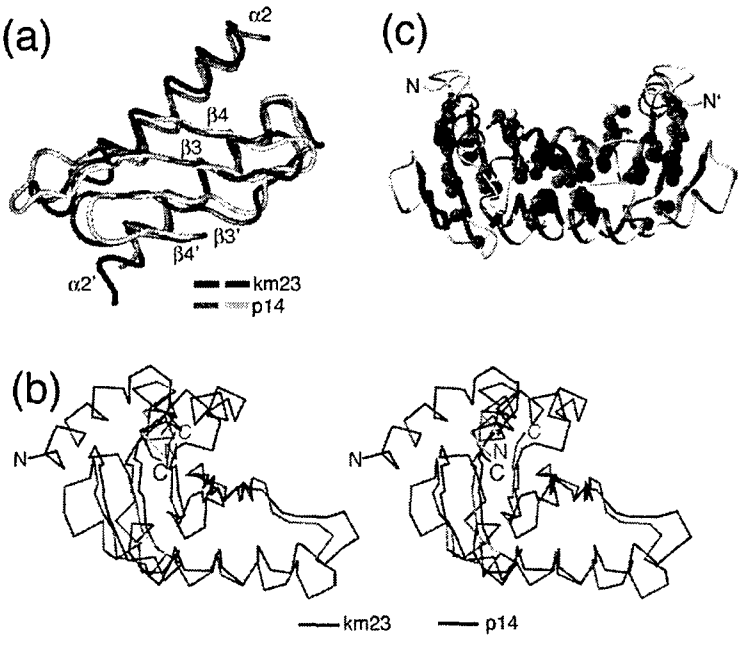

Figure 6. Structural comparison of the km23 homodimer with the crystal structure of the p14:MP1 heterodimer.[33] (a) An overlay of backbone ribbons of the km23 homodimer and p14:MP1 heterodimer in the region of the dimer interface. Region shown includes the interfacial α-helix and β-strand (α2 and β3, respectively) together with the flanking β-strand (β4). Ribbon corresponding to km23 is depicted in dark blue and magenta; ribbon corresponding to p14:MP1 is depicted in light blue and pink. (b) An overlay of C^{α} traces of the km23 monomer (red) and the p14 component of the p14:MP1 heterodimer (blue) shown in stereo. Structures were aligned by minimizing the deviation between the backbone atom positions of β1, β2, α2, β3, β4, and β5. km23 and p14 are shown to share a conserved arrangement of β1, β2, α2, β3, β4, and β5, but differ in that p14 includes a C-terminal α-helix, whereas km23 does not. km23 and p14 also differ in that the N-terminal helix lies nearly parallel with the underlying β-strands in km23, whereas in p14, the helix lies at an approximate 30 degree angle such that the N terminus is positioned close to β-strand 3 near the center of the dimer interface. (c) A ribbon diagram of the km23 homodimer (rotated by +90 degrees around the *x*-axis relative to that shown in Figure 3(b)) in which the side-chains of residues conserved among all known members of the MglB/robl superfamily are displayed. Residues included are V17, I20, I21, V22, G27, A43, F49, L66, I71, M79, V80, I89, and I91. Residues cluster in the area between the central ten-stranded antiparallel β-sheet and the α-helices (α1, α2) that pack against it. Ribbon is shaded such that the strands and helices from one monomer are dark blue and red/yellow, respectively, while those from the other monomer are light blue and magenta/yellow, respectively. Side-chains are displayed in CPK format with carbon atoms shaded green and sulfur atoms shaded yellow.

C-terminal α-helix, which is present in MglB, but not robl family members, to pack against the N-terminal α-helix without overlapping with the C-terminal helix from the other monomer.

The other feature that the p14:MP1 heterodimer and the km23 homodimer share in common is the fact that both form tight dimers. This has been directly shown in the case of the p14:MP1 heterodimer through the determination of the p14:MP1 dissociation constant ($K_d = 13$ nM) using surface plasmon resonance.[34] The K_d of the km23 monomers for one another has not been determined directly, although we estimate it to be about 10 nM or lower. This estimate is based on a dissociation rate constant (k_{off}) of about $5\ s^{-1}$ or slower and an association rate constant (k_{on}) of $5\times10^8\ M^{-1}\ s^{-1}$. The value for k_{off} is based upon the experimental observation of high intensity positive NOEs in the filtered NOESY experiments, which would only occur if the disassociation rate constant was slower than the inverse of the NOE mixing time (120 ms). The value for k_{on} is based upon the assumption that association is diffusion-controlled and that it occurs according to the translational rate constants determined from the sedimentation velocity analytical ultracentrifugation experiments in the absence of urea.

The high degree of structural similarity between these two dimers is rather remarkable given that their primary sequences are relatively poorly conserved (km23 exhibits 32% and 30% conservation relative to MP1 and p14, respectively, when residues at structurally equivalent positions are compared). The residues that are conserved between these proteins and other members of the MglB/robl superfamily are indicated in Figure 5 (purple squares with the letter c). These conserved residues are largely hydrophobic, and as illustrated in Figure 6(c), lie principally at the interface between the central ten-stranded β-sheet and α-helices 1 and 2 that pack on either side. These observations, together with the high stability of the two dimers that have been studied, suggest that all members of the MglB/robl superfamily adopt and function in the context of such dimeric structures. The significance of this is not yet clear, although one possibility, as suggested in the case of the p14:MP1 heterodimer, is to enable binding to multiple partners *via* distinct interactions through each of the monomeric subunits.[33,34] The significance of this in the case of homodimers is less clear, although one possibility as discussed below in the context of the km23 homodimer, may be to enhance affinities for binding *via* avidity effects.

Conserved surfaces and potential binding sites for Smad and DIC

The DIC binding function of km23 has been demonstrated previously.[10] km23 has also been shown to be serine-phosphorylated after TGFβ receptor activation[10] and to be partially required for TGFβ-mediated effects on both fibronectin expression and cell cycle progression.[10,28,48] The emerging picture from these findings is that TGFβ signaling leads to the phosphorylation of both Smad2 and km23 and that phosphorylated km23 plays an essential role in the dynein-mediated transport of Smad2 to the nucleus.[48] km23 may therefore bind TβRII, Smad2, and DIC, and such binding, as in the case of the DIC, may be regulated *via* phosphorylation.

To identify potential protein binding sites on the surface of km23, we analyzed the location of surface residues that are either invariant or conserved among km23 sequences from different species. The invariant and conserved residues were identified by aligning km23 sequences from different species and by assessing conservation using a flexible set-based method as implemented in the program AMAS.[49] The criterion used to distinguish surface residues from non-surface residues was based on the calculated residue-specific side-chain solvent accessible surface areas (the cutoff was set at 40%; those residues with greater than 40% solvent accessible surface areas were considered surface; those with less than 40% solvent accessible surface areas were considered non-surface). The invariant and conserved residues identified in this manner are indicated in Figure 5 (orange circles with an i and green circles with a c, respectively) and their location on the surface of the km23 homodimer is shown in Figure 7(a). The most striking feature is that the invariant (shaded red) and the conserved residues (shaded either green or yellow depending upon whether they are serine or non-serine, respectively) map to the face of the molecule and to the adjacent edge that includes the N-terminal α-helices (middle and left panels, respectively) but not the convex surface formed by the seven turn α-helices (right panel). The three conserved serine residues, S13, S32, and S73, are distributed amongst the invariant and conserved residues with S13 and S73 lying on the surface that includes the two N-terminal α-helices and with S32 lying on the adjacent edge. This is potentially significant as complementary biochemical studies (provided as Supplementary Data) have shown that the conserved serine residues, particularly S32 and S73, are critical sites for phosphorylation by the TGFβ receptors. Taken together, these observations

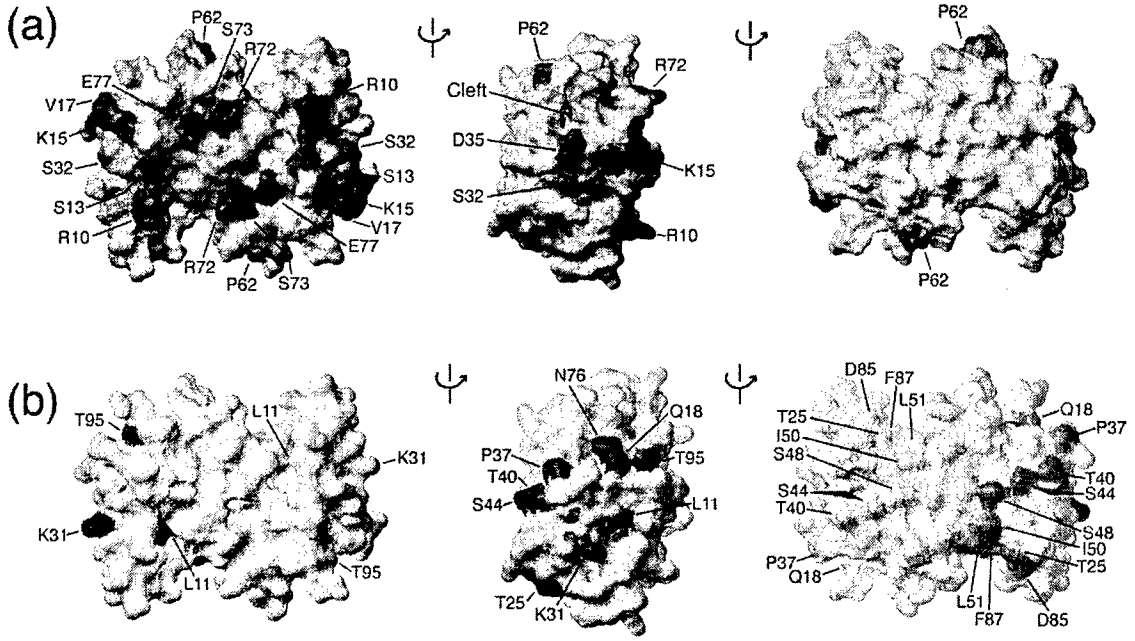

Figure 7. Potential binding sites on the surface of the km23 homodimer. (a) km23 residues that are invariant or conserved across a range of 15 different species and exhibit greater than 40% solvent exposure of their side-chains are shaded red, yellow, or green. Residues shaded red are invariant, residues shaded yellow correspond to conserved non-serine residues, and residues shaded green correspond to conserved serine residues. All other residues are shaded grey. The three surfaces shown correspond to different views of the same molecule. The view shown on the left corresponds to that shown in Figure 3(b). The other two views correspond to successive +90 degree rotations around the *y*-axis of that shown on the left. The "cleft" label designates the deep cleft formed by the incomplete overlap of loops 4 and loop 5 from opposing monomers. (b) km23 residues that differ relative to km23-2 are shaded red and yellow (the two colors correspond to whether these residues originate from monomer 1 or 2). All other residues are shaded grey. The three surfaces shown correspond to different orientations as in (a).

suggest that the surface that includes the two N-terminal α-helices may be involved in DIC binding and that phosphorylation of S32, S73, or both by the TGFβ receptors may regulate this process.

The cleft that is formed by incomplete overlap of loops 4 and 5 from the two monomers that lies adjacent to the putative DIC binding site (Figure 7(a), middle panel, labeled cleft) provides an ideal binding site for other molecules that km23 might bind, such as TβRII and Smad2. The key features of this site include its size, which is narrow (2–3 Å) and deep (11 Å), and the fact that it is lined with a number of hydrophobic residues, including A53, T56, V57, I60, and L66 from one subunit and Y42, M46, F49, I71, I78, V80, and I89 from the other subunit, all but two of which, M46 and T56, are conserved among km23 sequences from different species (Figure 5). The other interesting feature of this site includes the fact that it is flexible on both the ns-to-ps and ms-to-μs time-scales as shown by decreased order parameters (S^2) for most residues in loops 4 and 5 (Figure 4(a)) and non-zero R_{ex} terms for residues 61 and 64 in loop 4, residues 67 and 68 in the N-terminal end of β-strand 3, and residue 76 in loop 5 (Figure 4(c)), respectively. The flexibility inherent in this region of the protein is particularly intriguing, because if this indeed corresponds to the functional cargo binding site, it would provide a similar solution as to how to bind different partners using a single site as that of the LC8 DLCs.[22,27] There are clearly other possible binding modes that might utilize one of the other km23 serine residues to regulate DIC binding. There may also be as yet undetected surfaces through which km23 binds either DIC or other partners. Whatever the mechanism, the structure of the km23 presented here provides an invaluable resource with which to begin to dissect the diverse binding properties that this protein has been shown to exhibit.

km23 and km23-2 mainly differ through substitution of surface residues

The structure of the km23 homodimer presented here contributes to our understanding of the diversity of DLC subtypes in two important ways. The first is that it unequivocally establishes that the LC7/robl/km23 class of light chains is structurally distinct from that of the LC8 and Tctex classes. The LC7/robl/km23 class has an α–β–β–α–β–β–β topology with a strand order of β2–β1–β5–β4–β3, whereas the LC8 and Tctex class has an α–β–α–α–β–β–β–β topology with a strand order of β1–β4–β5–β2–β3′ (β3′ designates that β3 is from the other monomer). The two structurally distinct folds have likely arisen to enable diversification of cargo binding. The fact that both form stable homodimeric structures is curious and could be related to the fact that both bind their cargo peptides at the conformationally flexible dimer interface, as alluded to earlier. The homodimeric structures might alternatively enable tighter binding to other dimeric species through the existence of two weak non-interacting binding sites (i.e. through avidity effects). This could be important, for example, in binding and orienting km23 on the surface of the cytoplasmic domain of TβRII as homodimeric TGFβ assembles TβRI and TβRII into a heterotetrameric complex containing two type I and type II receptors. This type of binding would also be functionally advantageous, as this would ensure that km23 only binds and is phosphorylated upon ligand-induced assembly of the TβRI:TβRII tetrameric complex.

The second way in which the structure of the km23 homodimer contributes to our understanding of the diversity of light chains relates to the existence of the other mammalian homologue of km23, km23-2. km23-2 shares 77% sequence identity with km23, and as shown through the cell-based studies, forms complexes, likely heterodimers, with km23-2. There are not, as yet, any documented differences in either DIC or cargo binding properties of km23 and km23, although the two homologues have in some cases been shown to be differentially expressed.[50]

The fact that km23 and km23-2 can form a heterodimeric structure is not surprising in light of the structure presented here, since out of the 27 interfacial residues in km23, only three differ in km23-2. These include M46, F49, and N76 in km23, which are substituted to L46, L49, and H76 in km23-2 (Figure 5, red double-ended arrows). These differences are not anticipated to have a major effect on dimerization since the substitutions are, in general, conservative and since the interfacial contact area is extensive for just one of them (L49, which has an interfacial contact area of 83 Å^2; M46 and N76 have interfacial contact areas of just 7 and 16.5 Å^2, respectively).

To identify differences in potential binding properties of km23 and km23-2, we have analyzed the location of residues that differ between these isoforms, as shown in Figure 7(b) (yellow and red shading indicates whether the residues fall within the first or second monomer). The striking feature of the pattern is that it is the opposite of that shown in Figure 7(a). This suggests that residues that differ between km23 and km23-2 do not alter either DIC or cargo binding. What role then might such residue differences play? One possibility is that there may exist an as yet unidentified binding protein that differentially interacts with residues that are part of this surface to modulate function of one particular isoform over the other. One other possibility is that such differences play no real role other than accommodating the existing structure without altering either DIC or cargo binding. One way that this may have happened is through gene duplication, leading to a functionally equivalent protein with the same overall structure, but transcriptionally regulated in a distinct developmentally and tissue-specific manner. One advantage this would provide would be to regulate specific transport and/or motor regulatory activities in a manner most appropriate to individual cells and tissues.

Materials and Methods

Constructs

A construct encoding His-tagged human km23 was generated by PCR amplification of the km23 coding region and insertion into the NdeI and BamHI sites of the bacterial expression vector pET15b (Novagen, Madison, WI). The Flag-tagged km23 and km23-2 constructs were generated by inserting a PCR fragment of human km23 or km23-2 into the pFlag-CMV 5a vector (Sigma-Aldrich, St. Louis, MO) using the BglII and SalI cloning sites. The V5-tagged km23 construct was generated by cloning km23 into the pcDNA3.1/V5-His vector (Invitrogen, Carlsbad, CA) using the BamHI and XhoI cloning sites. All constructs were verified by DNA sequencing in both directions.

Expression and purification of km23

km23 protein samples were prepared by transforming the pET15b expression construct into BL21(DE3) host cells and then culturing the transformed cells on LB medium at 37 °C containing 100 μg/ml ampicillin. Protein expression was induced by the addition of 1 mM isopropyl-β-D-galactopyranoside (IPTG) when the absorbance of the cell culture at 600 nm reached 0.6–0.7. Cells were harvested three hours after induction and frozen. Cells from one liter of culture medium were resuspended in 40 ml of lysis buffer (50 mM NaCl, 20 mM Tris–HCl (pH 7.9), 5 mM imidazole, 1 mM phenylmethyl-sulfonyl fluoride, 10 μM leupeptin) and sonicated. Lysates were centrifuged at 14,000*g* for 20 minutes to remove the debris and the supernatant was filtered through a 0.45 μM membrane before loading onto a 5 ml bed of His·Bind resin (Novagen, Madison, WI) equilibrated with lysis buffer. The resin was sequentially washed with 45 ml of lysis buffer and 45 ml of wash buffer (50 mM NaCl, 20 mM Tris–HCl (pH 7.9), 60 mM imidazole) and the protein was then eluted with 30 ml of elution buffer (50 mM NaCl, 20 mM Tris–HCl (pH 7.9), 1 M imidazole). The protein was dialyzed against 25 mM sodium acetate, 0.02% sodium azide at pH 6.0 and then concentrated using a centrifugal filter with a 3000 molecular weight cutoff (VivaSciences, Palaiseau Cedex, France).

Cell culture

293T cells were purchased from American Type Culture Collection (ATCC, Rockville, MD) and were cultured in Dulbecco's Modified Eagle's Medium with glutamine supplemented with 10% (v/v) heat-inactivated fetal bovine serum. Cells were maintained in 5% CO_2 at 37 °C. Cultures were routinely screened for mycoplasma using Hoechst staining.

Immunoprecipitation/immunoblotting (IP/blot)

293T cells were transiently transfected with the indicated constructs using Lipofectamine PLUS (Invitrogen, Carlsbad, CA) following the manufacturer's protocol. 24 hours after transfection, cells were harvested using RIPA buffer (1x PBS, 1% (v/v) Nonidet P-40, 0.5% (w/v) sodium deoxycholate, 0.1% (w/v) SDS) supplemented with protease inhibitor cocktail (Roche, Indianapolis, IN). The cell lysates were incubated with 2 μg anti-V5 antibody (Invitrogen, Carlsbad, CA) for one hour at 4 °C, followed by incubation with 20 μl of Protein G-Plus agarose beads (Santa Cruz Biotechnology, Inc, Santa Cruz, CA) overnight at 4 °C. Agarose beads were washed three times with RIPA buffer and immune complexes were separated by 15% (w/v) SDS-PAGE, transferred to a PVDF membrane, and immunoblotted with an anti-Flag antibody (Sigma-Aldrich, St. Louis, MO).

Sedimentation velocity

The oligomeric state of km23 was investigated by monitoring its sedimentation properties in sedimentation velocity experiments as the urea concentration was varied. The samples used for these experiments were 0.50 ml in volume and consisted of 0.30 mM km23 in 25 mM sodium acetate (pH 6.0) with 0, 1.0, 2.0, 2.3, 2.6, and 3.0 M urea. The sedimentation velocity profiles were collected by monitoring the absorbance at 280 nm as the samples were centrifuged at 60,000 rpm and 20 °C in a Beckman Optima XL-I centrifuge fitted with a four-hole AN-60 rotor and double-sector aluminum centerpieces. Sedimentation coefficients and molecular masses were determined by fitting using both the C(*s*) method[35] and by finite element solutions to the Lamm equation,[36] both as implemented in UltraScan 7.0.[51] Buffer density and viscosity corrections were made using the method described by Laue *et al.*[52] as implemented in UltraScan.[51] The partial specific volume of km23 was estimated from the protein sequence as described by Cohn and Edsall.[53]

NMR samples

Samples of km23 for NMR were prepared in buffer consisting of 25 mM deuterated sodium acetate, 0.02% (w/v) sodium azide (pH 6.0) and were between 0.3 and 0.8 mM in concentration. Samples of km23 uniformly labeled with either ^{15}N or ^{15}N, ^{13}C were prepared by *E. coli* expression and purification as described above, except minimal medium with isotopically labeled growth substrates was used in place of LB medium. Samples of 10% fractionally ^{13}C labeled km23 for assignment of the side-chain methyl groups of valine and leucine were prepared by culturing the cells on minimal medium containing 0.03 g l^{-1} {^{13}C]glucose and 0.27 g l^{-1} unlabeled glucose.[54] Isotopic heterodimers of km23 were prepared by mixing an equal amount of unlabeled and ^{13}C, ^{15}N isotopically labeled km23 in 25 mM sodium acetate at pH 6.0 containing 6 M urea. The mixture was then dialyzed at 4 °C into NMR buffer and then concentrated to a final concentration of 0.6 mM.

NMR spectroscopy

All NMR experiments were performed at 42 °C on Bruker 600 MHz and 700 MHz spectrometers equipped with either conventional (700 MHz) or cryogenically cooled (600 MHz) 5 mm ^{1}H probes equipped with ^{13}C and ^{15}N decoupler and pulsed field gradient coils. All spectra were processed using NMRPIPE[55] and analyzed using the program NMRView.[56]

Resonance assignments

Backbone resonance assignments of km23 were obtained by collecting and analyzing HNCA,[57] HNCACB,[58] CBCA-(CO)NH,[59] and HNCO[60] data sets. Side-chain ^{1}H and ^{13}C assignments were obtained by collecting and analyzing (H)CC(CO)NH[61] and H(CC)HTOCSY[62] data sets. Aromatic

ring proton assignments were achieved by first recording a ^{1}H–^{13}C HSQC and a ^{1}H–^{13}C HSQC with a ^{1}H TOCSY relay using an unlabeled km23 sample. Assigned aromatic spin systems were correlated with those of the backbone through $^{1}H^{\beta}$–$^{1}H^{\delta}$ NOEs identified in a 3-D ^{13}C-separated NOESY spectrum.

Structural restraints

Intramolecular NOE distance restraints were identified through analysis of three-dimensional ^{15}N and ^{13}C-edited NOESY experiments performed using mixing times 120 ms and 200 ms, respectively. Ambiguities that arose in the assignment of amide-aliphatic NOEs in the three-dimensional ^{15}N-edited spectrum were further resolved by recording a 3-D ^{15}N-, ^{13}C-edited NOESY spectrum with a mixing time of 134 ms. Intermolecular NOEs were identified by recording 3-D ^{12}C-filtered, ^{15}N-edited and 3-D ^{12}C-filtered, ^{13}C-edited NOESY experiments[63,64] using a km23 isotopic heterodimer prepared in the manner described above. Residual dipolar couplings (RDCs) were measured by preparing ^{15}N or ^{15}N, ^{13}C labeled km23 in NMR buffer containing 10 mg ml^{-1} Pf1 phage (Asla Biotech, Riga, Latvia) and by recording the appropriate NMR experiment. One-bond ^{1}H–^{15}N RDCs ($^{1}D_{NH}$) were measured by recording a 2-D IPAP-HSQC[65] with ^{15}N labeled protein. One-bond ^{15}N–$^{13}C'$ ($^{1}D_{NC'}$), one-bond $^{13}C^{\alpha}$–$^{13}C'$ ($^{1}D_{C\alpha C'}$), one-bond $^{1}H^{\alpha}$–$^{13}C^{\alpha}$ ($^{1}D_{H\alpha C\alpha}$), and two-bond $^{13}C'$–^{1}H ($^{2}D_{C'H}$) RDCs were measured with ^{13}C, ^{15}N labeled protein by recording a 2-D ^{1}H–^{15}N HSQC with $^{13}C'$ coupling in the indirect dimension, a $^{13}C^{\alpha}$-coupled 3-D HNCO,[66] a 3-D (HA)CA(CO)NH,[67] and a $^{13}C'$-coupled 2-D ^{1}H–^{15}N HSQC, respectively. Backbone ϕ and ψ restraints were obtained by analysis of the assigned chemical shifts using the program TALOS,[39] and in the case of ϕ, by additionally measuring $^{3}J_{HN\alpha}$ couplings using an HNHA experiment.[68]

Structure calculations

NOE restraints were grouped into three distance ranges, 1.8–2.7 Å (1.8–2.9 Å for distances involving ^{15}N-bound protons), 1.8–3.3 Å (1.8–3.5 Å for distances involving ^{15}N-bound protons), and 1.8–5.0 Å. Upper distances for restraints involving methyl protons were increased by 0.5 Å. Distances involving methyl protons, aromatic ring protons, and non-stereospecifically assigned methylene protons were represented as r^{-6} sum, $\sqrt[-1/6]{(\sum_{ij} r_{ij}^{-6})}$. Structures were determined from a total of 1660 experimental restraints, including 1121 distance restraints, 70 chemical shift derived ϕ and ψ restraints, 66 $^{3}J_{HN\alpha}$ restraints, and 333 RDC restraints (Table 1). Symmetry of the dimer was enforced by additionally including non-crystallographic restraints for backbone N, C^{α}, and C′ atoms. Structures were calculated by using distance geometry and simulated annealing protocols[69] in torsion angle space[70] with the program X-PLOR-NIH.[38] Agreement of the calculated NMR structures with the experimentally measured RDC data was calculated using the program PALES.[41]

Backbone ^{15}N relaxation parameters

Backbone amide ^{15}N T_1, ^{15}N T_2, and ^{15}N–{^{1}H} NOE relaxation data sets were recorded in an interleaved manner at 42 °C at magnetic field strengths of 14.1 and 16.4 T (corresponding to ^{15}N frequencies of 60.81 MHz and 70.95 MHz, respectively) using ^{1}H-detected pulse schemes as described.[71] The T_1 and T_2 data sets were each collected using a total of 32 scans (eight scans per cycle, four cycles), an ^{15}N acquisition time of 136 ms, and a recycle time of 1.0 s. The T_1 and T_2 data sets were acquired using 12 delay times, which varied between 16–3600 ms and 16–400 ms, respectively. The spacing between the center of the ^{15}N π refocusing pulses (80 μs) in the CPMG of the ^{15}N T_2 experiment was 1 ms. The NOE data were recorded using 128 scans per point with a total ^{15}N acquisition time of 136 ms. The T_1 and T_2 relaxation times were obtained by fitting relative peak heights as a function of T_1 or T_2 delay time to a two parameter exponential. The errors in individual T_1 and T_2 measurements were estimated by Monte Carlo simulations.[72] NOE values were obtained by taking the ratio of peak intensities from experiments performed with and without ^{1}H presaturation and by applying a correction to take into account the incomplete recovery of both ^{15}N and ^{1}H magnetization.[73]

Modeling of the rotational diffusion tensor

The rotational diffusional anisotropy of km23 was modeled assuming axial symmetry. The relaxation data used for the calculation consisted of experimental T_1/T_2 ratios for 68 residues. Excluded from these calculations were 15 residues identified using the criteria described by Barbato[74] as undergoing exchange or high amplitude internal motion on the ns-ps time-scale. Amide bond vector orientations were calculated from the ten lowest energy NMR structures. The parameters describing the diffusion tensor, τ_{avg}, $D_{\|}/D_{\perp}$, θ, ϕ, were obtained by minimizing the quantity χ^2:

$$\chi^2 = \frac{1}{n}\sum_{1}^{n}[(T_1^{exp}/T_2^{exp}) - (T_1^{calc}/T_2^{calc})]/(T_1^{err}/T_2^{err}) \quad (1)$$

using the computational strategy described by Tjandra.[45] The statistical significance of the fit was assessed by repeating the fitting procedure after having randomized the residue numbers in the T_1/T_2 data table.

The km23 diffusion tensor was modeled by calculating the components of the inertia tensor from the coordinates of the km23 NMR structures. The axial ratio of the diffusion tensor was then approximated using the relation:

$$D_{\|}/D_{\perp} = [0.75(2(I_{\perp}/I_{\|}) - 1)]^{1/2} \quad (2)$$

This equation applies to a perfect ellipsoid[75] and therefore only roughly approximates the extent of diffusional anisotropy based upon the inertia calculation.

Modeling of internal motion

The internal dynamics of km23 were assessed by analyzing the experimental ^{15}N relaxation parameters using the model-free formalism[76,77] and by assuming that the protein tumbles as an axially symmetric rotor. This was accomplished using the program ModelFree4 and the model selection strategy based on F-statistics described by Mandel.[47] Five different models for internal motion were considered, S^2 (model 1), S^2, τ_e (model 2), S^2, R_{ex} (model 3), S^2,τ_e,R_{ex} (model 4), and S^2, S_f^2, τ_e (model 5).

Atomic coordinates accession codes

The km23 chemical shift assignments have been

deposited in the BMRB database under accession code 6527. The ensemble of low energy structures has been deposited in the RCSB database under accession code 1Z09.

Acknowledgements

Dr Virgil Schirff is thanked for collecting the analytical ultracentrifugation data. This work was supported by NCI grant CA100239, including an NMR Supplement awarded as CA100239-S1, to K.M.M. Additional financial support was provided by the Robert A. Welch Foundation (AQ1431 to A.P.H.), the Dept of Defense (DAMD17-03-0287 to K.M.M.), the NIH (GM58670 and RR13879 to A.P.H., CA92889 and CA90765 to K.M.M., and CA54174 to the Macromolecular Structure Shared Resource of the San Antonio Cancer Institute), the NSF (DBI-9974819 to B.D.) and the San Antonio Life Science Institute (10001642 to B.D.).

Supplementary Data

Supplementary data associated with this article can be found, in the online version, at doi:10.1016/j.jmb.2005.07.002

References

1. Vallee, R. B., Williams, J. C., Varma, D. & Barnhart, L. E. (2004). Dynein: an ancient motor protein involved in multiple modes of transport. *J. Neurobiol.* **58**, 189–200.
2. Gunawardena, S. & Goldstein, L. S. (2004). Cargo-carrying motor vehicles on the neuronal highway: transport pathways and neurodegenerative disease. *J. Neurobiol.* **58**, 258–271.
3. King, S. M. (2000). The dynein microtubule motor. *Biochim. Biophys. Acta*, **1496**, 60–75.
4. Vale, R. D. (2003). The molecular motor toolbox for intracellular transport. *Cell*, **112**, 467–480.
5. Vallee, R. B. & Sheetz, M. P. (1996). Targeting of motor proteins. *Science*, **271**, 1539–1544.
6. Harada, A., Takei, Y., Kanai, Y., Tanaka, Y., Nonaka, S. & Hirokawa, N. (1998). Golgi vesiculation and lysosome dispersion in cells lacking cytoplasmic dynein. *J. Cell Biol.* **141**, 51–59.
7. Vallee, R. B. & Hook, P. (2003). Molecular motors: a magnificent machine. *Nature*, **421**, 701–702.
8. Sakato, M. & King, S. M. (2004). Design and regulation of the AAA microtubule motor dynein. *J. Struct. Biol.* **146**, 58–71.
9. Bowman, A. B., Patel-King, R. S., Benashski, S. E., McCaffery, J. M., Goldstein, L. S. & King, S. M. (1999). Drosophila roadblock and Chlamydomonas LC7: a conserved family of dynein-associated proteins involved in axonal transport, flagellar motility, and mitosis. *J. Cell Biol.* **146**, 165–180.
10. Tang, Q., Staub, C. M., Gao, G., Jin, Q., Wang, Z., Ding, W. *et al.* (2002). A novel transforming growth factor-β receptor-interacting protein that is also a light chain of the motor protein dynein. *Mol. Biol. Cell*, **13**, 4484–4496.
11. Susalka, S. J., Nikulina, K., Salata, M. W., Vaughan, P. S., King, S. M., Vaughan, K. T. & Pfister, K. K. (2002). The roadblock light chain binds a novel region of the cytoplasmic Dynein intermediate chain. *J. Biol. Chem.* **277**, 32939–32946.
12. Jaffrey, S. R. & Snyder, S. H. (1996). PIN: an associated protein inhibitor of neuronal nitric oxide synthase. *Science*, **274**, 774–777.
13. Fan, J. S., Zhang, Q., Li, M., Tochio, H., Yamazaki, T., Shimizu, M. & Zhang, M. (1998). Protein inhibitor of neuronal nitric-oxide synthase, PIN, binds to a 17-amino acid residue fragment of the enzyme. *J. Biol. Chem.* **273**, 33472–33481.
14. Puthalakath, H., Huang, D. C., O'Reilly, L. A., King, S. M. & Strasser, A. (1999). The proapoptotic activity of the Bcl-2 family member Bim is regulated by interaction with the dynein motor complex. *Mol. Cell.* **3**, 287–296.
15. Puthalakath, H., Villunger, A., O'Reilly, L. A., Beaumont, J. G., Coultas, L., Cheney, R. E. *et al.* (2001). Bmf: a proapoptotic BH3-only protein regulated by interaction with the myosin V actin motor complex, activated by anoikis. *Science*, **293**, 1829–1832.
16. Schnorrer, F., Bohmann, K. & Nusslein-Volhard, C. (2000). The molecular motor dynein is involved in targeting swallow and bicoid RNA to the anterior pole of Drosophila oocytes. *Nature Cell Biol.* **2**, 185–190.
17. Raux, H., Flamand, A. & Blondel, D. (2000). Interaction of the rabies virus P protein with the LC8 dynein light chain. *J. Virol.* **74**, 10212–10216.
18. Vadlamudi, R. K., Bagheri-Yarmand, R., Yang, Z., Balasenthil, S., Nguyen, D., Sahin, A. A. *et al.* (2004). Dynein light chain 1, a p21-activated kinase 1-interacting substrate, promotes cancerous phenotypes. *Cancer Cell*, **5**, 575–585.
19. Nagano, F., Orita, S., Sasaki, T., Naito, A., Sakaguchi, G., Maeda, M. *et al.* (1998). Interaction of Doc2 with Tctex-1, a light chain of cytoplasmic dynein. Implication in dynein-dependent vesicle transport. *J. Biol. Chem.* **273**, 30065–30068.
20. Campbell, K. S., Cooper, S., Dessing, M., Yates, S. & Buder, A. (1998). Interaction of p59fyn kinase with the dynein light chain, Tctex-1, and colocalization during cytokinesis. *J. Immunol.* **161**, 1728–1737.
21. Tai, A. W., Chuang, J. Z., Bode, C., Wolfrum, U. & Sung, C. H. (1999). Rhodopsin's carboxy-terminal cytoplasmic tail acts as a membrane receptor for cytoplasmic dynein by binding to the dynein light chain Tctex-1. *Cell*, **97**, 877–887.
22. Fan, J., Zhang, Q., Tochio, H., Li, M. & Zhang, M. (2001). Structural basis of diverse sequence-dependent target recognition by the 8 kDa dynein light chain. *J. Mol. Biol.* **306**, 97–108.
23. Wang, W., Lo, K. W., Kan, H. M., Fan, J. S. & Zhang, M. (2003). Structure of the monomeric 8-kDa dynein light chain and mechanism of the domain-swapped dimer assembly. *J. Biol. Chem.* **278**, 41491–41499.
24. Liang, J., Jaffrey, S. R., Guo, W., Snyder, S. H. & Clardy, J. (1999). Structure of the PIN/LC8 dimer with a bound peptide. *Nature Struct. Biol.* **6**, 735–740.
25. Williams, J. C., Xie, H. & Hendrickson, W. A. (2005). Crystal structure of dynein light chain TCTEX-1. *J. Biol. Chem.* **23**, 21981–21986.
26. Wu, H., Maciejewski, M. W., Takebe, S. & King, S. M.

(2005). Solution structure of the Tctex1 dimer reveals a mechanism for dynein-cargo interactions. *Structure*, **13**, 213–223.
27. Fan, J. S., Zhang, Q., Tochio, H. & Zhang, M. (2002). Backbone dynamics of the 8 kDa dynein light chain dimer reveals molecular basis of the protein's functional diversity. *J. Biomol. NMR*, **23**, 103–114.
28. Jin, Q., Ding, W., Staub, C. M., Gao, G., Tang, Q. & Mulder, K. M. (2005). Requirement of km23 for TGFβ-mediated growth inhibition and induction of fibronectin expression. *Cell. Signal.* In the Press (available online March 31, 2005).
29. Massagué, J., Blain, S. W. & Lo, R. S. (2000). TGFβ signaling in growth control, cancer, and heritable disorders. *Cell*, **103**, 295–309.
30. Yue, J. & Mulder, K. M. (2001). Transforming growth factor-β signal transduction in epithelial cells. *Pharmacol. Ther.* **91**, 1–34.
31. Ding, W., Tang, Q., Espina, V., Liotta, L. A., Mauger, D. T. & Mulder, K. M. (2005). A TGF-β receptor-interacting protein frequently mutated in epithelial ovarian cancer. *Cancer Res.*. Aug 1, In the Press.
32. Koonin, E. V. & Aravind, L. (2000). Dynein light chains of the Roadblock/LC7 group belong to an ancient protein superfamily implicated in NTPase regulation. *Curr. Biol.* **10**, R774–R776.
33. Lunin, V. V., Munger, C., Wagner, J., Ye, Z., Cygler, M. & Sacher, M. (2004). The structure of the MAPK scaffold, MP1, bound to its partner, p14. A complex with a critical role in endosomal map kinase signaling. *J. Biol. Chem.* **279**, 23422–23430.
34. Kurzbauer, R., Teis, D., de Araujo, M. E., Maurer-Stroh, S., Eisenhaber, F., Bourenkov, G. P. *et al.* (2004). Crystal structure of the p14/MP1 scaffolding complex: how a twin couple attaches mitogen-activated protein kinase signaling to late endosomes. *Proc. Natl Acad. Sci. USA*, **101**, 10984–10989.
35. Schuck, P. (2000). Size-distribution analysis of macromolecules by sedimentation velocity ultracentrifugation and Lamm equation modeling. *Biophys. J.* **78**, 1606–1619.
36. Demeler, B. & Saber, H. (1998). Determination of molecular parameters by fitting sedimentation data to finite-element solutions of the Lamm equation. *Biophys. J.* **74**, 444–454.
37. Wishart, D. S. & Sykes, B. D. (1994). The ^{13}C chemical-shift index: a simple method for the identification of protein secondary structure using ^{13}C chemical shift data. *J. Biomol. NMR*, **4**, 171–180.
38. Schwieters, C. D., Kuszewski, J. J., Tjandra, N. & Clore, G. M. (2003). The Xplor-NIH NMR molecular structure determination package. *J. Magn. Reson.* **160**, 65–73.
39. Cornilescu, G., Delaglio, F. & Bax, A. (1999). Protein backbone angle restraints from searching a database for chemical shift and sequence homology. *J. Biomol. NMR*, **13**, 289–302.
40. Hansen, M. R., Mueller, L. & Pardi, A. (1998). Tunable alignment of macromolecules by filamentous phage yields dipolar coupling interactions. *Nature Struct. Biol.* **5**, 1065–1074.
41. Zweckstetter, M. & Bax, A. (2000). Prediction of sterically induced alignment in a dilute liquid crystalline phase: aid to protein structure determination by NMR. *J. Am. Chem. Soc.* **122**, 3791–3792.
42. Bax, A., Kontaxis, G. & Tjandra, N. (2001). Dipolar couplings in macromolecular structure determination. *Methods Enzymol.* **339**, 127–174.
43. Laskowski, R. A., MacArthur, M. W., Moss, D. S. & Thornton, J. M. (1993). PROCHECK: a program to check the stereochemical quality of protein structures. *J. Appl. Crystallog.* **26**, 283–291.
44. Osborne, M. J. & Wright, P. E. (2001). Anisotropic rotational diffusion in model-free analysis for a ternary DHFR complex. *J. Biomol. NMR*, **19**, 209–230.
45. Tjandra, N., Feller, S. E., Pastor, R. W. & Bax, A. (1995). Rotational diffusion anisotropy of human ubiquitin from ^{15}N NMR relaxation. *J. Am. Chem. Soc.* **117**, 12562–12566.
46. Tjandra, N., Wingfield, P., Stahl, S. & Bax, A. (1996). Anisotropic rotational diffusion of perdeuterated HIV protease from ^{15}N NMR relaxation measurements at two magnetic fields. *J. Biomol. NMR*, **8**, 273–284.
47. Mandel, A. M., Akke, M. & Palmer, A. G., III (1995). Backbone dynamics of *Escherichia coli* ribonuclease HI: correlations with structure and function in an active enzyme. *J. Mol. Biol.* **246**, 144–163.
48. Ding, W. & Mulder, K. M. (2004). km23: a novel TGFβ signaling target altered in ovarian cancer. In *Molecular Targeting and Signal Transduction (Cancer Treatment and Research)* (Kumar, R., ed.), vol. 119, pp. 315–327, Kluwer Academic Publishers, Boston/New York/Dordrecht/London.
49. Livingstone, C. D. & Barton, G. J. (1993). Protein sequence alignments: a strategy for the hierarchical analysis of residue conservation. *Comput. Appl. Biosci.* **9**, 745–756.
50. Jiang, J., Yu, L., Huang, X., Chen, X., Li, D., Zhang, Y. *et al.* (2001). Identification of two novel human dynein light chain genes, DNLC2A and DNLC2B, and their expression changes in hepatocellular carcinoma tissues from 68 Chinese patients. *Gene*, **281**, 103–113.
51. Demeler, B. (2005). UltraScan Software, University of Texas Health Science Center at San Antonio, Department of Biochemistry. http://ultrascan.uthscsa.edu
52. Laue, T. M., Shah, B. D., Ridgeway, T. M. & Pelletier, S. L. (1992). Analytical Ultracentrifugation in Biochemistry and Polymer Science. In *Proteins Amino Acids and Peptides as Ions and Dipolar Ions* (Harding, S. E., Rowe, A. J. & Horton, J. C., eds), pp. 90–125, Royal Society of Chemistry, Cambridge.
53. Cohn, E. J. & Edsall, J. T. (1943). *Proteins Amino Acids and Peptides as Ions and Dipolar Ions*, Reinhold, New York pp. 157.
54. Neri, D., Szyperski, T., Otting, G., Senn, H. & Wuthrich, K. (1989). Stereospecific nuclear magnetic resonance assignments of the methyl groups of valine and leucine in the DNA-binding domain of the 434 repressor by biosynthetically directed fractional ^{13}C labeling. *Biochemistry*, **28**, 7510–7516.
55. Delaglio, F., Grzesiek, S., Vuister, G. W., Zhu, G., Pfeifer, J. & Bax, A. (1995). NMRPIPE—a multidimensional spectral processing system based on Unix Pipes. *J. Biomol. NMR*, **6**, 277–293.
56. Johnson, B. A. & Blevins, R. A. (1994). NMRView—a computer-program for the visualization and analysis of NMR data. *J. Biomol. NMR*, **4**, 603–614.
57. Yamazaki, T., Lee, W., Revington, M., Mattiello, D. L., Dahlquist, F. W., Arrowsmith, C. H. & Kay, L. E. (1994). An HNCA pulse scheme for the backbone assignment of N-15,C-13,H-2-labeled proteins—application to a 37-kDa Trp repressor DNA complex. *J. Am. Chem. Soc.* **116**, 6464–6465.
58. Wittekind, M. & Mueller, L. (1993). HNCACB, a high-sensitivity 3-D NMR experiment to correlate amide-proton and nitrogen resonances with the alpha-carbon and beta-carbon resonances in proteins. *J. Magn. Reson. ser. B*, **101**, 201–205.

59. Grzesiek, S. & Bax, A. (1993). Amino acid type determination in the sequential assignment procedure of uniformLy $^{13}C/^{15}N$-enriched proteins. *J. Biomol. NMR*, **3**, 185–204.
60. Kay, L. E., Ikura, M., Tschudin, R. & Bax, A. (1990). 3-Dimensional triple-resonance NMR-spectroscopy of isotopically enriched proteins. *J. Magn. Reson.* **89**, 496–514.
61. Grzesiek, S., Anglister, J. & Bax, A. (1993). Correlation of backbone amide and aliphatic side-chain resonances in C-13/N-15-enriched proteins by isotropic mixing of C-13 magnetization. *J. Magn. Reson. ser. B*, **101**, 114–119.
62. Kay, L. E., Xu, G. Y., Singer, A. U., Muhandiram, D. R. & Formankay, J. D. (1993). A gradient-enhanced HCCH-TOCSY experiment for recording side-chain H-1 and C-13 correlations in H_2O samples of proteins. *J. Magn. Reson. ser. B*, **101**, 333–337.
63. Zwahlen, C., Legault, P., Vincent, S. J. F., Greenblatt, J., Konrat, R. & Kay, L. E. (1997). Methods for measurement of intermolecular NOEs by multinuclear NMR spectroscopy: application to a bacteriophage lambda N-peptide/boxB RNA complex. *J. Am. Chem. Soc.* **119**, 6711–6721.
64. Muhandiram, D. R., Farrow, N. A., Xu, G. Y., Smallcombe, S. H. & Kay, L. E. (1993). A gradient C-13 NOESY-HSQC experiment for recording NOESY spectra of C-13 labeled proteins dissolved in H_2O. *J. Magn. Reson. ser. B*, **102**, 317–321.
65. Ottiger, M., Delaglio, F. & Bax, A. (1998). Measurement of J and dipolar couplings from simplified two-dimensional NMR spectra. *J. Magn. Reson.* **131**, 373–378.
66. Grzesiek, S. & Bax, A. (1992). Improved 3D triple-resonance NMR techniques applied to a 31-kDa protein. *J. Magn. Reson.* **96**, 432–440.
67. Tjandra, N. & Bax, A. (1997). Large variation in $^{13}C^{\alpha}$ chemical shift anisotropy in proteins correlate with secondary structure. *J. Am. Chem. Soc.* **119**, 9576–9577.
68. Vuister, G. W. & Bax, A. (1994). Measurement of four-bond HN-H alpha *J*-couplings in staphylococcal nuclease. *J. Biomol. NMR*, **4**, 193–200.
69. Nilges, M., Clore, G. M. & Gronenborn, A. M. (1988). Determination of three-dimensional structures of proteins from interproton distance data by hybrid distance geometry-dynamical simulated annealing calculations. *FEBS Letters*, **229**, 317–324.
70. Schwieters, C. D. & Clore, G. M. (2001). Internal coordinates for molecular dynamics and minimization in structure determination and refinement. *J. Magn. Reson.* **152**, 288–302.
71. Kay, L. E., Nicholson, L. K., Delaglio, F., Bax, A. & Torchia, D. A. (1992). Pulse sequences for removal of the effects of cross-correlation between dipolar and chemical-shift anisotropy relaxation mechanism on the measurement of heteronuclear T_1 and T_2 values in proteins. *J. Magn. Reson.* **97**, 359–375.
72. Press, W. H., Flannery, B. P., Teukolsky, S. A. & Vetterling, W. T. (1988). *Numerical Recipes in C*, Cambridge University Press, Cambridge, UK.
73. Freedberg, D. I., Ishima, R., Jacob, J., Wang, Y. X., Kustanovich, I., Louis, J. M. & Torchia, D. A. (2002). Rapid structural fluctuations of the free HIV protease flaps in solution: relationship to crystal structures and comparison with predictions of dynamics calculations. *Protein Sci.* **11**, 221–232.
74. Barbato, G., Ikura, M., Kay, L. E., Pastor, R. W. & Bax, A. (1992). Backbone dynamics of calmodulin studied by ^{15}N relaxation using inverse detected two-dimensional NMR spectroscopy: the central helix is flexible. *Biochemistry*, **31**, 5269–5278.
75. Copie, V., Tomita, Y., Akiyama, S. K., Aota, S., Yamada, K. M., Venable, R. M. *et al.* (1998). Solution structure and dynamics of linked cell attachment modules of mouse fibronectin containing the RGD and synergy regions: comparison with the human fibronectin crystal structure. *J. Mol. Biol.* **277**, 663–682.
76. Lipari, G. & Szabo, A. (1982). Model-free approach to the interpretation of nuclear magnetic resonance relaxation in macromolecules. 2. Analysis of experimental results. *J. Am. Chem. Soc.* **104**, 4559–4570.
77. Clore, G. M., Szabo, A., Bax, A., Kay, L. E., Driscoll, P. C. & Gronenborn, A. M. (1990). Deviations from the simple 2-parameter model-free approach to the interpretation of N-15 nuclear magnetic-relaxation of proteins. *J. Am. Chem. Soc.* **112**, 4989–4991.
78. Woessner, D. E. (1962). Nuclear spin relaxation in ellipsoids undergoing rotational brownian motion. *J. Chem. Phys.* **37**, 647–654.

Edited by M. F. Summers

(Received 21 April 2005; received in revised form 5 July 2005; accepted 5 July 2005)
Available online 20 July 2005

4498 Requirement for the TGFB receptor interacting protein km23 in a Smad2-denpendent TGFB signaling pathway

Kathleen M. Mulder, Qunyan Jin, Xin Liu, Wei Ding. *Penn State College of Medicine, Hershey, PA.*

We previously identified km23 as a novel transforming growth factor B (TGFB) receptor-interacting protein that is also a light chain of the motor protein dynein (DLC). Further, we have demonstrated that km23 is altered in 42% of cancer tissues from ovarian cancer patients. Here we demonstrate that the phosphorylation of km23 is TGFB-dependent, and that EGF is unable to phosphorylate km23. In addition, we show that km23 is co-localized with the TGFB signaling component Smad2 at early time periods after TGFB treatment of Madin Darby canine kidney (MDCK) epithelial cells, prior to translocation of Smad2 to the nucleus. Further, km23 interacted with Smad2, but not Smad3, in both immunoprecipitation (IP) /blot and glutathione-S-transferase (GST) pull-down assays. Blockade of km23 using small interfering RNA (siRNA) significantly reduced nuclear expression of Smad2 and TGFB-dependent Smad2 transcriptional activation of the activin-responsive element (ARE). Other TGFB responses were also suppressed by km23 siRNA, including TGFB inhibition of cell growth. Our findings demonstrate that km23 is required in a Smad2-dependent TGFB signaling pathway, and that it is necessary, but not sufficient, for TGFB-mediated growth inhibition. We also show that stable, inducible over-expression of km23 in a TGFB-resistant ovarian cancer cell line results in growth suppression in monolayer culture and in soft agar. Thus, km23 may function as a tumor suppressor, and appears to be a novel anti-cancer therapeutic target. This work was supported by NIH grants CA90765, CA92889, CA100239, and DAMD17-03-1-0287 to KMM

Copyright © 2005 American Association for Cancer Research. All rights reserved.
Citation format: Proc Amer Assoc Cancer Res 2005;46: 4498.

American Association for Cancer Research

Back to Search Results Search Page Print This Page

3726 Role of the c-AMP responsive element in mediating TGFβ induction of TGFβ3 gene transcription

Guangming Liu, Lipai Chen, Jill Neiman, Kathleen M. Mulder. *Penn State University College of Medicine, Hershey, PA.*

Increased TGFβ production by tumor cells often contributes to cancer progression. We have previously reported that c-Fos is a major component binding at a proximal AP-1 DNA binding site of the TGFβ1 promoter and that blockade of c-Fos by siRNA suppresses TGFβ1 production and cell migration in FET human colon carcinoma cells. In similarity to TGFβ1, TGFβ3 can also promote migration and invasiveness of tumor cells, yet the TGFβ3 promoter is strikingly dissimilar from that for TGFβ1. In the current study, we identified the TGFβ3 promoter region that is critical for TGFβ3 gene transcription in both an untransformed epithelial cell line (IEC4-1) and a human colon carcinoma cell line (RKO). We also examined the transcription factors that bind to this region. Here we show that TGFβ stimulated TGFβ3 promoter reporter activity using the TGFβ inducible -221 to +110 region of the TGFβ3 promoter (termed Tβ3-P221/110-Luc) in luciferase assays. Further, DNA binding to Tβ3-P61/35, a portion of Tβ3-P221/110 containing an AP-2 site, a Smad binding element (SBE), and a c-AMP responsive element (CRE), was also induced by TGFβ in a time-dependent manner. Mutation of the CRE, but not the AP-2 or SBE sites, totally abolished complex formation in both IEC4-1 and RKO cells. EMSA supershift assays indicated that CRE binding protein 1 (CREB1) and Smad3, but not Smad4, were the major components in this complex. Dominant-negative TGFβRII effectively blocked the DNA binding activity induced by either TGFβ1 or TGFβ3, but not that induced by phorbol 12-myristate-13-acetate (PMA). Further, TGFβ induction of both complex formation at Tβ3-P61/35 and Tβ3-P221/110-Luc reporter activity were suppressed by both the JNK-selective inhibitor SP600125 and the p38-selective inhibitor SB203580, but not by the MEK/ERK inhibitor PD98059 or the PKA inhibitor H89 in IEC4-1 cells. siRNA-CREB1 also significantly inhibited both complex formation at Tβ3-P61/35 and Tβ3-P221/110-Luc reporter activity in both IEC4-1 and RKO cells. Collectively, our results indicate that the CRE site is critical for mediating TGFβ3 gene expression, with CREB1 and Smad3 being the major components bound at this site in response to TGFβ in IEC4-1 cells. Further, activation of the TGFβ3 promoter CRE site by TGFβ required TGFβRII, JNK, p38, and Smad3, but was independent of PKA. Identifying factors that modulate TGFβ3 auto-regulation improves our understanding of the mechanisms underlying TGFβ3 production in both untransformed cells and colon carcinoma cells, which may enable the design of novel strategies to regulate TGFβ3 secretion in cancers. Such strategies may prevent invasiveness and metastasis of the disease. This work was supported by NIH grants CA90765, CA92889, CA100239, and DAMD17-03-1-0287 to KMM

Copyright © 2005 American Association for Cancer Research. All rights reserved.
Citation format: Proc Amer Assoc Cancer Res 2005;46: 3726.

Abstract:
FASEB Summer Research Conference:
TGFβ Superfamily: Signaling & Development
Snomass Village, CO
June 2005

A new light chain of the motor protein dynein (km23-2) is involved in transforming growth factor-β signaling

Gao G.F. and Mulder K.M.

Pennsylvania State University College of Medicine, Hershey, PA

We have previously identified a novel TGFβ receptor-interacting protein, km23, which is also a light chain of the motor protein dynein. Here we show that a new member of this dynein light chain family, termed km23-2, is also involved in TGFβ signaling. km23-2 interacted with the TGFβ receptor complex intracellularly, and TGFβ mediated a rapid increase in km23-2 phosphorylation. The kinase activity of TβRII was required for km23-2 phosphorylation. In contrast, TβRI appeared to play no significant role in this phosphorylation event. Furthermore, TGFβ induced a rapid recruitment of km23-2 to the intermediate chain of dynein (DIC). A kinase-deficient form of TβRII prevented km23-2 phosphorylation and interaction with the DIC. This strengthens our previous work demonstrating a link between cytoplasmic dynein and TGFβ signaling. Furthermore, these results suggest that TGFβ signaling pathway components may use different motor protein light chains as motor receptors for the specific recruitment and transport of these cargos along microtubules.

Abstract:
FASEB Summer Research Conference:
TGFβ Superfamily: Signaling & Development
Snomass Village, CO
June 2005

km23 phosphorylation controls its function in transforming growth factor-β signaling

Zhong, Y., Ding, W., Tang, Q., and Mulder K.M.

Pennsylvania State University College of Medicine, Hershey, PA.

km23, a novel TGFβ receptor-interacting protein and also a dynein light chain, is known to be phosphorylated on serine residues and recruited to the dynein intermediate chain (DIC) after ligand-receptor activation. In vivo phosphorylation experiments have demonstrated that three conserved serine residues of km23 (S32, S55 and S73) are partially required for km23 phosphorylation by TGFβ. The three dimensional solution structure study has identified km23 as a stable homodimer. We have demonstrated that a single km23 mutant S32A can block the homodimerization of km23. Further, we have shown that two single phosphorylation mutants (S32A or S73A) completely block the interaction of km23 with the DIC, suggesting a defect in cargo recruitment to the dynein motor complex. In addition, a novel form of km23, which is missing exon 3 including 3 phosphorylation sites (Dexon3-km23), was found in two out of nineteen tumor tissues from patients with ovarian cancer. Functional studies have shown that the Dexon3-km23 mutant displayed not only a disruption in binding to the DIC, but also an inhibition of TGFβ-dependent transcriptional activation of both the p3TP-lux and activin responsive element (ARE) reporters. Therefore, the loss of key phosphorylation sites in km23 may represent a mechanism underlying the TGFβ resistance associated with ovarian tumors. Collectively, our results suggest that km23 phosphorylation controls its function in TGFβ signaling, presumably for the intracellular transport of TGFβ signaling components. Alteration of intercellular transport of TGFβ signaling components such as Smads would alter the growth suppression by TGFβ and may contribute to tumorigenesis.

CURRICULUM VITAE

NAME: KATHLEEN M. MULDER, Ph.D. **TITLE:** Professor with tenure

Website: : http://www.hmc.psu.edu/depts/cgi-bin/faculty.pl?name=mulder.html&folder=faculty&code=pharmacologydept
http://fred.hmc.psu.edu/ds/retrieve/fred/investigator/kmulder
http://www.genetics.psu.edu/Faculty/detail.asp?pkey=80

ADDRESS:

Home: 713 W. Elm St.
Palmyra, PA 17078
(717) 832-2203
FAX (717) 832-3450
Cell (717) 512-6560

Work: Dept. of Pharmacology – MC H078
Penn State College of Medicine
500 University Drive
Hershey, PA 17033
(717) 531-6789
(717) 531-5013 (FAX)

Email: kmm15@psu.edu

EDUCATION:

Muhlenberg College, Allentown, PA	B.S.	1979	Natural Sciences & Mathematics Psychology
State University of NY at Buffalo, NY	Ph.D.	1985	Pharmacology
Baylor College of Med., Houston, TX	Postdoc	1988	Cellular & Molecular Biology

OTHER TRAINING:

Reigle Aviation, Palmyra, PA	2002 Private Pilot License
Harrisburg Jet Center, Harrisburg, PA	2003 Instrument Rating
Federal Aviation Administration -- Pilot Proficiency Award Program	2003-04 Wings Phases I, II

APPOINTMENTS:

1980-1984	Graduate Research Assistant, State University of NY at Buffalo, Buffalo, NY
1985-1988	Research Associate, Department of Pharmacology, Baylor College of Medicine, Texas Medical Center, Houston, TX
1988-1991	Assistant Professor (tenure-track), Department of Pharmacology, Baylor College of Medicine, Houston, TX
1990-1991	Consultant, Bristol-Myers Squibb, Wallingford, CT
1991-1993	Assistant Professor (tenure-track), Department of Pharmacology, Pennsylvania State University College of Medicine, Hershey, PA
1993-1998	Tenured Associate Professor, Department of Pharmacology, Pennsylvania State University College of Medicine, Hershey, PA
1998-Pres	Tenured Professor, Department of Pharmacology, Pennsylvania State University College of Medicine, Hershey, PA

AWARDS:

1980-1983	NIH Pre-doctoral Training Grant recipient
1984	First Prize - Sigma XI Research Award Competition
1989-1994	NIH PHS First Independent Research Support and Transition Award: 5.2 percentile
1993-1998	NIH Research Career Development Award (NCI)

CURRENT RESEARCH GRANT SUPPORT (P.I. on all):

R01 CA90765-02; Mechanisms of TGFβ Production in Human Cancer Cells; $1,532,845 (total costs); 04/01/01-03/31/06; 1.8 percentile

R01 CA92889-01; Role of TGFβ in Microtubule Dynamics; $1,277,370 (total costs); 08/01/01-07/31/06

RO1 CA 100239-01; Role of km23 in ovarian cancer; $1,724,000 (total costs); 04/01/03-03/31/08; 1.7 percentile

DOD Ovarian cancer; Development of km23-based diagnostics and therapeutics; $561,375 (total costs); 04/15/03-05/15/06; 98 percentile; 1.3 priority score

CURRENT RESEARCH GRANT SUPPORT (Consultant)

2R01 HD33852-09 (McAllister, PI); 17α-Hydroxylase Expression in Human Ovarian Cells; $157,500 (annual total direct costs); 07/01/01-12/31/05

GRANTS COMPLETED (P. I. on all):

R01 CA 100239-01; Role of km23 in ovarian cancer (NIH Structural Studies Supplement High-Resolution NMR Structure of km23 Proteins); $40,000 (total direct costs); 04/01/03-03/31/05

DOD BC 996476; Mechanism of Ras Activation by TGFβ; 05/01-06/03.

NIH R01 CA51452-12; Mechanisms of TGFβ Signaling; 04/89-03/03.

NIH R01 CA68444 Intracellular Mediators of TGFβ Effects; 04/96-04/01.

NIH R01 CA54816 Role of MAPK's in TGFβ-Mediated Cellular Responses; 07/92 - 06/01.

RESEARCH CAREER DEVELOPMENT AWARD, NATIONAL CANCER INSTITUTE:
5 K04 CA59552 Mediators of Growth Factor Independence in Colon Cancer; 05/93-04/98.

PATENT PENDING: Control of TGFβ signaling by km23 superfamily members

PEER REVIEW SERVICE

Grants:

NCDDG Grant Review - 10/89
NIH Program Grant Site Visits- 6/90, 3/94, 9/95, 9/03

NIH R13 Grant Review - 12/90, 12/96
Veterans Administration Merit Review Applic. - 3/92, 9/92, 8/95
Institutional Research Grant Review Committee - 3/93-present
Israel Science Foundation - 5/93
National Cancer Institute of Canada, Program Project Site Visit - 10/93
American Cancer Society, Local Chapter - 10/94-9/97
Active Member, NIH Special Study Section SSS2 - SBIR/STTR awards - 11/94-11/96
NIH R03/RFA Study Section - 3/95
USAMRMC (DOD) Breast Cancer Reviews - 11/95, 9/96, 9/97, 9/98, 8/99
North Carolina Biotech Center - 4/96
Ad Hoc Member, Metabolic Pathology Study Section (MEP), NIH - 6/96-3/97
National Science Foundation - 9/97
Regular Member, Metabolic Pathology Study Section (MEP), NIH - 6/97-7/01
Reviewer, NCI Phased Application Awards/SBIR-STTR Initiative,
Cancer Prognosis & Prediction, 10/02
Reviewer, Tobacco Settlement Research Funds RFA, PSCOM, 4/03
Reviewer, Tumor Cell Biology Study Section (TCB) – NIH Oncological Sciences
Integrated Review Group, Center for Scientific Review – 2/04
Reviewer, NCI-F, KO1 Mentored Career Development Awards & T32 Institutional
National Research Awards – 3/05
ZRG1 ONC-U, Molecular Oncogenesis Study Section (MONC), Oncological Sciences
IRG, Center for Scientific Review, National Institutes of Health – 6/05

Manuscripts:

Reviewer for:

American Journal of Pathology
American Journal of Physiology
Cancer Chemotherapy and Pharmacology
Cancer Communications/Oncology Research
Cancer Detection and Prevention
Cancer Research
Carcinogenesis
Cell Growth and Differentiation
EMBO Journal
Experimental Cell Research
FEBS Letters
Gastroenterology
International Journal of Cancer
Journal of Biological Chemistry
Journal of Cellular Physiology
Journal of Cell Science
Journal of Clinical Endocrinology and Metabolism
Molecular Biology of the Cell
Molecular and Cellular Biology
Molecular Pharmacology
Oncogene
Regulatory Peptides

EDITORIAL BOARD MEMBER: **The Journal of Biological Chemistry**, 07/01/01-06/30/06

PROFESSIONAL AFFILIATIONS

American Association for Cancer Research
American Association for the Advancement of Science
Women in Cancer Research
Federation of American Societies for Experimental Biology
American Society for Biochemistry and Molecular Biology
American Society for Cell Biology
Association for Molecular Pathology

NATIONAL COMMITTEES

Joint Steering Committee on Public Policy, District Leader, Pennsylvania Congressional Liaison Committee, 1997-1999
American Association for Cancer Research, Science Policy and Legislative Affairs Committee, 2004-present

INVITED SPEAKER

Albert Einstein School of Medicine, Bronx, NY	1988
National Institute of Environmental Health Sciences, Chapel Hill, NC	1988
Bristol-Myers Co., Wallingford, CT	1988
University of Maryland, Baltimore, MD	1989
University of Tennessee, Memphis, TN	1989
Bristol-Myers Co., Wallingford, CT	1989
15th International Cancer Congress, Hamburg, Germany	1990
Northwestern University School of Medicine, Chicago, IL	1990
M.D. Anderson Cancer Center, Houston, TX	1990
University of Connecticut Health Center, Farmington, CT	1990
University of Alabama College of Medicine, Birmingham, AL	1990
Triton Biosciences, Oakland, CA	1990
Univ. of North Dakota School of Medicine, Grand Forks, ND	1990
Dartmouth Medical School, Hanover, NH	1990
Cell and Molecular Biology Program, Penn State College of Medicine, Hershey, PA	1991
Medical College of Wisconsin Cancer Center, Milwaukee, WI	1992
Case Western Reserve University, Cleveland, OH	1992
Michigan Cancer Foundation, Detroit, MI	1992
Medical College of Ohio, Toledo, OH	1992
Chicago Medical School, North Chicago, IL	1992
Cellular and Molecular Physiology, Penn State College of Medicine, Hershey, PA	1992
Division of Endocrinology, Department of Medicine, Penn State College of Medicine, Hershey, PA	1992
Instituto Nationale per la ricerca Sul Cancro, Genova, Italy	1992
Bloomsburg University, Bloomsburg, PA	1992
Roswell Park Cancer Institute, Buffalo, NY	1993
Symposium of the American Gastroenterological Assoc., Vail, CO	1994
Bristol Myers Squibb, Princeton, NJ	1994
Fifth International Congress on Anti-Cancer Chemotherapy, Paris, France	1995

Division of Endocrinology, Department of Medicine, Penn State College of Medicine, Hershey, PA	1995
Department of Biological Chemistry and Molecular Biology, Penn State College of Medicine, Hershey, PA	1995
Cancer Research Center of Hawaii, Honolulu, HI	1995
Bowman Gray Medical School of Wake Forest Univ., Winston-Salem, NC	1995
AACR Annual Meeting, Toronto, Canada	1995
University of Miami Medical Center, Miami, FL	1995
Division of Endocrinology, Department of Medicine, PSCOM, Hershey, PA	1996
Department of Cellular and Molecular Physiology, Penn State College of Medicine, Hershey, PA	1996
AACR Special Conference: Cell Signaling and Cancer Treatment, Telfs-Buchen, Austria	1997
Penn State University Cancer Center, Hershey, PA	1997
National Cancer Institute, Biological Carcinogenesis and Development Program, Frederick, MD	1997
Onyx Pharmaceuticals, Inc., Richmond, CA	1997
Indiana University Cancer Center, Indianapolis, IN	1997
Creative BioMolecules, Inc, Boston, MA	1998
Baylor College of Medicine, Houston, TX	1998
Department of Microbiology & Immunology, Penn State College of Medicine, Hershey, PA	1998
University of Arizona at Tucson, Tucson, AZ	1998
Division of Endocrinology, Department of Medicine, Pennsylvania State University College of Medicine, Hershey, PA	1999
Laboratory of Cell Regulation and Carcinogenesis, NIH, Bethesda, MD	1999
Lombardi Cancer Center, Georgetown University Medical Center, Washington, D.C.	1999
TGFβ: Biological Mechanisms and Clinical Applications; 3rd Inter. Conf., National Institutes of Health, Bethesda, MD	1999
Session Chair, AACR Symposium: Cell Signaling thru the Cytoplasm, San Francisco, CA	2000
Program in Genetics, Pennsylvania State University, University Park, PA	2000
MD Anderson Cancer Center, Houston, TX	2000
Division of Surgery, Department of Medicine, Penn State College of Medicine, Hershey, PA	2000
MCP - Hahnemann School of Medicine, Philadelphia, PA	2001
Jefferson Medical College, Thomas Jefferson University, Philadelphia, PA	2001
11th International Conference on Second Messengers and Phosphoproteins: 2nd Messengers, Melbourne, Australia	2001
Southern Research Institute, Birmingham, AL	2001
Virginia Commonwealth University, Richmond, VA	2001
Medical College of Ohio, Toledo, OH	2001
University of Alabama at Birmingham Cancer Center	2001
FASEB Summer Research Conference, Tucson, AZ	2001
MD Anderson Cancer Center, Houston, TX	2001
Duke University School of Medicine, Durham, NC	2001
Penn State University, University Park, PA	2002

Penn State Cancer Institute, Hershey, PA	2002
University of Texas, San Antonio, TX	2003
AACR Annual Meeting, Toronto, CA	2003
Penn State College of Medicine IBIOS Program	2003
Fox Chase Cancer Center, Philadelphia, PA	2004
H. Lee Moffitt Cancer Center and Research Institute, Tampa, FL	2004
University of South Carolina School of Medicine, Columbia, SC	2004
Medical University of South Carolina, Charleston, SC	2005
University of Arizona Cancer Center & College of Medicine, Tucson, AZ	2005

TEACHING EXPERIENCE

Graduate Courses - *Division of Molecular Biology, Department of Pharmacology*
Baylor College of Medicine, 1988-1990

Polypeptide Growth Factors and Their Receptors: Transforming Growth Factor-beta (TGF-β)-Structure and Cellular Effects, Receptor/Ligand Interaction and Associated Events

Oncogenes and Growth Control: Nuclear Oncogenes and Regulatory Factors, Regulation of c-myc Expression in Normal and Transformed Cells

Graduate Courses - *Penn State University College of Medicine*

Pharmacology 501: Tyrosine Kinase Receptor Signaling, Serine/Threonine Kinase Receptor Signaling

Pharmacology 502: Growth Factors, Oncogenes, and Cell Cycle in Cancer

Molecular Pharmacology Techniques

Reproductive Hormones: Inhibins, Activins, and Follistatins: Endocrine/Paracrine/Autocrine Regulators of the Reproductive System

The Biology of Neoplasia: Growth Factor/Cytokine Signal Transduction Pathways

Cell Communication: Growth Factors, Receptors, and Signal Transduction

Core Cell Biology, CMBIO 540: Actin Microfilaments
Microtubules
Intermediate Filaments
Serine/Threonine Receptor Kinase Signaling

Medical Pharmacology Course

Teaching Committee, Baylor College of Medicine, 1989-1991

Lectures: Adrenergic Drugs, Penn State Univ. College of Medicine, 1991-1993

INSTITUTIONAL COMMITTEE SERVICE

Student Affairs Committee, Baylor College of Medicine, 1988-1991

Medical Pharmacology Teaching Committee, Baylor College of Medicine, 1989-1991

Summer Medical and Research Training Program, Baylor College of Medicine, 1989-1991

Graduate Faculty, Penn State University College of Medicine, 1991-present

Library Advisory Committee, Penn State University College of Medicine, 1991-present

Medical Student Selection Committee, Penn State University College of Medicine, 1992-1995

Pharmacology Faculty Search Committee, Penn State University College of Medicine, 1993-2000

Medical Student Curriculum Committee, Penn State University College of Medicine, 1995-1998

Summer Symposium in Molecular Biology, Penn State University, University Park, 1996-present
Faculty Member, Life Sciences Consortium, Graduate Program in Integrative Biosciences, Penn State University, College of Medicine (PSCOM), 1996-present
Faculty Member, Penn State University Graduate Programs:
Pharmacology, 1991-present
Cell and Molecular Biology, 1992-present
MD/PhD Program, 1995-present
Molecular Medicine, 1996-present
Chemical Biology, 1999-present
Cellular and Molecular Mechanisms of Toxicity/Molecular Toxicology, 1999-present
Genetics, 1999-present
Biomolecular Transport Dynamics, 2000-present
Chair, Appointment, Promotion, Tenure Committee, Dept. of Pharmacology, PSCOM, 2001- present
Co-Chair, Seminar Committee, Dept. of Pharmacology, PSCOM, 2001-2003
Member, Education Committee, Penn State Cancer Institute (PSCI), 2001-present
Member, Search Committee for Director, PSCI, 2002-2003
Member, Search Committee for Director, Jake Gittlen Cancer Research Institute, 2003

SELECTED NEWS RELEASES ABOUT RESEARCH FROM THE MULDER LAB

09/04/2002	*Penn State Newswire*, Study finds new target for development of anti-cancer drugs
09/04/2002	*Penn State College of Medicine News Release*, Study finds new target for development of anti-cancer drugs: Protein found effective in nearly half of human cancer tissues
09/11/2002	*Hummelstown Sun*, Anti-Cancer Target
09/12/2002	*Espicom Business Intelligence*, New target for anticancer therapies identified
09/27/2002	*Central Penn Business Journal*, Help for Cancer
08/12/2005	*Penn State Newswire*, Study suggests protein may be early warning for ovarian cancer
08/15/2005	*Pharmaceutical Business Review Online*, Researchers find ovarian cancer target
08/16/2005	*Science Daily*, Study suggests protein may be early warning for ovarian cancer

PUBLICATIONS

1. Roth, J.A., Eddy, B.J., Pearce, B., and **Mulder, K.M.**: Phenylhydrazine: Selective inhibition of human brain type B monoamine oxidase. *Biochem. Pharmacol.,* 30:945-950, 1981.
2. **Mulder, K.M.**, and Kostyniak, P.J.: Stabilization of glutathione in urine and plasma: Relevance to urinary metal excretion studies. *J. Anal. Toxicol.,* 9:31-35, 1985.
3. **Mulder, K.M.**, and Kostyniak, P.J.: Involvement of glutathione in the enhanced renal excretion of methyl mercury in CFW Swiss mice. *Tox. Appl. Pharmacol.,* 78:451-457, 1985.
4. **Mulder, K.M.**, and Kostyniak, P.J.: Effect of L-(alpha-S,5S)-alpha-amino-3-dichloro-4,5-dihydro-5-isoxazoleacetic acid on urinary excretion of methyl mercury in the mouse. J. *Pharmacol. Expt. Ther.,* 234:156-160, 1985.
5. **Mulder, K.M.**, Levine, A.E., Hernandez, X., McKnight, M.K., Brattain, D.E., and Brattain, M.G.: Modulation of c-myc by transforming growth factor-β in human colon carcinoma cells. *Biochem. Biophys. Res. Commun.,* 150:711-716, 1988.
6. **Mulder, K.M.**, and Brattain, M.G.: Alterations in c-myc expression in relation to maturational status of human colon carcinoma cells. *Int. J. Cancer,* 42:64-70, 1988.
7. **Mulder, K.M.**, McKnight, M.K., Hoosein, N.M., Levine, A.E., Hernandez, X., Brattain, D.E., and Brattain, M.G.: Characterization of TGF-β-resistant subclones isolated from a TGF-β-sensitive human colon carcinoma cell line. *Cancer Res.,* 48:7120-7125, 1988.
8. **Mulder, K.M.**, and Brattain, M.G.: Continuous maintenance of transformed fibroblasts under reduced serum conditions: Utility as a model system for investigating growth factor-specific effects in non-quiescent cells. *J. Cell. Physiol.,* 138:450-458, 1989.
9. Hoosein, N.M., McKnight, M.K., Levine, A.E., **Mulder, K.M.**, Childress, K.E., Brattain, D.E., and Brattain, M.G.: Differential sensitivity of subclasses of human colon carcinoma cell lines to the growth inhibitory effects of transforming growth factor-β. *Exp. Cell Res.,* 181:442-453, 1989.
10. **Mulder, K.M.**, and Brattain, M.G.: Growth factor expression and response in human colon carcinoma cells: In: *The Cell and Molecular Biology of Colon Cancer* (Augenlicht, L., ed.), CRC Press: Boca Raton, FL, pp. 45-67, 1989.
11. **Mulder, K.M.**, Levine, A.E., and Hinshaw, X.H.: Up-regulation of c-myc in a transformed cell line approaching stationary phase growth in culture. *Cancer Res.,* 49:2320-2326, 1989.
12. **Mulder, K.M.**, and Brattain, M.G.: Effects of growth stimulatory factors on mitogenicity and c-myc expression in poorly-differentiated and well-differentiated human colon carcinoma cells. *Mol. Endocrinol.,* 3:1215-1222, 1989.
13. **Mulder, K.M.** and Childress-Fields, K.E.: Characterization of a serum-free culture system comparing growth factor requirements of transformed and untransformed cells. Exp. Cell Res., 188:254-261, 1990.
14. **Mulder, K.M.**, Humphrey, L.E., Choi, H.-G., Childress-Fields, K.E., and Brattain, M.G.: Evidence for c-myc in the signaling pathway for TGF-β in well-differentiated human colon carcinoma cells. *J. Cell. Physiol.,* 145:501-507, 1990.
15. **Mulder, K.M.**, Zhong, W., Choi, H.-G., Humphrey, L.E., and Brattain, M.G.: Inhibitory effects of transforming growth factor-β_1 on mitogenic response, transforming growth factor-α, and c-myc in well-differentiated human colon carcinoma cells. *Cancer Res.,* 50:7581-7586, 1990.

16. **Mulder, K.M.**: Differential regulation of c-myc and TGF-α mRNA expression in poorly-differentiated and well-differentiated colon carcinoma cells during the establishment of a quiescent state. *Cancer Res.*, 51:2256-2262, 1991.
17. Wu, S.P., Theodorescu, D., Kerbel, R.S., Willson, J.K.V., **Mulder, K.M.**, Humphrey, L.E., and Brattain, M.G.: TGF-β_1 is an autocrine negative growth regulator of human colon carcinoma FET cells *in vivo* as revealed by transfection of an anti-sense expression vector. *J. Cell. Biol.*, 116:187-196, 1992.
18. **Mulder, K.M.** and Morris, S.L. Activation of $p21^{ras}$ by transforming growth factor β in epithelial cells. *J. Biol. Chem.*, 267:5029-5031, 1992.
19. Brattain, M.G., **Mulder, K.M.**, Wu, S.P., Howell, G., Sun, L., Willson, J.K.V., and Ziober, B.L. Altered expression of transforming growth factor-α and transforming growth factor-β autocrine loops in cancer cells. *Adv. Molec. Cell Biol.* 7:35-59, 1993.
20. **Mulder, K.M.**, Segarini, P.R., Morris, S.L., Ziman, J.M., and Choi, H.G.: Role of receptor complexes in resistance or sensitivity to growth inhibition by TGFβ in intestinal epithelial cell clones. *J. Cell. Physiol.* 154:162-174, 1993.
21. Zipfel, P.A., Ziober, B.L., Morris, S.L., and **Mulder, K.M.**: Up-regulation of TGFα expression by TGFβ_1, EGF, and DMF in human colon carcinoma cells. *Cell Growth Differen.* 4:637-645, 1993.
22. Brattain, M.G. and **Mulder, K.M.**: Therapeutic approaches for colon cancer based on transcriptional regulation of specific growth factors. In *Cancer Therapy:* Differentiation, Immunomodulation, and Angiogenesis, edited by N. D'Alessandro, E. Mihich, L. Rausa, H. Tapiero, and T. Tritton. The NATO ASI series H, Cell Biol. 75:51-70, 1993.
23. Zhou, G.H.K., Sechrist, G.L., Brattain, M.G., and **Mulder, K.M.**: Clonal heterogeneity of the sensitivity of human colon carcinoma cell lines to TGFβ isoforms. *J. Cell. Physiol.* 165:512-520, 1995.
24. Hartsough, M.E. and **Mulder, K.M.**: Transforming growth factor β activation of $p44^{mapk}$ in proliferating cultures of epithelial cells. *J. Biol. Chem.* 270:7117-7124, 1995.
25. Zhou, G.H.K., Sechrist, G.L., Periyasamy, S., Brattain, M.G., and **Mulder, K.M.**: Transforming growth factor β isoform-specific differences in interactions with type I and II transforming growth factor β receptors. *Cancer Res.* 55:2056-2062, 1995.
26. Buard, A., Zipfel, P.A., Frey, R.S. and **Mulder, K.M.**: Maintenance of growth factor signaling through Ras in human colon carcinoma cells containing K-ras mutations. *Int. J. Cancer* 67:539-546, 1996.
27. Hartsough, M.T., Frey, R.S., Zipfel, P.A., Buard, A., Cook, S.J., McCormick, F. and **Mulder, K.M.**: Altered TGFβ signaling in epithelial cells when Ras activation is blocked. *J. Biol. Chem.* 271:22368-22375, 1996.
28. Frey, R.S. and **Mulder, K.M.**: Involvement of ERK2 and SAPK/JNK activation by TGFβ in the negative growth control of breast cancer cells. *Cancer Res.*, 57:628-633, 1997.
29. Hartsough, M.T. and **Mulder, K.M.** TGFβ signaling in epithelial cells. *Pharmacol. and Ther.*, 75:21-42, 1997.
30. Frey, R.S. and **Mulder, K.M.** TGFβ regulation of mitogen-activated protein kinases in human breast cancer cells. *Cancer Lett.*, 117:41-50, 1997.
31. Yue, J., Buard, A., and **Mulder, K.M.** Blockade of TGFβ up-regulation of $p27^{Kip1}$ and $p21^{Cip1}$ by expression of RasN17 in epithelial cells. *Oncogene*. 17:47-55, 1998.
32. Liu, X., Yue, J., Frey, R.S., Zhu, Q. and **Mulder, K.M.** TGFβ signaling through Smad1 in human breast cancer cells. *Cancer Res.*, 58:4752-4757, 1998.

33. Yue, J., Frey, R.S. Hartsough, M.T., Frielle, T., and **Mulder, K.M.** Cloning and expression of a rat Smad1: Regulation by TGFβ and modulation by the Ras/MEK pathways. *J. Cell. Physiol.*, 178:387-396, 1999.
34. Yue, J., Frey, R.S., and **Mulder, K.M.** Cross-talk between the Smad1 and Ras/MEK signaling pathways for TGFβ. *Oncogene*, 18:2033-2037, 1999.
35. **Mulder, K.M.** Role of Ras/Mapk pathways in TGFβ signaling. *Cytokine & Growth Factor Reviews* 11:23-35,2000.
36. Yue, J. and **Mulder, K.M.** Activation of the mitogen-activated protein kinase pathways by transforming growth factor-β. In Howe, P. (Ed.): *Transforming Growth Factor Beta Protocols*. The Humana Press, Inc. 142:125-131, 2000.
37. Yue, J. and **Mulder, K.M.** Requirement of Ras/MAPK pathway activation by TGFβ for $TGF\beta_1$ production in a Smad-dependent pathway. *J. Biol. Chem.* 275:30765-30773, 2000.
38. Yue, J. and **Mulder, K.M.** Transforming growth factor-beta signal transduction in epithelial cells. *Pharmacol & Ther*, 91:1-34, 2001.
39. Tang, Q., Staub, C., Gao, G., Jin, Q., Wang, Z., Ding, W., Aurigemma, R., and **Mulder, K.M.** A novel transforming growth factor-β receptor-interacting protein that is also a light chain of the motor protein dynein. *Mol. Biol. Cell,* 13: 4484-4496, 2002.
40. Yue, J., Sun, B., Liu, G., and **Mulder, K.M.** Requirement of TGFβ receptor-dependent activation of c-Jun N-terminal kinases (JNKs)/Stress-activated protein kinases (Sapks) for TGFβ up-regulation of the urokinase-type plasminogen activator receptor. *J. Cell. Physiol.* 199: 284-292, 2004.
41. Jin, Q., Ding, W., Staub, C.M., Gao, G., Tang, Q., and **Mulder, K.M.** Requirement of km23 for TGFβ-mediated growth inhibition and induction of fibronectin expression. In Press, *Cell. Signaling* 17: 1363-72, 2005.
42. Ding, W. and **Mulder, K.M.** km23: A novel TGFβ signaling target altered in ovarian cancer. In Molecular Targeting and Signal Transduction., Ed, Kumar, R. Kluwer Academic Publishers, Cancer Treatment and Research Book Series. 43. Chap. 15, 315-327, 2004.
43. Ding, W., Tang, Q., Espina, V., Liotta, L.A., Mauger, D., and **Mulder, K.M.** A TGFβ receptor-interacting protein frequently mutated in epithelial ovarian cancer. *Cancer Res.* 65, 6526-6533, 2005.
44. Ilangovan, U., Ding, W., Zhong, Y., Willson, C. L., Groppe, J. C., Trbovich, J. T., Zuniga, J., Demeler, B., Tang, Q., Gao, G., Hinck, A. P., **Mulder, K.M.** Structure and dynamics of the homodimeric dynein light chain km23. *J. Molec. Biol.*, 352:338-54, 2005.
45. Liu, G. Chen, L., Neiman, J., and **Mulder, K.M.** Critical role of the c-AMP-responsive element in TGFß-mediated regulation of TGFβ3 gene expression. In Revision, *J. Biol. Chem.*, 2005.
46. Jin, Q, Ding, W., and **Mulder, K.M.** Requirement for km23 in a Smad2-dependent TGFβ signaling pathway. In Revision, *Mol. Biol. Cell,* 2005.
47. Liu, G., Ding, W., and **Mulder, K.M.** c-Fos plays a Critical Role in TGFβ1 Promoter AP-1 binding and transactivation in human colon carcinoma cells. Submitted, 2005.
48. **Mulder, K.M.** A new target for the development of anti-cancer diagnostics and therapeutics. *Amer. Clin. Lab.*, In Preparation, 2005.
49. Liu, X., Ding, W., Sun, B., **Mulder, K.M.** Suppression of tumor growth by stable expression of wild-type km23 in human ovarian cancer cells expressing a mutant form of km23. In Prep., 2005.
50. Gao, G. and **Mulder, K.M.** Involvement of km23 dynein light chains in TGFβ signaling and intracellular transport. In: Transforming Growth Factor-Beta in Cancer Therapy.Ed,

Jakowlew, S.B. The Humana Press, Inc, Beverly Teicher's Methods in Molecular Biology series on Cancer Drug Discovery and Development. In Prep., 2005.

51. Liu, G. and **Mulder, K.M.** km23: A novel TGFβ signaling intermediate involved in TGFβ1 production in human colon carcinoma cells. In Prep., 2005.
52. Ding, W. and **Mulder, K.M.** km23 siRNA blockade of TGFβ-dependent AP-1 promoter reporter activity in untransformed epithelial cells. In Prep., 2005.
53. Gao, G. and **Mulder, K.M.** A new light chain of the motor protein dynein (km23-2) involved in transforming growth factor-β signaling. In Prep., 2005.
54. Zhong, Y., Ding, W., and **Mulder, K.M.** Control of km23 function in TGFβ signaling by phosphorylation. In Prep., 2005.

SELECTED ABSTRACTS

1. **Mulder, K.M.**, Rickling, S., Levine, A.E., and Brattain, M.G.: Effect of differentiation agents on c-myc expression in transformed fibroblasts and in human colon carcinoma cells. Fed. Proc., 45:1707, 1986.
2. **Mulder, K.M.**, and Brattain, M.G.: Loss of cell contact-mediated c-myc regulation in chemically transformed fibroblasts is restored by N,N-dimethylformamide (DMF) and retinoic acid (RA). J. Cell Biochem. (Suppl.) 11A:76, 1987.
3. Brattain, M.G., Hoosein, N., Boyd, D., **Mulder, K.**, Levine, A.E., Watkins, L., Chakrabarty, S., Ramey, M.K., and Brattain, D.E.: Regulation of growth in colon carcinoma. J. Cell. Biochem. (Suppl.) 11D, 91, 1987.
4. **Mulder, K.M.**, Hernandez, X., Gee, A., and Brattain, M.G.: Transforming growth factor-β (TGF-β) organizes the growth pattern of murine embryonic fibroblasts adapted to growth in low serum. Fed. Proc., May, 1988.
5. McKnight, K., **Mulder, K.**, and Brattain, M.G.: Differences in growth factor sensitivity by well differentiated and poorly differentiated colon carcinomas. Proc. AACR, 19:132, 1988.
6. **Mulder, K.M.**, Lynch, M.J., Childress-Fields, K.E., Hinshaw, X.H., Ramey, M.K., and Brattain, M.G.: Transforming growth factor β inhibition of growth factor-stimulated mitogenesis and c-myc expression in human colon carcinoma cells under serum-free conditions. UCLA Symposia, January, 1989.
7. Miller, G.S., Hinshaw, X.H., and **Mulder, K.M.**: Modulation of TGF-α secretion in human colon carcinoma cells. Proc. AACR, 30:74, 1989.
8. **Mulder, K.M.**: Differential regulation of c-myc and TGF-α expression in poorly-differentiated colon carcinoma cells during the establishment of a quiescent state. 15th International Cancer Congress, Hamburg, Germany, 1990.
9. **Mulder, K.M.**, Morris, S.L., Choi, H.G., Ziman, J., and Segarini, P.R.: Isolation and characterization of intestinal epithelial cell clones displaying hypersensitivity or resistance to growth inhibition by transforming growth factor-beta (TGF-β). 1991 Keystone Symposia, Steamboat Springs, CO.
10. **Mulder, K.M.**, Morris, S.L., Choi, H.G., Ziman, J., and Segarini, P.R.: Resistance and hypersensitivity to transforming growth factor-β (TGF-β) in chemically mutagenized intestinal epithelial cells. Proc. AACR, 32:42, 1991.
11. **Mulder, K.M.**, and Morris, S.L.: Activation of $p21^{ras}$ by transforming growth factor β in epithelial cells. 1992 Keystone Symposia, Keystone, CO.

12. **Mulder, K.M.,** and Morris, S.L.: Transforming growth factor-β stimulates formation of an active $p21^{ras}$. GTP complex in epithelial cells. Proc. AACR, San Diego, CA, May, 1992.
13. Zipfel, P.Z., Ziober, B.L., Morris, S.L., and **Mulder, K.M.**: Up-regulation of TGFα mRNA and protein by EGF, $TGF\beta_1$, and DMF in human colon carcinoma cells. 11th Summer Symposium in Molecular Biology, Cell Growth and Regulation, Pennsylvania State University, University Park, PA., July 1992.
14. Hartsough, M.T., Sechrist, G.L., Zhou, G.H., Brattain, M.G., and **Mulder, K.M.**: Differential binding to TGFβ receptor subtypes in clonal variants with differential sensitivities to TGFβ isoforms. 11th Summer Symposium in Molecular Biology, Cell Growth & Regulation, Pennsylvania State University, University Park, PA, July 1992.
15. Brattain, M.G., and **Mulder, K.M.**: Therapeutic approaches for colon cancer based on transcriptional regulation of specific growth factors. NATO Advanced Study Institute; Specific Approaches in Cancer Therapy: Differentiation, Immunomodulation and Angiogenesis. Erice, Italy, October 1992.
16. Hartsough, M.T. and **Mulder, K.M.**: MAPK and PKC involvement in the signaling pathway for TGFβ in colon carcinoma and intestinal epithelial cells. Academic Development Program Symposium, Merck Research Labs, Rahway, NJ, October, 1993.
17. Zipfel, P.A., Buard, A., and **Mulder, K.M.**: Analysis of K-*ras* point mutations and growth factor activation of $p21^{ras}$ in human colon carcinoma and intestinal epithelial cell lines. AACR, San Francisco, CA, April, 1994.
18. **Mulder, K.M.**: TGFβ signaling in colon carcinoma and intestinal epithelial cells. Peptide growth factors in the GI tract. Amer. Gastroenterological Assoc., Vail, CO, June, 1994.
19. Hartsough, M.T. and **Mulder, K.M.**: TGFβ activation of $p44^{mapk}$ in proliferating cultures of intestinal epithelial cells. AACR, Toronto, Canada, March, 1995.
20. Zipfel, P.A. and **Mulder, K.M.**: Altered growth factor activation of Ras in human colon carcinoma cells with K-ras mutations. FASEB, Atlanta, GA, April, 1995.
21. **Mulder, K.M.** and Hartsough, M.T.: TGFβ activation of ERK1 in proliferating cultures of intestinal epithelial cells. Fifth International Congress on Anti-Cancer Chemotherapy, Paris, France, February, 1995.
22. Hartsough, M.D. and **Mulder, K.M.**: Transforming growth factor-β activation of $p44^{mapk}$ in proliferating intestinal epithelial cells. Proc. AACR Meeting, Washington, DC, April, 1996.
23. Hartsough, M.T., Zipfel, P.A., Buard, A., Cook, S.J., McCormick, F., and **Mulder, K.M.**: Requirement of Ras for TGFβ-induced activation of extracellular signal-regulated kinase-1 (Erk1) and inhibition of cyclin-dependent kinase-2 (Cdk2) in epithelial cells. Keystone Symposia on Molecular and Cellular Biology, Tamarron, CO, January, 1996.
24. Frey, R.S. and **Mulder, K.M.**: TGFβ regulation of ERK2 and SAPK/JNK activation in the negative growth control of breast cancer cells. FASEB, New Orleans, LA, April, 1997.
25. Hartsough, M.T., Frey, R.S., Zipfel, P.A., Buard, A., Cook, S.J., McCormick, F., and **Mulder, K.M.**: TGFβ signaling in epithelial cells. AACR Special Conference: Cell Signaling and Cancer Treatment, Telfs-Buchen, Austria, February, 1997.
26. Yue, J., Buard, A., and **Mulder, K.M.**: Blockade of $TGF\beta_3$ Up-regulation of $p27^{Kip1}$ and $p21^{Cip1}$ by Expression of RasN17 in Intestinal Epithelial Cells. Keystone Symposium on Molecular and Cellular Biology, Keystone, CO, April, 1997.
27. Frey, R.S, Yue, J., Zhu, Q., Fletcher, T.M., Liu, X., and **Mulder, K.M.**: TGFβ signaling and cross-talk between the Smad and Ras Mapk Signaling Cascades in Epithelial Cells. AACR, New Orleans, LA, 1998.

28. Liu, X., Yue, J., Frey, R.S., Zhu, Q., and **Mulder, K.M.**: TGFβ signaling through Smad1 in human breast cancer cells. Gordon Conference on Peptide Growth Factors, Meridan, NH, 1998.
29. Yue, J., Frey, R.S., and **Mulder, K.M.**: Cross-talk between the Smad1 and Ras/MEK signaling pathway for TGFβ. Gordon Conference on Peptide Growth Factors, Meridan, NH, 1998.
30. Liu, X.J. and **Mulder, K.M.**: The effects of mutation of erk consensus phosphorylation sites (4SP/AP) in Smad1 on TGFβ signaling. AACR Annual Meeting; Philadelphia, PA, April, 1999.
31. Yue, J. and **Mulder, K.M.:** Requirement of the Ras pathway for TGFβ autoinduction. Annual Meeting of American Society for Biochem. and Molec. Biol., San Francisco, CA, May, 1999.
32. Liu, X. and **Mulder, K.M.** Role of Erk consensus phosphorylation sites in Smad1 on TGFβ-mediated responses. TGF-β: Biological Mechanisms and Clinical Applications, 3rd International Conference, Bethesda, MD, 1999.
33. Yue, J. and **Mulder, K.M.** Requirement of Ras, SAPK/JNK, and Erk for TGFβ1 autoinduction in a Smad4 independent pathway. TGF-β: Biological Mechanisms and Clinical Applications, 3rd International Conference, Bethesda, MD, 1999.
34. **Mulder, K.M.** TGFβ activation of Ras/Mapks/Sapks: Biological significance for TGFβ autoinduction and Smad signaling. AACR Annual Meeting, San Francisco, CA, April 1, 2000.
35. Staub, C.M., Tang, Q., Charboneau, L., Liotta, L.A., and **Mulder, K.M.** km23: Role in TGFβ signaling and alterations in human ovarian cancer. AACR Annual Meeting, New Orleans, LA, March, 2001.
36. Tang, Q., Staub, C.M., and **Mulder, K.M.** Identification of a TGFβ signaling component that interacts with dynein molecular motors. ASBMB Annual Meeting, Orlando, FL, April, 2001.
37. Tang, Q., Staub, C.M., and **Mulder, K.M.** km23: A novel TGFβ receptor-associated protein that interacts with dynein molecular motors. 2nd Messengers: 11th International Conference on Second Messengers and Phosphoproteins, Melbourne, Australia, April, 2001.
38. **Mulder, K.M.** km23: A TGFß signaling intermediate that interacts with the molecular motor dynein. FASEB Summer Research Conference: The TGFβ Superfamily: Signaling and Development, July 7-12, 2001.
39. Tang, Q., Staub, C.M. and **Mulder, K.M.** km23: A TGFβ signaling intermediate that interacts with dynein. 55th Annual Meeting and Symposium of the Society of General Physiologists, Molecular Motors, Marine Biological Laboratory, Woods Hole, Massachusetts, September, 2001.
40. Tang, Q., Staub, C.M., Ding, W., Jin, Q., Wang, Z., and **Mulder, K.M.** km23: A novel TGFβ signaling component that is truncated in human ovarian cancer. Penn State Univ., University Park, PA, April 2002.
41. Tang, Q., Staub, C.M., Gao, G., Jin, Q., Wang, Z., Ding, W., Aurigemma, R., and **Mulder, K.M.** km23: A novel TGFβ receptor-interacting protein that is also a light chain of the motor protein dynein. Anti-Cancer Drug Discovery and Development Summit, Princeton, NJ, June 17-19, 2002.
42. **Mulder, K.M.** km23—A novel TGF-beta-related target that is altered in human cancers. Drug Discovery Technology, IBC Life Sciences, Boston, MA, August 3-8, 2002.

43. **Mulder, K.**M. km23: A novel target for the development of anti-cancer therapeutics and diagnostics. Protein-Protein Interaction, Newark, NJ, November 4-6, 2002.
44. **Mulder, K.M.** A novel TGFβ receptor-interacting protein altered in human cancers that is also a light chain of the motor protein dynein. TGFβ Superfamily: Roles in the Pathogenesis of Cancer and Other Diseases, La Jolla, CA, January 15-19, 2003.
45. Jin, Q., Ding, W., Staub, C.M., Gao, G., Tang, Q., and **Mulder, K.M.** A TGF-β receptor-interacting protein frequently mutated in epithelial ovarian cancer. AACR Annual Meeting, Washington, DC, July, 2003.
46. Jin, Q., Ding, W., Staub, C.M., Gao, G., and **Mulder, K.M.** A novel Target for the Development of Anti-Cancer Diagnostics and Therapeutics. Innoventure 2003, Hershey, PA, May 2, 2003.
47. Liu, G., Ding, W., Zehner, G., Jin, Q., and **Mulder, K.M**. c-Fos plays a Critical Role in TGFβ1 Promoter AP-1 binding and transactivation in human colon carcinoma cells. AACR Annual Meeting, March, 2004.
48. **Mulder, K. M.**, Jin, Q., Liu, X., and Ding, W. Requirement for the TGFβ receptor Interacting protein km23 in a Smad2-dependent TGFß signaling pathway. AACR Annual Meeting, April, 2005.
49. Liu, G., Chen, L., Neiman, J., and **Mulder, K.M.** Role of the c-AMP Responsive Element in Mediating TGFβ induction of TGFβ3 Gene Transcription. AACR Annual Meeting, April, 2005.
50. Zhong, Y., Ding, W., Tang, Q., and **Mulder K.M.** Control of km23 function in TGF-β signaling by its phosphorylation. The FASEB Summer Research Conference: TGF-β Superfamily: Signaling and Development, June, 2005.
51. Gao G.F. and **Mulder K.M.** A new light chain of the motor protein dynein (km23-2) is involved in transforming growth factor-b signaling. The FASEB Summer Research Conference: TGF-β Superfamily: Signaling and Development, June, 2005.

10/07/0